NOTICE

AVIS

The quality of this microform is heavily dependent upon the quality of the original thesis submitted for microfilming. Every effort has been made to ensure the highest quality of reproduction possible.

La qualité de cette microforme dépend grandement de la qualité de la thèse soumise au microfilmage. Nous avons tout fait pour assurer une qualité supérieure de reproduction.

If pages are missing, contact the university which granted the degree.

S'il manque des pages, veuillez communiquer avec l'université qui a conféré le grade.

Some pages may have indistinct print especially if the original pages were typed with a poor typewriter ribbon or if the university sent us an inferior photocopy.

La qualité d'impression de certaines pages peut laisser à désirer, surtout si les pages originales ont été dactylographiées à l'aide d'un ruban usé ou si l'université nous a fait parvenir une photocopie de qualité inférieure.

Canada

Ab Initio Studies of Fluorinated Ethanes: Electronic and Energetic Properties and Reactions with Hydroxyl Radicals

by

Jaime M. Martell

Submitted in partial fulfilment of the requirements for the degree of

Doctor of Philosophy

at

Dalhousie University

Halifax, Nova Scotia

April, 1995

THE AUTHOR HAS GRANTED AN
IRREVOCABLE NON-EXCLUSIVE
LICENCE ALLOWING THE NATIONAL
LIBRARY OF CANADA TO
REPRODUCE, LOAN, DISTRIBUTE OR
SELL COPIES OF HIS/HER THESIS BY
ANY MEANS AND IN ANY FORM OR
FORMAT, MAKING THIS THESIS
AVAILABLE TO INTERESTED
PERSONS.

L'AUTEUR A ACCORDE UNE LICENCE
IRREVOCABLE ET NON EXCLUSIVE
PERMETTANT A LA BIBLIOTHEQUE
NATIONALE DU CANADA DE
REPRODUIRE, PRETER, DISTRIBUER
OU VENDRE DES COPIES DE SA
THESE DE QUELQUE MANIERE ET
SOUS QUELQUE FORME QUE CE SOIT
POUR METTRE DES EXEMPLAIRES DE
CETTE THESE A LA DISPOSITION DES
PERSONNE INTERESSEES.

THE AUTHOR RETAINS OWNERSHIP
OF THE COPYRIGHT IN HIS/HER
THESIS. NEITHER THE THESIS NOR
SUBSTANTIAL EXTRACTS FROM IT
MAY BE PRINTED OR OTHERWISE
REPRODUCED WITHOUT HIS/HER
PERMISSION.

L'AUTEUR CONSERVE LA PROPRIETE
DU DROIT D'AUTEUR QUI PROTEGE
SA THESE. NI LA THESE NI DES
EXTRAITS SUBSTANTIELS DE CELLE-
CI NE DOIVENT ETRE IMPRIMES OU
AUTREMENT REPRODUITS SANS SON
AUTORISATION.

ISBN 0-612-05283-4

Canada

Name _J____ M__h__l_ M__t_ll_

_P_y____l_ C__m_st_y__

SUBJECT TERM

| 0 | 4 | 9 | 4 | U·M·I

SUBJECT CODE

Subject Categories

THE HUMANITIES AND SOCIAL SCIENCES

COMMUNICATIONS AND THE ARTS
Architecture	0729
Art History	0377
Cinema	0900
Dance	0378
Fine Arts	0357
Information Science	0723
Journalism	0391
Library Science	0399
Mass Communications	0708
Music	0413
Speech Communication	0459
Theater	0465

EDUCATION
General	0515
Administration	0514
A l ran	
Art	0273
Bilingual and Multicultural	0282
Business	0688
Early Childhood	0518
Elementary	0524
Finance	0277
Guidance and Counseling	0519
Health	0680
Higher	0745
History of	0520
Home Economics	0278
Industrial	0521
Language and Literature	0279
Mathematics	0280
Music	0522
Philosophy of	0998
Physical	0523

Psychology	0525
Reading	0535
Religious	0527
Sciences	0714
Secondary	0533
Social Sciences	0534
Sociology of	0340
Special	0529
Teacher Training	0530
Technology	0710
Tests and Measurements	0288
Vocational	0747

LANGUAGE, LITERATURE AND LINGUISTICS
Language
General	0679
Ancient	0289
Linguistics	
Modern	
Literature
General	0401
Classical	0294
Comparative	0295
Medieval	0297
Modern	0298
African	0316
American	0591
Asian	0305
Canadian (English)	0352
Canadian (French)	0355
English	0593
Germanic	0311
Latin American	0312
Middle Eastern	0315
Romance	0313
Slavic and East European	0314

PHILOSOPHY, RELIGION AND THEOLOGY
Philosophy	0422
Religion
General	0318
Biblical Studies	0321
Clergy	
History of	
Philosophy of	
Theology	0469

SOCIAL SCIENCES
American Studies	0323
Anthropology
Archaeology	0324
Cultural	0326
Physical	0327
Business Administration
General	0310
Accounting	0272
Banking	0770
Management	0454
Marketing	0338
Canadian Studies	0385
Economics
General	0501
Agricultural	0503
Commerce Business	0505
Finance	0508
History	0509
Labor	0510
Theory	0511
Folklore	0358
Geography	0366
Gerontology	0351
History
General	0578

Ancient	0579
Medieval	0581
Modern	0582
Black	0328
African	0331
Asia Australia and Oceania	0332
Canadian	0334
European	0335
Latin American	0336
Middle Eastern	0333
United States	0337
History of Science	0585
Law	0398
Political Science
General	0615
International Law and Relations	0616
Public Administration	0617
Recreation	0814
Social Work	0452
Sociology
General	0626
Criminology and Penology	0627
Demography	0938
Ethnic and Racial Studies	0631
Individual and Family Studies	0628
Industrial and Labor Relations	0629
Public and Social Welfare	0630
Social Structure and Development	0700
Theory and Methods	0344
Transportation	0709
Urban and Regional Planning	0999
Women s Studies	0453

THE SCIENCES AND ENGINEERING

BIOLOGICAL SCIENCES
Agriculture
General	0473
Agronomy	0285
Animal Culture and Nutrition	0475
Animal Pathology	0476
Food Science and Technology	0359
Forestry and Wildlife	
Plant Culture	
Plant Pathology	0480
Plant Physiology	0817
Range Management	0777
Wood Technology	0746
Biology
General	0306
Anatomy	0287
Biostatistics	0308
Botany	0309
Cell	0379
Ecology	0329
Entomology	0353
Genetics	0369
Limnology	0793
Microbiology	0410
Molecular	0307
Neuroscience	0317
Oceanography	0416
Physiology	0433
Radiation	0821
Veterinary Science	0778
Zoology	0472
Biophysics
General	0786
Medical	0760

EARTH SCIENCES
Biogeochemistry	0425
Geochemistry	0996

Geodesy	0370
Geology	0372
Geophysics	0373
Hydrology	0388
Mineralogy	0411
Paleobotany	0345
Paleoecology	0426
Paleontology	0418
Paleozoology	0985
Palynology	0427
Physical Geography	0368
Physical Oceanography	0415

HEALTH AND ENVIRONMENTAL SCIENCES
Environmental Sciences	0768
Health Sciences
General	0566
Audiology	0300
Chemotherapy	0992
Dentistry	0567
Education	0350
Hospital Management	0769
Human Development	0758
Immunology	0982
Medicine and Surgery	0564
Mental Health	0347
Nursing	0569
Nutrition	0570
Obstetrics and Gynecology	0380
Occupational Health and Therapy	0354
Ophthalmology	0381
Pathology	0571
Pharmacology	0419
Pharmacy	0572
Physical Therapy	0382
Public Health	0573
Radiology	
Recreation	

Speech Pathology	0460
Toxicology	0383
Home Economics	0386

PHYSICAL SCIENCES

Pure Sciences
Chemistry
General	0485
Agricultural	0749
Analytical	0486
Biochemistry	0487
Inorganic	0488
Nuclear	0738
Organic	0490
Pharmaceutical	0491
Physical	0494
Polymer	0495
Radiation	0754
Mathematics	0405
Physics
General	0605
Acoustics	0986
Astronomy and Astrophysics	0606
Atmospheric Science	0608
Atomic	0748
Electronics and Electricity	0607
Elementary Particles and High Energy	0798
Fluid and Plasma	0759
Molecular	0609
Nuclear	0610
Optics	0752
Radiation	0756
Solid State	0611
Statistics	0463

Applied Sciences
Applied Mechanics	0346
Computer Science	0984

Engineering
General	0537
Aerospace	0538
Agricultural	0539
Automotive	0540
Biomedical	0541
Chemical	0542
Civil	0543
Electronics and Electrical	
Hydraulic	0545
Industrial	0546
Marine	0547
Materials Science	0794
Mechanical	0548
Metallurgy	0743
Mining	0551
Nuclear	0552
Packaging	0549
Petroleum	0765
Sanitary and Municipal	0554
System Science	0790
Geotechnology	0428
Operations Research	0796
Plastics Technology	0795
Textile Technology	0994

PSYCHOLOGY
General	0621
Behavioral	0384
Clinical	0622
Developmental	0620
Experimental	0623
Industrial	0624
Personality	0625
Physiological	0989
Psychobiology	0349
Psychometrics	0632
Social	0451

To my family

Table of Contents

List of Figures

List of Tables

Abstract

Geometries for the molecules in the series $C_2H_nF_{6-n}$ ($n = 0-6$), and the radicals produced by homolytic cleavage of the $C-C$ and $C-H$ bonds, have been optimized at the HF/6-31G(d) and MP2/6-31G(d,p) levels. Total energies were calculated with inclusion of electron correlation, up to the MP2/6-311G(d,p) level for all species, at the MP4/6-311G(d,p) level for species with less than four fluorines, and at the G2 level for species with less than three fluorines. The $C-C$ and $C-H$ bond dissociation energies are reported as $D_0(298 \text{ K})$. The $C-C$ bond dissociation energies exhibit three interesting trends, two of which may be rationalized in terms of electronegativity arguments. The C-H bond dissociation energies indicate that $C-H$ bonds can be stabilized by an inductive effect from the β-group. Inclusion of electron correlation in the geometry optimizations improves the geometrical parameters, in particular lengthening the $C-F$ bonds, and improves the total energies, but has little effect on the bond dissociation energies. The hyperfine structure in the ethyl radicals was calculated using density functional theory, at the MP2/6-31G(d,p) optimized geometries, giving good agreement with experiment in most cases where comparison is possible.

The reactions of the title molecules with hydroxyl radicals have been investigated by optimizing the transition state geometries at the HF/6-31G(d) level, and also at the MP2/6-31G(d,p) level for species with less than four fluorines, and calculating energies at the MP2/6-311G(d,p) level, at MP4/6-311G(d,p) for species with less than three fluorines, and at the G2 level for species with less than two fluorines. Inclusion of electron correlation in the geometry optimizations gives an earlier transition state. The calculated activation barriers and reaction enthalpies are affected by substitution patterns and the level of theory used.

Properties of the bond critical points for all species were also calculated. Charge development in the course of the reactions was monitored using Mulliken population analysis at four levels of theory, and Bader population analysis at the highest common level of theory. As with all the results presented, electronegativity plays a dominant role in the observed trends.

List of Symbols

δ_{ij}	Krönecker delta	Δ	energy correction factor
E	energy of stationary state	$\rho(x)$	electron (charge) density
ϵ_i	orbital energy	$\hat{V}_{ext}$	potential energy operator
ζ	variational parameter	T	kinetic energy
$\mathcal{H}$	Hamiltonian operator	E_{xc}	exchange and correlation energy
λ	parameter	A_{iso}	isotropic hyperfine constant
Φ	trial function	T_{aniso}	anisotropic hyperfine tensor
ϕ	basis function	∇^2	Laplacian
Ψ	wavefunction	x_c	critical point
Ψ_0	ground-state wavefunction	V_b	potential energy barrier height
$c_{\mu i}$	expansion coefficient	$\Delta E_0^{\ddagger}$	vibrationally adiabatic barrier
$d_{\mu s}$	basis function coefficient	E_A	Arrhenius activation energy
$\hat{F}$	Hartree-Fock operator	g	Landé splitting factor
g_s	primitive Gaussian function	β	magneton
P	electron probability density matrix	ΔH	enthalpy change
$S_{\mu\nu}$	overlap integral		

Acknowledgements

As is often the case, a supposedly individual contribution is actually a team effort. This work would not have been possible without help from many people. I have tried to list them all below; my apologies go to any I may have neglected to include.

Successful postgraduate research is rarely possible without guidance and support from a good supervisor. In addition to this, Dr. Russell Boyd has in many ways helped me realize my potential as a researcher in computational chemistry.

I am indebted to all the members of the Boyd group. In particular, I thank Dr. Zheng Shi for teaching me almost everything I know about GAUSSIAN, and for much guidance in computational strategies. Thanks go to Zheng Shi, Natalie Cann, Jian Wang, Mimi Lam, Kent Worsnop and Jing Kong for many stimulating discussions. I also thank Dr. Leif Eriksson for kindly giving me a copy of his Ph.D. thesis, which has served as a model for much of Chapter 2. In addition, his guidance and many suggestions were essential to the completion of the study of hyperfine constants.

Several members of the department merit my thanks. The members of my supervisory committee (Drs. Don Arnold, Neil Burford and Phil Pacey) have all provided input to this project. In particular, Dr. Pacey was a second supervisor on the work on the reaction of ethane with hydroxyl, and his attention to detail greatly enhanced the manuscript. Big thank yous go to Drs. Jim Pincock and Susan Boyd for helping to restore my morale. I am also grateful to Dr. Jan Kwak and Mr. Ian MacLeod for their advice and assistance, and to David Burkholder for helping me to at least pretend I can

still do experiments.

The support of both my families has been critical from day one. Thanks to Mom and Dad for providing an environment which instilled in me a thirst for knowledge, and for all their support, moral and otherwise, through the years. Last, but not least, thank you Lois for your love, support, and encouragement, to Leanne, for walking me to the elevator, and to my unborn child, for giving me the incentive to finish when I did.

Chapter 1. Global Introduction

1.1 Background

The world was first warned of the possibility of stratospheric ozone destruction initiated by fully halogenated chlorofluorocarbons (CFCs) in 1974 by Molina and Rowland.[1] Unfortunately, decisive action was not taken until after the discovery of the Antarctic "ozone hole" in 1985 by Farman *et al.*[2] The 1987 Montreal Protocol,[3] which has since been strengthened by further agreements, as well as recent unilateral government actions, mandates the rapid phase-out of CFC use. The prudence of these (belated) decisions has been underscored by recent observations of reduced levels of stratospheric ozone over the Arctic[4,5] (which could lead to another "ozone hole"[6]), and even at mid-latitudes.[7] A clear case has been made that catastrophic ozone destruction would not have occurred had certain chlorine and bromine containing compounds, primarily CFCs, not been synthesized and introduced into the atmosphere.[8,9] The search for replacements is complicated by the fact that many of the possibilities share the undesirable effects of CFCs, including being potent greenhouse gases.[10]

Research on CFC replacements has concentrated on hydrohalocarbons, which because they contain a hydrogen atom, can be removed in the troposphere by reaction with hydroxyl radicals, significantly shortening their atmospheric lifetimes.[11] This causes the ozone depletion potentials (ODPs) of hydrochlorofluorocarbons (HCFCs) to be on an order of magnitude less than those of CFCs.[12] However, the presence of ozone destroying chlorine atoms in HCFCs means that they are, at best, short-term

1

solutions until more suitable replacements can be developed. Moreover, calculation of time-dependent ODPs by Solomon and Albritton[13] shows that some of the HCFCs proposed as replacements may induce significant ozone destruction in the short term. Since fluorine has not been identified in any of the catalytic cycles which destroy stratospheric ozone (fluorine radicals are converted to HF which is highly stable under normal stratospheric conditions[14]), hydrofluorocarbons (HFCs) have been assigned ODPs of zero.[12]

The wisdom of this assignment has been the subject of some debate. It has been suggested[15] that the CF_3 radical may be involved in ozone destruction through a CF_3O_x cycle, but recent studies[16,17] concluded that this would have a negligible ODP. However, the reactions of OH radicals with HFCs in the troposphere are relatively slow[18] and hence CF_3O radicals, which are rapidly formed by the reaction of CF_3 with O_2 and NO,[19] will be formed fairly uniformly throughout the troposphere. The complexity of the subsequent chemistry ensures that the actual ODP of a given CF_3-bearing species cannot be determined solely on the basis of the measurement of a single rate constant.[20] For an excellent review of the entire subject of the environmental impact of CFC replacements, see the article by Wallington et al.[21]

This discussion is relevant to the topic of CFC replacements since most of the investigated compounds contain CF_3 groups. HFCs in the ethane series currently being developed for use include CF_3-CHF_2 (HFC-125), CF_3-CH_2F (HFC$-134a$), CF_3-CH_3 (HFC$-143a$), and CHF_2-CH_3 (HFC$-152a$). In particular, HFC-125 and HFC$-134a$ are being considered as replacement coolants for refrigeration and air-conditioning units.[22]

While fluorinated ethanes, and their reactions with hydroxyl radicals, are thus of interest to the atmospheric community, the associated fluorinated methyl and ethyl radicals, in particular the latter, are also of interest because they would be tropospheric degradation products. Both radical series attract interest from synthetic organic chemists as well, since they are common reactive intermediates. Thus, many experimentalists as well as theoreticians will be interested in the work described below.

1.2 Overview of This Work

Chapter 2 outlines the theoretical background necessary to understand the computational techniques used in this study. Chapter 3 gives details of research on the structural and energetic properties of the radical series produced by homolytic cleavage of the $C-C$ and $C-H$ bonds in the ethane series. Included are optimized geometries, vibrational frequencies, and total energies, for each series. Details of hyperfine structure calculations on the ethyl radicals are given in Chapter 4. Chapter 5 describes studies of the full series of fluorinated ethanes, including optimized geometries, vibrational frequencies, and total energies, as well as $C-C$ and $C-H$ bond dissociation energies. Results of research into properties of transition species in the reaction of ethane with OH are given in Chapter 6. A description of investigations of the transition states for the reactions of the fluorinated ethanes with hydroxyl radicals is presented in Chapter 7. Chapter 8 gives the results of topological analyses of the reactants, transition states and products of the reactions of the title series with OH. Global conclusions and suggestions for further study are given in Chapter 9.

All of the calculations described herein were performed by the author, under the supervision of Professor Russell J. Boyd, with the following exceptions. The work described in Chapter 4 was done under the co-supervision of Dr. Leif A. Eriksson (Stockholm University), who also performed a few of the calculations. Professor Philip D. Pacey was co-supervisor of the work described in Chapter 6, which was part of a collaborative effort of which he was the coordinator. Most of the calculations reported in Chapter 8 were performed by James B. Tee, a summer student who was co-supervised by the author and Professor Boyd. The supervisor and co-supervisors have given input to some of the points of discussion below, but the author remains solely responsible for the contents of this document.

Chapter 2. Theoretical Background

2.1 Introduction[23,24]

According to quantum mechanics, the energy and many properties of a stationary state of a molecule can be obtained by solution of the time-independent Schrödinger partial differential equation[25]

$$\hat{\mathcal{H}}\Psi = E\Psi \tag{1}$$

where $\mathcal{H}$ is the Hamiltonian operator, and E is the energy of the stationary state. The Schrödinger equation for any molecule will have many solutions, corresponding to different stationary states, with the lowest energy state being the ground state. It would appear to be unfortunate that this equation can only be solved exactly for a few special cases (the harmonic oscillator, the rigid rotor, and the hydrogen atom and molecular cation). However, the rapid advances in computer hardware and software of the past few decades have led to significant advances in mathematical models that can closely approximate solutions to the Schrödinger equation, thus yielding useful information.

A satisfactory model should possess a number of important characteristics. First, the method should be *well defined* and *applicable in a continuous manner to any arrangement of nuclei and any number of electrons*. Second, there must not be such a rapid increase in required computation with molecular size as to preclude its use in systems of chemical interest. A third requirement is *size-consistency*, i.e., it must give additive results when applied to an assembly of isolated molecules. A fourth desirable feature is that the calculated electronic energy be *variational*, that is, it should correspond

5

to an *upper bound* to the energy that would derive from an exact solution of the Schrödinger equation.

There are two basic approaches used in contemporary quantum chemistry. *Perturbation theory* operates from the general equation

$$\hat{\mathcal{H}} = \hat{\mathcal{H}}_0 + \hat{\mathcal{H}}' \tag{2}$$

where $\mathcal{H}_0$ is the unperturbed Hamiltonian operator, $\mathcal{H}'$ is a perturbation, and $\mathcal{H}'$ can be written in terms of a power series expansion. Typically, the first few orders provide nearly all of the correction energy needed to make the energies and wavefunctions exact. This method requires knowing the solution of a related problem ($\mathcal{H}_0$), which is not always possible.

Conversely, the *variation method* will always lead to a solution. For the ground state of a system

$$\hat{\mathcal{H}}\Psi_0 = E\Psi_0 \tag{3}$$

$$\langle\Psi_0|\hat{\mathcal{H}}|\Psi_0\rangle = E_0\langle\Psi_0|\Psi_0\rangle \tag{4}$$

hence

$$E_0 = \frac{\langle\Psi_0|\hat{\mathcal{H}}|\Psi_0\rangle}{\langle\Psi_0|\Psi_0\rangle} \tag{5}$$

Given some function Φ which satisfies the boundary conditions for the problem,

$$E_\Phi = \frac{\langle\Phi|\hat{\mathcal{H}}|\Phi\rangle}{\langle\Phi|\Phi\rangle} \geq E_0 \tag{6}$$

Only when $\Phi = \Psi_0$ will $E = E_0$. Otherwise E provides an upper bound to the true energy. Normally Φ is chosen to depend on a set of parameters, and can be written as

a function of the parameters and the coordinate' of the system. Through differentiation, the parameters are varied to make the energy a minimum.

Among the most powerful of the approximate methods (at least for small molecules) are *ab initio* techniques, which, as the name implies, operate from first principles, being independent of any experiment other than the determination of a small number of physical constants (Planck's constant, the velocity of light, and the masses and charges of electrons and nuclei). The techniques used in this study are based on *molecular orbital (MO) theory*, which assigns individual electrons to one-electron functions termed *spin orbitals*. These comprise a product of spatial functions, termed *molecular orbitals*, and either α or β *spin functions*. The spin orbitals are allowed complete freedom to spread throughout the molecule, their exact form being determined variationally to minimize the total energy.

One of the most fundamental approximations used in MO theory is the *separation of electronic and nuclear motion*, better known as the Born-Oppenheimer approximation.[26] Since electrons are much lighter than nuclei, and move much faster, nuclear kinetic terms in the Hamiltonian can be neglected, and the internuclear repulsion term treated as a constant. A further simplification is the *independent particle model*, which assumes that the electrons are non-interacting. This allows the total n-electron Hamiltonian to be rewritten as a sum of n one-electron Hamiltonians, although this is an oversimplification, since the electron-electron repulsion term is neglected.

2.2 Basis Functions and Basis Sets[23]

In practical calculations the molecular orbitals are restricted to be linear combinations of a set of N known one-electron functions:

$$\psi_i = \sum_{\mu=1}^{N} c_{\mu i} \phi_\mu \qquad (7)$$

The functions ϕ_1, ϕ_2, $\cdots$, ϕ_n are known as *basis functions*, which constitute a *basis set*, and the $c_{\mu i}$ are the *molecular orbital expansion coefficients*. These coefficients provide the orbital description with some flexibility, but a complete set ϕ_μ is required for complete freedom.

Two types of basis functions have received widespread use. *Slater-type orbitals*[27] (STOs) have exponential radial parts. They have the general form

$$\phi = A e^{-\zeta r} \qquad (8)$$

where A is a pre-exponential term, also dependent on the parameter ζ, containing the radial function and spherical harmonics. STOs provide reasonable representations of atomic orbitals, but are not well suited to numerical work, so their use in practical MO calculations has been limited.

Gaussian-type functions are powers of the Cartesian coordinates x, y, z multiplied by exp $(-\alpha r^2)$, α being a constant determining the size, i.e., radial extent, of the function. They were suggested for use in MO computations by Boys.[28] As representations of atomic orbitals, they are less satisfactory than STOs, particularly because they do not have a cusp at the origin and they fall off too rapidly at large radial distances. However, they are readily implemented as all the integrals in the computations can be evaluated explicitly without recourse to numerical integration. This property is due to the Gaussian

product theorem: the product of two Gaussian functions centered at two different points is equal to a single Gaussian centered at a third point. Thus all three- and four-center two-electron repulsion integrals are reduced to two-center integrals.[29]

In practice, linear combinations of Gaussians are often used as basis functions. For example, an s-type basis function ϕ_μ may be expanded in terms of s-type Gaussians,

$$\phi_\mu = \sum_s d_{\mu s} g_s \qquad (9)$$

where the coefficients $d_{\mu s}$ are fixed. Basis functions of this type are called *contracted Gaussians*, the individual g_s being termed *primitive Gaussians*. Whereas in an uncontracted basis set each coefficient is treated as a variational parameter, contracting a basis set reduces the number of variational parameters, thus speeding up the calculation.

Early *ab initio* calculations (and even still, calculations on large systems) used *minimal basis sets* (a.k.a. single zeta), consisting of one function for each orbital in the inner and valence shells. More sophisticated calculations require extended basis sets, which may take several forms:

i) double zeta - contain double the number of functions as a minimal basis set;

ii) split-valence - contain double (or triple) the number of basis functions in the valence shell;

iii) double zeta or split-valence plus polarization - functions of higher angular momentum are added to the above basis sets. For hydrogen atoms, a set of p functions is added, and for heavy atoms d (for p-block) or f (for transition metals) functions are added.

iv) diffuse functions - functions with a small α value (giving a large radial extent) can

also be added to the above basis sets, providing a better description of loosely bound electrons.

2.2.1 Basis Set Notation

Because of the large number of basis sets available for use in MO calculations, a standard notation is required to denote them succinctly and unambiguously. Following is an explanation of the notation for the standard basis sets available in the widely used GAUSSIAN series of programs, developed by John Pople's group at Carnegie-Mellon University.

The minimal basis sets used in the GAUSSIAN programs are the STO-NG series, in which each STO is approximated by a contraction of N primitive Gaussians. The doubly split-valence basis sets are denoted as K-LMG, where K,L,M are the number of primitive Gaussians in the core, inner valence, and outer valence shells, respectively. An additional number is required for the third valence shell in the case of a triply split-valence basis set.

There are two common conventions used to denote the addition of polarization functions. The first uses asterisks after the G, one for polarization functions on heavy atoms, and two for functions on hydrogens as well. This system breaks down if one wants to use two sets of polarization functions. This can be handled by the alternative convention, which uses (id,jp) after the G, where i and j are the number of sets of d (or f) and p functions to use on the heavy and hydrogen atoms, respectively. The convention for addition of diffuse functions is analogous to the first one for polarization functions,

with plus signs used before the G.

The commonly used notation to denote the level of theory used is A/B//C/D where A is the method used to calculate the energy, C is the method used for the geometry optimization, and B and D are the respective basis sets used. If the energy calculation and geometry optimization were done with the same method and basis set, the notation would simply be A/B.

2.3 Hartree-Fock Theory[23,30]

Once the determinantal wavefunction has been constructed from MOs, and the orbitals have been expanded in terms of a set of basis functions, it remains to specify a method for fixing the expansion coefficients. The most commonly used method is *Hartree-Fock theory*, which is based on the variational method. As formulated by Hartree,[31] and later modified by Fock,[32] the independent particle model is used to reduce the many-body problem, which cannot be solved exactly, to solving n single-particle equations. Within the limitations imposed by the single-determinant wavefunction, and the particular basis set employed, the best such wavefunction, in an energy sense, is found by minimizing E with respect to the expansion coefficients. This implies the variational equations

$$\frac{\partial E}{\partial c_{\mu i}} = 0 \quad (all\ \mu, i) \tag{10}$$

which lead to a set of algebraic equations for $c_{\mu i}$. They were derived independently for the closed-shell wavefunction by Roothaan[33] and by Hall.[34]

Direct solution of the Hartree-Fock equations

$$\hat{F}\psi_i = \epsilon_i\psi_i \tag{11}$$

where ϵ_i are the orbital energies, is not practical for polyatomic molecules. When an MO is expanded in terms of a set of AOs, the orthogonality of AOs leads to

$$\langle\psi_i|\psi_i\rangle = \sum_\mu \sum_\nu C_{\mu i}C_{\nu j}S_{\mu\nu} = \delta_{ij} \tag{12}$$

where $S_{\mu\nu}$ is the overlap integral between atomic orbitals. Application of the variation principle leads to the Roothaan-Hall equations

$$\sum_\nu (F_{\mu\nu} - \epsilon_i S_{\mu\nu})C_{\nu i} = 0, \quad \mu = 1,2,3... \tag{13}$$

where $F_{\mu\nu}$ are matrix elements of the HF-Hamiltonian. Expressing the coefficients and eigenvalues as matrices, we obtain the matrix form of the Roothaan-Hall equations

$$FC = SC\epsilon \tag{14}$$

Because the spin functions α and β are associated with the same spatial functions, i.e.

$$\psi_i^\alpha = \psi_i^\beta \tag{15}$$

this method is called *restricted* Hartree-Fock (RHF).

In the case of open-shell systems, which have an unpaired electron, the *unrestricted* Hartree-Fock (UHF) method gives a much more accurate description of the system than can be obtained with RHF. In the UHF formalism the set of spatial orbitals for electrons of α spin is different from that for electrons of β spin. This leads to a double set of equations, matrices and integrals to compute. The unrestricted form of the Roothaan-Hall equations are called the Pople-Nesbet equations.[35]

2.3.1 Self Consistent Field Method

Even when all the integrals are known we cannot calculate E and $F_{\mu\nu}$ because both depend on the electron probability density matrix P which, in turn, is constructed from C and it is the quantity C which we want to obtain, as the solution, from the Hartree-Fock equations. This requires that the eigen-problem equation be solved in an iterative manner by a process referred to as the *self consistent field* (SCF) method. The initial wavefunction is used to generate a potential, which is applied in order to refine the coefficient matrix. The modified MOs form the new input in the Roothaan-Hall equations, and a new potential is generated. The iterative procedure is repeated until convergence is reached, i.e. when the changes in energy and/or charge density in two subsequent iterations are below a pre-set threshold value.

2.4 Perturbation Theory and Configuration Interaction[23,30]

Most SCF methods satisfy the four model requirements outlined in the introduction to this chapter. The primary deficiency of Hartree-Fock theory is the inadequate treatment of the correlation between motions of electrons. Practical models incorporating electron correlation do not usually satisfy all the requirements. Nevertheless, they are gaining widespread use because they give improved electronic energies.

The difference between the Hartree-Fock and exact (nonrelativistic) energies is the *correlation energy*, which represents only about 1% of the total energy, but is very important for a correct description of molecular reactions and properties. One approach

to calculating this energy is perturbation theory, the most popular application of which is due to Møller and Plesset.[36] This computational scheme is based on applying Rayleigh-Schrödinger perturbation theory[37] to the HF-Hamiltonian, and treating the non-HF part of the Hamiltonian as a perturbation.

A generalized electronic Hamiltonian is given by

$$\mathcal{H}_\lambda = \mathcal{H}_0 + \lambda V \tag{16}$$

where $\mathcal{H}_0$ is an operator such that the matrix with elements

$$\int \cdots \int \psi_s \mathcal{H}_0 \psi_t \, d\tau_1 d\tau_2 \cdots d\tau_n \tag{17}$$

is diagonal. The perturbation is defined by

$$\lambda V = \lambda (\mathcal{H} - \mathcal{H}_0) \tag{18}$$

where $\mathcal{H}$ is the correct Hamiltonian and λ is a dimensionless parameter.

The exact (within a given basis set) ground-state wavefunction and energy for a system described by the Hamiltonian $\mathcal{H}_\lambda$ may be expanded in powers of λ

$$\begin{aligned}
\Psi_\lambda &= \Psi^{(0)} + \lambda \Psi^{(1)} + \lambda^2 \Psi^{(2)} + \dots \\
E_\lambda &= E^{(0)} + \lambda E^{(1)} + \lambda^2 E^{(2)} + \dots
\end{aligned} \tag{19}$$

Practical correlation methods may now be formulated by setting the parameter λ to 1, and by truncation of the series in equation (19) to various orders. The methods are referred to by the highest-order energy term allowed, that is, truncation after second-order as MP2, after third-order as MP3, and so on.

The MPn methods have the advantage of being size-consistent, but the disadvantage of not obeying the variation principle. In particular, MP2 calculations have been shown to overestimate the correlation energy. The estimated CPU times for MP2, MP3 and MP4 calculations are 1.5, 3.6 and 5.8 times the corresponding HF calculation,

respectively. MP3 gives a lower total energy than MP2, but very small corrections to the wavefunctions and properties, at a high computational cost. If one decides to go beyond MP2, it is thus necessary to go to MP4 in order to obtain a qualitative improvement of the results. At the present time, cost considerations make MP2 the most popular of the MPn methods.

A more accurate, but much more costly method of determining the correlation energy is *configuration interaction* (CI). This method has the advantage of being variational, but the disadvantage of not being size-consistent (unless full CI is used). Interaction can be based on a single reference determinant, or on several references, the latter giving multi-configuration or multi-reference CI (MRCI).

The HF wavefunction is commonly used as the ground state reference determinant, Ψ_0. A configuration expansion can be based on all single, double, triple, etc. excitations from Ψ_0. This *full CI expansion* is formally exact if all possible excitations are used, and gives the exact energy for the particular basis set used. For ground state orbitals a,b,c... and excited state orbitals r,s,t... the full CI wavefunction has the form

$$|\Psi^{CI}\rangle = c_0|\Psi_0\rangle + \sum_{a,r} c_a^r|\Psi_a^r\rangle + \sum_{a<b,r<s} c_{ab}^{rs}|\Psi_{ab}^{rs}\rangle + \sum_{a<b<c,r<s<t} c_{abc}^{rst}|\Psi_{abc}^{rst}\rangle + \dots \quad (20)$$

where the expansion coefficients are optimized variationally.

For any but the smallest systems, the CI expansion is truncated after a certain set of excitations, commonly after single and double ones. The rationale for this choice is that the double excitations are responsible for the main contribution to the correlation energy. The single excitations influence the ground state wavefunction indirectly,

through mixing with the double excitations. If a triples contribution to the energy is added, the resultant method is called QCISD(T).[38] This method gives improved accuracy, but at considerable additional computational cost.

2.5 Geometry Optimization Techniques[30]

Most of the optimized geometries reported in the literature are of ground state equilibrium structures, the global minimum on the potential energy surface. Optimizations of excited state and transition state geometries are also possible. All geometry optimizations require an initial guess. The better the guess, the fewer the number of iterations needed to reach a converged structure. This is particularly important for optimizations of transition states, which often need an excellent initial guess to converge at all.[39] The general rule-of-thumb is that the larger the basis set or more refined the method used, the better the agreement with experiment.

The general strategy in a geometry optimization is to solve the SCF equations for a given geometry, then calculate the energy gradients of the potential surface. If the gradients, or forces, are below a pre-set threshold, the geometry has converged. If not, the structure is varied along the energy gradient, according to some kind of quasi-Newton algorithm, with a pre-set or dynamically varied step length, to obtain a new prediction for the geometry. The integrals are recalculated for this new geometry, and the SCF equations are solved. The gradient optimization cycle is repeated until the forces are below the convergence threshold. It is often necessary to use tighter convergence criteria to find a transition state than for an equilibrium structure.[39]

2.6 Characterizing Stationary Points[30,40]

The equilibrium structure of a molecule will be located at a minimum on the potential energy surface; transition states will be at saddle points. Minima, maxima, and saddle points can be characterized by their first and second derivatives. For a function of several variables, the first derivatives with respect to each of the variables form a vector termed the *gradient*. The second derivatives form a matrix called the *Hessian*. The first derivative of the potential energy of a particle is minus the force on the particle, and the second derivative is the force constant. Thus, the negatives of the components of the gradient are the forces on the atoms in a molecule, and the Hessian is the force-constant matrix.

At a local minimum, maximum, or saddle point, all of the forces on the atoms in a molecule must be zero; hence such a point is known as a *stationary point*. The nature of the stationary point can be determined from the eigenvalues of the second derivative matrix. If all the eigenvalues are positive, the point is a local minimum; if all are negative, it is a local maximum. A transition structure, or first-order saddle point, has one negative eigenvalue and all the rest are positive. An nth order saddle point has n negative eigenvalues. A zero eigenvalue indicates a point of inflection for motion along the associated eigenvector.

When a stationary point has been found, it should be characterized by examining the eigenvalues of the Hessian. When possible, this characterization should be confirmed by calculating the harmonic frequencies for the structure, using the same basis set as for the optimization. A minimum will have no imaginary frequencies, a transition state one,

an nth order saddle point n, and for a maximum all the frequencies will be imaginary.

2.7 Single-Point Energy Calculations and Gaussian-2 Theory

When one is primarily interested in calculating energies, a computationally cheap technique is to use single-point energy calculations. The first step is to optimize the geometry of a system using a moderately sized basis set which gives reasonable agreement with experiment. Next, a larger basis set and/or more refined method is chosen, and the SCF equations are solved for the previously optimized geometry, yielding the energy of the system. Since calculations are performed only on this single point, a highly sophisticated method can be used for about the same cost as a geometry optimization at a much lower level.

Curtiss et al.[41] have recently developed a theoretical procedure for accurate energy calculations that they have designated as "Gaussian-2" ("G2") theory, which involves making several single-point energy calculations on an MP2/6-31G(d) optimized geometry. The first energy calculation is done at MP4/6-311G(d,p), and added to this are corrections obtained by subtracting this result from other energy calculations, i.e. $\Delta_i = E_i - E_{MP4/6-311G(d,p)}$. These corrections (level of theory in parentheses) are for energy differences due to diffuse sp-functions on nonhydrogen atoms (MP4/6-311+G(d,p)), higher polarization functions on nonhydrogen atoms (MP4/6-311G(2df,p)), and for correlation beyond fourth-order perturbation using quadratic configuration interaction (QCISD(T)/6-311G(d,p)). A final higher level correction (HLC) to make the

E_e exact for the hydrogen atom and hydrogen molecule is included by multiplying the number of valence electron pairs and unpaired electrons by respective constants. A zero-point energy (ZPE) from scaled HF/6-31G(d) frequencies is then added to obtain E_0. The method described thus far constitutes the earlier developed "Gaussian-1" ("G1") theory.[42]

In G2 theory a correction Δ is added to the G1 energy. This is composed of two parts, both computed at the MP2 level (the validity of using MP2 rather than MP4 energies was examined in several test calculations and found to be valid[41]). The first part Δ_1 corrects for nonadditivity caused by the assumption of separated basis set extensions for diffuse-sp functions and higher polarization functions in G1 theory,

$$\Delta_1 = \Delta(+2df) - \Delta(+) - \Delta(2df) \tag{21}$$

where the individual corrections are obtained as before but now subtracting the MP2/6-311G(d,p) energy. The levels of theory required are, respectively, MP2/6-311+G(2df,p), MP2/6-311+G(d,p), and MP2/6-311G(2df,p). The second part Δ_2 is a correction for addition of a third d function to the nonhydrogen atoms and a second p function to the hydrogens,

$$\Delta_2 = E[MP2/6-311+G(3df,2p)] - E[MP2/6-311+G(2df,p)] \tag{22}$$

The only additional calculation required beyond those done for G1 theory is MP2/6-311+G(3df,2p), the other MP2 values already being done as part of the MP4 calculations. The final correction is to adjust HLC to be equal to -5.00*npair - 0.19*upe, where npair is the number of valence pairs, upe is the number of unpaired electrons, and the constants are in millihartrees.

The calculation of the individual corrections in G2 theory can be useful for a detailed analysis of the energy factors, but for a straightforward total energy calculation, the G2 expression can be simplified to the following:

$$
\begin{aligned}
E_0(G2) = \; & E[MP4/6\text{-}311\text{+}G(d,p)] + E[MP4/6\text{-}311G(2df,p)] \\
& + E[QCISD(T)/6\text{-}311G(d,p)] + E[MP2/6\text{-}311\text{+}G(3df,2p)] \\
& - E[MP2/6\text{-}311G(2df,p)] - E[MP2/6\text{-}311\text{+}G(d,p)] \\
& + E[MP2/6\text{-}311G(d,p)] - 2.0*E[MP4/6\text{-}311G(d,p)] \\
& - 0.005*npair - 0.00019*upe + SCALE*ZPE
\end{aligned}
\tag{23}
$$

where the originally recommended scale value was 0.8929.

2.8 Density Functional Theory and Hyperfine Structure Calculations[30,43]

Density functional theory (DFT) is based on using the *electron density*,

$$
\rho(r) = \sum_{i=1}^{occ.} |\psi_i(r)|^2
\tag{24}
$$

as a basic variable, where r is the matrix of spatial coordinates. The total energy is expressed as a functional of $\rho(r)$. The theory began as a model, based on studies of electron density by Thomas[44] and Fermi,[45] with further development by Slater[46] and Gáspár,[47] who introduced expressions for an approximate exchange potential in band theory calculations. In its modern form DFT was first formulated for an electron gas by Hohenberg and Kohn,[48] and further developed by Kohn and Sham.[49]

Given an external (nuclear) potential energy operator $\hat{V}_{ext}$ and kinetic energy T, the total energy is expressed as

$$
E[\rho(r)] = \int \hat{V}_{ext}(r)\,\rho(r)\,dr + \frac{1}{2}\int\int \frac{\rho(r)\,\rho(r')}{|r - r'|}\,dr\,dr' + G[\rho(r)]
\tag{25}
$$

where

$$G[\rho(r)] = T[\rho(r)] + E_{xc}[\rho(r)] \tag{26}$$

with E_{xc} being the *exchange and correlation energy*. If the density is assumed to be slowly varying, the *local density approximation* (LDA) can be formulated:

$$E_{xc}[\rho(r)] = \int \rho(r)\varepsilon_{xc}[\rho(r)]dr \tag{27}$$

where ε_{xc} is the single-particle exchange correlation potential. Treating the electrons with α- and β-spin separately gives the *local spin-density* (LSD) approximation.

It is possible to include the exchange effects directly,

$$E_{xc}[\rho(r)] = E_x[\rho_1(r,r')] + \int \rho(r)\varepsilon_c[\rho(r)]dr \tag{28}$$

where E_x is the exchange energy, ε_c is the single-particle correlation energy, and the *density matrix* is defined by:

$$\rho_1(r,r') = \sum_{i=1}^{N} \psi_i(r)\psi_j^*(r'). \tag{29}$$

Given

$$\mu_c[\rho(r)] = \frac{d\{\rho(r)\varepsilon_c[\rho(r)]\}}{d\rho(r)} \tag{30}$$

and

$$\Omega(r) = \hat{V}_{ext}(r) + \int \frac{\rho(r')}{|r - r'|}dr \tag{31}$$

the Kohn-Sham equations can be obtained:

$$\{-\frac{1}{2}\nabla_i^2 + \Omega(r) + \mu_c[\rho(r)]\}\psi_i(r) - \int \frac{\rho_1(r,r')}{|r - r'|}\psi_i(r')dr' = \varepsilon_i\psi_i(r). \tag{32}$$

Here, ε_i is the DFT counterpart to the single-particle energies, and the set of single particle-orbitals $\psi_i(r)$ is referred to as the *Kohn-Sham orbitals*. As formulated by

Kohn and Sham, DFT may be regarded as a Hartree-Fock method, corrected for correlation effects, with the total energy given by:

$$E_{tot}^{DFT} = \sum_{i=1}^{N} e_i - \frac{1}{2} \iint \frac{\rho(r)\rho(r')}{|r - r'|} \, dr\,dr' + \frac{1}{2} \iint \frac{\rho_1(r,r')\rho_1(r,r')}{|r - r'|} \, dr\,dr'$$

$$+ \int \rho(r)\{e_c[\rho(r)] - \mu_c[\rho(r)]\}\,dr. \tag{33}$$

There are now a wide variety of DFT methods available, with the main differences being in the choice of basis sets for the Kohn-Sham orbitals, and in the potential type. The form of the latter is generally a pseudopotential, where the valence part is treated as an orbital in the potential created by the inner shells and the nucleus.

The isotropic hyperfine coupling constant for a nucleus N is obtained from the formula

$$A_{iso}^{(N)} = \frac{4\pi}{3} g_e \, \beta_e \, g_N \, \beta_N \langle S_z \rangle^{-1} \sum_{\mu,\nu} P_{\mu\nu}^{\alpha-\beta} \langle \psi_\mu(r_{kN}) \,|\, \delta(r_{kN}) \,|\, \psi_\nu(r_{kN}) \rangle \tag{34}$$

where g_e and g_N are the Landé splitting factors for the electron and nucleus, respectively, β_e is the Bohr magneton and β_N is the nuclear magneton. The spin density at the nucleus is obtained from the corresponding atomic orbitals, and $P_{\mu\nu}^{\alpha-\beta}$ is an element of the unpaired spin density matrix. The remaining terms of the traceless 3x3 hyperfine tensor form the anistropic hyperfine coupling constants. The ijth element of the anisotropic tensor can be obtained through the relation

$$T_{ij}^{(N)} = \frac{1}{2} g_e \, \beta_e \, g_N \, \beta_N \langle S_z \rangle^{-1} \sum_{\mu,\nu} P_{\mu\nu}^{\alpha-\beta} \langle \psi_\mu(r_{kN}) \,|\, r_{kN}^{-5}(r_{kN}^2 \delta_{ij} - 3r_{kN,i} \, r_{kN,j}) \,|\, \psi_\nu(r_{kN}) \rangle \tag{35}$$

2.9 Topological Analyses[50,51]

Bader and coworkers[52] have developed a theory of "atoms in molecules", in which the *gradient vector field* and the *scalar field of the electronic charge distribution* $\rho(r)$ are used to study the bonds, atomic interactions, reactivities and stabilities of molecular systems. The properties of the gradient vector field $\nabla\rho(r)$ provide a definition of the elements of molecular structure. The molecular charge density, which is synonymous with the electron density as defined in equation (24), is uniquely partitioned into atoms bounded by the *zero-flux surfaces* in $\nabla\rho(r)$ and chemical bonds are manifested by the existence of bond paths in $\nabla\rho(r)$.

On the other hand, the properties of the scalar field of the charge density, the Laplacian distribution $\nabla^2\rho(r)$, provide an understanding of atomic interactions and the reactivity of the molecule. In particular, the *Laplacian of the charge density*

$$\nabla^2\rho(r) = \frac{\partial^2\rho}{\partial x^2} + \frac{\partial^2\rho}{\partial y^2} + \frac{\partial^2\rho}{\partial z^2} \tag{36}$$

identifies the regions of space wherein the electronic charge of a molecule is locally concentrated or depleted. In three dimensions, when $\nabla^2\rho(r) < 0$, then the ρ at point r is greater than its average value at neighbouring points, and when $\nabla^2\rho(r) > 0$, the ρ at point r is less than its average value at neighbouring points. Thus a minimum in $\nabla^2\rho(r)$ with a negative value means that the electronic charge is locally concentrated in that region of space, even though the charge density itself exhibits no corresponding maximum.

The essential topological properties of ρ can be summarized by the complete

specification of its critical points at which $\nabla\rho = 0$. A critical point, $\mathbf{r}_c$, is classified according to its rank and signature.[52a] The rank λ of a critical point equals the number of non-zero eigenvalues of the Hessian matrix of $\rho(\mathbf{r}_c)$, while the signature σ is the algebraic sum of the signs of the eigenvalues, and the classification is written as (λ,σ). If the eigenvalue is positive its associated eigenvector or gradient path originates at, and is directed away from, the critical point. For negative eigenvalues the gradient path terminates at, and is directed toward, the critical point.

In the case of a nondegenerate critical point, four types of critical points are possible: $(3,-3)$, which usually occurs only at a nucleus; $(3,+3)$, a cage critical point; $(3,+1)$, a ring critical point; and $(3,-1)$, a bond critical point. Only bond critical points are considered in this study.

The gradient paths defined by the eigenvectors associated with the negative eigenvalues of the Hessian matrix of a $(3,-1)$ critical point generate an interatomic surface. The interatomic surface and the surfaces at infinity are the only closed surfaces which satisfy the zero-flux surface condition[53]

$$\nabla\rho(r) \cdot n(r) = 0 \tag{37}$$

where $n(\mathbf{r})$ is the unit vector normal to the surface at $\mathbf{r}$. An atom is defined by a real space (the "atomic basin") surrounded by a zero-flux surface.

The zero-flux surface condition leads to a variational definition of its average properties, and as a consequence any atomic property is the average over the atomic basin of an effective single-particle density. It follows that the average value for a total molecular system is given by the sum over the atoms in the molecule of the

corresponding atomic values. The atomic charge of an atom is obtained by integrating

$\rho(r)$ over the basin of the atom to obtain its average electron population N, and then

subtracting this from the nuclear charge Z, *i.e.*, $Q = Z - N$.

2.10 Computational Methods Used

Ab initio MO calculations were carried out with the GAUSSIAN 90[54] and

Gaussian 92/DFT[55] program packages. All geometries were fully optimized at the

restricted Hartree-Fock level with the 6-31G(d) basis set[56] using analytical gradient

methods.[57] Energies were calculated to second order in Møller-Plesset perturbation

theory (MP2) using polarized basis sets with doubly-split (6-31G(d) and 6-31G(d,p))[56]

and triply-split (6-311G(d) and 6-311G(d,p))[58] valence shells, using the HF/6-31G(d)

optimized geometries. Similarly, the geometries were reoptimized at the MP2/6-

31G(d,p) level, and single-point energy calculations were performed on these geometries

at the MP2/6-311G(d,p) level. Additional single-point calculations on some systems

were done at the MP4/6-311G(d,p) level, and for a subset using G2 theory (see above),

modified by using the more accurate MP2/6-31G(d,p) geometries. For the reaction of

ethane with hydroxyl, the reaction path was followed in mass-weighted internal

coordinates, using the intrinsic reaction coordinate (IRC) method of Gonzalez and

Schlegel,[59] at the MP2/6-31G(d,p) level.

To allow for direct comparison with experimental values, the calculated bond

dissociation energies (BDEs) include corrections for the zero-point vibrational energy

(ZPE) calculated at the HF/6-31G(d) level (scaled by a factor of 0.90 to compensate for

systematic overestimation[60]), or ZPEs calculated at the MP2/6-31G(d,p) level scaled by a factor of 0.9646, as recommended by Pople *et al.*[61], in the case of the G2 calculations. A temperature correction of 4RT for $C-C$ BDEs and 2.5RT for $C-H$ BDEs, as recommended by Hehre et al.[62], was also applied. The vibrational contribution to the temperature correction has been ignored in order to eliminate the risk of introduction of large errors by low-frequency modes. This can result because the vibrational contribution is given by[63]

$$\Delta H_{vib}(T) = Nh \sum_i^{normalmodes} \frac{v_i}{e^{hv_i/kT} - 1} \qquad (38)$$

Thus for small values of v_i the denominator can approach zero. As a result the vibrational contribution depends almost exclusively on the very-low-frequency modes, which are not reproduced as accurately or as uniformly as the high-frequency vibrations.

The DFT calculations were performed using the linear combination of Gaussian type orbitals-density functional theory (LCGTO-DFT) program deMon,[64] and a modified version with the improvements as described in ref 65. The loosely contracted IGLO-III[66] basis sets (5111111/211111/11) for carbon and fluorine and (3111/11) for hydrogen were employed in conjunction with the auxiliary bases (5,2;5,2) for carbons and fluorines and (5,1;5,1) for hydrogens (IGLO = individual gauge of localized orbitals).[66a] A routine by Malkin *et al.*[67] was employed for the DFT-ESR calculations. Two functionals were used: a local density approximation (LDA) due to Vosko, Wilk and Nusair,[68] and a non-local functional with gradient corrections due to Perdew and Wang[69] for the exchange functional and to Perdew[70] for the correlation part (PWP).

For some cases, where good agreement with experiment was not obtained, ESR parameters were also calculated from DFT optimized structures, using the PWP functional and the same basis sets as above.

The topological analysis calculations were performed using a vectorized version of the PROAIM[71] program package. Wavefunction files from the highest common level of theory employed in this study (MP2/6-311G(d,p)//HF-6-31G(d)) were used as input. For each bond a $(3, -1)$ critical point was located. Integration of atomic charges was performed for each atom, using 96 ϕ and 64 θ planes outside of the β sphere, and the maximum values of 140 points per surface path and 80 basic gradient paths. Threshold values of 0.001 and 0.002 were used for the volume calculation, and the primitive cutoff algorithm was employed.

Chapter 3. Structural and Energetic Properties of the Series $C_2H_nF_{5-n}$, n = 0−5, and CH_nF_{3-n}, n = 0−3

3.1 Introduction

Many of the radicals in the two title series have been studied extensively, by a variety of theoretical and experimental methods. The short lifetimes of these and other free radicals limit the availability of experimental methods for determination of electron distributions and structure, with electron spin resonance (ESR) spectroscopy being the most useful technique. Theoretical studies can complement experimental ones even more so than is the case with closed-shell species.

Ab initio studies of the structures of the series of fluoromethyl radicals have been reported by Bernardi *et al.*,[72] Leroy and Peeters,[73] Baird,[74] Luke *et al.*,[75] and Pasto *et al.*[76] The latter authors also calculated radical stabilization energies, and their study also included some radicals in the ethyl series (CH_2F-CH_2, CHF_2-CH_2, and CF_3-CH_2). Radical stabilization energies for this series, as well as C_2H_5, have also been published by Leroy *et al.*[77] Dearden *et al.*[78] recently published a spectroscopic and *ab initio* study of CHF_2, including the optimized geometry and vibrational frequencies.

In the series of ethyl radicals, the parent, C_2H_5 has been the most extensively studied, both by experiment and theory. The structure of this and other alkyl radicals has been studied at several levels of theory by Pacansky and co-workers,[79] with their latest work on this subject also including infrared and Raman spectra.[80] The structure and vibrational frequencies of C_2H_5, as well as CH_2F-CH_2, was also reported by

Schlegel.[81] Paddon-Row and Houk[82] examined the ethyl radical in their study of the conformational dependence of alkyl radicals.

Paddon-Row et $al.$ also reported structures and conformational analysis,[83] and vibrational frequencies,[84] of CF_3-CH_2, CH_3-CF_2, and CF_3-CF_2. A conformational analysis of CH_2F-CH_2 was reported by Pross and Radom.[85] Brum et $al.$[86] complemented a spectroscopic study with ab $initio$ calculations of the structures, vibrational frequencies, and relative energies of CH_3-CF_2 and CHF_2-CH_2 radicals and cations.

The most comprehensive study of the full series $C_2H_nF_{5-n}$, n $=$ 0$-$5 has been reported by Chen et $al.$,[87-91] who calculated optimized geometries, vibrational frequencies, ideal gas thermodynamic functions, and barriers for rotation and inversion. The highest levels of theory used were HF/6-31G(d) for geometries and frequencies, and MP2/6-311G(d,p)//HF/6-31G(d) for energies.

In the present study, geometries were optimized at the HF/6-31G(d) level for the radicals in the methyl series, and at the MP2/6-31G(d,p) level for both the methyl and ethyl series. In the latter case all the minima determined by Chen et $al.$, who optimized the structures at the HF/6-31G(d) level, were reoptimized. Frequency analyses were performed for all species, and energy minima were confirmed. In particular, Chen et $al.$[90] had speculated that one of the minima for CH_2F-CHF (their structure **1b**, the present **1f**) might not be a local minimum at a higher level of theory, but the MP2 frequency analysis has verified this as a minimum.

3.2 Optimized Geometries

Optimized geometries for the radicals produced by $C-H$ bond dissociation (hereafter denoted as ethyl radicals) are presented in Figure 1a–t. Extensive discussions of the HF/6-31G(d) optimized geometries for each radical are given in the series of papers by Chen et al.[88–91] Here the general trends and differences between the two levels of optimization are discussed. For ease of comparison with the previous results, the authors' naming convention (a, b, and c) for the CH_2F-CHF and CHF_2-CHF radicals, where all the conformers have the same (C_1) symmetry, has been adopted. The $C-C$ bond lengths vary from 1.473–1.505 Å, with a tendency towards longer lengths when there are two fluorines on the α-carbon. In other cases, there is a tendency towards shorter bond lengths when the number of fluorines on the β-carbon is greater than or equal to the number on the α-carbon.

There are three distinct trends in the $C-F$ bond lengths, which have a large range (1.330–1.409 Å). They decrease with increasing substitution, both at the individual carbons and in the radical as a whole. For each radical, the shorter lengths are always at the α-carbon, as expected from the simple argument of increased s character in going from an sp^3 to sp^2 hybridized carbon. For the different positions at the β-carbon, the longer lengths are always for the $C-F$ bond eclipsing the SOMO (i.e. the bond bisecting the radical centre as seen in Figure 1). This may be attributed to a weak three-electron hyperconjugative interaction as discussed by Paddon-Row and Houk[82] for alkyl radicals. For the $C-H$ bond lengths, there is no discernible trend with substitution patterns, but the other two trends observed for the $C-F$ bond lengths are seen.
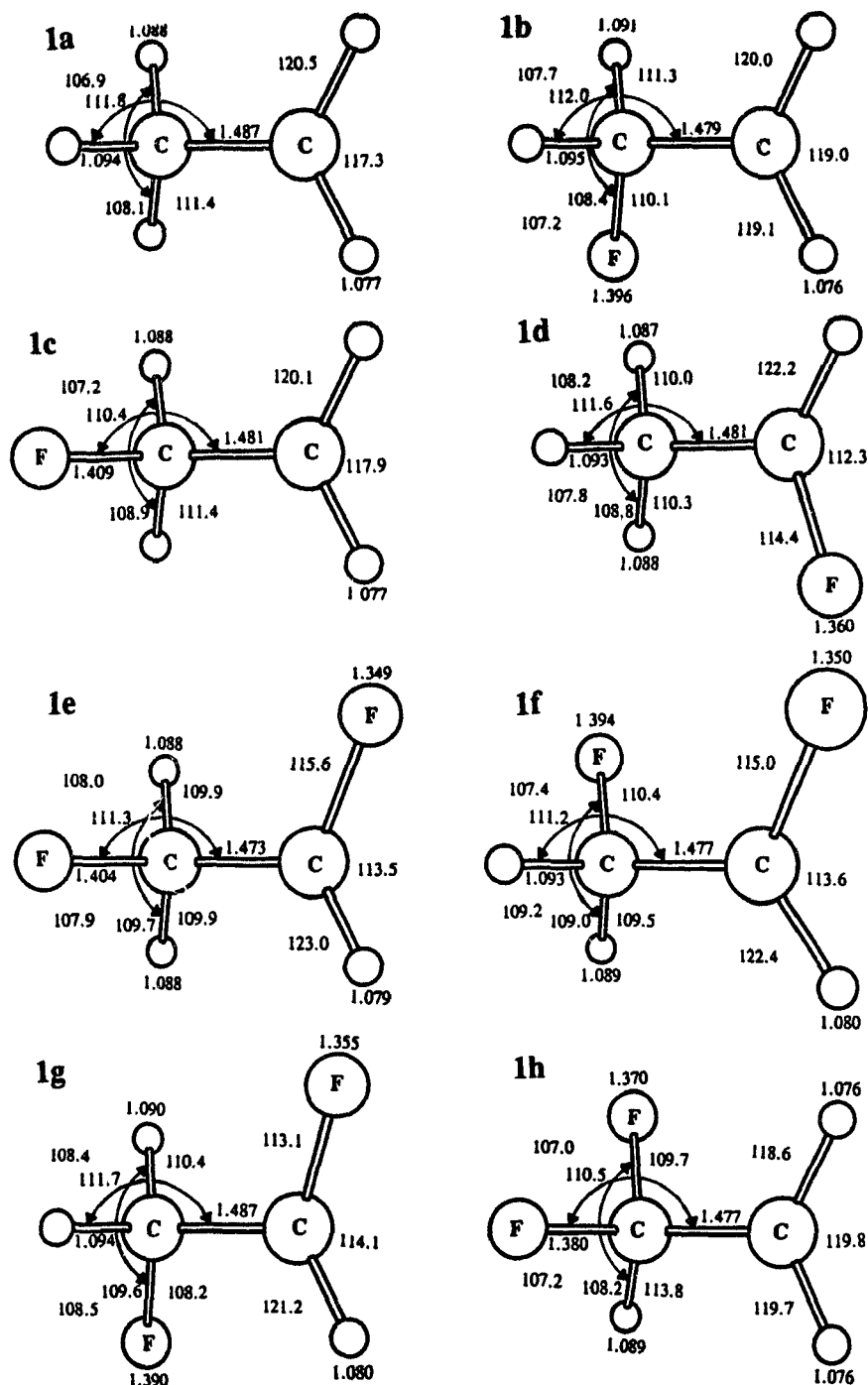
Figure 1. MP2/6-31G(d,p) optimized geometries for radicals: **1a**, ethyl (C₅); **1b**, β-fluoroethyl (C₁); **1c**, β-fluoroethyl (C₅); **1d**, α-fluoroethyl (C₁); **1e**, α,β-difluoroethyl (a) (C₁); **1f**, α,β-difluoroethyl (b) (C₁); **1g**, α,β-difluoroethyl (c) (C₁); **1h**, β,β-difluoroethyl (C₁). Bond lengths are in angstroms, bond angles in degrees. Drawings are in perspective, with relative radii of 1 : 1.667 : 2 for H, F, and C atoms, respectively. For curved arrows, the corresponding bond angle is that written closest to the arrow. Unlabelled atoms are hydrogens.

1i

1.372
F
107.1
114.3
119.2
C
1.478
C
120.2
1.092
108.2 110.0
F
1.075

1j

1.085
F
114.4
109.0
109.8
C
1.486
C
109.8
1.090
109.5 109.8
F
1.347

1k

1.088
1.346
F
107.8 112.7
114.1
110.8
F
1.481
C
115.2
1.375
109.7 108.0
121.2
107.6
F
1.366
1.079

1l

1.342
1.365
F
F
107.2 109.7
114.5
110.7
F
1.480
C
114.7
1.376
109.3 111.7
108.2
121.6
F
1.089
1.079

1m

1.366
1.345
F
F
107.4 110.0
113.7
114.0
1.485
C
115.0
1.092
108.6 109.0 107.8
121.2
F
1.367
1.078

1n

1.087
F
108.9
115.0
110.0
F
1.487
C
110.7
1.395
110.1 109.4
F
1.339

Figure 1 (cont.) MP2/6-31G(d,p) optimized geometries for radicals: 1i, β,β-difluoroethyl (C$_s$); 1j, α,α-difluoroethyl (C$_s$) 1k, α,β,β-trifluoroethyl (a) (C$_1$); 1l, α,β,β-trifluoroethyl (b) (C$_1$); 1m, α,β,β-trifluoroethyl (c) (C$_1$); 1n, α,α,β-trifluoroethyl (C$_s$). Bond lengths are in angstroms, bond angles in degrees. Drawings are in perspective, with relative radii of 1 : 1.667 : 2 for H, F, and C atoms, respectively. For curved arrows, the corresponding bond angle is that written closest to the arrow. Unlabelled atoms are hydrogens.
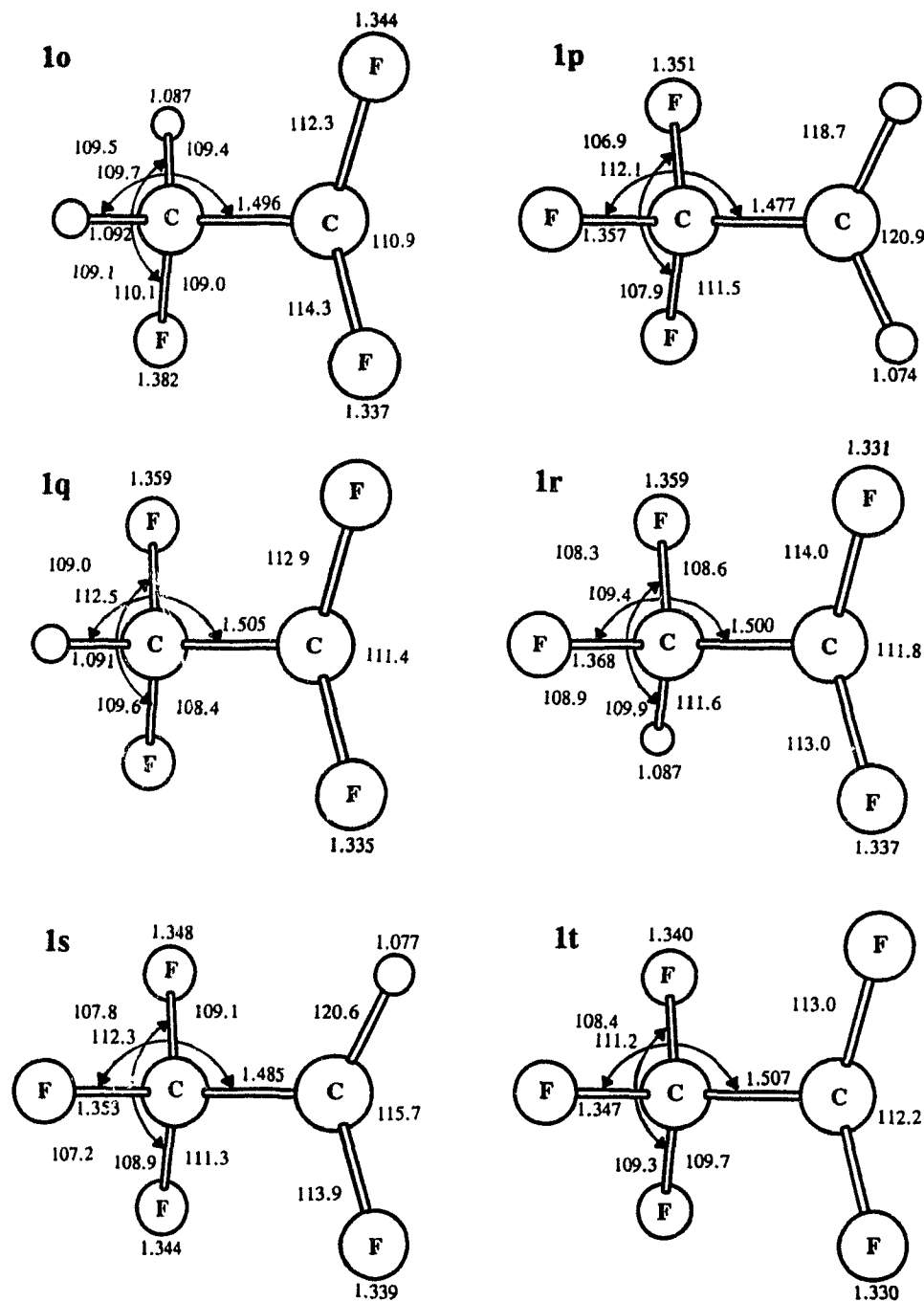
Figure 1 (cont.) MP2/6-31G(d,p) optimized geometries for radicals: 1o, α,α,β-trifluoroethyl (C₁); 1p, β,β,β-trifluoroethyl (Cₛ); 1q, α,α,β,β-tetrafluoroethyl (Cₛ); 1r, α,α,β,β-tetrafluoroethyl (C₁); 1s, α,β,β,β-tetrafluoroethyl (C₁); 1t, pentafluoroethyl (Cₛ). Bond lengths are in angstroms, bond angles in degrees. Drawings are in perspective, with relative radii of 1 : 1.667 : 2 for H, F, and C atoms, respectively. For curved arrows, the corresponding bond angle is that written closest to the arrow. Unlabelled atoms are hydrogens.

On the α-carbon, HCH angles are greater than HCF, as expected because of the increased s character in the C$-$H bonds in the presence of an electronegative substituent.[92] The latter angles are greater than FCF, consistent with FCF angles being small because of the relatively small radii of the F atoms.[93] The HCC angles are greater than FCC, which can be rationalized by the different atomic sizes when the difference in the C$-$H and C$-$F bond lengths is taken into account.[93] The latter trend is also observed for substituents on the β-carbon. For angles between substituents at this centre, the greatest value in a species is always for those substituents pointing away from the α-substituents (this angle is denoted with a curved arrow in Figure 1), as these substituents have more space in which to avoid steric repulsions.

As compared to the HF/6-31G(d) optimized structures, the present structures have C$-$C bonds shorter by up to 0.01 Å, C$-$F bonds longer by about 0.02$-$0.03 Å, and slightly longer C$-$H bonds. Differences in interatomic angles are for the most part slight, particularly for conformers with C_s symmetry, but the variance is greater than that observed for the closed-shell structures (see Chapter 5).

An interesting structural feature of the ethyl radicals is the out-of-plane angle γ, defined by the C$-$C axis and the plane formed by the radical site group. Chen *et al.*[88-91] have discussed this topic previously. All alkyl radicals except for CH_3, and all haloalky- and halo-substituted radicals, are predicted to be pyramidal from a σ inductive effect when attached substituents are at least as electronegative as the atom at the trigonal centre.[94] The degree of nonplanarity is determined by three types of π-type conjugative interactions superimposed on the inductive effect.[88] The effect of fluorine substitution

Table 3.1: Out-of-Plane Angles for Ethyl Radicals

Structure	HF/6-31G(d)	MP2/6-31G(d,p)
1a	13.6[a]	12.4
1b	14.6[b]	13.9
1c	13.8[b]	13.3
1d	32.6[a]	31.8
1e	29.8[c]	26.8
1f	32.0[c]	30.5
1g	34.1[c]	33.3
1h	13.9[b]	13.7
1i	11.7[b]	11.6
1j	43.6[a]	44.2
1k	31.7[c]	30.0
1l	31.4[c]	29.4
1m	32.8[c]	31.9
1n	43.6[d]	42.1
1o	47.1[d]	45.8
1p	13.1[b]	13.2
1q	47.0[d]	46.3
1r	45.4[d]	44.8
1s	32.3[c]	30.8
1t	45.7[d]	45.6

[a] Reference 88. [b] Reference 89. [c] Reference 90. [d] Reference 91.

is much greater at the α position.

In Table 3.1 the MP2/6-31G(d,p) out-of-plane angles are compared with those previously calculated at the HF/6-31G(d) level.[88-91] Except for structures **1j** and **1p**,which have slightly higher values, inclusion of electron correlation has lowered the γ values by 0.1 to 3.0°. The trends in the relative magnitudes of γ remain essentially the same. The exceptions are two interchanges of relative magnitudes (**1a ↔ 1p**, **1q ↔ 1o**) and a divergence of values for **1j** and **1n**, which were equal at the HF/6-31G(d) level.

Geometrical parameters for the methyl radicals are given in Table 3.2. Trends in these parameters are similar to those discussed above for the ethyl radicals, and to those noted in fluorochloromethanes by Ignacio and Schlegel.[95] These authors explained the trends as a balance between electrostatic and negative hyperconjugation effects.

Table 3.2: Geometrical Parameters for the Radicals CH_nF_{3-n}, n = 0-3[a]

Parameter	CH_3 (D_{3h})	CH_2F (C_s)	CHF_2 (C_s)	CF_3 (C_{3v})
C-H	1.073 (1.073)	1.078 (1.074)	1.084 (1.075)	
C-F		1.347 (1.330)	1.336 (1.314)	1.327 (1.300)
∠ HCH		120.0 (120.0)		
∠ HCF		114.7 (114.2)	113.7 (113.8)	
∠ FCF			115.5 (111.1)	111.2 (111.3)

[a] Bond lengths in angstroms, bond angles in degrees. First value is for the MP2/6-31G(d,p) optimized geometry, second value (in parentheses) is for the HF/6-31G(d) optimized geometry.

3.3 Vibrational Frequencies

Values of vibrational frequencies at the MP2/6-31G(d,p) level of theory (and from experiment where available[80,96-99]), along with their reduced masses, symmetry, and approximate type, are given in Table 3.3. The assignment of modes was made by examining the normal coordinate vectors. The descriptions of modes follow the naming conventions used by Shimanouchi.[100] In this context "symmetric" and "degenerate" should be interpreted loosely, especially for C_1 species, where such a designation indicates a motion essentially equivalent to that occuring in a symmetrical species. For cases where equivalent groups are at both carbons, α- and β- designations, where α- is the radical centre, are used to distinguish the motions. If no designations appear in these cases, the motion occurs in both groups. There is a high degree of modal coupling in the asymmetrical radicals, but coupling also occurs in those with C_s symmetry, particularly for low frequency modes.

For the ethyl radicals, there is a tendency for stretching frequencies to be higher at the radical (α-) centre, as expected since the bond lengths are shorter. The same reason (but in the opposite direction) can be used to explain why $C-H$ stretching frequencies decrease with increasing fluorine substitution, with the effect being more pronounced in the methyl radicals. In contrast to the stretches, bending modes tend to have lower frequencies at the radical centre. Again, this is as expected since the substituents are more tightly held to the central carbon atom, rendering bending more difficult.

Table 3.3: Vibrational Frequencies of Radicals at MP2/6-31G(d,p) Level

Frequency (cm^{-1})		Reduced mass (amu)	Sym	Approximate type of mode
MP2	Expt[a]			
CH$_3$[b]				
395	617	1.236	a$_2''$	CH$_3$ symmetric deformation
1491	1396	1.102	e$'$	CH$_3$ degenerate deformation
3243		1.008	a$_1'$	CH$_3$ symmetric stretch
3441	3162	1.119	e$'$	CH$_3$ degenerate stretch
CH$_2$F				
830		1.292	a$'$	CH$_2$ rock
1216		5.898	a$'$	C$-$F stretch
1217		1.218	a$''$	CH$_2$ twist
1561		1.151	a$'$	CH$_2$ scissor
3239		1.043	a$'$	CH$_2$ symmetric stretch
3387		1.126	a$''$	CH$_2$ asymmetric stretch
CHF$_2$[c]				
542		15.063	a$'$	CF$_2$ scissor
1094	949	1.402	a$'$	C$-$H bend + CF$_2$ wag
1206	1164	10.313	a$'$	CF$_2$ symmetric stretch
1235	1173	3.026	a$''$	CF$_2$ asymmetric stretch
1412	1317	1.479	a$''$	C$-$H bend + CF$_2$ twist
3239		1.088	a$'$	C$-$H stretch
CF$_3$				
504		18.255	e	CF$_3$ degenerate deformation
704		16.460	a$_1$	CF$_3$ symmetric deformation
1126		14.311	a$_1$	CF$_3$ symmetric stretch
1318		13.336	e	CF$_3$ degenerate stretch
CH$_3$$-CH_2$[b]				
169		1.008	a$''$	CH$_3$$-CH_2$ torsion

Table 3.3 (continued)

Frequency (cm⁻¹) MP2	Expt[a]	Reduced mass (amu)	Sym	Approximate type of mode
469	540	1.214	a'	CH_2 wag
837		1.049	a"	CH_3 rock + CH_2 twist
1025		1.327	a'	CH_3 rock
1109	1138	3.100	a'	C—C stretch
1247	1175	1.460	a"	CH_3 rock + CH_2 twist
1463	1366	1.213	a'	CH_3 symmetric deformation
1540		1.079	a'	CH_3 degenerate deformation
1553	1440	1.037	a"	CH_3 degenerate deformation
1554		1.154	a'	CH_2 scissors
3096	2842	1.046	a'	CH_3 symmetric stretch
3184	2920	1.088	a'	CH_3 degenerate stretch
3230	2987	1.103	a"	CH_3 degenerate stretch
3270	303ʒ	1.052	a'	CH_2 symmetric stretch
3385	3112	1.119	a"	CH_2 asymmetric stretch

$CH_2F—CH_2$ $(C_1)^d$

189		1.074	a	$CH_2F—CH_2$ torsion
419	427	2.002	a	C—F bend + α-CH_2 rock
496		1.510	a	α-CH_2 rock + C—F bend
882		1.547	a	β-CH_2 rock + C—F stretch
1020		2.280	a	C—C stretch + α-CH_2 wag
1145	1047	3.202	a	C—F stretch + β-CH_2 rock
1168		2.047	a	C—C stretch + α-CH_2 twist
1281		1.076	a	β-CH_2 twist
1460		1.292	a	β-CH_2 wag
1525		1.255	a	α-CH_2 scissors
1567		1.087	a	β-CH_2 scissors

Table 3.3 (continued)

Frequency (cm⁻¹) MP2	Expt[a]	Reduced mass (amu)	Sym	Approximate type of mode
3089	2879	1.063	a	β-CH$_2$ symmetric stretch
3163		1.100	a	β-CH$_2$ asymmetric stretch
3279		1.052	a	α-CH$_2$ symmetric stretch
3403		1.120	a	α-CH$_2$ asymmetric stretch

CH$_2$F−CH$_2$ (C$_s$)

Frequency (cm⁻¹) MP2	Expt[a]	Reduced mass (amu)	Sym	Approximate type of mode
94		1.079	a″	CH$_2$F−CH$_2$ torsion
382		2.018	a′	α-CH$_2$ wag + C−F bend
640		2.087	a′	α-CH$_2$ wag + C−F bend
824		1.073	a″	α- + β-CH$_2$ rock
1033		8.559	a′	C−F stretch
1129		3.021	a′	C−C stretch
1223		1.528	a″	α- + β-CH$_2$ rock
1329		1.095	a″	β-CH$_2$ twist
1442		1.233	a′	β-CH$_2$ wag
1546		1.167	a′	α-CH$_2$ scissors
1584		1.130	a′	β-CH$_2$ scissors
3150		1.057	a′	β-CH$_2$ symmetric stretch
3215		1.110	a″	β-CH$_2$ asymmetric stretch
3274		1.050	a′	α-CH$_2$ symmetric stretch
3395		1.120	a″	α-CH$_2$ asymmetric stretch

CH$_3$−CHF

Frequency (cm⁻¹) MP2	Expt[a]	Reduced mass (amu)	Sym	Approximate type of mode
212		1.182	a	CH$_3$−CHF torsion
414		2.948	a	CH$_3$ rock + C−F bend
669		1.195	a	CH$_3$ rock + C−F bend
948		2.103	a	C−C−F bend
1082		1.467	a	CH$_3$ rock

Table 3.3 (continued)

Frequency (cm⁻¹)		Reduced	Sym	Approximate type of mode
MP2	Expt[a]	mass (amu)		
1175		2.229	a	C−C stretch
1226		2.645	a	C−F stretch
1423		1.287	a	C−H bend
1482		1.494	a	CH₃ symmetric deformation
1531		1.047	a	CH₃ degenerate deformation
1553		1.053	a	CH₃ degenerate deformation
3109		1.043	a	CH₃ symmetric stretch
3203		1.093	a	CH₃ degenerate stretch
3247		1.102	a	CH₃ degenerate stretch
3279		1.090	a	C−H stretch

CH₂F−CHF (a)

121		5.448	a	CH₂F−CHF torsion
321		2.162	a	α- + β-C−F bend
475		2.080	a	α- + β-C−F bend
691		2.620	a	C−C−Fα bend
943		2.281	a	C−C−Fβ bend
1044		8.255	a	β-C−F stretch
1156		2.394	a	C−C stretch
1250		2.210	a	α-C−F stretch
1308		1.106	a	CH₂ twist
1423		1.256	a	CH₂ wag + C−H bend
1498		1.691	a	CH₂ wag + C−H bend
1556		1.133	a	CH₂ scissor
3157		1.058	a	CH₂ symmetric stretch
3229		1.110	a	CH₂ asymmetric stretch
3308		1.090	a	C−H stretch

Table 3.3 (continued)

Frequency (cm⁻¹)		Reduced	Sym	Approximate type of mode
MP2	Expt[a]	mass (amu)		

CH₂F−CHF (b)

110		3.988	a	CH_2F-CHF torsion
322		2.765	a	α- + β-C−F bend
467		1.767	a	α- + β-C−F bend + CH_2 rock
684		3.096	a	$C-C-F_\beta$ bend
942		2.529	a	$C-C-F_\alpha$ bend
1058		3.239	a	β-C−F stretch
1133		2.919	a	C−C stretch
1240		2.044	a	α-C−F stretch
1316		1.154	a	CH_2 twist
1443		1.335	a	CH_2 wag + C−H bend
1480		1.799	a	CH_2 wag + C−H bend
1557		1.114	a	CH_2 scissor
3120		1.060	a	CH_2 symmetric stretch
3199		1.104	a	CH_2 asymmetric stretch
3302		1.091	a	C−H stretch

CH₂F−CHF (c)

103		4.153	a	CH_2F-CHF torsion
284		5.221	a	α- + β-C−F bend
478		10.397	a	α- + β-C−F bend
677		1.165	a	CH_2 rock + C−H bend
1059		1.939	a	C−C stretch + CH_2 rock
1124		5.208	a	β-C−F stretch
1154		3.353	a	C−C stretch + α-C−F bend
1211		2.586	a	α-C−F stretch
1261		1.109	a	CH_2 twist

Table 3.3 (continued)

Frequency (cm^{-1}) MP2	Expt[a]	Reduced mass (amu)	Sym	Approximate type of mode
1367		1.288	a	CH_2 wag + C−H bend
1501		1.722	a	CH_2 wag + C−H bend
1575		1.088	a	CH_2 scissor
3107		1.062	a	CH_2 symmetric stretch
3185		1.102	a	CH_2 asymmetric stretch
3295		1.090	a	C−H stretch

CHF$_2$−CH$_2$ (C$_1$)

157	1.043	a	CHF_2−CH_2 torsion
361	2.014	a	CF_2 twist + CH_2 wag
465	3.658	a	CF_2 + CH_2 rock
538	3.041	a	CF_2 twist + CH_2 wag
638	2.902	a	CF_2 scissor
921	2.175	a	CH_2 twist + CF_2 rock
1094	6.784	a	CF_2 asymmetric stretch
1187	2.471	a	C−C stretch
1195	2.870	a	CF_2 symmetric stretch
1425	1.161	a	C−H bend
1458	1.309	a	C−H bend
1532	1.361	a	CH_2 scissor
3182	1.088	a	C−H stretch
3287	1.051	a	CH_2 symmetric stretch
3417	1.121	a	CH_2 asymmetric stretch

CHF$_2$−CH$_2$ (C$_s$)

153	1.041	a″	CH_2 twist
397	2.928	a″	CH_2F−CH_2 torsion
432	1.535	a′	CH_2 wag

Table 3.3 (continued)

Frequency (cm^{-1})		Reduced mass (amu)	Sym	Approximate type of mode
MP2	Expt[a]			
493		4.129	a'	CF$_2$ scissors
655		6.333	a'	CF$_2$ rock
955		1.737	a''	CH$_2$ + CF$_2$ twist
1025		4.684	a'	C−C + CF$_2$ symmetric stretch
1198		3.122	a''	CF$_2$ asymmetric stretch
1201		2.692	a'	C−C + CF$_2$ symmetric stretch
1434		1.389	a'	C−H bend
1448		1.226	a''	C−H bend
1522		1.332	a'	CH$_2$ scissors
3134		1.084	a'	C−H stretch
3294		1.051	a'	CH$_2$ symmetric stretch
3425		1.121	a''	CH$_2$ asymmetric stretch
CH$_3$−CF$_2$				
196		1.072	a''	CH$_3$−CF$_2$ torsion
374		3.080	a''	CF$_2$ twist + CH$_3$ rock
466		3.923	a'	CF$_2$ wag + CH$_3$ rock
541		5.997	a'	CF$_2$ scissors
896		3.550	a'	CF$_2$ wag + CH$_3$ rock
1018		1.712	a''	CH$_3$ rock + CF$_2$ twist
1143		1.938	a'	C−C stretch
1306		4.866	a''	CF$_2$ asymmetric stretch
1321		3.740	a'	CF$_2$ symmetric stretch
1472		1.538	a'	CH$_3$ symmetric deformation
1536		1.048	a'	CH$_3$ degenerate deformation
1539		1.054	a''	CH$_3$ degenerate deformation
3142		1.041	a'	CH$_3$ symmetric stretch

Table 3.3 (continued)

Frequency (cm^{-1})		Reduced mass (amu)	Sym	Approximate type of mode
MP2	Expt[a]			
3246		1.095	a'	CH_3 degenerate stretch
3284		1.104	a"	CH_3 degenerate stretch
CHF$_2$–CHF (a)				
95		5.776	a	CHF_2–CHF torsion
245		4.804	a	C–C–F bend
433		4.167	a	CF_2 wag
450		3.033	a	CF_2 rock + C–F bend
574		8.016	a	CF_2 twist
728		2.798	a	CF_2 scissors
1100		7.776	a	β-C–F stretch
1158		5.912	a	CF_2 asymmetric stretch + C–F bend
1176		3.802	a	CF_2 asymmetric stretch + C–F bend
1239		2.100	a	C–F stretch
1348		1.337	a	α- + β-C–H bend
1429		1.167	a	β-C–H bend
1525		2.093	a	C–C stretch
3199		1.088	a	β-C–H stretch
3315		1.090	a	α-C–H stretch
CHF$_2$–CHF (b)				
90		6.952	a	CHF_2–CHF torsion
231		13.080	a	C–F bend + CF_2 wag
365		2.083	a	CF_2 twist + α-C–H bend
517		11.909	a	CF_2 rock
703		2.345	a	CF_2 twist + α-C–H bend

Table 3.3 (continued)

Frequency (cm⁻¹) MP2	Expt[a]	Reduced mass (amu)	Sym	Approximate type of mode
792		7.624	a	CF_2 symmetric stretch + C−F bend
950		3.337	a	CF_2 symmetric stretch + C−F bend
1115		6.906	a	CF_2 asymmetric stretch
1168		3.981	a	C−C−F bend
1271		1.936	a	C−F stretch
1422		1.167	a	β-C−H bend
1460		1.442	a	α- + β-C−H bend
1500		2.405	a	C−C stretch
3188		1.088	a	β-C−H stretch
3310		1.091	a	α-C−H stretch

CHF_2−CHF (c)

Frequency (cm⁻¹) MP2	Expt[a]	Reduced mass (amu)	Sym	Approximate type of mode
96		4.909	a	CHF_2−CHF torsion
247		7.119	a	C−F bend + CF_2 rock
430		8.837	a	C−F bend + CF_2 rock
478		2.140	a	CF_2 twist
577		7.685	a	CF_2 scissors
729		2.650	a	CF_2 wag
1053		4.940	a	CF_2 symmetric stretch + C−F bend
1167		4.267	a	CF_2 asymmetric stretch
1191		4.839	a	CF_2 symmetric stretch + C−F bend
1241		2.416	a	C−F stretch
1367		1.251	a	α- + β-C−H bend
1447		1.226	a	β-C−H bend

Table 3.3 (continued)

Frequency (cm^{-1})		Reduced mass (amu)	Sym	Approximate type of mode
MP2	Expt[a]			
1506		2.307	a	C$-$C stretch
3151		1.085	a	β-C$-$H stretch
3319		1.091	a	α-C$-$H stretch
CH$_2$F$-$CF$_2$ (C$_s$)				
97		6.056	a''	CH$_2$F$-$CF$_2$ torsion
208		16.973	a'	CF$_2$ wag + C$-$F bend
371		2.673	a''	CF$_2$ twist + CH$_2$ rock
523		11.500	a'	CF$_2$ scissors + CH$_2$ wag
755		10.219	a'	CF$_2$ rock + C$-$F bend
880		5.772	a'	CF$_2$ scissors + CH$_2$ wag
1019		1.868	a''	CH$_2$ rock + CF$_2$ twist
1080		7.644	a'	C$-$F stretch
1257		1.736	a''	CH$_2$ twist + CF$_2$ asymmetric stretch
1361		3.195	a'	CF$_2$ symmetric stretch
1375		1.964	a''	CH$_2$ twist + CF$_2$ asymmetric stretch
1480		1.703	a'	C$-$C stretch
1557		1.103	a'	CH$_2$ scissors
3174		1.058	a'	CH$_2$ symmetric stretch
3248		1.111	a''	CH$_2$ asymmetric stretch
CH$_2$F$-$CF$_2$ (C$_1$)				
106		4.338	a	CH$_2$F$-$CF$_2$ torsion
236		7.466	a	CF$_2$ twist + C$-$F bend
433		8.848	a	CF$_2$ rock + C$-$F bend
465		3.403	a	CF$_2$ + CH$_2$ rock
581		12.912	a	CF$_2$ twist + C$-$F bend

Table 3.3 (continued)

Frequency (cm^{-1})		Reduced mass (amu)	Sym	Approximate type of mode
MP2	Expt^a			
934		3.531	a	CF$_2$ symmetric stretch
1101		2.450	a	C$-$C stretch
1144		5.365	a	β-C$-$F stretch
1258		2.828	a	α-C$-$F stretch + CH$_2$ twist
1293		1.533	a	CH$_2$ + CF$_2$ wag
1352		3.207	a	α-C$-$F stretch + CH$_2$ twist
1484		1.786	a	CH$_2$ + CF$_2$ wag
1563		1.090	a	CH$_2$ scissors
3130		1.062	a	CH$_2$ symmetric stretch
3223		1.103	a	CH$_2$ asymmetric stretch
CF$_3$$-CH_2$				
153		1.033	a$''$	CF$_3$$-CH_2$ torsion
342		2.355	a$'$	CF$_3$ rock
378		3.863	a$''$	CF$_3$ rock
504		3.052	a$'$	CF$_3$ degenerate deformation
536		6.607	a$''$	CF$_3$ degenerate deformation
610		5.824	a$'$	CF$_3$ symmetric deformation + CH$_2$ rock
622		5.030	a$'$	CF$_3$ symmetric deformation + CH$_2$ rock
874		8.243	a$'$	CF$_3$ symmetric stretch
978		1.732	a$''$	CF$_3$ degenerate stretch + CH$_2$ twist
1200		12.383	a$'$	CF$_3$ degenerate stretch
1307		5.341	a$''$	CF$_3$ degenerate stretch + CH$_2$ twist
1359		3.698	a$'$	C$-$C stretch + CH$_2$ scissors

Table 3.3 (continued)

Frequency (cm⁻¹) MP2	Frequency (cm⁻¹) Expt[a]	Reduced mass (amu)	Sym	Approximate type of mode
1526		1.414	a'	$C-C$ stretch + CH_2 scissors
3301		1.051	a'	CH_2 symmetric stretch
3436		1.123	a″	CH_2 asymmetric stretch
CHF₂−CF₂ (Cₛ)				
74		13.617	a″	CHF_2-CF_2 torsion
202		18.588	a″	CF_2 twist
360		17.393	a'	CF_2 rock
405		5.466	a'	CF_2 wag
496		13.813	ɔ″	CF_2 twist
538		15.146	a'	CF_2 scissors
644		14.389	a'	CF_2 scissors
1048		8.610	a'	CF_2 rock
1171		6.855	a'	β-CF_2 symmetric stretch
1202		5.048	a″	β-CF_2 asymmetric stretch
1299		2.066	a'	α-CF_2 symmetric stretch
1308		12.770	a″	α-CF_2 asymmetric stretch
1436		1.249	a″	$C-H$ bend
1488		2.619	a'	$C-C$ stretch
3161		1.086	a'	$C-H$ stretch
CHF₂−CF₂ (C₁)				
68		14.681	a	CHF_2-CF_2 torsion
216		17.102	a	β-CF_2 twist + α-CF_2 wag
233		14.021	a	β-CF_2 wag + α-CF_2 twist
413		15.460	a	CF_2 rock
530		12.074	a	CF_2 scissors
607		14.604	a	CF_2 scissors

Table 3.3 (continued)

| Frequency (cm^{-1}) | | Reduced | Sym | Approximate type of mode |
MP2	Expt[a]	mass (amu)		
785		10.635	a	β-CF$_2$ rock + α-CF$_2$ wag
921		5.295	a	α-CF$_2$ rock
1136		7.102	a	β-CF$_2$ symmetric stretch
1185		5.147	a	β-CF$_2$ asymmetric stretch
1281		4.905	a	α-CF$_2$ asymmetric stretch
1377		3.773	a	α-CF$_2$ symmetric stretch
1435		1.198	a	C$-$H bend
1497		2.283	a	C$-$C stretch
3214		1.089	a	C$-$H stretch
CF$_3$-CHF				
86		6.458	a	CF$_3$$-$CHF torsion
213		14.421	a	CF$_3$ rock + C$-$F bend
352		2.638	a	CF$_3$ rock + C$-$H bend
420		14.662	a	CF$_3$ rock + C$-$F bend
517		5.532	a	CF$_3$ rock + C$-$H bend
557		12.607	a	CF$_3$ degenerate deformation
674		10.284	a	CF$_3$ symmetric deformation
721		2.263	a	CF$_3$ degenerate deformation
886		7.416	a	CF$_3$ symmetric stretch
1213		11.682	a	C$-$F + CF$_3$ degenerate stretch
1231		3.018	a	C$-$H bend + C$-$F stretch
1256		8.500	a	CF$_3$ degenerate stretch
1341		2.478	a	C$-$H bend + CF$_3$ degenerate stretch
1507		3.363	a	C$-$C stretch
3332		1.091	a	C$-$H stretch

Table 3.3 (continued)

Frequency (cm^{-1})		Reduced mass (amu)	Sym	Approximate type of mode
MP2	Expt[a]			
CF$_3$—CF$_2$[c]				
62		18.888	a"	CF$_3$—CF$_2$ torsion
206	211	18.570	a"	CF$_3$ rock + CF$_2$ twist
222	227	18.258	a'	CF$_3$ rock + CF$_2$ wag
366	366	18.716	a'	CF$_3$ + CF$_2$ rock
420	419	18.250	a"	CF$_3$ rock + CF$_2$ twist
515	514	17.620	a'	CF$_3$ degenerate deformation
591	604	17.835	a"	CF$_3$ degenerate deformation
604	694 (604)[f]	17.156	a'	CF$_3$ symmetric deformation + CF$_2$ scissors
721	703	15.536	a'	CF$_3$ symmetric deformation + CF$_2$ scissors
860	956 (820)[f]	14.991	a'	CF$_3$ + CF$_2$ symmetric stretch
1175	1117	13.804	a'	CF$_3$ + CF$_2$ symmetric stretch
1258	1184	13.199	a'	CF$_3$ degenerate stretch
1297	1227	13.026	a"	CF$_3$ degenerate stretch
1331	1273	13.408	a"	CF$_2$ asymmetric stretch
1475	1398	12.596	a'	C—C stretch

[a] References to experimental determinations given at headings for individual radicals.
[b] Reference 80. [c] Reference 96. [d] Reference 97. [e] Reference 98, except where indicated. [f] Reference 99.

Where comparison with experiment is possible, the deviation is well within 10 %, with a systematic overestimation, as expected, except for a few of the low frequency bends where the calculated value is lower. The agreement is particularly good for CF_3-CF_2, with the exception of two modes where the calculated values are much lower than those measured by Jacox.[98] However, excellent agreement is obtained with the assignments of Snelson et al.[99] (which are shown in parentheses), suggesting that the latter assignments are correct.

3.4 Total Energies and Zero-Point Energies

Symmetry point groups, total energies at the MP2/6-311G(d,p)//MP2/6-31G(d,p) level for all radicals, and at the MP4/6-311G(d,p)//MP2/6-31G(d,p) level for the methyl radicals, and those ethyl radicals with two or fewer fluorines, unscaled ZPEs at the MP2/6-31G(d,p) level, and experimental ΔH_f values[90,91,101 - 113] used to calculate the experimental BDEs are given in Table 3.4. It should be noted that, due to lack of data, some of the experimental ΔH_f values are calculated by means of the triatomic additivity method[114], and some others are estimated or derived values, some with large uncertainties. Where data is available from several sources, there is often a wide range of values. Leroy et al.[115] have recently published recommended experimental ΔH_f values for some radicals based on the best agreement with their calculated values. (Unfortunately, they only worked on two of the radicals in this study.) The most recent values given in standard references have been used, where possible (not necessarily those which would give the best agreement with the calculated results).

Table 3.4: Symmetry Point Groups, Total Energies, Zero-Point Energies, and Experimental Heats of Formation of Radicals

Radical	sym	MP2/6-311G(d,p)[a]	MP4/6-311G(d,p)[a]	ZPE[b]	$\Delta H_{f,298}{}^c$	ref
CH_3	D_{3h}	−39.707172	−39.730634	30.762	145.7 ± 0.8	104
CH_2F	C_s	−138.772821	−138.798591	26.085	−29.0[f]	105
CHF_2	C_s	−237.855372	−237.882487	19.883	−238.9 ± 4.2	106
CF_3	C_{3v}	−336.942272	−336.970361	12.471	−468.6 ± 4.2	107
CH_3-CH_2	C_s	−78.902838	−78.944350	61.816	117.2	108
CH_2F-CH_2	C_1	−177.968344	−178.012454	54.869		
CH_2F-CH_2	C_s	−177.968009	−178.012252	55.270		
CH_3-CHF	C_1	−177.975770	−178.019678	55.938	−71.5 ± 4.6[g]	109
CH_2F-CHF (a)	C_1	−277.039136	−277.085944	48.935		
CH_2F-CHF (b)	C_1	−277.037264	−277.084013	48.692		
CH_2F-CHF (c)	C_1	−277.036451	−277.083189	48.711		
CHF_2-CH_2	C_1	−277.052965	−277.099007	47.515		
CHF_2-CH_2	C_s	−277.052807	−277.098761	47.311		
CH_3-CF_2	C_s	−277.061373		48.937	−302.5 ± 7.5	110
CHF_2-CHF a	C_1	−376.119666		41.044		
CHF_2-CHF b	C_1	−376.117926		41.193		

Table 3.4 (continued)

Radical	sym	MP2/6-311G(d,p)[a]	MP4/6-311G(d,p)[a]	ZPE[b]	ΔH$_{f,298}$[c]	ref
CHF$_2$−CHF c	C$_1$	−376.118731		41.003	.	
CH$_2$F−CF$_2$	C$_s$	−376.119797		41.884		
CH$_2$F−CF$_2$	C$_1$	−376.119124		41.702		
CF$_3$−CH$_2$	C$_s$	−376.146393		39.016	−517.1 ± 5.0	111
CHF$_2$−CF$_2$	C$_s$	−475.198160		33.789		
CHF$_2$−CF$_2$	C$_1$	−475.197611		33.939		
CF$_3$−CHF	C$_1$	−475.210073		32.597	−680.7	112
CF$_3$−CF$_2$	C$_s$	−574.286901		25.298	−891.2 ± 5.4[g]	113
H		−0.499810		0.0	217.965	104

[a] Single-point energy, in hartrees, at MP2/6-31G(d,p) geometry. [b] Unscaled, in millihartrees, at MP2/6-31G(d,p) level. [c] In kJ mol^{-1}. [d] Derived from correlative procedures. [e] Calculated by the triatomic additivity method of Reference 114. [f] Estimated from the reaction Br + CH$_3$F ⇆ HBr + CH$_2$F [g] Estimated from kinetic parameters.

Table 3.5: Total Energies of Radicals at the Additional Levels of Theory Required for G2 Method[a]

Species/ G2 energy[b]	MP2/6-311+G(d,p)	MP2/6-311G(2df,p)	MP2/6-311+G(3df,2p)	MP4/6-311+G(d,p)	MP4/6-311G(2df,p)	QCISD(T)/6-311G(d,p)
CH_3 −39.742997	−39.708454	−39.724093	−39.731398	−39.731911	−39.748742	−39.73207
CH_2F −138.891534	−138.78¨	−138.838734	−138.856246	−138.807492	−138.867984	−138.799130
CHF_2 −238.055633	−237.868460	−237.971032	−237.996532	−237.896587	−238.004152	−237.881445
CH_3-CH_2 −78.967355	−78.904436	−78.938601	−78.950852	−78.946021	−78.982086	−78.946362
CH_3-CHF −178.124225	−177.984552	−178.060864	−178.083417	−178.029031	−178.109094	−178.020453
CH_2F-CH_2 C_1 −178.118806	−177.978043	−178.053161	−178.076799	−178.022744	−178.101577	−178.013192
CH_2F-CHF −277.274298	−277.055820	−277.173478	−277.207177	−277.103728	−277.226944	−277.085512
CHF_2-CH_2 C_1 −277.286952	−277.067720	−277.187499	−277.219477	−277.114942	−277.240391	−277.098054
CH_3-CF_2 −277.292801	−277.074986	−277.196458	−277.227268	−277.121591	−277.248812	−277.105922

a All values given are single-point energies, in hartrees at the MP2/6-31G(d,p) geometries given above. The MP4/6-311G(d,p) and MP2/6-311G(d,p) single-point energies and ZPEs are given in Table 3.4. b Scaled ZPEs included. To obtain the energy without the ZPE correction subtract the MP2/6-31G(d,p) ZPE listed in Table 3.4 multiplied by the scaling factor of 0.9646.

The total energies given in Table 3.4 are universally lower than those calculated previously with the same basis set using HF/6-31G(d) optimized geometries, while the relative stabilities remain qualitatively the same. As with the fluorinated ethanes and methyl radicals, the ethyl radicals decrease in energy with increasing fluorine substitution, and when there is an equal number of fluorines the lowest energy occurs when as many as possible are on one carbon, consistent with the geminal effect.[116] There is also a secondary preference for having as many fluorines as possible on the α-carbon, which will lower the energy of the SOMO.

Total energies at the additional levels of theory required for the G2 method, and the resultant G2 extrapolated energies (using the modified G2 method as described in section 2.10), for the most stable conformer of each radical with two or fewer fluorines, are given in Table 3.5. Once again, energies decrease with increasing level of theory, both in terms of electron correlation and basis-set size, with the MP4/6-311G(2df,p) level of theory giving the lowest energy in every case.

The present results for the ethyl radicals suggest that the gauche effect[117] also operates in radicals. For CH_2F-CHF the two gauche conformers 1e and 1f are more stable than the anti conformer 1g. Furthermore, the gauche conformer which has the fluorine on the β-carbon ($r_{C-F} = 1.404$ Å) eclipsed with the SOMO (1e) is the most stable one. For CH_2F-CF_2 the conformer (1n) which has the fluorine on the β-carbon ($r_{C-F} = 1.395$ Å) gauche to the two fluorines on the α-carbon and eclipsed with the SOMO is the more stable one. Conversely, a saturated species with one fluorine gauche to two fluorines is relatively unstable (see Chapter 5). This can be explained by reduced

repulsions in the radicals due to the large FCCF dihedral angles and long $C_\beta - F_\beta$ bond lengths. Having the fluorine on the β-carbon eclipsed with the SOMO also makes the radical more stable, possibly due to an attractive two-centre three-electron hyperconjugative interaction.[90,91]

As in the saturated case, it is unfavorable to have the two fluorines on the β-carbon gauche to a fluorine on the α-carbon. Thus, for $CHF_2 - CHF$ 1l is less stable than 1k and 1m. Since 1k has a fluorine on the β-carbon eclipsed with the SOMO, it is more stable than 1m. Also, for $CHF_2 - CF_2$ 1r is less stable than 1q.

3.5 Conclusions

The inclusion of electron correlation in geometry optimizations gives shorter $C-C$, longer $C-F$ and slightly longer $C-H$ bond lengths, and minor differences in interatomic bond angles, as compared to structures optimized with HF theory. The observed trends in geometrical parameters through the series can be rationalized in terms of simple bonding arguments.

The calculated vibrational frequencies show that many modes are coupled, particularly in the asymmetrical radicals. Trends in the term values are also consistent with simple bonding arguments.

The calculated total energies are lowered as increasingly higher levels of theory are used, but the relative stabilities remain the same. The geminal effect and the gauche effect, which have been noted previously in the literature for many closed-shell species, are also operative in the ethyl radicals.

Chapter 4. Hyperfine Structures of the Series $C_2H_nF_{5-n}$, n = 0−5

4.1 Introduction

The coupling of nuclear and electronic magnetic moments produces hyperfine splitting in ESR spectra. The hyperfine coupling constant can be factored into an isotropic part (A_{iso}, Fermi contact term), which provides a measure of the spin density at the various nuclei in the molecule, and an anisotropic part (T_{aniso}), which provides a measure of the asymmetry of the spin density. Because of the global nature of the operator, *ab initio* predictions of T_{aniso} are comparatively accurate (although good agreement with experiment is not always obtained), whereas predictions of A_{iso} are highly dependent on the geometry and the "local" quality of the wavefunction at the nuclei (which is often poor, as in the case of Gaussian-type basis sets), and can be complicated by contributions from such effects as spin polarization. Fermi contact spin densities are thus highly sensitive to both the quality of the one-particle basis and the level of theory employed to account for electron correlation. Despite this, theoretical determinations of A_{iso} are more common, since the integrals are far easier to evaluate than those for T_{aniso}.

Both ease and accuracy favour A_{iso} in experimental determinations, as demonstrated by the volume of ESR reports in the literature. Isotropic spectra have been reported for most of the radicals[118 − 124] in the title series, but anisotropic spectra have been limited to the parent ethyl radical,[125,126,127] CH_3-CF_2,[128] and CF_3-CH_2.[123] Some of the experimental studies also included semiempirical INDO calculations, specifically on CH_3-CH_2,[122] CH_3-CHF,[121,122] CH_3-CF_2,[121,122,128] and

59

CF_3-CF_2.[121] Recently there have been some extensive *ab initio* investigations of the hyperfine structure (hfs) of the ethyl radical, including isotropic[129,130,131] and anisotropic[129] values. For the fluorinated radicals, *ab initio* studies have been limited to the β-proton in CH_2F-CH_2.[132]

Below are presented results of hfs calculations using density functional theory (DFT) on the most stable conformer for each radical in the series $C_2H_nF_{5-n}$ (n = 0−5). The DFT calculations were performed on the MP2/6-31G(d,p) optimized structures presented in Chapter 3. This level of theory has been shown to give sufficiently accurate geometries,[23] which are essential for obtaining accurate hfs parameters.[133] Both isotropic and anisotropic coupling constants were calculated.

The numbering system used for the nuclei in the data tables below is shown in Figure 2, along with the directions for the principal axes. The x axis lies along the $C-C$ bond; the y axis approximately bisects the plane of the radical site, and is in the $C_\alpha-C_\beta-X_{\beta 0}$ plane; the z axis is perpendicular to this plane. The designations LDA and PWP refer to results from these functionals (see section 2.10) on the MP2 optimized geometries, and PWP' refers to results from DFT optimizations with the PWP functional (the latter calculations were performed by Leif Eriksson, who also co-supervised the work described in this chapter). Where there is more than one experimental determination, solution spectra were used where possible, to avoid matrix effects, and the one done at the lowest temperature chosen, since the calculations are done at 0 K and the experimental hfs of many of these radicals are known to be affected by temperature,[121] due to increased vibrational and/or rotational motion in the sample.
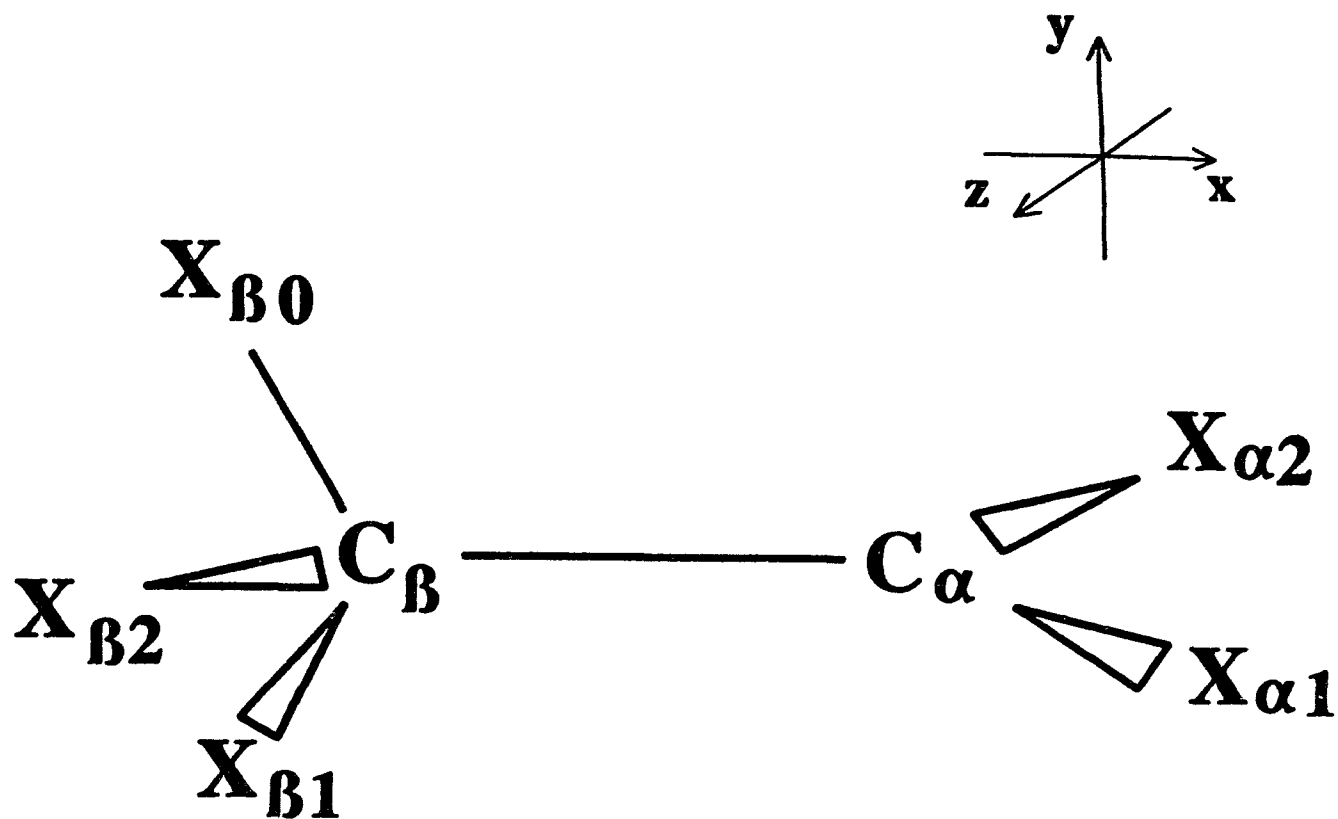
Figure 2. Atom numbering and principal axes labelling systems for the radicals under study. X can be a F or H atom.

4.2 Isotropic Hyperfine Coupling Constants

The isotropic hyperfine coupling constants (in gauss) for all nuclei in each radical are presented in Table 4.1. The PWP functional gives better agreement with experiment than LDA in almost all cases where comparison is possible. This has also been shown in great detail in previous work[67b,c,134] and is related to the build-up of spin density at the core and outer valence parts, obtained with the gradient corrected functionals. Large relative errors still remain in some cases, such as for H_β in CHF_2-CH_2 (45%) and H_α in CF_3-CHF (51%). For couplings at the radical (α) centre, PWP invariably gives values with larger magnitudes, and where comparison with experiment is possible, this always gives better agreement than does LDA (assuming that in cases of dispute the calculated sign is correct rather than the experimental assignment; this assumption is valid as all the disputes are for α-protons, which are expected to have negative isotropic coupling constants,[135] as all the present ones do). The situation is not as clearcut for couplings to atoms at the β-centre. Better agreement with experiment is usually obtained with PWP, but the two methods give results close in magnitude.

For the carbon couplings, the larger magnitude is always at the radical centre. This can be taken as an indication of the localization of the SOMO; in the simplest possible picture, the unpaired electron may be thought of as residing in a non-bonding p_y or (with increasing pyramidal angle) sp^3 orbital on the α-carbon. Couplings to hydrogen are always positive at the β-centre (except for a small negative coupling in CH_2F-CF_2), and negative at the α-centre. The value of the coupling for the hydrogens in the CH_3 group of CH_3-CF_2 (12.34 by PWP cf. 13.99 from experiment) is strikingly

Table 4.1: Isotropic Hyperfine Coupling Constants in gauss[a]

Radical (sym)	Method	C_α	C_β	$H_\alpha{}^j$	F_α	H_β	F_β
CH_3-CH_2	LDA	15.17	−10.08	−15.33		25.82	
(C_s)	PWP	39.19	−10.63	−19.34		26.48	
	Expt[b]	39.07	−13.57	(−)22.38		26.87	
CH_2F-CH_2	LDA	17.25	−11.46	−14.59		34.70	23.55
(C_1)	PWP	40.74	−12.54	−18.38		34.47	19.80
	PWP′	32.98	−10.13	−19.78		27.43	53.76
	Expt[c]			(−)22.15		27.35	47.59
CH_3-CHF	LDA	55.45	−4.23	−4.50	22.30	20.98	
(C_1)	PWP	79.35	−4.18	−6.20	51.49	21.94	
	PWP′	35.57	−11.88	−22.85	37.19	26.35	
	Expt[d]			(−)17.31	59.21	24.48	
CH_3-CF_2	LDA	132.88	15.28		64.96	11.95	
(C_s)	PWP	157.19	17.07		87.35	12.34	
	Expt[e]				94.01	13.99	
CH_2F-CHF	LDA	37.41	10.31	−9.78	15.32	1.79	117.17
(C_1)	PWP	61.21	9.26	−12.48	45.37	2.13	115.35
CHF_2-CH_2	LDA	16.12	−6.50	−15.83		6.83	46.34
(C_1)	PWP	38.56	−6.55	−19.18		6.60	49.88
	Expt[f]			(−)23.16		12.05	49.28
CH_2F-CF_2	LDA	113.30	34.41		46.49	−0.16	8.08
(C_s)	PWP	140.33	35.78		70.62	−0.32	7.68
CF_3-CH_2	LDA	16.02	−13.43	−16.36			21.71
(C_s)	PWP	39.39	−13.85	−19.59			23.98
	PWP′	34.36	−15.02	−21.05			26.30
	Expt.[g]			(−)23.77			29.61

Table 4.1 (continued)

Radical (sym)	Method	C_α	C_β	H_α^j	F_α	H_β	F_β
CHF$_2$–CHF	LDA	47.38	2.40	−7.90	17.17	4.44	41.03
(C$_1$)	PWP	71.63	1.47	−9.98	47.88	4.32	40.77
CHF$_2$–CF$_2$	LDA	132.17	0.13		55.88	18.31	15.27
(C$_s$)	PWP	159.77	2.62		80.53	19.08	11.23
CF$_3$–CHF	LDA	49.68	−7.26	−8.55	18.06		17.90
(C$_1$)	PWP	73.89	−7.26	−10.57	47.25		19.10
	PWP'	52.48	−11.69	−17.46	39.48		20.56
	Expt.[h]			(−)21.47	66.18		25.25
CF$_3$–CF$_2$	LDA	133.47	15.26		51.81		7.93
(C$_s$)	PWP	160.13	19.34		76.40		8.30
	Expt.[i]				87.64		11.35

[a] Values averaged where applicable for comparison to experiment. All experimental values are taken from solution spectra. [b] Carbon couplings from ref 118; 95 K. Hydrogen couplings from ref 119; 93 K. [c] Reference 121; 179 K. [d] Reference 121; 167 K. [e] Reference 121; 195 K. [f] Reference 121; 181 K. [g] Reference 121; 160 K. [h] Reference 121; 167 K. [i] Reference 124; 179 K. [j] (−) indicates value was reported as positive.

small in comparison to those of other alkyl radicals, which are in the range 23−26 G.[119] The large out-of-plane angle (44.2° in the MP2 structure) confirms the suspicion of earlier workers[122] that the most important factor in causing this unusually small value is the degree of pyramidalization at the α-carbon. The electron withdrawing properties of the fluorine atoms relative to the alkyl hydrogens gives a polarization of the SOMO towards the CF_2 moiety, whereby there is very little unpaired spin density at the hydrogens. All couplings to fluorine are positive, a well-known trend which has been seen in both planar and non-planar radicals.[136]

Experimental carbon couplings are only available for the ethyl radical; the PWP results give excellent agreement, particularly for C_α, but this is somewhat fortuitous All the $R-CH_2$ radicals in this series have very low barriers to inversion at the radical centre, allowing rapid inversion to occur, which creates a vibrational averaging effect. Chipman[129] has calculated this effect to be about 8 G for CH_3CH_2. To investigate the effect at the level of theory used here, the hfs was calculated using the PWP method at 61 additional points, in which the pyramidal angle was varied up to ±39.4° (the equilibrium value is 12.4°). It was assumed that all other geometrical parameters did not vary   the equilibrium values at the MP2/6-31G(d,p) level. This assumption was checked by optimizing the geometry for the structure at −12.4°, which showed that these parameters were indeed almost unchanged. In agreement with Chipman[129] it was found that the vibrational averaging effect is important only for the C_α coupling. A plot of this coupling versus pyramidal angle is given in Figure 3.
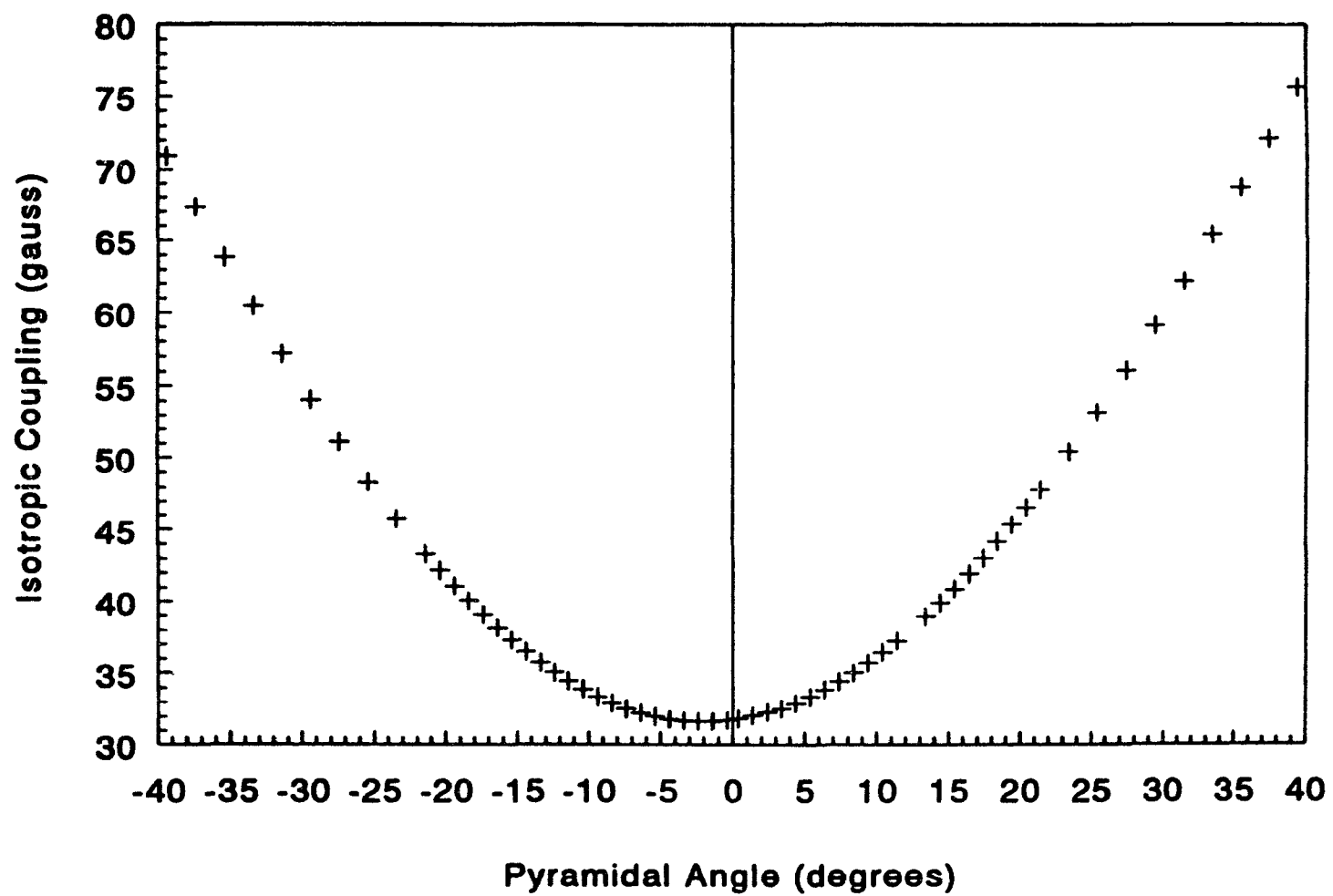
Figure 3. Variation of the C_α isotropic coupling in CH_3-CH_2 with pyramidal angle as radical undergoes inversion.
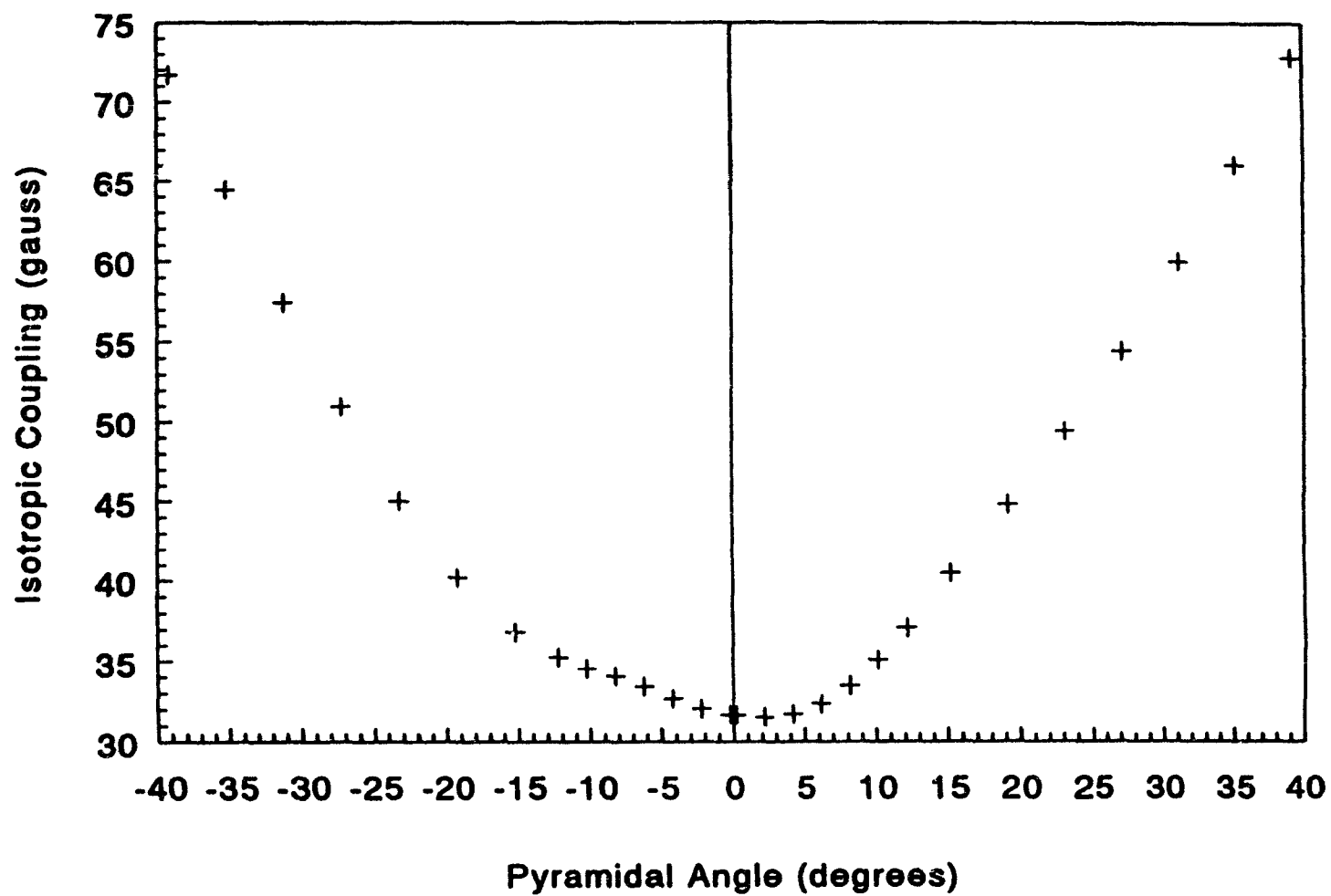
Figure 4. Variation of the C_α isotropic coupling in CF_3-CH_2 with pyramidal angle as radical undergoes inversion.

To investigate the effect of β-fluorine substitution on the vibrational averaging effect, a similar study on CF_3-CH_2 was performed, using 28 additional points spanning pyramidal angles to $\pm 39.2°$ (equilibrium value is $13.2°$). The effect on the other species is expected to be between these two extremes. As seen in Figure 4, the distribution of couplings about the inversion centre is more nearly symmetrical than in Figure 3, thus it can be expected that the vibrational averaging effect is smaller here, perhaps on the order of 2 G.

The relatively large couplings seen for all atoms at the radical centre are indicative of a pyramidal centre. This is illustrated in Figure 5, which shows a fair correlation between the hyperfine couplings constants and the out-of-plane angle at the radical centre. This correlation has been noted previously experimentally for H_α and F_α couplings,[121] and in general for substituted alkyl radicals,[118,137] where all coupling constants increase in magnitude with the pyramidality at the radical centre, the effect being much more pronounced at the radical centre than at surrounding atoms. This is seen in Figure 5, where the degree of dependence of the couplings with the out-of-plane angle decreases in the order $C > F > H$. This can be explained in terms of an increased sp^3 hybridization of the radical centre, whereby there is more s mixing in the orbital of the unpaired electron, an argument originally postulated by Pauling[94] in terms of electronegativity arguments. In the case of a planar radical centre (sp^2 hybridized), the unpaired electron instead resides in a p_y orbital, with a nodal plane through the carbon atom. Bingham et al.[138] argue that conjugative destabilization associated with the presence of two or three donor dominant substituents is the primary electronic factor
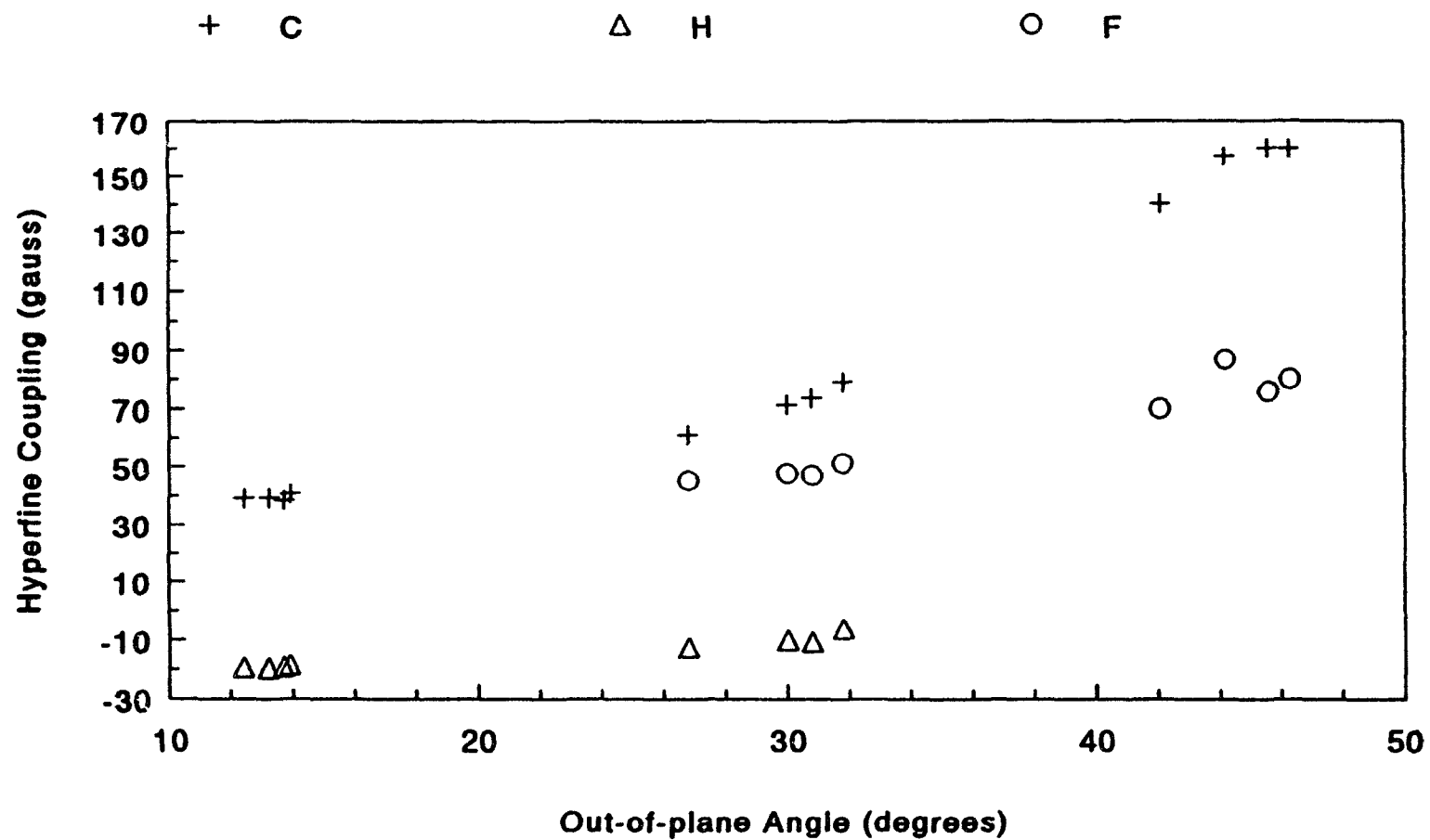
Figure 5. Hyperfine coupling constants for atoms at the radical (α-) centre versus out-of-plane angle.

giving rise to nonplanar radical structures. They cite support from studies[139] showing "that two donor substituents induce pyramidality to a far greater extent than would be expected on the basis of the effect of one alone".[138b] However, the calculated out-of-plane angles for these radicals shows that the first fluorine substituent has a slightly greater effect than the second in increasing pyramidality.

4.3 Anisotropic Hyperfine Coupling Constants

Anisotropic hyperfine coupling constants (in gauss) computed along the principal axes are presented in Table 4.2. These constants are remarkably similar throughout the series, suggesting that substituent effects are unimportant to the asymmetry of the spin density for these radicals. The C_α couplings are nearly constant, with lower magnitudes in the case of a CF_2 group. The C_β couplings are all near zero, with slightly larger magnitudes for the $R-CF_2$ radicals. There is very little change in the H_α and H_β couplings, with the latter all being very small, as expected since they are much farther away from the radical centre. In contrast the F_α couplings are large (an effect also noted but not quantified experimentally by Chen et al.[121]), particularly for CHF groups, with more variability than for the other centres. The F_β couplings also show a high degree of variability, with larger magnitudes for $F_{\beta 0}$ (the position eclipsing the SOMO), and smaller magnitudes for cases where the α-group is CF_2. This is again due to the form of the SOMO, leading to large couplings for the β-atoms in the same plane as the orbital with the main unpaired spin component.

Table 4.2: Anisotropic Hyperfine Tensor in Principal Axes in gauss[a]

Nucleus	Method	T_x	T_y	T_z
CH₃−CH₂				
C_α	LDA	−26.82	−26.55	53.37
	PWP	−28.04	−27.67	55.71
C_β	LDA	−1.34	0.07	1.27
	PWP	−1.04	0.07	0.97
$H_{\alpha 1}$, $H_{\alpha 2}$	LDA	−13.50	0.02	13.48
	PWP	−13.98	0.29	13.70
	Expt.[b]	−6.8		
$H_{\beta 0}$	LDA	−2.28	−1.07	3.35
	PWP	−2.08	−1.03	3.10
$H_{\beta 1}$, $H_{\beta 2}$	LDA	−1.75	−1.49	3.24
	PWP	−1.67	−1.54	3.21
H_β ave.	LDA	−1.93	−1.35	3.28
	PWP	−1.80	−1.37	3.18
	Expt.[b]	1.9		
CH₂F−CH₂				
C_α	LDA	−26.67	−26.52	53.19
	PWP	−27.97	−27.81	55.78
	PWP'	−28.03	−27.66	55.69
C_β	LDA	−1.22	−0.47	1.69
	PWP	−1.03	−0.57	1.60
	PWP'	−1.21	−0.34	1.56
$H_{\alpha 1}$	LDA	−13.35	−0.19	13.54
	PWP	−13.89	0.08	13.81
	PWP'	−13.64	−0.13	13.77
$H_{\alpha 2}$	LDA	−13.37	−0.23	13.59

Table 4.2 (continued)

Nucleus	Method	T_x	T_y	T_z
	PWP	−13.80	0.15	13.64
	PWP′	−13.69	0.07	13.61
$H_{\beta 0}$	LDA	−2.61	−0.51	3.12
	PWP	−2.43	−0.51	2.94
	PWP′	−2.61	−0.49	3.11
$F_{\beta 1}$	LDA	−9.08	−7.78	16.86
	PWP	−9.02	−5.48	14.50
	PWP′	−21.06	−17.88	38.94
$H_{\beta 2}$	LDA	−2.12	−1.71	3.83
	PWP	−2.11	−1.61	3.72
	PWP′	−2.08	−1.57	3.65
CH_3-CHF				
C_α	LDA	−26.86	−25.85	52.71
	PWP	−28.00	−27.14	55.14
	PWP′	−30.20	−29.30	59.51
C_β	LDA	−1.23	−0.41	1.64
	PWP	−1.02	−0.53	1.55
	PWP′	−0.81	0.01	0.80
$F_{\alpha 1}$	LDA	−90.88	−76.22	167.10
	PWP	−87.32	−74.25	161.57
	PWP′	−89.22	−73.05	162.27
$H_{\alpha 2}$	LDA	−12.50	−1.07	13.58
	PWP	−12.77	−0.78	13.55
	PWP′	−14.25	0.46	13.79
$H_{\beta 0}$	LDA	−1.94	−0.96	2.91
	PWP	−1.77	−1.04	2.81
	PWP′	−1.85	−1.37	3.22

Table 4.2 (continued)

Nucleus	Method	T_x	T_y	T_z
H$_{\beta1}$	LDA	−1.96	−1.81	3.78
	PWP	−1.97	−1.77	3.74
	PWP′	−1.65	−1.47	3.12
H$_{\beta2}$	LDA	−1.95	−1.59	3.54
	PWP	−2.00	−1.57	3.57
	PWP′	−1.74	−1.62	3.36
CH$_3$−CF$_2$				
C$_\alpha$	LDA	−25.22	−24.50	49.73
	PWP	−26.02	−25.81	51.83
C$_\beta$	LDA	−1.85	−1.65	3.50
	PWP	−1.88	−1.66	3.53
F$_{\alpha1}$, F$_{\alpha2}$	LDA	−74.28	−66.44	140.72
	PWP	−71.42	−64.97	136.38
	Expt.[c]	−59.11	−59.11	118.1
H$_{\beta0}$	LDA	−2.02	−0.87	2.89
	PWP	−1.89	−0.96	2.86
H$_{\beta1}$, H$_{\beta2}$	LDA	−2.42	−1.81	4.24
	PWP	−2.48	−1.75	4.23
CH$_2$F−CHF				
C$_\alpha$	LDA	−26.31	−25.28	51.60
	PWP	−27.64	−26.58	54.22
C$_\beta$	LDA	−0.91	0.04	0.87
	PWP	−0.68	−0.17	0.85
H$_{\alpha1}$	LDA	−12.22	−1.13	13.36
	PWP	−12.60	−0.73	13.33
F$_{\alpha2}$	LDA	−102.92	−89.37	192.29
	PWP	−97.69	−85.58	183.28

Table 4.2 (continued)

Nucleus	Method	T_x	T_y	T_z
$F_{\beta0}$	LDA	−43.77	−41.09	84.86
	PWP	−43.34	−40.13	83.47
$H_{\beta1}$	LDA	−2.70	−1.21	3.91
	PWP	−2.69	−1.21	3.89
$H_{\beta2}$	LDA	−2.50	−1.30	3.81
	PWP	−2.51	−1.31	3.82
CHF$_2$·–CH$_2$				
C_α	LDA	−27.16	−27.07	54.24
	PWP	−28.30	−28.06	56.36
C_β	LDA	−0.96	0.29	0.67
	PWP	−0.91	0.28	0.63
$H_{\alpha1}$	LDA	−13.51	−0.48	13.99
	PWP	−13.89	−0.04	13.93
$H_{\alpha2}$	LDA	−13.44	−0.56	14.00
	PWP	−13.86	−0.23	14.09
$F_{\beta0}$	LDA	−39.13	−36.41	75.54
	PWP	−36.64	−35.45	72.09
$H_{\beta1}$	LDA	−2.53	−1.16	3.69
	PWP	−2.49	−1.19	3.68
$F_{\beta2}$	LDA	−13.26	−10.56	23.83
	PWP	−15.01	−11.50	26.51
CH$_2$F–CF$_2$				
C_α	LDA	−25.42	−24.63	50.05
	PWP	−26.31	−25.73	52.04
C_β	LDA	−1.47	−1.24	2.71
	PWP	−1.45	−1.44	2.89
$F_{\alpha1}$, $F_{\alpha2}$	LDA	−83.15	−73.38	156.53

Table 4.2 (continued)

Nucleus	Method	T_x	T_y	T_z
	PWP	−81.82	−70.20	152.02
$F_{\beta 0}$	LDA	−6.77	−6.46	13.23
	PWP	−6.23	−6.15	12.38
$H_{\beta 1}$, $H_{\beta 2}$	LDA	−2.74	−1.62	4.36
	PWP	−2.74	−1.63	4.37
CF₃−CH₂				
C_α	LDA	−27.66	−27.64	55.30
	PWP	−28.72	−28.63	57.35
	PWP′	−28.87	−28.73	57.61
C_β	LDA	−1.23	0.43	0.80
	PWP	−1.18	0.41	0.77
	PWP′	−1.30	0.59	0.71
$H_{\alpha 1}$, $H_{\alpha 2}$	LDA	−13.69	−0.60	14.29
	PWP	−14.09	−0.17	14.26
	PWP′	−13.86	−0.30	14.15
	Expt.[d]	−5.3	3.3	1.9
$F_{\beta 0}$	LDA	−34.14	−33.15	67.30
	PWP	−33.23	−31.54	64.77
	PWP′	−35.91	−33.82	69.73
$F_{\beta 1}$, $F_{\beta 2}$	LDA	−12.50	−11.42	23.92
	PWP	−12.47	−11.51	23.97
	PWP′	−13.83	−11.96	25.79
F_β ave.	LDA	−19.72	−18.66	38.38
	PWP	−19.39	−18.18	37.57
	PWP′	−21.19	−19.25	40.44
	Expt.[d]	19.3	−8.3	−11.0

CHF₂−CHF

Table 4.2 (continued)

Nucleus	Method	T_x	T_y	T_z
C_α	LDA	−26.85	−25.82	52.66
	PWP	−28.00	−27.08	55.09
C_β	LDA	−0.95	−0.19	1.14
	PWP	−0.86	−0.36	1.23
$H_{\alpha 1}$	LDA	−12.41	−1.31	13.72
	PWP	−12.68	−0.92	13.60
$F_{\alpha 2}$	LDA	−103.78	−88.69	192.47
	PWP	−98.90	−84.79	183.69
$F_{\beta 0}$	LDA	−34.55	−31.88	66.43
	PWP	−33.22	−30.20	63.42
$F_{\beta 1}$	LDA	−9.04	−7.74	16.78
	PWP	−9.95	−7.91	17.86
$H_{\beta 2}$	LDA	−2.50	−1.30	3.80
	PWP	−2.50	−1.3.)	3.80
CHF$_2$−CF$_2$				
C_α	LDA	−24.55	−23.78	48.33
	PWP	−25.32	−24.88	50.20
C_β	LDA	−2.76	−2.68	5.43
	PWP	−2.96	−2.62	5.58
$F_{\alpha 1}$, $F_{\alpha 2}$	LDA	−80.52	−71.66	152.18
	PWP	−79.97	−69.23	148.20
$H_{\beta 0}$	LDA	−2.39	−0.57	2.96
	PWP	−2.29	−0.69	2.98
$F_{\beta 1}$, $F_{\beta 2}$	LDA	−3.50	−1.28	4.78
	PWP	−3.30	−0.70	3.90
CF$_3$−CHF				
C_α	LDA	−26.92	−25.93	52.85

Table 4.2 (continued)

Nucleus	Method	T_x	T_y	T_z
	PWP	−28.19	−27.09	55.29
	PWP′	−28.87	−27.67	56.54
C_β	LDA	−1.41	−0.52	1.93
	PWP	−1.32	−0.68	2.00
	PWP′	−1.48	−0.42	1.89
$F_{\alpha 1}$	LDA	−106.16	−90.44	196.60
	PWP	−102.39	−86.09	188.48
	PWP′	−99.11	−87.27	186.38
$H_{\alpha 2}$	LDA	−12.51	−1.31	13.82
	PWP	−12.85	−1.00	13.85
	PWP′	−13.14	−0.58	13.72
$F_{\beta 0}$	LDA	−28.53	−27.92	56.45
	PWP	−27.57	−25.85	53.42
	PWP′	−25.50	−24.10	49.60
$F_{\beta 1}$	LDA	−10.21	−10.04	20.25
	PWP	−10.00	−9.40	19.39
	PWP′	−17.35	−16.59	33.94
$F_{\beta 2}$	LDA	−7.82	−6.28	14.10
	PWP	−7.67	−6.94	14.62
	PWP′	−8.68	−7.00	15.68
$CF_3 - CF_2$				
C_α	LDA	−24.71	−23.88	48.59
	PWP	−25.54	−24.96	50.50
C_β	LDA	−2.26	−2.22	4.48
	PWP	−2.54	−2.20	4.74
$F_{\alpha 1}$, $F_{\alpha 2}$	LDA	−82.70	−75.24	157.94
	PWP	−78.84	−73.64	152.48

Table 4.2 (continued)

Nucleus	Method	T_x	T_y	T_z
$F_{\beta 0}$	LDA	-24.25	-23.17	47.42
	PWP	-23.76	-21.65	45.41
$F_{\beta 1}$, $F_{\beta 2}$	LDA	-3.14	-3.03	6.17
	PWP	-4.02	-2.59	6.62

[a] direction of principal axes given in Figure 2. [b] argon matrix at 4.2 K.; Ref. 125; determined to be axially symmetric about the $C-C$ bond. [c] solution spectra, 77 K; Ref. 128; given as $A_\perp = 34.9$, $A_\parallel = 212.1$, $2B = 118.1$; calculated from the relations $A_\perp = A_{iso} + 1/2\,(T_x + T_y)$, $A_\parallel = A_{iso} + T_z$, $2B = T_z$. [d] in argon matrix at 4.2 K.; Ref. 123. Their A_{iso} values subtracted from $A_{x/y/z}$ to get $T_{x/y/z}$.

Due to decreasing overlap with increasing out-of-plane angle, the hfs of the out-of-plane β-atoms (with respect to the C_α p_y orbital) decreases in magnitude. This has also been observed in the case of, $e.g.$, the couplings on β-hydrogens in alkene radical cations.[133a] Furthermore, note that the functional dependence is much smaller for the anisotropic couplings than for the isotropic ones, in agreement with the results reported in, $e.g.$, ref. 67b, 134a and 134b.

Experimental anisotropic spectra have been reported for only three radicals in the series, and none of these assigned tensors to all nuclei. The agreement of the present results to experiment is mixed. For CH_3-CH_2 the experimental hfs has been analyzed as being axially symmetric about the $C-C$ bond (x direction). The H_α results are several gauss higher than experiment, while the H_β results agree almost exactly in magnitude; the signs are opposite, but it could be that, as for the isotropic spectra, the experimental assignment is incorrect. For CH_3-CF_2 the agreement is fairly good, with relative errors ranging from 10% to 21% for the PWP results. The worst agreement is for CF_3-CH_2; this case is discussed in more detail below.

4.4 Hyperfine Coupling Constants from DFT Optimized Geometries

For cases where calculations on the MP2 geometries gave poor agreement with experiment the geometries were also optimized by Leif Eriksson[140] at the DFT/PWP level (see Table 4.3 for geometrical parameters; numbering system as shown in Figure 2). In general, DFT gives slightly shorter $C-C$ bond lengths, slightly longer $C-H$ bond lengths, sometimes significantly longer $C-F$ bond lengths, and deviations of up to a few

degrees in interatomic angles in comparison to the MP2 structures. Since there are no accurate experimental geometries to compare to, it is difficult to say which method is more accurate, although the MP2 method gave satisfactory agreement with experiment for the parent ethanes (see Chapter 5), and previous work on fluorine species[67b,c,141] shows that DFT has a tendency to overestimate bond lengths to fluorine. The hyperfine coupling constants as calculated by Leif Eriksson are listed in Tables 4.1 and 4.2 as the PWP' method. As a whole the results are very similar to those obtained from the MP2 geometries (see PWP method), with some minor improvements.

For CH_3-CHF coupling constants were calculated for both C_1 and C_s conformers with the PWP' method. While the latter conformer is unlikely to be the most stable (only a C_1 conformer was found to be a minimum in a search of the potential energy surface using the HF/6-31G(d) method[142]) as it has an artificial constraint of a 180° FCCH dihedral angle, the results are nevertheless almost identical for both conformers. This suggests that rotation about the $C-C$ bond is unimportant to the hyperfine structure, in agreement with the results of Chen et al.[121] who found no evidence for restricted rotation of the CH_3 group.

For CH_2F-CH_2, the main difference between the hfs of the DFT and MP2 optimized geometries is in the fluorine couplings. The DFT geometry gave better agreement with experiment for the isotropic fluorine, as well as H_β, couplings. The C_s conformer was also optimized, but the resultant couplings gave very poor agreement with experiment, suggesting that the most stable conformer is asymmetric, in agreement with the ab initio energy results (see Chapter 3).

Table 4.3: Selected Geometrical Parameters for CH_2F-CH_2, CH_3-CHF, CF_3-CH_2, and CF_3-CHF Using DFT and MP2 Theory[a]

Parameter	DFT[b]	MP2[c]
CH_2F-CH_2		
$C_\alpha-C_\beta$	1.472	1.479
$C_\beta-F_\beta$	1.433	1.396
$C_\beta-H_{\beta0}$	1.102	1.095
$C_\beta-H_{\beta2}$	1.096	1.091
$F_\beta-C_\beta-C_\alpha$	110.2	110.1
$H_\alpha-C_\alpha-H_\alpha$	119.4	119.0
$H_\beta-C_\beta-H_\beta$	108.4	107.7
CH_3-CHF		
$C_\alpha-C_\beta$	1.473	1.481
$C_\alpha-F_\alpha$	1.375	1.360
$C_\alpha-H_\alpha$	1.082	1.081
$C_\beta-H_{\beta0}$	1.104	1.093
$F_\alpha-C_\alpha-C_\beta$	117.5	114.4
$H_\alpha-C_\alpha-C_\beta$	128.8	122.2
$H_{\beta0}-C_\beta-C_\alpha$	113.2	111.6
CF_3-CH_2		
$C_\alpha-C_\beta$	1.471	1.477
$C_\beta-F_{\beta0}$	1.389	1.357
$C_\beta-F_{\beta1,2}$	1.370	1.351
$C_\alpha-H_\alpha$	1.082	1.074
$F_{\beta0}-C_\beta-C_\alpha$	111.8	112.1
$F_{\beta1,2}-C_\beta-C_\alpha$	112.1	111.7
$H_\alpha-C_\alpha-H_\alpha$	121.7	120.9

Table 4.3 (continued)

Parameter	DFT[b]	MP2[c]
CF_3-CHF		
$C_\alpha-C_\beta$	1.481	1.485
$C_\alpha-H_\alpha$	1.084	1.077
$C_\alpha-F_\alpha$	1.348	1.339
$C_\beta-F_{\beta 0}$	1.375	1.353
$F_{\beta 0}-C_\beta-C_\alpha$	112.7	112.3
$F_{\beta 1}-C_\beta-F_{\beta 2}$	108.2	108.9
$H_\alpha-C_\alpha-F_\alpha$	117.0	115.7
$H_\alpha-C_\alpha-C_\beta$	122.9	120.6

[a] Bond lengths in angstroms, bond angles in degrees. [b] This chapter; see text for details.
[c] Chapter 3, which gives a more complete geometry description.

A problem case is CF_3-CH_2, for which the DFT and MP2 optimized structures gave similar results. After subtracting the isotropic couplings to get "experimental" $T_{x/y/z}$ values, and interchanging the x and z axes to obtain correspondence, the agreement is poor, except that the T_x values are close in magnitude. It could be that DFT does not work in this case, but there is also the possibility that the experimental interpretation is wrong, given the logical consistencies noted in the general trends of the present results, the good agreement obtained for isotropic couplings for the other radicals, and the well-documented trend for DFT to give more accurate results for anisotropic versus isotropic couplings.[67b,134a,b,143] Note that the authors[123] were not completely confident in their interpretation of their spectra. There were strong singularities that were not completely accounted for, and they concluded that "... features of the spectra can be explained at

least qualitatively". If it is the theoretical results that are incorrect, one explanation can be sought in an insufficiency to describe the very strongly electron withdrawing CF_3 group properly, *i.e.*, that the unpaired electron becomes too strongly associated with the radical centre. However, since the isotropic couplings (*cf.* Table 4.1) are in excellent agreement with experiment, such an explanation seems less likely. Also, since both the MP2 and DFT geometries give very similar results, a faulty geometry also seems improbable.

For CF_3-CHF, better agreement with experiment was obtained for the hydrogen A_{iso} value, but somewhat worse agreement for the F_α coupling. The anisotropic PWP′ results are in good agreement with those obtained by the PWP method using the MP2 geometries. These results are consistent with a very simplistic picture, that at first approximation (due to the nature of the integrals) the bond lengths strongly affect the isotropic couplings, while the anisotropic part is more sensitive to changes in bond angles. Thus a too long $C-F$ bond leads to an inaccurate fluorine isotropic coupling, while minor variations in bond angles (see Table 4.3) have minor effects on the anisotropic hyperfine structure.

4.5 Conclusions

For most of the radicals in the series satisfactory agreement with experiment is obtained with the gradient corrected method (PWP). While the LDA method is less satisfactory the same qualitative trends can be seen in the results. When the hyperfine structures are calculated from DFT optimized geometries, the results are very similar to

those from the MP2 optimized geometries. The high level of agreement obtained for the radicals for which there are experimental determinations, and the logical consistencies in the noted trends, suggest that these results will be useful as a guide in completing the remaining experiments in the series.

Chapter 5. Structural and Energetic Properties of the Series $C_2H_nF_{6-n}$, n = 0−6

5.1 Introduction

There have been many *ab initio* studies of the HFCs noted in Chapter 1, and other fluorinated ethanes. One of the earliest presented maps of the electrostatic potential around halogenated anaesthetics, including CHF_2-CH_3, CF_3-CH_3, and CF_3-CHF_2.[144] Sana *et al.*[145] calculated heats of formation of several organic compounds, including CHF_2-CH_3, CF_3-CH_3, and CF_3-CH_2F. Challocombe and Cioslowski[146] calculated the harmonic and anharmonic force constants for C_2H_6, CHF_2-CH_3, CF_3-CH_3, CHF_2-CHF_2, and C_2F_6. For CHF_2-CH_3 there has also been an evaluation of the strain energy,[147] and a study of basis set and correlation energy dependence of geometry and harmonic frequencies.[148] Cooper and co-workers have reported *ab initio* SCF geometry optimizations, using various basis sets, of perfluoroalkane molecules, including perfluoroethane,[149] and a similar study (also including semi-empirical results) on several fluorine and chlorine substituted alkanes, including CF_3-CH_3, CF_3-CH_2F, and CF_3-CHF_2.[150] Perfluoroethane was also included in a study of structural changes as a function of torsional motion, by Mastryukov *et al.*[151] Magnusson has published two systematic studies which included CF_3-CH_3, one on conformational preference,[152] the other on the structural and energetic consequences of hyperconjugation.[153] A study of substituent effects in methyl derivatives, including CF_3-CH_3, reported geometries, bond path angles, and electron populations.[154] Other studies on this molecule include one on the chirality of the electron distribution in the methyl group,[155] and a scale of direct

substituent polarizability parameters from polarization potentials.[156] Esseffar *et al.*[157] performed a topological analysis of bond activations by protonation on several alcohols and fluoroalkanes, including fluoroethane. A study of the structures, barriers for internal rotation, vibrational frequencies, and thermodynamic functions of CHF_2-CH_2F and CHF_2-CHF_2 was recently reported by Chen *et al.*[158] Another recent report was the calculation of vibrational frequencies and infrared intensities for the global warming potential of CF_3-CH_2F, by Papasavva *et al.*[159]

The most extensively studied molecule in the series is 1,2-difluoroethane, which is of structural interest because it exhibits the gauche effect.[160] The energy differences and rotational barrier between the gauche and *anti* forms have been the subject of several *ab initio* investigations.[161 − 168] Geometry optimizations have also been performed at various levels of theory.[169] A recent publication of experimental and *ab initio* results[170] included conformational analysis, barriers to internal rotation and vibrational assignments.

While the previous literature on theoretical studies of fluorinated ethanes is fairly extensive, the first systematic studies of the full series, $C_2H_nF_{6-n}$ (n = 0−6) were reported as part of this research.[171,172] Geometries were optimized at the HF/6-31G(d) level for all the staggered conformers in the title series. Frequency analyses indicated energy minima in all cases. Single-point energy calculations up to the MP2/6-31G(d,p)//HF/6-31G(d) level were performed on all these conformers; further calculations were performed (and results are presented) only for the most stable conformer of each structural isomer. The relative stabilities determined using HF and

MP2 theory were the same except for the case of 1,2-difluoroethane. Results at the HF/6-31G(d) level indicated that the *anti* conformer was more stable; however, experimental and theoretical results[173] have shown that the gauche form is the most stable. The present MP2 energy results have confirmed the latter finding. Geometries were optimized at the MP2/6-31G(d,p) level only for the most stable conformer of each structural isomer in the title series.

5.2 Optimized Geometries

Optimized geometries at the HF/6-31G(d) level are presented in Figure 6. Full geometry specification of CHF_2-CH_2F, which has C_1 symmetry, requires a dihedral angle, which is given in the figure caption. There are two opposing trends in the $C-C$ bond lengths: they decrease as more F atoms are added to one C atom, but increase again as more F atoms are added to the second C atom. This is consistent with an increasing electronegativity difference between bonded atoms leading to a stronger bond. The $C-H$ bond lengths generally decrease slightly with increasing number of F atoms in the molecule, with shorter lengths on the more highly substituted carbon. An electronegative substituent should lead to increased s character in the $C-H$ bonds, and it is well recognized that this leads to shorter bonds.[174] The $C-F$ bond lengths are the most variable (range = 0.062Å). The general trend is similar to that for $C-H$, but the correlation is not as strong. These results lend credence to the simple electrostatic model of Cooper *et al.*,[150] who were unable to reproduce the desired trend in $C-F$ bond lengths using semi-empirical methods.
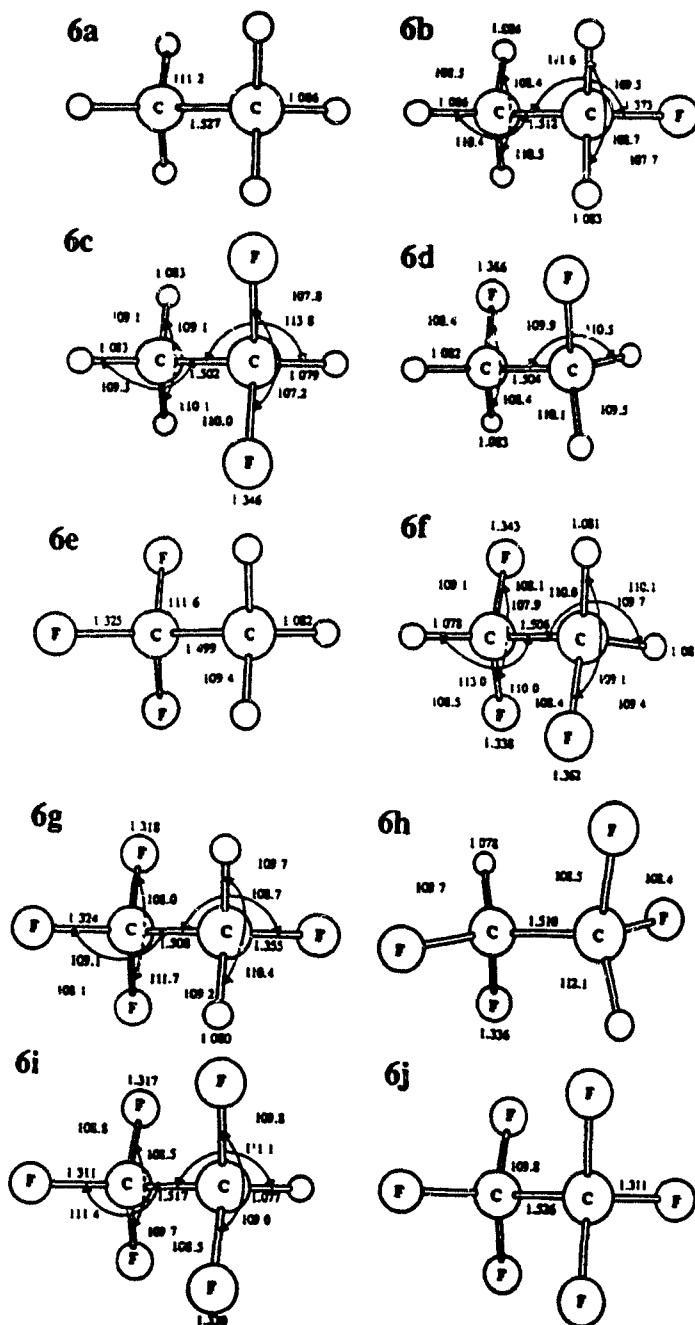
Figure 6. HF/6-31G(d) optimized geometries for molecules: **6a** ethane (D_{3d}); **6b** fluoroethane (C_s); **6c** 1,1-difluoroethane (C_s); **6d** gauche-1,2-difluoroethane (C_2); **6e** 1,1,1-trifluoroethane (C_{3v}); **6f** 1,1,2-trifluoroethane (C_1) $\phi_{FCCF} = 67.3°$; **6g** 1,1,1,2-tetrafluoroethane (C_s); **6h** trans-1,1,2,2-tetrafluoroethane (C_{2h}); **6i** pentafluoroethane (C_s); **6j** hexafluoroethane (D_{3d}). Bond lengths in angstroms, bond angles in degrees. Drawings are in perspective, with relative radii of 1 : 1.667 : 2 for H, F, and C atoms, respectively. For curved arrows, the corresponding bond angle is that written closest to the arrow. Dashed arrows through an atom indicate the bond angle is behind. Unlabelled atoms are hydrogens.

Angles between atoms attached to the same carbon show little variance. HCH angles vary about $\pm 1°$ from the tetrahedral angle, with lower values for molecules which contain only one or two fluorines, and higher values for more highly substituted molecules. HCF angles have a somewhat similar trend, but with a bias towards lower values, as expected because of the increased s character in the C−H bonds.[92] FCF angles are all smaller than tetrahedral, with the effect more pronounced for less substituted molecules. The FCC and HCC angles are more variable, with the only easily discernible pattern being that FCC angles tend to be smaller than HCC angles within the same molecule.

Optimized geometries at the MP2/6-31G(d,p) level are presented in Figure 7. Most of the trends seen in the HF/6-31G(d) optimized structures are also manifested here, so comments will be restricted to differences between the two levels of optimization. The most obvious difference is the lengthening of the C−F bonds when electron correlation is included, as expected. The C−C bond lengths are slightly shorter, with the degree of difference inversely correlated with number of fluorines, except for the highly substituted structures **7h** − **7j**, which have lengths longer by 0.001 − 0.002 Å compared with the HF/6-31G(d) optimized structures. There is almost no variability in the C−H bond lengths (1.088 ± 0.002 Å, except for a minimum of 1.085 Å in **7e**, cf. 1.077 − 1.086 Å previously). Shorter lengths within a molecule are on the less substituted carbon, contrary to the HF/6-31G(d) optimized structures, and the model of increased s character leading to shorter bonds,[174] but it is risky to call this a trend since the bond length differences are almost negligible. The interatomic angles are all
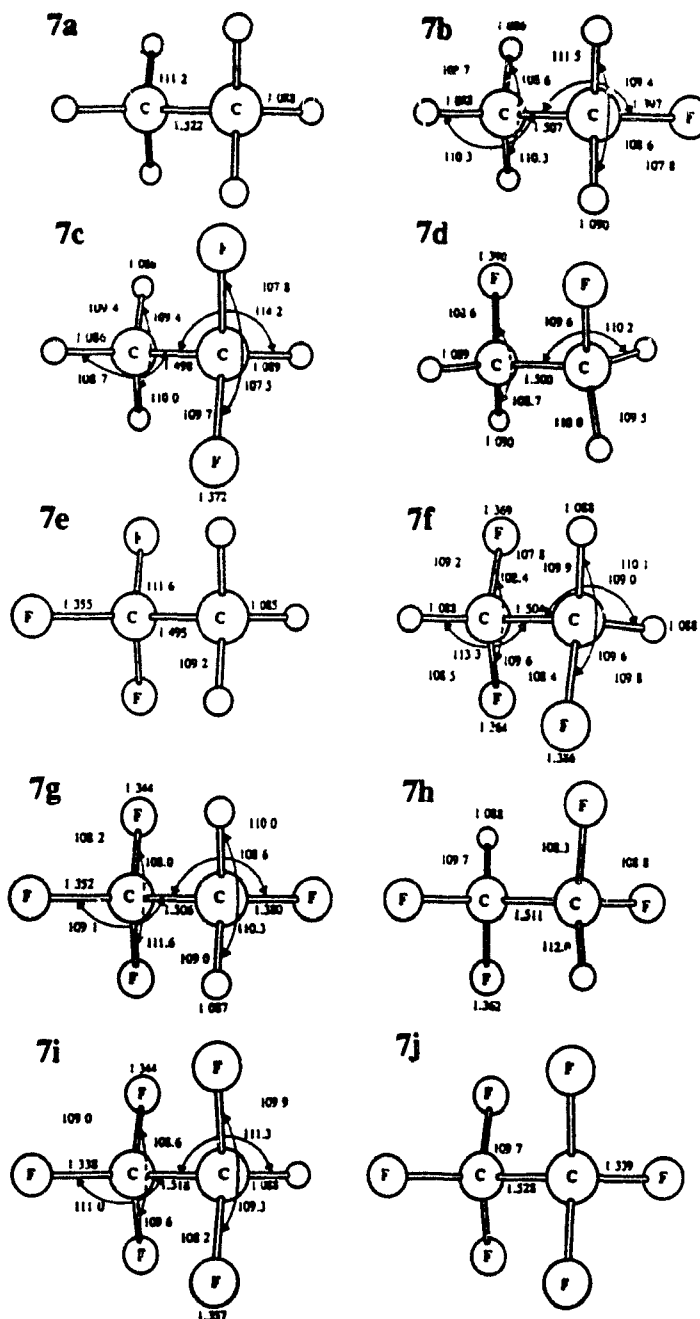
Figure 7. MP2/6-31G(d,p) optimized geometries for molecules: **7a**, ethane (D_{3d}); **7b**, fluoroethane (C_s); **7c**, 1,1-difluoroethane (C_s); **7d**, gauche-1,2-difluoroethane (C_2); **7e**, 1,1,1-trifluoroethane (C_{3v}); **7f**, 1,1,2-trifluoroethane (C_1) $\phi_{FCCF} = 66.3°$; **7g**, 1,1,1,2-tetrafluoroethane (C_{3v}); **7h**, trans-1,1,2,2-tetrafluoroethane (C_{2h}); **7i**, pentafluoroethane (C_s); **7j**, hexafluoroethane (D_{3d}) Bond lengths are in angstroms and bond angles in degrees. Drawings are in perspective, with relative radii of 1 : 1.667 : 2 for H, F, and C atoms, respectively. For curved arrows, the corresponding bond angle is that written closest to the arrow. Dashed arrows through an atom indicate the bond angle is behind. Unlabelled atoms are hydrogens.

within 0.5 (and usually 0.2) degrees of those previously optimized.

A complete comparison of the optimized geometries with experiment is precluded by a lack of experimental data for some of the molecules. In any case, the reliability of HF/6-31G(d) geometries has already been documented.[175] Lengths for single bonds have a mean absolute error of 0.02 Å (usually to the low side of experiment), with the largest deviations being for polar bonds such as C–F. Bond angles can be expected to be accurate to within $\pm 2.0°$ in most cases, and often within $\pm 1.0°$. There is as yet insufficient data to accurately quantify the agreement with experiment of MP2 optimized structures, but a higher level of theory is expected to give more accurate results. Indeed, Schleyer et al.[176,177] have recently claimed that structures calculated at this level of theory can be more accurate than experimentally determined structures.

Table 5.1 compares the results obtained at the two levels of theory with experiment[178,179] for two molecules for which extensive experimental data is available, fluoroethane and 1,2-difluoroethane. While the HF/6-31G(d) results give satisfactory agreement with experiment for most parameters, a significant improvement is observed for all bond lengths with inclusion of electron correlation. For bond angles, both methods give about equal agreement with experiment, with some minor improvements due to inclusion of electron correlation.

Table 5.1: Comparison of Geometrical Parameters of Fluoroethane and 1,2-Difluoroethane Using Different Levels of Theory with Experimental Results[a]

Parameter	Fluoroethane			1,2-Difluoroethane		
	HF/6-31G(d)	MP2/6-31G(d,p)	exptl[b]	HF/6-31G(d)	MP2/6-31G(d,p)	exptl[c]
C−C	1.512	1.507	1.505	1.504	1.500	1.493
C−F	1.373	1.397	1.398	1.366	1.390	1.390
C−H[d]	1.084	1.086	1.090	1.082	1.089	1.099
	1.086	1.088	1.091	1.083	1.090	1.093
	1.083	1.090	1.095			
∠CCF	109.5	109.4	109.7	109.9	109.6	110.6
∠CCH[d]	110.5	110.3	N/A	110.5	110.2	108.4
	110.4	110.3	109.7	110.1	110.0	111.3

Table 5.1 (c⁻ ntinued)

Parameter	Fluoroethane			1,2-Difluoroethane		
	HF/6-31G(d)	MP2/6-31G(d,p)	exptl[b]	HF/6-31G(d)	MP2/6-31G(d,p)	exptl[e]
	111.6	111.5	112.9			
∠HCF[c]	107.7	107.8	106.1	108.4	108.6	109.6
				108.4	108.7	107.8
∠HCH[f]	108.5	108.7	108.7	109.5	109.5	109.1
	108.4	108.6	108.9			
	108.7	108.6	108.8			

[a] Bond lengths in angstroms, bond angles in degrees. [b] Reference 178. [c] Reference 179. [d] First value is for H gauche to F. Second value is for H trans to F. Third value is for H geminal to F. [e] First value is for H gauche to F. Second value is for H trans to F. [f] First value is for Hs gauche and trans to F. Second value is for Hs gauche and gauche to F. Third value is for Hs geminal to F.

5.3 Vibrational Frequencies

Values of vibrational frequencies at both levels of theory used for geometry optimizations (and from experiment where available[100,159]), along with their reduced masses, symmetry, and approximate type, are given in Table 5.2. All frequencies are lower using MP2 theory, except for the torsion mode, which is slightly higher. In general, there is little coupling between modes, and the type of mode is the same at both levels of theory. Exceptions occur for CH_2F-CH_3, CHF_2-CH_3, and CHF_2-CH_2F, where the $C-H$ stretching modes are coupled at HF, but not MP2, theory. For each molecule the mode types are as expected from the principles given by Shimanouchi,[100] except for CHF_2-CHF_2, where there is only one CF_2 rock, but three $C-H$ bends. The reduced masses and eigenvectors of the frequencies leave no doubt as to the assignment; there is virtually no motion of the fluorines in any of the three $C-H$ bending modes.

The calculated frequencies are in most cases systematically high in comparison to experiment, by ~10% at the HF level and ~6% at MP2, although the amount varies within a few % for individual frequencies. For some of the low frequency $C-F$ bending modes, the MP2 results are equal to or slightly less than experiment, and for some others they are only ~3% too high. This excellent agreement is encouraging, given the challenges that fluorine atoms provide to computational chemists.

Table 5.2: Vibrational Frequencies for Each Molecule at Two Levels of Theory

Frequency (cm^{-1})			Reduced mass (amu)		Sym	Approx. type of mode
HF	MP2	Expt[a]	HF	MP2		
CH$_3$–CH$_3$						
326	337	289	1.008	1.008	a$_{1u}$	CH$_3$–CH$_3$ torsion
889	847	822	1.056	1.057	e$_u$	CH$_3$ rock
1062	1051	995	3.132	3.068	a$_{1g}$	C–C stretch
1338	1270	1190	1.455	1.460	e$_g$	CH$_3$ rock
1548	1460	1379	1.198	1.198	a$_{2u}$	CH$_3$ symmetric deformation
1580	1489	1388	1.274	1.284	a$_{1g}$	CH$_3$ symmetric deformation
1644	1567	1468	1.021	1.020	e$_g$	CH$_3$ degenerate deformation
1650	1570	1469	1.063	1.062	e$_u$	CH$_3$ degenerate deformation
3200	3138	2896	1.034	1.034	a$_{2u}$	CH$_3$ symmetric stretch
3206	3138	2954	1.038	1.039	a$_{1g}$	CH$_3$ symmetric stretch
3249	3221	2969	1.103	1.103	e$_g$	CH$_3$ degenerate stretch
3274	3241	2985	1.104	1.103	e$_u$	CH$_3$ degenerate stretch
CH$_2$F–CH$_3$						
273	281	243	1.130	1.130	a″	CH$_2$F–CH$_3$ torsion
440	414	415	2.929	2.894	a′	C–C–F bend
877	835	810	1.078	1.075	a″	CH$_2$ + CH$_3$ rock
971	928	1048	2.178	2.130	a′	CH$_3$ rock
1169	1121	1048	3.115	3.429	a′	C–C stretch
1240	1169	880	2.296	2.172	a′	C–F stretch
1309	1233	1108	1.540	1.502	a″	CH$_3$ + CH$_2$ rock

Table 5.2 (continued)

Frequency (cm⁻¹)			Reduced mass (amu)		Sym	Approx. type of mode
HF	MP2	Expt[a]	HF	MP2		
1587	1490	1395	1.350	1.378	a'	CH_3 symmetric deformation + CH_2 wag
1627	1548	1449	1.042	1.041	a″	CH_3 degenerate deformation
1645	1564	1449	1.067	1.057	a″	CH_3 degenerate deformation
1683	1593	1479	1.097	1.096	a'	CH_2 scissors
3213	3145	2915	1.037	1.039	a'	CH_3 symmetric stretch
3244	3141	2941	1.059	1.055	a'	CH_2 symmetric stretch
3276			1.108		a″	CH_2 asymmetric + CH_3 degenerate stretch
	3201	3003		1.110	a″	CH_2 asymmetric stretch
3281	3243	3003	1.101	1.102	a'	CH_3 degenerate stretch
3302			1.109		a″	CH_2 asymmetric + CH_3 degenerate stretch
	3256	3003		1.105	a″	CH_3 degenerate stretch
CH₂F−CH₂F						
150	152		4.701	5.237	a	CH_2F-CH_2F torsion
348	331		2.641	2.491	a	$C-C-F$ bend
541	508		2.437	2.407	b	$C-C-F$ bend
956	915		2.540	2.525	a	CH_2 rock
1002	938		1.979	1.988	b	CH_2 rock
1211	1132		3.685	3.676	b	C-F asymmetric stretch
1230	1163		2.953	3.265	a	$C-C$ stretch
1251	1179		2.195	1.996	a	$C-F$ symmetric stretch
1383	1293		1.110	1.110	b	CH_2 twist

Table 5.2 (continued)

Frequency (cm⁻¹)			Reduced mass (amu)		Sym	Approx. type of mode
HF	MP2	Expt[a]	HF	MP2		
1606	1501		1.531	1.569	a	CH_2 wag
1658	1563		1.094	1.093	b	CH_2 scissors
1662	1567		1.111	1.102	a	CH_2 scissors
3242	3138		1.059	1.057	b	CH_2 symmetric stretch
3258	3147		1.060	1.060	a	CH_2 symmetric stretch
3300	3209		1.110	1.109	a	CH_2 asymmetric stretch
3314	3220		1.108	1.109	b	CH_2 asymmetric stretch
CHF₂−CH₃						
258	267		1.065	1.063	a″	CH_3 rock
408	386		3.083	3.033	a″	CHF_2-CH_3 torsion
503	469		4.360	4.725	a′	CF_2 rock
614	571		4.238	3.878	a′	CF_2 scissor
948	905		2.216	2.2000	a′	CF_2 wag
1072	1000		1.839	1.937	a″	CF_2 twist
1254	1190		2.305	2.868	a′	CF_2 symmetric stretch
1283	1202		2.841	2.266	a′	C−C stretch
1298	1208		2.708	2.554	a″	CF_2 asymmetric stretch
1540	1443		1.235	1.237	a′	CH_3 rock
1558	1455		1.213	1.220	a″	C−H bend
1603	1500		1.486	1.576	a′	CH_3 symmetric deformation
1630	1550		1.084	1.053	a′	CH_3 degenerate deformation
1633	1551		1.068	1.059	a″	CH_3 degenerate deformation

Table 5.2 (continued)

Frequency (cm^{-1})			Reduced mass (amu)		Sym	Approx. type of mode
HF	MP2	Expt[a]	HF	MP2		
	3179			1.089	a'	C−H stretch
3306	3264		1.104	1.104	a"	CH$_3$ degenerate stretch
3324			1.095		a'	C−H + CH$_3$ degenerate stretch
	3269			1.104	a'	CH$_3$ degenerate stretch
CF$_3$−CH$_3$						
251	261		1.042	1.041	a$_2$	CF$_3$−CH$_3$ torsion
392	368		3.898	3.974	e	CF$_3$ rock
585	538		7.944	7.471	e	CF$_3$ degenerate deformation
646	604		6.174	6.768	a$_1$	CF$_3$ symmetric deformation
908	845		7.808	7.344	a$_1$	CF$_3$ symmetric stretch
1095	1014		1.718	1.840	e	CH$_3$ rock
1415	1301		4.768	4.146	e	CF$_3$ degenerate stretch
1430	1340		3.366	3.172	a$_1$	CH$_3$ symmetric deformation
1601	1496		1.642	1.677	a$_1$	C−C stretch
1627	1548		1.062	1.055	e	CH$_3$ degenerate deformation
3246	3170		1.036	1.035	a$_1$	CH$_3$ symmetric stretch
3330	3282		1.106	1.105		CH$_3$ degenerate stretch
CHF$_2$−CH$_2$F						
128	128		4.353	4.459	a	CHF$_2$−CH$_2$F torsion
263	243		6.121	6.092	a	CF$_2$ rock
462	431		8.980	8.860	a	CF$_2$ wag

Table 5.2 (continued)

Frequency (cm^{-1})			Reduced mass (amu)		Sym	Approx. type of mode
HF	MP2	Expt[a]	HF	MP2		
1003	946		2.263	2.265	a	CH$_2$ rock + C−F stretch
1210	1132		5.910	5.685	a	C−C−F bend
1244	1161		3.312	5.918	a	C−F stretch
1259	1184		2.949	2.282	a	C−F stretch + CH$_2$ rock
1292	1206		2.832	2.765	a	C−F stretch
1386	1299		1.151	1.150	a	CH$_2$ twist
1492	1391		1.229	1.226	a	CH$_2$ wag
1570	1466		1.286	1.270	a	C−H bend
1631	1519		1.698	1.745	a	C−C stretch
1664	1568		1.118	1.095	a	CH$_2$ scissors
3274	3163		1.058	1.058	a	CH$_2$ symmetric stretch
3327			1.102		a	CH$_2$ asymmetric + C−H stretch
	3196			1.089	a	C−H stretch
3344			1.010		a	C−H + CH$_2$ asymmetric stretch
	3240			1.111	a	CH$_2$ asymmetric stretch

CF$_3$−CH$_2$F[b]

117	116	110	5.031	5.243	a″	CF$_3$−CH$_2$F torsion
233	216	225	15.826	15.744	a′	CF$_3$ rock
382	359	358	3.271	3.262	a″	CH$_2$ + CF$_3$ rock
446	414	408	13.539	13.804	a′	F−C−C bend
578	531	540	8.373	7.883	a″	CF$_3$ + CH$_2$ rock

Table 5.2 (continued)

Frequency (cm⁻¹)			Reduced mass (amu)		Sym	Approx. type of mode
HF	MP2	Expt[a]	HF	MP2		
928	867	843	7.213	6.984	a′	CF₃ symmetric stretch
1098	1022	973	1.856	1.923	a″	CF₃ degenerate deformation
1234	1149	1104	5.827	5.962	a′	C−F stretch
1344	1250	1191	1.474	1.644	a″	CH₂ twist
1362	1249	1185	6.255	7.607	a′	CF₃ degenerate stretch + CH₂ wag
1460	1362	1301	3.695	3.320	a′	CF₃ degenerate stretch + CH₂ wag
1472	1366	1294	2.483	2.036	a″	CF₃ degenerate stretch
1621	1511	1428	1.863	1.965	a′	C−C stretch
1663	1566	1462	1.143	1.100	a′	CH₂ scissors
3286	3172	2981	1.058	1.058	a′	CH₂ symmetric stretch
3349	3249	3010	1.113	1.111	a″	CH₂ asymmetric stretch
CHF₂−CHF₂						
95	91		10.696	10.783	aᵤ	CHF₂−CHF₂ torsion
220	204		18.595	18.552	aᵤ	CF₂ twist
390	364		17.985	18.180	a_g	CF₂ wag
454	418		3.570	3.560	bᵤ	CF₂ wag
533	496		11.530	11.397	b_g	CF₂ twist
585	537		15.149	15.236	bᵤ	CF₂ scissors
679	629		10.427	10.356	a_g	CF₂ scissors
1226	1149		6.911	6.730	a_g	CF₂ symmetric stretch
1258	1169		9.166	9.003	bᵤ	CF₂ symmetric stretch
1276	1174		4.245	4.693	b_g	CF₂ asymmetric stretch

Table 5.2 (continued)

Frequency (cm^{-1})			Reduced mass (amu)		Sym	Approx. type of mode
HF	MP2	Expt[a]	HF	MP2		
1462	1361		1.283	1.288	b$_u$	C−H bend
1526	1419		1.238	1.209	a$_u$	C−H bend
1556	1448		1.313	1.275	b$_g$	C−H bend
1657	1534		2.053	2.024	a$_g$	C−C stretch
3344	3203		1.091	1.090	a$_g$	C−H symmetric stretch
3354	3213		1.090	1.089	b$_u$	C−H asymmetric stretch

CF$_3$−CHF$_2$

81	78		13.481	13.578	a″	CHF$_2$−CF$_3$ torsion
225	210		18.649	18.650	a″	CF$_2$ twist
263	246		14.259	14.169	a′	CF$_2$ wag
393	366		17.857	18.125	a′	CF$_2$ rock
455	418		15.513	15.519	a″	CF$_3$ rock
565	518		15.320	15.515	a′	CF$_3$ rock
626	576		9.803	9.755	a′	CF$_2$ scissors
638	589		16.221	16.110	a″	CF$_3$ degenerate deformation
791	728		12.503	13.230	a′	CF$_3$ degenerate deformation
962	898		5.914	5.845	a′	CF$_3$ symmetric deformation
1266	1174		6.514	6.354	a′	CF$_2$ symmetric stretch
1309	1202		4.234	4.878	a″	CF$_2$ asymmetric stretch
1363	1253		3.454	4.286	a′	CF$_3$ degenerate stretch
1407	1284		12.977	13.166	a″	CF$_3$ degenerate stretch
1483	1373		3.615	3.078	a′	CF$_3$ symmetric stretch

Table 5.2 (continued)

Frequency (cm^{-1})			Reduced mass (amu)		Sym	Approx. type of mode
HF	MP2	Expt[a]	HF	MP2		
3355	3211		1.090	1.089	a$'$	C$-$H stretch
CF$_3$$-CF_3$						
70	68	68	18.998	18.998	a$_{1u}$	CF$_3$$-CF_3$ torsion
230	214	220	18.652	18.653	e$_u$	CF$_3$ rock
378	354	348	18.635	18.663	a$_{1g}$	CF$_3$ symmetric deformation
415	380	372	18.758	18.762	e$_g$	CF$_3$ rock
564	517	520	18.221	18.233	e$_u$	CF$_3$ degenerate deformation
674	622	619	17.863	17.905	e$_g$	CF$_3$ degenerate deformation
774	707	714	17.025	17.087	a$_{2u}$	CF$_3$ symmetric deformation
888	815	807	18.280	18.332	a$_{1g}$	CF$_3$ symmetric stretch
1243	1153	1117	13.909	13.868	a$_{2u}$	CF$_3$ symmetric stretch
1426	1293	1250	12.869	12.840	e$_g$	CF$_3$ degenerate stretch
1434	1308	1251	13.374	13.367	e$_u$	CF$_3$ degenerate stretch
1627	1505	1228	12.463	12.427	a$_{1g}$	C$-$C stretch

[a] Taken from ref 100, except where indicated.   [b] Reference 159.

5.4 Total Energies and Zero-Point Energies

Total energies calculated with various basis sets at the MP2 level, using the HF/6-31G(d) optimized geometries, are given in Table 5.3. For all the fluorinated ethanes, a small improvement is seen when polarization functions are included on hydrogens, while going from a double to triple split-valence basis set gives a more dramatic improvement. Energies become more negative with increasing number of fluorines. In all cases where there is more than one isomer, the most stable one is that in which as many fluorines as possible are on one carbon. This can be readily understood in terms of the geminal effect.[116] When two substituents on the same atom are both strong σ-acceptors and strong π-donors, (e.g., F) there is a strongly stabilizing interaction. Thus, having a carbon atom fully substituted with fluorines should be particularly stabilizing.

The gauche effect for 1,2-difluoroethane has been explained by Wiberg et al.,[180] using the bond path method of Bader,[181] as being due to a destabilizing interaction in the trans rotamer, in which the C−C bond orbitals are bent in opposite directions, giving decreased overlap and thus a weaker bond. On the other hand, the gauche rotamer has bond orbitals bent in roughly the same direction, giving better overlap. It might be expected that the same effect would be operative in 1,1,2-trifluoro- and 1,1,2,2-tetrafluoroethane. However, in these cases the gauche rotamers have three fluorines mutually cis, so repulsive interactions are greatly increased in comparison to 1,2-difluoroethane. Indeed, the MP2/6-31G(d,p)//HF/6-31G(d) calculations showed these gauche rotamers to be significantly less stable (by 6.72 kJ mol^{-1} for 1,1,2-trifluoroethane as compared to the C_1 isomer, which has two fluorines in a near *anti*

Table 5.3: Total Energies of Molecules at MP2 Level Using Several Basis Sets[a]

Molecule[b]	6-31G(d)	6-31G(d,p)	6-311G(d)	6-311G(d,p)
CH_3-CH_3 (D_{3d})	-79.495412	-79.543349	-79.525737	-79.570654
CH_2F-CH_3 (C_s)	-178.507859	-178.548409	-178.601017	-178.638856
CH_2F-CH_2F (C_2)	-277.516712	-277.549700	-277.671623	-277.702617
CHF_2-CH_3 (C_s)	-277.541751	-277.573778	-277.695819	-277.725742
CHF_2-CH_2F (C_1)	-376.547194	-376.571241	-376.762697	-376.785952
CF_3-CH_3 (C_{3v})	-376.584708	-376.608468	-376.798342	-376.820167
CHF_2-CHF_2 (C_{2h})	-475.574929	-475.590792	-475.850928	-475.866528
CF_3-CH_2F (C_s)	-475.586630	-475.602577	-475.861700	-475.877015
CF_3-CHF_2 (C_s)	-574.611171	-574.619046	-574.946600	-574.954378
CF_3-CF_3 (D_{3d})	-673.647002	-673.647002	-674.042028	-674.042028

[a] in hartrees; all calculations have been carried out at the HF/6-31G(d) optimized geometries shown in Figure 6. [b] Symmetry point groups also given in parentheses.

conformation; and 6.86 kJ mol^{-1} for 1,1,2,2-tetrafluoroethane, as compared to the trans isomer). In 1,2-difluoroethane the gauche conformer is 2.57 kJ mol^{-1} more stable at this level of theory.

Total energies at the MP2/6-311G(d,p)//MP2/6-31G(d,p) level for all molecules in the series, and at the MP4/6-311G(d,p)//MP2/6-31G(d,p) level for molecules with three or fewer fluorines, unscaled ZPEs at the HF/6-31G(d) and MP2/6-31G(d,p) levels, and experimental ΔH_f values[90,91,101-104] used to calculate the experimental BDEs are given in Table 5.4. It should be noted that, due to lack of data, some of the experimental ΔH_f values are calculated by means of the triatomic additivity method[114], and some others are estimated or derived values. Both zero-point and total energies are lower when electron correlation is employed in the geometry

Table 5.4: Total Energies,[a] Zero-Point Energies,[b] and Experimental Heats of Formation[c] of Molecules

Molecule	MP2/6-311G(d,p) //MP2/6-31G(d,p)	MP4/6-311G(d,p) //MP2/6-31G(d,p)	ZPE// HF/6-31G(d)	ZPE// MP2/6-31G(d,p)	$\Delta H_{f,298}$	ref
CH_3-CH_3	−79.570739	−79.614234	79.760	77.565	−83.8 ± 0.4	101
CH_2F-CH_3	−178.639255	−178.685358	73.141	70.524	−263.2 ± 1.7[d]	102
CH_2F-CH_2F	−277.703348	−277.752149	66.315	63.232	−443.5[e]	90
CHF_2-CH_3	−277.726464	−277.774393	65.524	62.798	−500.8 ± 6.3	102
CHF_2-CH_2F	−376.786986	−376.837836	58.550	55.456	−664.8 ± 4.2	103
CF_3-CH_3	−376.821147	−376.870570	56.882	54.260	−745.6 ± 1.7	102
CHF_2-CHF_2	−475.867848		50.592	47.438	−884.5[e]	91
CF_3-CH_2F	−475.878430		49.872	46.968	−904.2[e]	90
CF_3-CHF_2	−574.956045		41.862	38.924	−1104.6 ± 4.6[d]	102
CF_3-CF_3	−674.044061		32.952	30.235	−1343.9 ± 5.0	104

[a] In hartrees. [b] Unscaled, in millihartrees. [c] In kJ mol^{-1}. [d] Derived from correlative procedures. [e] Calculated by the triatomic additivity method of Reference 114. [f] Estimated from the reaction Br + CH_3F ⇆ HBr + CH_2F [g] Estimated from kinetic parameters.

Table 5.5: Total Energies of Molecules at the Additional Levels of Theory Required for G2 Method[a]

Species/ G2 energy[b]	MP2/6-311+G(d,p)	MP2/6-311G(2df,p)	MP2/6-311+G(3df,2p)	MP4/6-311+G(d,p)	MP4/6-311G(2df,p)	QCISD(T)/6-311G(d,p)
CH_3-CH_3 −79.627161	−79.571325	−79.607285	−79.620290	−79.614882	−79.652670	−79.615478
CH_2F-CH_3 −178.782113	−178.648072	−178.724712	−178.749351	−178.694743	−178.775024	−178.685266
CH_2F-CH_2F C_2 −277.932684	−277.719834	−277.838134	−277.873724	−277.769697	−277.893478	−277.750697
CHF_2-CH_3 −277.953302	−277.740330	−277.861834	−277.894829	−277.789372	−277.916516	−277.772646

[a] All values given are single-point energies, in hartrees at the MP2/6-31G(d,p) geometries given above. The MP4/6-311G(d,p) and MP2/6-311G(d,p) single-point energies and ZPEs are given in Table 5.3. [b] Scaled ZPEs included. To obtain energy without ZPE correction subtract the MP2/6-31G(d,p) ZPE listed in Table 5.3 multiplied by the scaling factor of 0.9646.

optimizations. There is also a significant lowering of total energies when higher-order correlation corrections are employed.

Total energies at the additional levels of theory required for the G2 method, and the resultant G2 extrapolated energies (using the modified G2 method described in section 2.10), for molecules with two or fewer fluorines, are given in Table 5.5. Once again, energies decrease with increasing level of theory, both in terms of electron correlation and basis-set size, with the MP4/6-311G(2df,p) level always giving the lowest energies. The next lowest energies are given by the MP2/6-311+G(3df,2p) level, which combines the largest basis set employed in the method with the lowest level of electron correlation.

5.5 C−C Bond Dissociation Energies

Calculated and experimental C−C homolytic bond dissociation energies are given in Table 5.6. Single-point calculations using the HF/6-31G(d) optimized geometries were carried out using several basis sets. In most cases agreement with experiment improves as basis-set size increases. With the 6-311G(d,p) basis set, agreement is within the absolute experimental error (where this is known) in the majority of cases, and can be considered acceptable in all cases. The MP2/6-311G(d,p)//MP2/6-31G(d,p) results not only show the same trends but are nearly identical to the MP2/6-311G(d,p)//HF/6-31G(d)results, varying by no more than 2 kJ mol^{-1}. While this may seem surprising given the improvements in geometry seen above, it is yet another example of cancellation of errors which can make lower level calculations useful for determination of derived values such as BDEs.

Table 5.6: C—C Bond Dissociation Energies[a]

Molecule	6-31G(d)[b]	6-31G(d,p)[b]	6-311G(d)[b]	6-311G(d,p)[b]	6-311G(d,p)[c]	6-311G(d,p)[c,d]	G2[c,e]	expt
CH₃—CH₃	380	383	378	378	379	369	380	375
CH₂F—CH₃	395	396	393	392	393	384	397	380
CH₂F—CH₂F	398	398	394	393	395	388	403	386
CHF₂—CH₃	413	413	409	407	409	401	416	408
CHF₂—CH₂F	408	407	402	400	402	397		397
CF₃—CH₃	439	438	432	431	432	427		423
CHF₂—CHF₂	411	410	402	410	402			407
CF₃—CH₂F	424	423	417	415	417			407
CF₃—CHF₂	419	418	408	407	409			397
CF₃—CF₃	426	426	413	413	415			407

[a] In kJ mol⁻¹; calculated as D_0(298 K), using 4RT as temperature correction. All single-point calculations used MP2 theory, except where noted, at the indicated basis set. [b] Using the HF/6-31G(d) optimized geometries shown in Figure 6. [c] Using the MP2/6-31G(d,p) optimized geometries shown in Figure 7. [d] Using MP4 theory. [e] Using the modified G2 theory described in Chapter 2.

To investigate whether higher-order correlation effects would change any of the trends, BDEs were also calculated at the MP4/6-311G(d,p)//MP2/6-31G(d,p) level for ethanes with three or fewer fluorines. This level of theory lowers the calculated BDEs by $5-10$ kJ mol^{-1} but does not qualitatively affect the trends. Trends are also not affected by using G2 theory, which gives the highest BDEs of the levels of theory used here. Overall the best agreement with experiment was given by the MP2/6-311G(d,p)//MP2/6-31G(d,p) level of theory, so for these molecules at least it appears that nothing is to be gained by calculating BDEs at higher levels of theory.

Analysis of the computed BDEs reveals three interesting trends, two of which may be rationalized in terms of electronegativity arguments. Successive substitution on one carbon increases the BDE: $CH_3-CH_3 < CH_2F-CH_3 < CHF_2-CH_3 < CF_3-CH_3$. The monotonic increments (at the MP2/6-311G(d,p)//MP2/6-31G(d,p) level) of 14, 16, and 23 kJ mol^{-1} are consistent with Pauling's original ideas about the connection between the bond dissociation energy and the electronegativity difference between two bonded atoms. Thus, for substitution on a single carbon, each additional fluorine increases the electronegativity difference between the two methyl fragments and therefore the BDE increases, as noted above. A similar analysis has been used to explain the remarkable effect of protonation on BDEs.[182] For molecules containing equal numbers of fluorine atoms, the higher BDE of the unsymmetrically substituted molecule is also consistent with the electronegativity explanation. Thus, the BDE of CHF_2-CH_3 is greater than that of CH_2F-CH_2F, and the BDE of CF_3-CH_2F is greater than that of CHF_2-CHF_2.

Electronegativity considerations are insufficient, however, to explain the monotonic

increase in the BDEs of symmetrically substituted molecules: $CH_3-CH_3 < CH_2F-CH_2F$

$< CHF_2-CHF_2 < CF_3-CF_3$.

There is only a rough correlation between the calculated BDEs and $C-C$ bond

lengths. The shortest and longest $C-C$ bonds correspond with the highest and lowest

BDE. However, ethane and perfluoroethane have nearly the same $C-C$ bond length,

but a large difference in BDE; 1,2-difluoroethane has the third shortest $C-C$ distance,

but the third lowest BDE.

5.6 C−H Bond Dissociation Energies

Calculated and (where available) experimental homolytic $C-H$ BDEs, for each

unique hydrogen in the parent ethane, are given in Table 5.7. In cases where there are

more radical conformers than inequivalent hydrogens, the conformer that would be

formed directly upon hydrogen abstraction (i.e., before a subsequent rotation about the

$C-C$ bond) was used. Once again, the two levels of theory produce almost identical

results, with a maximum variance of only 1 kJ mol^{-1}. The comparisons available with

experimental data indicate the agreement is reasonable, although not as close as with the

$C-C$ BDEs. There is insufficient data to make a judgment on the accuracy of these

results, but it is expected that they will be useful as a predictive tool for experimentalists.

In the present case, one of the fragments produced by bond dissociation is

constant, so it is to be expected that the range of BDEs will be smaller, and the trends

not as apparent, as for the $C-C$ BDEs, where different substituted methyl fragments

Table 5.7: C−H Bond Dissociation Energies[a]

Molecule[b]	MP2/6-311G(d,p)// HF/6-31G(d)	MP2/6-311G(d,p)// MP2/6-31G(d,p)	Expt
CH_3CH_2-H **1a**	413	413	419
CH_2FCH_2-H g **1b**	421	421	
CH_2FCH_2-H t **1c**	423	423	
CH_3CHF-H **1d**	412	413	410
$CH_2FCHF-H$ g **1f**	411	411	
$CH_2FCHF-H$ t **1e**	406	406	
CHF_2CH_2-H g,t **1h**	429	428	
CHF_2CH_2-H g,g **1i**	429	428	
CH_3CF_2-H **1j**	409	410	416
CHF_2CHF-H g,t **1k**	414	414	
CHF_2CHF-H g,g **1l**	419	419	
CH_2FCF_2-H **1o**	416	417	
CF_3CH_2-H **1p**	432	432	446
CHF_2CF_2-H **1q**	421	422	
CF_3CHF-H **1s**	417	417	
CF_3CF_2-H **1t**	420	421	431

[a] In kJ mol^{-1}; calculated as D_0(298 K), using 4RT as temperature correction.
[b] For cases where there are inequivalent hydrogens, the g and t designations indicate hydrogens gauche and trans, respectively, to fluorine(s) on the β-carbon. The figure numbers of the resultant ethyl radicals are given for clarity.

were produced. Indeed, the range of C−H BDEs is only 26 kJ mol⁻¹. For a given R

group at the β-carbon, the relative BDEs are RCH_2-H > RCF_2-H > $RCHF-H$, with

an exception for R = CH_3, where there is no fluorine on the β-carbon (CH_3CH_2-H >

CH_3CHF-H > CH_3CF_2-H). For a given R group at the α-carbon, the relative BDEs

are CF_3R-H > CHF_2R-H > CH_2FR-H > CH_3R-H, consistent with a C−H bond

stabilization due to an inductive effect. The exceptions to this trend are CH_3CHF-H >

$CH_2FCHF-H$ and CHF_2CF_2-H > CF_3CF_2-H, although in the latter case the

difference (1 kJ mol⁻¹) may be insignificant. The inductive effect is also suggested by

the relative BDEs in cases where hydrogen abstraction is possible from inequivalent

carbon atoms in the parent ethanes. In these cases the higher BDE is when the β-group

has the higher number of fluorines. Again, there is an exception (CH_2FCF_2-H >

CHF_2CHF-H), but only for the case where the hydrogen being abstracted from

CHF_2CHF-H is gauche/trans to β−fluorines. It is interesting that CH_3CHF-H

provides an exception to two trends, suggesting an error in the calculated value for this

species, although this value gave the closest agreement with experiment.

All other things being equal, shorter bonds are stronger bonds, so shorter C−H

bonds in the parent molecules can be expected to lead to greater C−H BDEs. However,

this is not always the case here. For CH_2FCH_2-H the shorter C−H bond has the lower

BDE. As well, in CHF_2CHF-H the C−H bond lengths are equal but the difference in

BDEs is relatively large (5 kJ mol⁻¹). It appears that the favoured H-atom abstraction

is not governed by the length of the C−H bond but rather by the relative stability of the

resultant ethyl radicals (see discussion in Chapter 3). Alternatively, the strength of a

bond is dependent not only on its length but also on other effects.

5.7 Conclusions

Results from the total energy calculations show that for fluorinated ethanes, as in the fluorinated ethyl radicals, the most stable isomer is always that in which as many fluorines as possible are on one carbon. It is also observed that the gauche effect is operative in 1,2-difluoroethane, but not in more highly substituted members of the series, where three fluorines are mutually *cis*.

The computed $C-C$ BDEs show some intriguing trends, which can be largely explained using electronegativity arguments. The net result of these trends is that CF_3-CH_3 has the greatest $C-C$ bond dissociation energy. Trends in the computed $C-H$ BDEs suggest that an inductive effect from an electronegative β-group can stabilize $C-H$ bonds. Where hydrogen atom abstraction is possible from inequivalent positions in the parent molecules, the favourability of the process is controlled by the nature of the products, rather than the reactants.

The inclusion of electron correlation in geometry optimization leads to improvements in structural parameters, most notably the $C-F$ bond lengths, and in total energies, but has a negligible effect on the calculated BDEs.

These results compare favourably with those from experimental studies. However, the incompleteness of the experimental data for these molecules, and some conflicting results where more than one value has been reported, render an absolute determination of the accuracy of these results impossible. From the comparisons that are

possible, it appears that the MP2/6-311G(d,p) level of theory gives accurate predictions for the bond dissociation energies and the associated trends, and that accurate geometries can be obtained with the MP2/6-31G(d,p) level.

Chapter 6. Properties of Transition Species in the Reaction of Hydroxyl with Ethane

6.1 Introduction

Hydroxyl radicals are important chain carriers in combustion,[183] and are the most likely .iitiators of tropospheric degradation for the hydrochlorofluorocarbon (HCFC) and hydrofluorocarbon (HFC) classes of chlorofluorocarbon replacement compounds.[184] The reaction (R1)

$$OH + C_2H_6 \rightarrow H_2O + C_2H_5$$
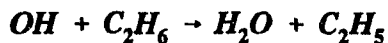
can serve as a prototype for theoretical understanding of combustion reactions and hydrogen abstractions from HFCs and HCFCs with two or more carbons, and in the present context will provide a base for comparison with the reactions studied in the following chapter.

This reaction has been the subject of numerous experimental investigations.[185−207] Theoretical investigations have been less numerous. The geometry for the transition state (TS) of reaction R1, calculated at the HF/6-31G(d) level of theory, has been reported previously by Tully et al.[194] (hereafter referred to as TDKM). More accurate geometries can be obtained when the effects of electron correlation are included. This can be done using Møller-Plesset perturbation theory,[36] usually applied at second order (denoted MP2). Melissas and Truhlar[208] (hereafter referred to as MT) published results of an MP2 optimization of the transition state for reaction R1, from which they calculated the barrier height and treated the kinetics of the

115

reaction in the range 200 to 3000 K using transition state theory (TST).

The present work is the most detailed description to date of the potential energy surface for this reaction. Included are high-level *ab initio* calculations on the TS, twelve additional points along the reaction coordinate, and on the two saddle points for internal rotation about the C...H...O axis. This work was done as part of a collaborative effort with Philip D. Pacey and Anil K. Mehta,[209] who performed bond-energy-bond-order (BEBO) calculations, and a fit of TST parameters to the experimental data. The work of these coauthors will hereafter be referred to as PM.

6.2 Geometries and Moments of Inertia

According to the BEBO calculations of PM, in the activated complex the C−H bond has stretched by only 5% to 1.166 Å, whereas the O−H internuclear distance is 1.389 Å, 45% longer than its final value. This corresponds to an early transition state, with the order of the breaking bond being 0.81, which is in agreement with Hammond's postulate for an exothermic reaction with a low activation barrier. TDKM, by means of HF/6-31G(d) calculations, predicted that the O−H internuclear distance would, instead, be shorter than the C−H distance. The higher level *ab initio* calculations of MT are in agreement with the BEBO results for the C−H distance and predict an O−H distance only 2% shorter than BEBO theory.

The present *ab initio* results confirm that the inclusion of electron correlation with MP2 theory dramatically changes the lengths of the C−H bond being broken and the O−H bond being formed. The present MP2 structure shows the C−H bond to be

stretched by only about 9% (*cf.* C_2H_6 at same level of theory, Chapter 5), to 1.187 Å, while the O−H contact is 1.322 Å, confirming an early TS. This HF/MP2 bond length dichotomy has been noted in other hydrogen abstraction reactions.[210,211] At the HF level, the computed barrier is high compared to the exothermicity, making the barrier appear almost symmetrical; both bonds are stretched by a similar amount. At the MP2 level, or in BEBO theory, the barrier height is less than the exothermicity and the TS is early. The optimization performed by MT using an adjusted version of Dunning's (10s5p2d1f/5s2p1d)/[4s3p2d1f/3s2p1d] basis set,[212] which is larger than the one used here, showed a slightly earlier TS (C−H bond stretched by 8%). Their geometrical parameters have only minor differences with the present work.

Sixteen points on the potential energy surface (PES) of reaction R1 have been optimized in the present work, at the MP2/6-31G(d,p) level of theory: four saddle points and twelve points (six on either side of the TS) along the reaction coordinate. The geometries for the saddle points and the extreme points determined from the intrinsic reaction coordinate (IRC) calculation are illustrated in Figure 8, with bond lengths and angles tabulated in Table 6.1. The optimized geometry for the transition state of reaction R1 is shown in Figures 8a and 8b (a mirror image transition state of exactly the same energy also exists). While the HF/6-31G(d) optimized structure of TDKM has C_s symmetry (with the OH group *anti* to the β-CH_3 group), as one would expect intuitively from the approach of OH to the stable staggered conformer of ethane, here the point group is C_1. When the MP2 optimization (using various basis sets) was attempted using a C_s symmetry constraint, the resultant saddle point was always second-order. The C_s
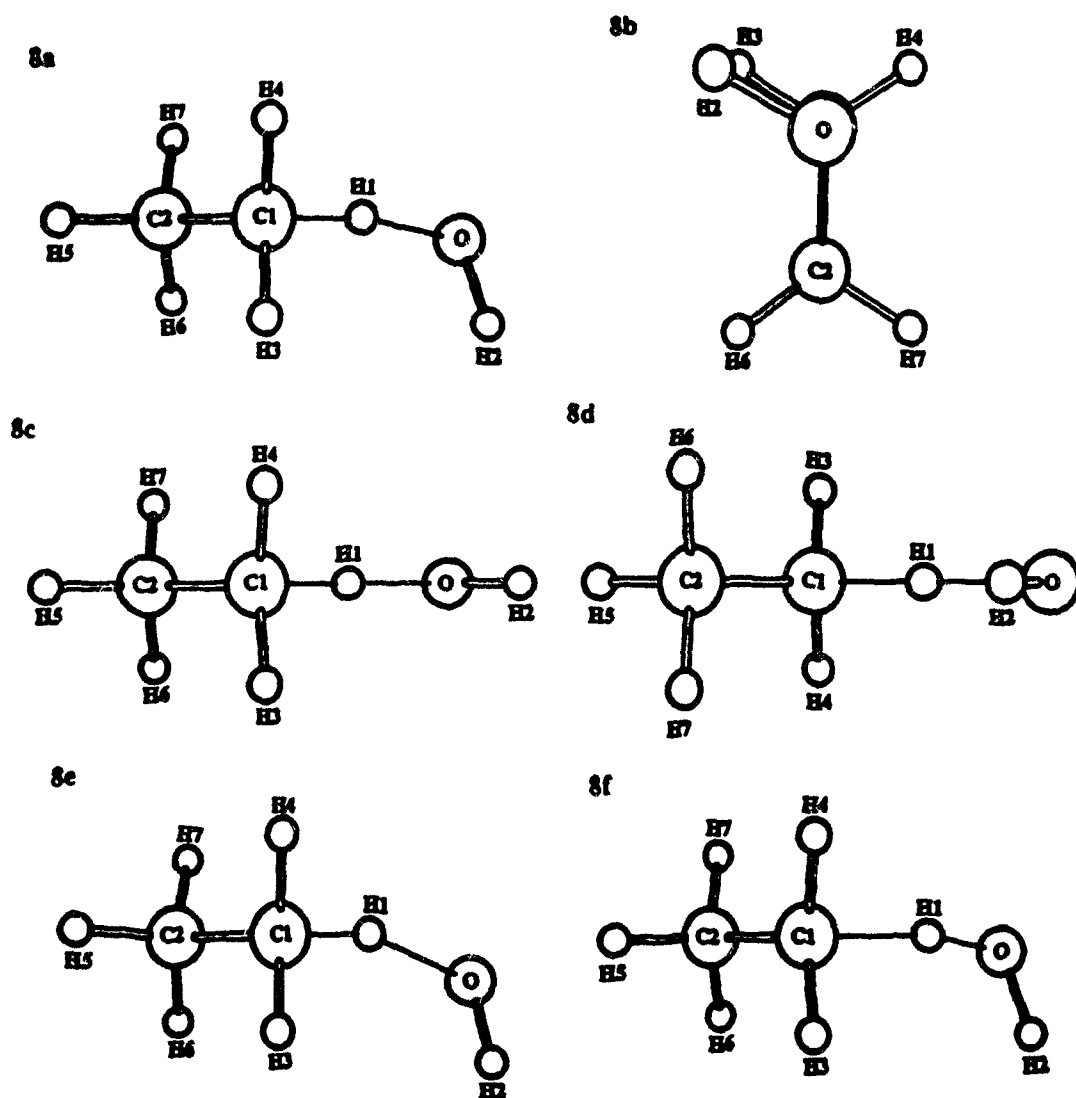
Figure 8. MP2/6-31G(d,p) optimized geometries for points in reaction R1: **8a** TS; **8b** TS, viewed along O−C1 axis; **8c** second-order TS, with OH group *anti* to β-CH₃; **8d** second-order TS, with OH group *syn* to β-CH₃; **8e** furthest point reached towards reactants in IRC calculation; **8f** furthest point reached towards products in IRC calculation. Drawings are in perspective, with relative radii of 1 : 1.667 : 2 for H, O, and C atoms respectively.

Table 6.1: Geometrical Parameters for the Transition Species Illustrated in Figure 8[a]

Parameter	Structure				
	8a	**8c**	**8d**	**8e**	**8f**
C1−C2	1.511	1.512	1.512	1.516	1.503
C1−H1	1.187	1.187	1.189	1.088	1.492
H1−O	1.322	1.321	1.319	1.581	1.017
O−H2	0.971	0.971	0.971	0.973	0.966
C1−H3	1.087	1.086	1.086	1.089	1.085
C1−H4	1.087	1.086[b]	1.086[b]	1.089	1.085
C2−H5	1.089	1.090	1.089	1.089	1.093
C2−H6	1.086	1.087	1.088	1.089	1.088
C2−H7	1.087	1.087[b]	1.088[b]	1.088	1.088
C1−H1−O	169.6	175.8	169.3	159.4	169.9
H1−O−H2	97.6	97.5	97.6	95.1	100.4
H3−C1−H1	106.7	106.0	104.2	109.1	103.4
H4−C1−H1	104.3	106.0[b]	104.2[b]	105.0	102.8
H3−C1−H4	110.0	110.3	110.5	108.3	112.0
H1−C1−C2	107.7	106.8	110.3	109.7	106.5
H3−C1−C2	113.5	113.5	113.4	112.4	115.0
H4−C1−C2	113.9	113.5[b]	113.4[b]	112.0	115.5
H5−C2−H6	108.0	108.0	107.5	108.4	107.9
H5−C2−H7	108.0	108.0[b]	107.5[b]	108.4	107.8
H6−C2−H7	108.0	108.1	108.3	107.7	108.2
H5−C2−C1	110.8	110.7	110.8	110.1	109.8
H6−C2−C1	111.0	111.0	111.3	111.3	111.5
H7−C2−C1	111.0	111.0[b]	111.3[b]	110.8	111.5
C1−H1−O−H2	39.3	180.0	0.0	52.5	36.0

* Geometries optimized at the MP2/6-31G(d,p) level. Bond lengths in angstroms, bond
and dihedral angles in degrees. b Value is equivalent by symmetry to that immediately
above.

---

symmetry saddle point obtained at MP2/6-31G(d,p), with the OH group *anti* to the β-

CH_3, is shown in Figure 8c. Another second-order saddle point of C_s symmetry, with

the OH group *syn* to the β-CH_3, also exists; its geometry is shown in Figure 8d.

Perhaps more surprisingly, in the C_1 structure the hydroxyl hydrogen (H2) is

nearly eclipsed with a methylene hydrogen (H3). In an eclipsed conformation there

should be nuclear repulsions between the H atoms, electron repulsions between the $C-H$

and $O-H$ bonds, and electron-nuclear attractions between the nuclei and the bonding

electrons, with the repulsive terms expected to outweigh the attractive terms. However,

as seen in Figure 8b, which shows the view along the O...C1 axis, the bend in the

H...O...C bond angle has brought H2 slightly outside H3. This should reduce the

repulsion between the H nuclei, and increase the attraction between the methylene H

nucleus and the $H-O$ bonding electrons, allowing the attractive terms to now outweigh

the repulsive ones. An alternative explanation could be that the internuclear distance

between the two hydrogen atoms (2.804 Å) is one at which London dispersion attractive

forces are significant. From MM3 calculations Allinger *et al.* have determined the van

der Waals radius of an alcoholic hydrogen[213] to be 1.60 Å, and that for a hydrogen in

a saturated hydrocarbon[214] to be 1.62 Å. Thus, the ideal distance between these two

hydrogens for London dispersion attractive forces to be optimized is 3.22 Å, about 0.4

Å greater than in the TS. By comparison, in 8c and 8d this distance is 3.042 and 3.350

Å, slightly below and above the MM3 ideal distance, respectively. The energies of these species (see below) increases in the order **8a → 8c → 8d**, with the H2...H3 distance increasing in the same order. Thus, thermodynamic stability is not correlated with favorability of London dispersion forces, making it unlikely that these forces can explain the calculated structures.

The furthest points reached along the IRC towards the reactants and products are shown in Figures 8e and 8f, respectively. In **8e** the OH group is relatively remote from the reaction site, and the geometrical parameters of the C_2H_6 fragment are close to those of staggered ethane (see Chapter 5). In **8f** the abstraction of H to form H_2O is nearly complete, and the contraction of the C-C bond length and the flattening of the α-CH_2 group, which occur in forming an ethyl radical (see Chapter 3) from ethane, are becoming apparent. Thus, there is no doubt that the optimized TS is that for the reaction of OH with staggered C_2H_6 to give H_2O and C_2H_5.

Figure 9 shows the motion along the reaction coordinate where the vertical coordinate (r) is proportional to the C−H distance, and the horizontal coordinate (R) is almost proportional to the C−O distance,[215] with the coordinates scaled[216] to represent motion of a constant mass of 1.008 amu. The BEBO distances calculated by PM are compared with the results of the IRC calculation. The BEBO curve, which covers a greater extent of reaction, has a sharper curvature. For this potential energy surface the heavy atoms continue to drift together after the barrier is crossed. In contrast, for the IRC surface, the reaction coordinate at the transition state corresponds essentially to the hydrogen atom moving from the carbon atom toward the oxygen atom.
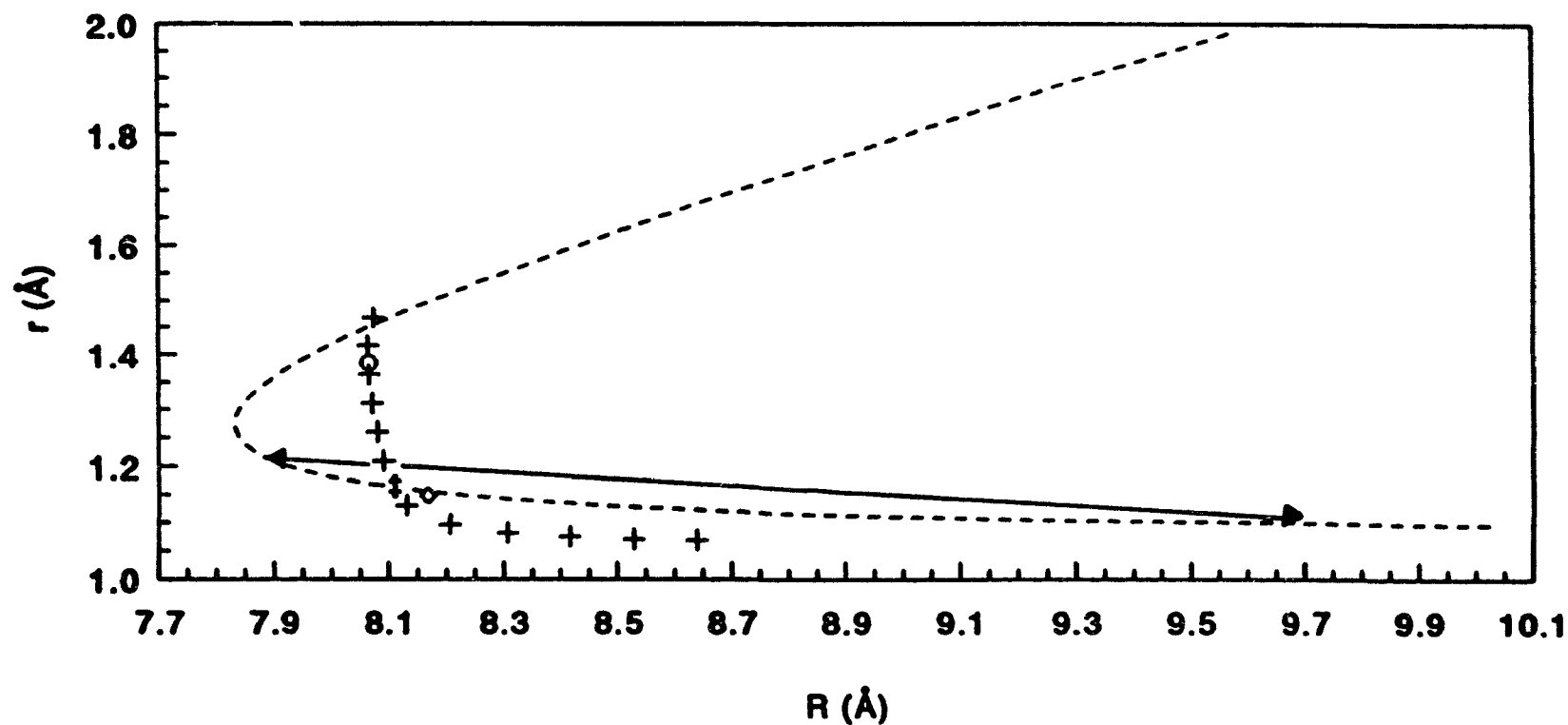
Figure 9. Motion along the reaction coordinate using the scaled coordinates recommended in ref. 215, using both the IRC (crosses) and BEBO (dashed line) results. The double-headed arrow shows the transition from half-way up one side of the BEBO barrier to a point of equal energy on the other side. The circle shows a point on the product side of the IRC barrier at an energy equal to half the height of the forward barrier. The double dagger represents the TS on the IRC curve, and the diamond the TS according to MT.

This switch, which PM calculated to be from 92% R motion in BEBO to 67% r motion by MP2, is striking, and may be caused by the decrease in the asymmetry of the barrier from BEBO to MP2, or by the simplifying assumptions in the BEBO model geometry.

The square roots of the products of the overall moments of inertia $(I_A I_B I_C)^{1/2}$ for the TS are listed in the first column of Table 6.2. The values for the various theoretical methods are seen to be in good agreement.

Table 6.2: Transition State Parameters from Various Sources

Source	$\dfrac{(I_A I_B I_C)^{1/2}}{10^{-68}\ \mathrm{kg}^{3/2}\ \mathrm{m}^3}$	$v_b^{\ddagger}$, cm^{-1}	V_b, kJ mol^{-1}	T^*, K	$\Delta\,s_{1/2}$, Å
Fits to Experiment[a]					
Basic data		350 ± 7	9.3 ± 0.3	119 ± 15	0.74 ± 0.11
Reduced data[b]		351 ± 8	9.2 ± 0.3	118 ± 18	0.74 ± 0.12
Theory					
BEBO[a]	3.315		11.3	60	1.82
TDKM	3.161				
MT	3.163	366	10.2	323	0.44
Fit to MT[a]		378 ± 1	9.8 ± 0.1	277 ± 3	0.33 ± 0.01
This work	3.137	345	12.4[c]	403	0.88, 0.53[d]

[a] Performed by Mehta and Pacey. See ref 209. [b] Experimental studies at a single temperature near room temperature were deleted from the data set. [c] At G2 level of theory; energy of internal rotational mode about C...H...O axis not included in ZPE. [d] At MP2/6-31G(d,p) and MP4/6-311G(d,p)//MP2/6-31G(d,p) levels of theory, respectively, from the fitted Eckart curves.

6.3 Vibrational Frequencies

The *ab initio* normal mode vibrational frequencies, their reduced masses and descriptions of their motions are given in Table 6.3 for the TS, at the MP2/6-31G(d,p) level of theory. The reaction coordinate, as expected, consists of movement of the hydrogen atom being abstracted, away from the carbon atom to which it is bonded, and towards the abstracting oxygen atom. As discussed in the previous section, the lowest frequency mode in the TS (60 cm^{-1}) is a rotation of the OH group about the O...H...C axis. The second-order points **8c** and **8d** have similar frequencies for the reaction coordinate, with second low frequency imaginary modes at 72 and 97 i cm^{-1}, respectively, which also correspond to the OH rotation. Thus, the two C_s structures are saddle points in the respective rotations between the two mirror image C_1 structures.

Many of the other TS modes, in particular those with low frequencies, are strongly coupled. Many assignments are complicated by the lack of symmetry in the complex. The mode at 110 cm^{-1} is best described as a skeletal bend involving the three heavy atoms (note the high reduced mass). This motion could correspond to a rotation of C_2H_6 in the reactants. The CH_3-CH_3 torsion is split over two modes, the vibration at 182 cm^{-1} consisting mostly of rotation of the β-CH_3 group with restricted motion of the α-CH_3, and the vibration at 400 cm^{-1} being a more symmetrical rotation. In comparison, this mode occurs at 337 cm^{-1} in ethane. A lowering of this value is expected in the TS because of the increase in the moment of inertia on attachment of the OH group. An averaging of the two torsional modes in the TS does give the expected lower value.

Table 6.3: Vibrational Frequencies Calculated at the MP2/6-31G(d,p) Level for the

Transition State of Reaction R1.

Frequency (cm^{-1})	Reduced Mass (amu)	Description
1761i	1.122	reaction coordinate
60^a	1.096	OH rotation
110	2.753	C$-$C$-$O bend
182	1.118	β-CH$_3$ rotation
400	1.106	CH$_3$$-CH_3$ torsion
751	1.563	TS sym. stretch + CH$_3$ rock
816	1.253	CH$_3$ rock + C$-$H$-$O bend
873	1.175	CH$_3$ rock
985	1.274	H$-$O$-$H bend
1070	2.675	C$-$C stretch
1216	1.350	CH$_3$ rock
1280	1.397	CH$_3$ rock
1352	1.222	α-CH$_3$ deformation
1468	1.226	β-CH$_3$ inversion
1505	1.038	α-CH$_3$ deformation
1533	1.114	α-CH$_3$ deformation
1556	1.041	β-CH$_3$ deformation
1561	1.046	β-CH$_3$ deformation
3136	1.037	C$-$H stretch
3180	1.057	C$-$H stretch
3226	1.100	C$-$H stretch
3242	1.104	C$-$H stretch
3265	1.107	C$-$H stretch
3841	1.067	O$-$H stretch

^{a} This mode not included in ZPE calculation.

The "symmetrical" stretching frequency of the TS ($C-H$ and $O-H$ bonds at the reaction center) occurs at 751 cm^{-1}. There is some coupling with the lowest CH_3 rocking frequency at 816 cm^{-1}. In the latter vibration the coupled mode is best described as a $C-H-O$ bend. The vibration at 985 cm^{-1} is an $H-O-H$ bend, accompanied by motion towards the OH group of the methylene hydrogen which is eclipsing the hydroxyl hydrogen. The remaining modes are similar to those seen in the reactants, with some shifting of frequencies due to symmetry breaking.

The geometric means of the five lowest frequency vibrational term values in the transition state from the fits performed by PM of TST to the experimental data are shown in the second column of the upper part of Table 6.2. The results of fitting the TST model to all the experimental data are shown in the first line. Deleting the data from studies at a single temperature near room temperature led to the results in the second line; this deletion did not make a significant difference in this parameter. PM's quoted uncertainties are standard deviations and are about 2% of the fitted values. PM's fitted vibrational term value is the lowest found for any hydrogen atom abstraction reaction and is 40% less than the value for the reaction of OH with CH_4.[217] They attribute this to the low frequency values of the $C-C...O$ bend and the torsional mode about the $C-C$ bond, as seen in the *ab initio* frequencies in Table 6.3.

The *ab initio* $v_b^{\ddagger}$ values are in excellent agreement with those obtained from experiment. The values quoted are the geometric means of the five lowest frequencies, with the exception of the internal rotation about the $C...H...O$ axis. For MT, the mean was taken at a non-stationary point 0.0026 Å along the reaction coordinate past the

classical barrier top. MT found the sum of electronic plus zero-point energy was greater at this point than at the classical barrier top. The mean of the five lowest frequencies at the classical barrier top was identical with the present *ab initio* value. There is also reasonable agreement between MT's result and PM's fit to their calculated rate constants.

6.4 Barrier Heights

The calculated *ab initio* energies for reactants, products and the TS of reaction R1, and the classical barrier heights (not including ZPEs) are given in Table 6.4 for the various levels of theory required by the G2 method. The ZPE difference, multiplied by the appropriate scaling factor, can be added to the quoted heights to obtain barriers with ZPEs included. The barriers decrease in magnitude both with increasing level of electron correlation and with increasing basis-set size, with the largest effect seen when the extrapolated G2 method is employed. Although the G2 method explicitly includes scaled ZPEs, Table 6.4 also gives the results from the G2 method excluding ZPEs (in parentheses), to allow a direct comparison with the best energies calculated by MT (see last line of Table 6.4). The G2 method gives consistently lower energies than the PMP2 method used by MT.

Activation barriers from various sources are given in Table 6.2. The effective barrier height (including ZPEs), V_b, which PM obtained by fitting their TST model to the experimental data, listed in the fourth column, upper half of Table 6.2, is about half the value of 19 kJ mol^{-1} found[217] for the reaction of OH with CH_4 and reflects the greater exothermicity of the present reaction. Some theoretical values of these reaction

Table 6.4: Total Energies at MP2/6-31G(d,p) Optimized Geometries, for Reactants, Products, and Transition State of Reaction R1, and Classical Barrier Heights, at Levels of Theory Required for G2 Method, and G2 Extrapolated Values[a]

	C_2H_6	OH	TS	C_2H_5	H_2O	$E_{TS}-E_{reac}$[b]
MP4/6-311G(d,p)	−79.614234	−75.588329	−155.190337	−78.944350	−76.276272	32.1
MP4/6-311+G(d,p)	−79.614882	−75.595394	−155.199232	−78.946021	−76.287030	29.0
MP4/6-311G(2df,p)	−79.652670	−75.623671	−155.265443	−78.982086	−76.313602	28.6
QCISD(T)/6-311G(d,p)	−79.615478	−75.589267	−155.194278	−78.946362	−76.276270	27.5
MP2/6-311+G(3df,2p)	−79.620290	−75.617526	−155.227861	−78.950852	−76.318271	26.1
MP2/6-311G(2df,p)	−79.607285	−75.605468	−155.201626	−78.938601	−76.299124	29.2
MP2/6-311+G(d,p)	−79.571325	−75.579714	−155.139201	−78.904436	−76.274712	31.1
MP2/6-311G(d,p)	−79.570739	−75.572879	−155.130898	−78.902838	−76.263894	33.4
ZPE[c]	0.077565	0.008758	0.083263[d]	0.061431[d]	0.021898	−8.03
G2[e]	−79.627161	−75.643638	−155.266086	−78.967355	−76.331566	12.4
	(−79.701980)	(−75.652087)	(−155.346402)	(−79.026612)	(−76.352689)	(20.1)
PMP2/adj2-cc-pVTZ[f]	−79.662134	−75.626008	−155.281789	−78.991808	−76.324444	16.7

[a] Energies in hartrees, except where indicated. [b] Total energy of TS minus reactants, in kJ mol⁻¹, ZPE not included, except for G2, which includes scaled ZPEs. [c] Unscaled, from MP2/6-31G(d,p) frequencies. [d] Internal rotation mode removed; see text for details. [e] Scaled ZPEs are included in the first line of this row, but not in the second, to allow direct comparison with the results of MT. [f] As calculated by MT.

parameters are presented in the second half of the table. Included are BEBO results from PM, G2 results of the present work, and the results of the *ab initio* calculations of MT. In the case of MT, the quoted value is again for a point 0.0026 Å further along the reaction coordinate than the classical barrier top, near the maximum of electronic energy plus zero-point energy. The barrier height from the fit to MT's data is slightly lower than theirs. The BEBO value also agrees well with the others. In fact, all the barrier heights presented in Table 6.2 agree within the often quoted chemical accuracy limit of four kJ mol^{-1}.

G2 theory contains higher-order correlation terms, and nonadditivity corrections not contained in either the PMP2 or MP-SAC2[218] methods used by MT, and has the further advantage of not requiring basis set adjustment for each application, as in the MP-SAC2 method. The basis sets used are of comparable or larger size to that used by MT (the same as for their geometry optimization; see above). A disadvantage is that spin projection is not included for open-shell species, as in the PMP2 method. The expectation value of S^2 (0.75 indicates no spin contamination) at the various levels of theory ranges from $0.755-0.757$ for OH, $0.762-0.763$ for C_2H_5, suggesting very minor contamination in these species, but from $0.779-0.783$ for the TS, suggesting moderate contamination which may affect the results slightly. On balance the modified G2 method described herein (see section 2.10) appears to be a higher level of theory than either of those used by MT, so it should give a better description of the reaction energetics (as noted above, it does give a better description of the energetics of each species, assuming the correlation energy has not been overestimated). However, the G2 barrier for the

forward reaction, is 12.4 kJ mol^{-1}, whereas the best calculated value of MT is 10.2 kJ mol^{-1}, in better agreement with the value of 9.3 kJ mol^{-1} from PM's fit to experimental data. This apparent contradiction is the result of two well-known facts: *ab initio* methods overestimate activation barriers[23] (sometimes by tens of kJ mol^{-1}; the agreement with experiment of the G2 result and that of MT are both much better than that reported in most *ab initio* studies) and fortuitous cancellation of errors can sometimes make a lower level of theory more accurate. It would certainly be unwise to condemn G2 theory on the basis of one result which is only marginally inaccurate. It can be further noted that the G2 result is a significant improvement on the MP4/6-311G(d,p) level of theory, which yielded a forward barrier height of 24.4 kJ mol^{-1}.

The latter level of theory on the second-order points **8c** and **8d** gives energies of -155.190135 and -155.190015 au, placing them 0.53 and 0.84 kJ mol^{-1}, respectively (or 0.09 and 0.64 kJ mol^{-1}, respectively, when scaled ZPEs are included), higher in energy than the TS. MT calculate an even lower barrier of 0.07 kJ mol^{-1} through a geometry analogous to the present **8c**. These low barriers to rotation through the four saddle points, together with the low, real or imaginary, vibrational frequencies for OH rotation at each point, suggest that the PES for OH rotation is very flat. The harmonic vibrational zero-point energy in this degree of freedom is 0.36 kJ mol^{-1} and the average thermal energy in one degree of freedom at 138 K is 0.57 kJ mol^{-1}. It follows that this degree of freedom is a nearly free internal rotation and it is not realistic to add the zero-point energy for this degree of freedom to the barrier height; the quoted barrier for reaction R1 from the present work has been reduced by this amount.

The $\Delta H_0^{\ddagger}$ value calculated from G2 theory is -73.8 kJ mol^{-1}. Here the zero-point energy for the lowest frequency mode in C_2H_5 has not been included, as this mode is also a nearly free internal rotation. Using experimental heats of formation,[104,219,220] the enthalpy of reaction at 0 K is -80 ± 2 kJ mol^{-1}. Using bond strengths at 0 K recommended in a recent review article[221] gives an experimental enthalpy of -76 ± 2 kJ mol^{-1}. MT obtained -80.5 kJ mol^{-1} by adjusting the Gaussian exponential parameter for the oxygen f-shell to improve agreement with experimental bond dissociation energies. Their reverse barrier height is higher than the G2 one, at 90.8 vs. 86.2 kJ mol^{-1}.

6.5 Tunneling and Barrier Thickness

PM's fitted values of T^* in Table 6.2 are within the range of values obtained for the reaction of OH with CH_4,[217] but they are more reliably determined, because the lower limit (138 K) of the experimental temperature range for the present reaction is closer to T^*. The theoretical values were calculated from the imaginary frequency in the transition state. The parameter from BEBO is about half the value obtained from experimental data, but the *ab initio* values are substantially larger than the experimental value.

The differences between the experimental and *ab initio* values of T^* deserve further discussion. The electronic energies of points along the reaction coordinate (as output from the IRC calculation), relative to the sum of the reactant energies, are plotted

in Figure 10. While the energies in the top curve are at the MP2/6-31G(d,p) level, which grossly overestimates the barrier at 72.5 kJ mol^{-1}, here it is the shape and width of the barrier which are of concern. The three energy calculations at the MP4/6-311G(d,p) level indicate that only moderate changes in the barrier shape would be seen using the higher level of theory.

An unsymmetrical Eckart function was fitted to the barriers.

$$V(x) = \frac{Ay}{(1+y)^2} + \frac{By}{(1+y)} \; , \; y = \exp\left(\frac{x-x_0}{b}\right)$$

Here x_0 is the origin of the barrier, b is a thickness parameter, the force constant at the barrier top is $-(A^2-B^2)/(8A^3b^2)$, and the forward and reverse barriers are $(A+B)^2/4A$ and $(A-B)^2/4A$, respectively. From the fitted curves in Figure 10 values of T^* were calculated to be 285 K at the MP2 level and 313 K at the MP4 level, both somewhat less than the value of 403 K found by analytical gradient techniques at the MP2 level. The difference is caused by the different shapes of the Eckart and IRC barriers. The top three points on the IRC barrier give a value of 417 K for T^*, in good agreement with the analytical value.

The equation for the experimental barrier, plotted as the lower curve in Figure 10, was derived from PM's fitted parameters in the upper part of Table 6.2. Note that this curve is vibrationally adiabatic. The *ab initio* curves do not include ZPEs, as meaningful frequency analyses cannot be done on non-stationary points.[222] Inclusion of scaled ZPE at the TS lowers the barriers by 7.7 kJ mol^{-1}.
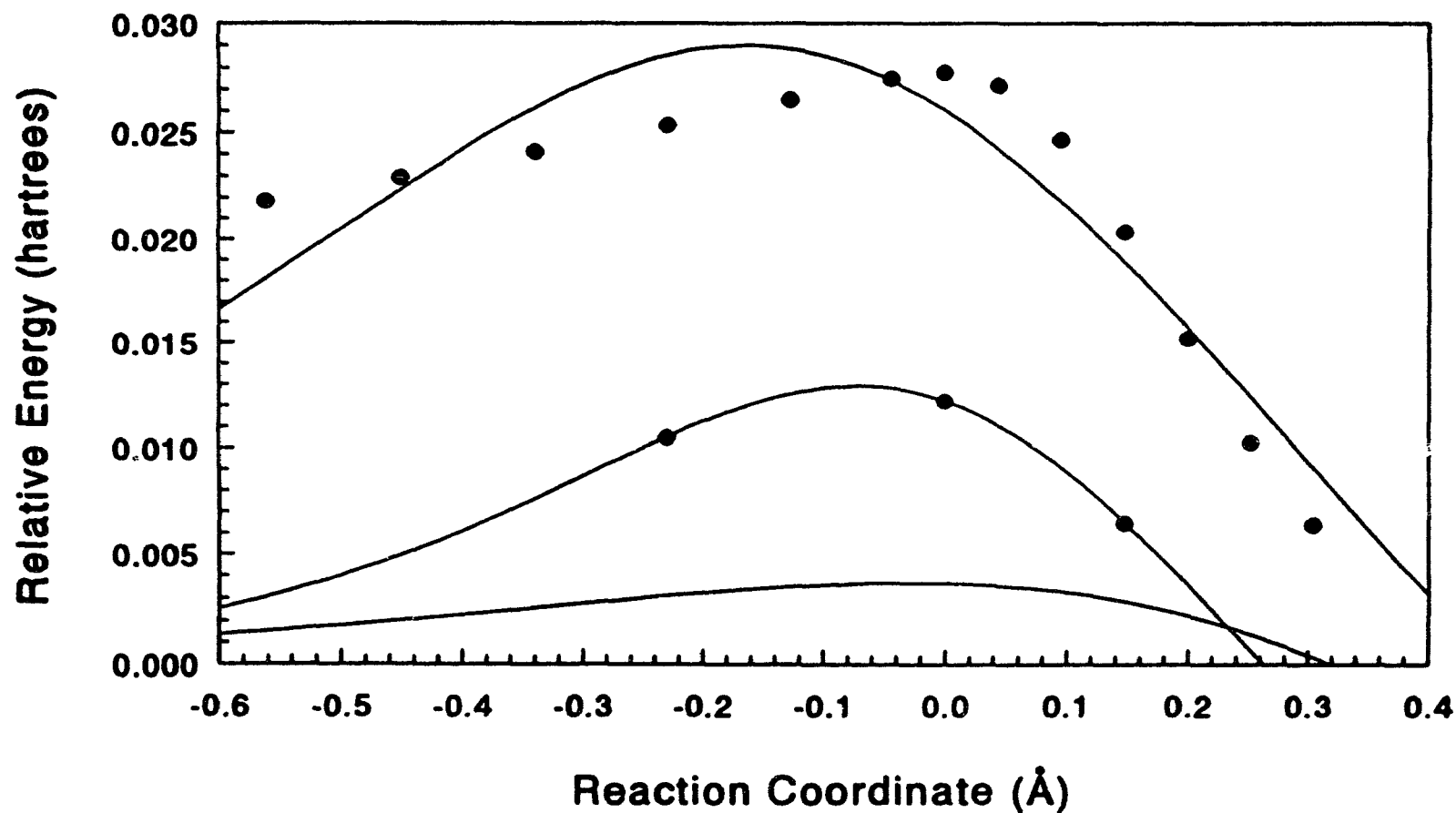
Figure 10. Profiles through the activation barrier. The upper circles are electronic energies directly from the IRC calculation (MP2/6-31G(d,p) level), while the middle circles are single-point energies (MP4/6-311G(d,p) level) at the geometries from the IRC calculation. The upper and middle curves are fits to these results using the unsymmetrical Eckart function. The lower curve is from PM's fit to experimental data.

A useful measure of barrier width is the full width, $\Delta\ s_{1/2}$, of the barrier at half

its height in the forward direction. As PM point out, this may be determined by setting $V(x)$

equal to $(A + B)^2/8A$ in equation 4 and taking the difference between the two roots for

x. The results for a number of barriers are listed in the final column of Table 6.2.

The barrier obtained by the BEBO method is more than twice as broad as the

barrier obtained from experiment. The double-headed arrow on Figure 9 represents a

transition from half-way up one side of the BEBO barrier to a point at equal energy on

the other side.

The barrier width in Table 6.2 calculated from MT's values of V_b and T^* is

smaller. It is interesting to note that the same value of 0.44 Å is obtained from MT's

values at the HF and MP2 levels, even though the barrier height differed by a factor of

four and T^* by a factor of two. This gives reason to hope that *ab initio* methods may

give more consistent values of barrier widths than of barrier heights. For their TST

calculations MT used an "interpolated" barrier obtained from the reactant, TS and

product energies (including zero-point energies) and one additional energy for a point

slightly on the product side of the TS. Measuring the width of the barrier in their Figure

2 at 5.1 kJ mol^{-1} below its peak, and adjusting to the reduced mass of a hydrogen atom,

gives a width of 0.33 Å. This is in excellent agreement with the value of 0.33 ± 0.01 Å

which PM obtained by fitting their TST model to MT's data, confirming that differences

in models (different treatment of tunneling and grouping of vibrational frequencies) do

not seriously affect this parameter.

From the present *ab initio* calculations, a value of 0.88 Å is obtained from the

Eckart curve fitted to the MP2 barrier in Figure 10. This is about one standard deviation wider than the barrier obtained from experimental results. However, the Eckart barrier fitted to the MP4 points has a width of only 0.53 Å. This is close to the MT result, and within two standard deviations of the experimer .' ·ult.

Thus a difference remains between the highest level *ab initio* barrier widths, at 0.53 Å, and the experimental result, at 0.74 Å. One possible explanation would be that the effective barrier for experimental particles is the sum of electronic and zero-point energies, whereas the theoretical values quoted are for electronic energy barriers only. The addition of zero-point energies affects the vertical, and as shown by MT, the horizontal position of the top of the barrier, so it is not unreasonable to conjecture that it would have a similar effect at other points along the barrier, thus modifying the width. Another possibility (pointed out by PM) is that the curvature of the reaction path makes it more difficult for real particles to tunnel through the multidimensional barrier. Also note that the MP2 points at the left side of Figure 10 approach the reactant energy more gradually than the Eckart curve does; the true barrier width at half-height of the MP4 curve may also exceed the value calculated from the Eckart curve. It is likely that a combination of these reasons is responsible for the difference between theory and experiment.

6.6 Conclusions

The optimized transition state geometry is consistent with an early TS. The surface for OH internal rotation is very flat. The normal mode frequency analysis

reveals several low frequency vibrations in the transition state, including modes for CH_3-CH_3 torsions, and bending and stretching modes at the reaction center, with the harmonic mean of the five lowest frequencies being 345 cm^{-1}, in excellent agreement with the value which PM inferred from experiment (350 cm^{-1}). The calculated activation barrier height of 12.4 kJ mol^{-1} is in reasonable agreement with the value from the fit to experimental data (9.3 kJ mol^{-1}). The calculated enthalpy of reaction at 298 K of -73.8 kJ mol^{-1} also agrees fairly well with experimental results. Although *ab initio* calculations of the characteristic tunneling temperature suggest tunneling would be significant at room temperature, the experimental evidence suggests it is only dominant at the lowest experimental temperatures. The width of the activation barrier at half its height was found to be 0.53 Å at the MP4 level, 0.88 Å at the MP2 level and 0.74 $\pm$ 0.11 Å from experiment.

Chapter 7. Structural and Energetic Properties of Reactions of Hydroxyl Radicals with Fluorinated Ethanes

7.1 Introduction

Hydroxyl radicals are the most likely initiators of tropospheric degradation for the hydrochlorofluorocarbon (HCFC) and hydrofluorocarbon (HFC) classes of chlorofluoro-carbon (CFC) replacement compounds.[223] In the HFC class several fluorinated ethanes have been investigated, and in particular CF_3-CH_2F (HFC-134a) has been chosen for use in home refrigeration units. Since the reactions of OH with hydrofluorinated ethanes (HFEs) are potentially of great significance in atmospheric chemistry, it is desirable to increase the knowledge base on them. There have been no published *ab initio* studies of these reactions. Experimental studies have included the determination of rate coefficients for reactions of OH with C_2H_5F,[224,225] CHF_2-CH_3,[226-228] CF_3-CH_3,[225,229] CF_3-CH_2F,[226,228-231] CHF_2-CHF_2,[231] and CF_3-CHF_2.[226,229] Cohen and Benson used conventional transition-state theory to extrapolate rate coefficients,[232] and derived empirical correlations for the activation energy and entropy,[233] for reactions of OH with several haloalkanes, including C_2H_5F, CHF_2-CH_3, CH_2F-CH_2F, CF_3-CH_3, CHF_2-CH_2F, CF_3-CH_2F, CHF_2-CHF_2, and CF_3-CHF_2.

The optimized geometries and vibrational frequencies for the fifteen transition states which occur when OH abstracts an inequivalent hydrogen atom from the most stable conformer for each of the eight molecules in the series $C_2H_nF_{6-n}$, $n = 1-5$ have been calculated. Energy calculations include total and zero-point energies, classical

barrier heights and enthalpies of reaction.

7.2 Optimized Geometries

The HF/6-31G(d) optimized geometries are presented in Figure 11, the MP2/6-31G(d,p) optimized geometries are presented in Figure 12 and geometrical parameters at both levels of theory are given in Table 7.1. The structures are asymmetrical except for $CH_3-CF_2H + OH$, which has C_s symmetry at HF/6-31G(d), but again has C_1 symmetry at MP2/6-31G(d,p). As with the parent $C_2H_6 + OH$ reaction (see Chapter 5), and other reactions where hydrogen is abstracted by hydroxyl,[234,235] the MP2 geometries indicate a relatively early transition state, with the breaking bond stretched by only a small amount from its equilibrium value and the forming bond still relatively long, while the HF geometries show a long $C-H$ bond and a short $O-H$ one. The other major difference in the two levels of theory is the greater deviation from linearity for the $C-H-O$ angle at the reaction centre seen with MP2 theory.

Many of the trends seen in the geometrical parameters are similar to those noted in Chapter 5 for the series $C_2H_nF_{6-n}$. $n = 0-6$, and Chapter 3 for the series $C_2H_nF_{5-n}$, $n = 0-5$. The $C-C$ bond lengths have two opposing trends, decreasing with increasing fluorine substitution for less than three fluorines, reaching a minimum for $CF_3-CH_3 +$ OH, then increasing to reach a maximum for $CF_3-CHF_2 + OH$. There is also a tendency to shorter lengths when there is more than one fluorine on a given carbon, indicative of a geminal effect. The lengths are slightly shorter at the MP2 level, except for $CH_2F-CHF_2 + OH$, where it is 0.001 Å longer.
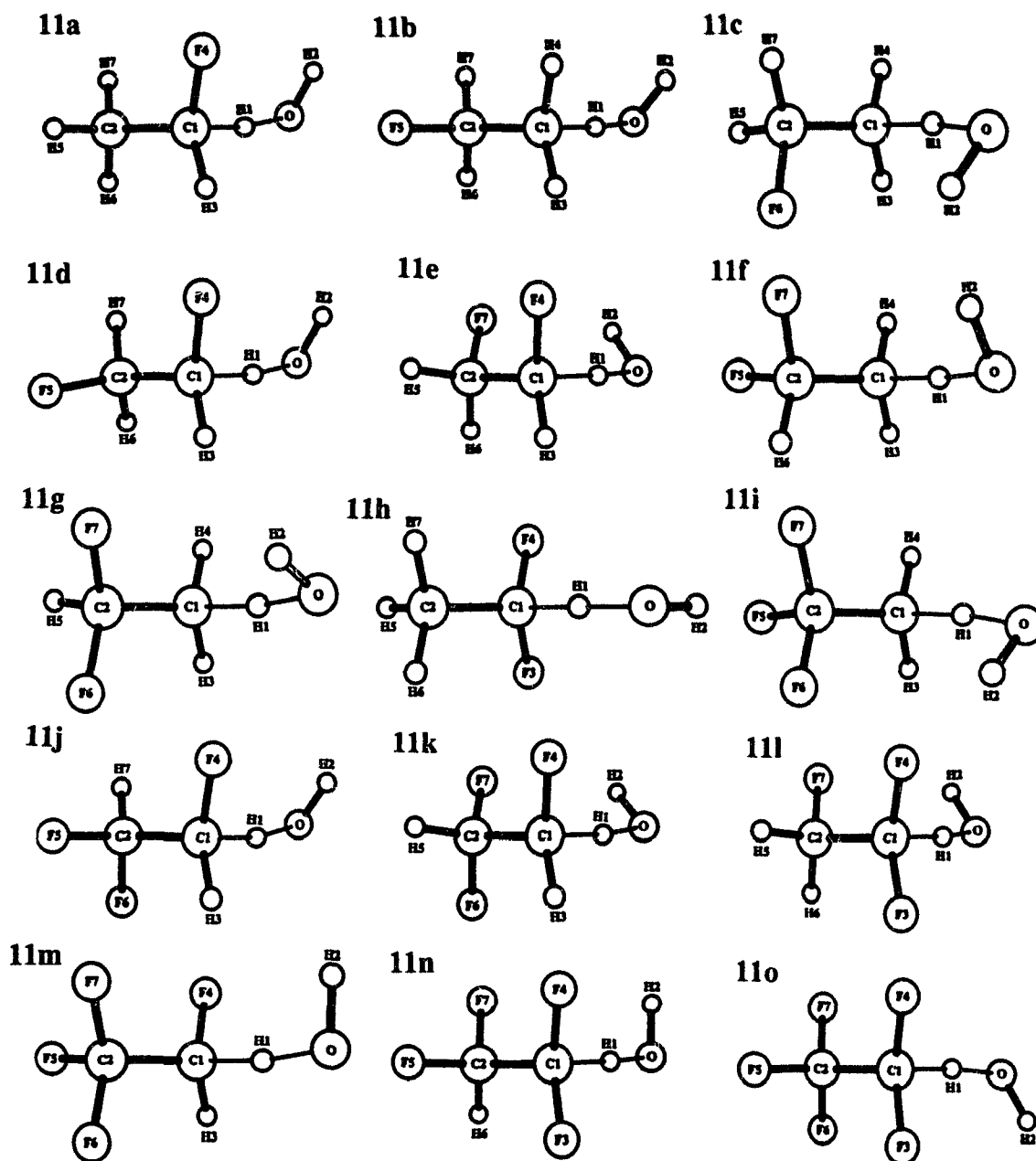
Figure 11. HF/6-31G(d) optimized transition states for the reactions: **11a** CH_3-CH_2F + OH; **11b** CH_2F-CH_3 + OH t; **11c** CH_2F-CH_3 + OH g; **11d** CH_2F-CH_2F + OH t; **11e** CH_2F-CH_2F + OH g; **11f** CHF_2-CH_3 + OH g,t; **11g** CHF_2-CH_3 + OH g,g; **11h** CH_3-CF_2H + OH; **11i** CF_3-CH_3 + OH; **11j** CHF_2-CH_2F + OH g,t; **11k** CHF_2-CH_2F + OH g,g; **11l** CH_2F-CHF_2 + OH; **11m** CF_3-CH_2F + OH; **11n** CHF_2-CHF_2 + OH; **11o** CF_3-CHF_2 + OH. The designations t and g refer to the abstracted H being trans or gauche to a β-F, respectively.
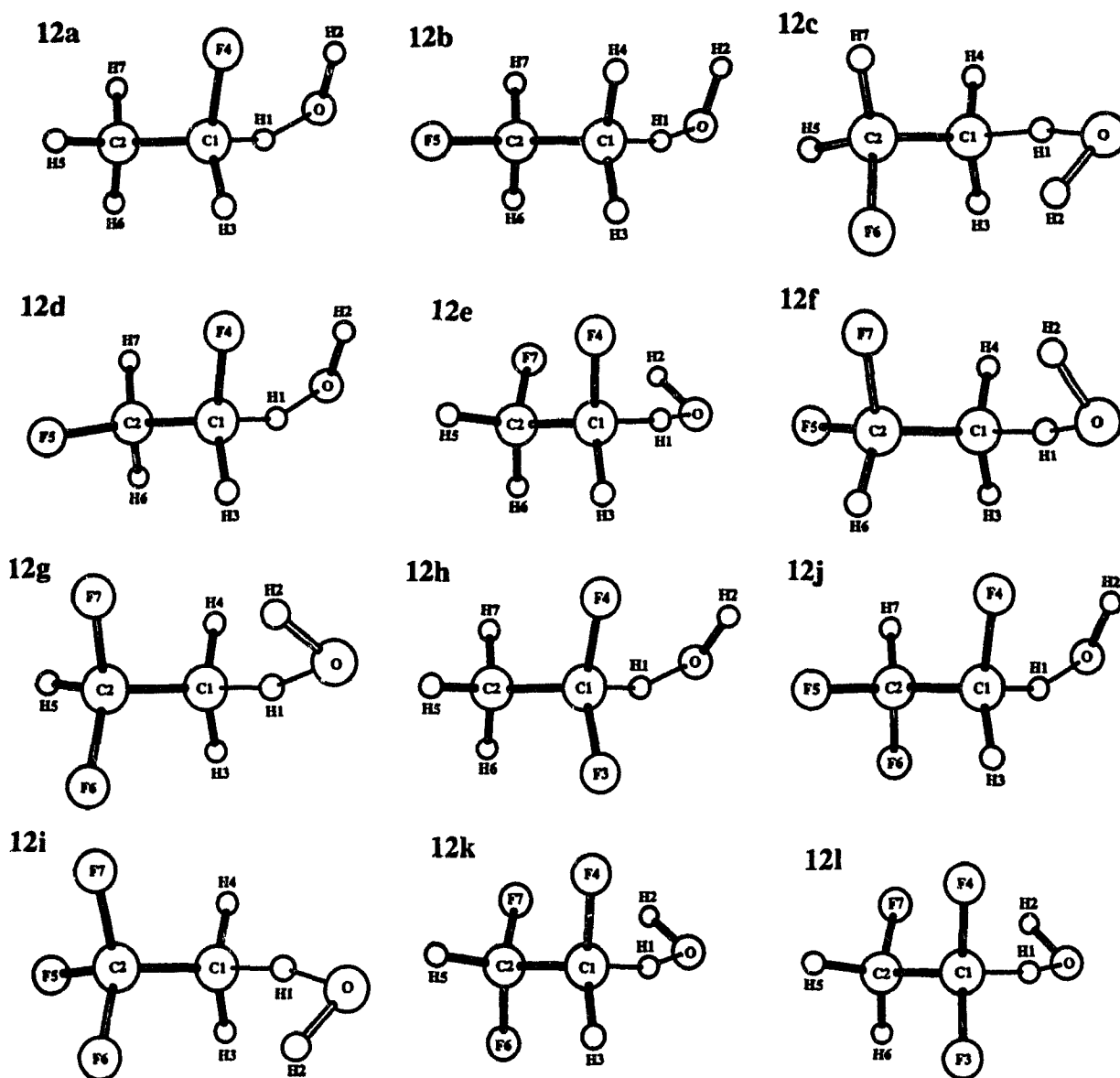
Figure 12. MP2/6-31G(d,p) optimized transition states for the reactions: **12a** CH₃−CH₂F + OH; **12b** CH₂F−CH₃ + OH t; **12c** CH₂F−CH₃ + OH g; **12d** CH₂F−CH₂F + OH t; **12e** CH₂F−CH₂F + OH g; **12f** CHF₂−CH₃ + OH g,t; **12g** CHF₂−CH₃ + OH g,g; **12h** CH₃−CF₂H + OH; **12i** CF₃−CH₃ + OH; **12j** CHF₂−CH₂F + OH g,t; **12k** CHF₂−CH₂F + OH g,g; **12l** CH₂F−CHF₂ + OH. The designations t and g refer to the abstracted H being trans or gauche to a β-F, respectively.

Table 7.1: Geometrical Parameters for Each TS at Two Levels of Theory[a]

Parameter[b]	HF/6-31G(d)	MP2/6-31G(d,p)
CH₃−CH₂F + OH		
C1−C2	1.500	1.498
C1−H1	1.299	1.190
H1−O	1.210	1.314
O−H2	0.955	0.971
C1−H3	1.080	1.089
C1−F4	1.354	1.387
C2−H5	1.086	1.088
C2−H6	1.084	1.087
C2−H7	1.083	1.086
C1−H1−O	171.4	157.8
H1−O−H2	99.1	95.2
H3−C1−H1	104.5	106.6
F4−C1−H1	106.0	105.9
H3−C1−F4	109.7	109.0
H1−C1−C2	107.5	108.9
H3−C1−C2	116.3	115.1
F4−C1−C2	112.0	110.9
H5−C2−H6	108.8	108.9
H5−C2−H7	108.6	109.0
H6−C2−H7	108.8	108.8
H5−C2−C1	110.2	110.2
H6−C2−C1	110.1	110.1
H7−C2−C1	110.3	109.9
C1−H1−O−H2	25.1	19.1
H2...F4	2.896	2.525

Table 7.1 (continued)

Parameter[b]	HF/6-31G(d)	MP2/6-31G(d,p)
CH₂F−CH₃ + OH t		
C1−C2	1.505	1.502
C1−H1	1.313	1.200
H1−O	1.201	1.292
O−H2	0.955	0.971
C1−H3	1.080	1.085
C1−H4	1.081	1.085
C2−F5	1.374	1.398
C2−H6	1.081	1.088
C2−H7	1.081	1.088
C1−H1−O	174.1	165.1
H1−O−H2	100.1	98.3
H3−C1−H1	103.9	105.1
H4−C1−H1	106.0	107.8
H3−C1−H4	112.4	111.3
H1−C1−C2	104.4	105.8
H3−C1−C2	114.7	113.4
H4−C1−C2	114.1	112.8
F5−C2−H6	108.0	108.2
F5−C2−H7	107.9	108.2
H6−C2−H7	109.1	108.8
F5−C2−C1	109.1	109.2
H6−C2−C1	111.3	111.2
H7−C2−C1	111.3	111.1
C1−H1−O−H2	87.1	64.1
H2...F5	4.949	4.740
CH₂F−CH₃ + OH g		

Table 7.1 (continued)

Parameter[b]	HF/6-31G(d)	MP2/6-31G(d,p)
C1−C2	1.502	1.498
C1−H1	1.316	1.210
H1−O	1.194	1.273
O−H2	0.955	0.972
C1−H3	1.080	1.085
C1−H4	1.080	1.086
C2−H5	1.084	1.090
C2−F6	1.375	1.404
C2−H7	1.081	1.088
C1−H1−O	166.0	157.1
H1−O−H2	99.2	96.9
H3−C1−H1	104.4	106.4
H4−C1−H1	104.0	105.5
H3−C1−H4	112.9	111.9
H1−C1−C2	105.4	106.0
H3−C1−C2	114.4	113.2
H4−C1−C2	114.4	113.2
H5−C2−F6	107.6	107.4
H5−C2−H7	109.1	109.3
F6−C2−H7	107.8	107.7
H5−C2−C1	111.7	112.2
F6−C2−C1	109.0	108.7
H7−C2−C1	111.5	111.4
C1−H1−O−H2	22.0	20.3
H2...F6	2.515	2.193
CH₂F−CH₂F + OH t		
C1−C2	1.497	1.494

Table 7.1 (continued)

Parameter[b]	HF/6-31G(d)	MP2/6-31G(d,p)
C1−H1	1.309	1.198
H1−O	1.199	1.298
O−H2	0.955	0.972
C1−H3	1.079	1.088
C1−F4	1.347	1.378
C2−F5	1.368	1.392
C2−H6	1.080	1.089
C2−H7	1.081	1.088
C1−H1−O	171.6	158.5
H1−O−H2	99.6	96.1
H3−C1−H1	105.6	107.6
F4−C1−H1	107.0	107.2
H3−C1−F4	110.6	110.0
H1−C1−C2	105.0	106.2
H3−C1−C2	115.6	114.2
F4−C1−C2	112.3	111.3
F5−C2−H6	108.6	109.1
F5−C2−H7	108.6	109.0
H6−C2−H7	109.8	109.6
F5−C2−C1	109.5	109.6
H6−C2−C1	110.0	109.8
H7−C2−C1	110.3	109.8
C1−H1−O−H2	52.8	39.5
H2...F4	2.971	2.647
CH₂F−CH₂F + OH g		
C1−C2	1.497	1.495
C1−H1	1.314	1.206

Table 7.1 (continued)

Parameter[b]	HF/6-31G(d)	MP2/6-31G(d,p)
H1–O	1.191	1.285
O–H2	0.955	0.972
C1–H3	1.080	1.089
C1–F4	1.344	1.373
C2–H5	1.083	1.089
C2–H6	1.081	1.088
C2–F7	1.369	1.398
C1–H1–O	167.9	157.9
H1–O–H2	99.5	96.9
H3–C1–H1	104.6	106.1
F4–C1–H1	108.1	108.7
H3–C1–F4	110.9	110.6
H1–C1–C2	105.7	106.7
H3–C1–C2	115.0	113.2
F4–C1–C2	112.0	111.2
H5–C2–H6	110.0	110.2
H5–C2–F7	108.1	108.0
H6–C2–F7	108.6	108.7
H5–C2–C1	110.7	110.8
H6–C2–C1	110.1	110.1
F7–C2–C1	109.3	109.1
C1–H1–O–H2	36.8	33.1
H2...F7	2.340	2.195
CHF$_2$–CH$_3$ + OH g,t		
C1–C2	1.497	1.492
C1–H1	1.323	1.216
H1–O	1.184	1.259

Table 7.1 (continued)

Parameter[b]	HF/6-31G(d)	MP2/6-31G(d,p)
O−H2	0.955	0.972
C1−H3	1.079	1.084
C1−H4	1.079	1.084
C2−F5	1.345	1.369
C2−H6	1.077	1.088
C2−F7	1.348	1.379
C1−H1−O	167.8	158.1
H1−O−H2	100.2	98.0
H3−C1−H1	103.7	105.8
H4−C1−H1	105.7	107.4
H3−C1−H4	113.6	112.8
H1−C1−C2	105.1	105.9
H3−C1−C2	114.2	113.0
H4−C1−C2	113.2	111.6
F5−C2−H6	108.2	108.4
F5−C2−F7	107.2	107.3
H6−C2−F7	108.1	107.8
F5−C2−C1	110.1	110.2
H6−C2−C1	113.6	114.0
F7−C2−C1	109.5	109.0
C1−H1−O−H2	39.7	35.8
H2...F7	2.697	2.340
CHF₂−CH₃ + OH g,g		
C1−C2	1.496	1.492
C1−H1	1.327	1.220
H1−O	1.181	1.252
O−H2	0.955	0.972

Table 7.1 (continued)

Parameter[b]	HF/6-31G(d)	MP2/6-31G(d,p)
C1−H3	1.079	1.084
C1−H4	1.079	1.084
C2−H5	1.080	1.090
C2−F6	1.341	1.365
C2−F7	1.349	1.380
C1−H1−O	169.8	161.1
H1−O−H2	100.1	98.1
H3−C1−H1	104.8	106.0
H4−C1−H1	104.2	106.6
H3−C1−H4	113.6	112.6
H1−C1−C2	106.2	105.8
H3−C1−C2	113.7	112.6
H4−C1−C2	113.6	112.6
H5−C2−F6	108.0	108.2
H5−C2−F7	107.7	107.3
F6−C2−F7	107.2	107.3
H5−C2−C1	113.5	114.4
F6−C2−C1	110.4	110.2
F7−C2−C1	109.7	109.2
C1−H1−O−H2	12.9	9.8
H2...F7	2.587	2.262
CH₃−CF₂H + OH		
C1−C1	1.496	1.494
C1−H1	1.303	1.194
H1−O	1.197	1.305
O−H2	0.955	0.971
C1−F3	1.329	1.357

Table 7.1 (continued)

Parameter[b]	HF/6-31G(d)	MP2/6-31G(d,p)
C1−F4	1.329[c]	1.365
C2−H5	1.085	1.087
C2−H6	1.082	1.085
C2−H7	1.082[c]	1.085
C1−H1−O	178.9	162.0
H1−O−H2	100.1	96.8
F3−C1−H1	107.0	107.8
F4−C1−H1	107.0[c]	106.3
F3−C1−F4	108.3	108.0
H1−C1−C2	108.5	111.0
F3−C1−C2	112.9	112.0
F4−C1−C2	112.9[c]	111.4
H5−C2−H6	109.3	109.6
H5−C2−H7	109.3[c]	109.7
H6−C2−H7	109.4	109.5
H5−C2−C1	109.2	108.7
H6−C2−C1	109.8	109.7
H7−C2−C1	109.8[c]	109.6
C1−H1−O−H2	0.0	32.7
H2...F4	2.357	2.682
CF₃−CH₃ + OH		
C1−C2	1.495	1.491
C1−H1	1.331	1.223
H1−O	1.173	1.241
O−H2	0.955	0.972
C1−H3	1.077	1.083
C1−H4	1.078	1.083

Table 7.1 (continued)

Parameter[b]	HF/6-31G(d)	MP2/6-31G(d,p)
C2–F5	1.324	1.351
C2–F6	1.327	1.359
C2–F7	1.320	1.346
C1–H1–O	171.9	163.1
H1–O–H2	101.0	99.1
H3–C1–H1	104.8	107.1
H4–C1–H1	103.9	106.0
H3–C1–H4	114.1	113.1
H1–C1–C2	106.7	106.4
H3–C1–C2	112.9	111.8
H4–C1–C2	113.2	112.0
F5–C2–F6	107.2	107.1
F5–C2–F7	107.5	107.6
F6–C2–F7	107.4	107.3
F5–C2–C1	111.4	111.8
F6–C2–C1	111.1	110.9
F7–C2–C1	111.9	111.9
C1–H1–O–H2	6.4	0.3
H2...F6	2.739	2.411
CHF$_2$–CH$_2$F + OH g,t		
C1–C2	1.502	1.500
C1–H1	1.318	1.206
H1–O	1.184	1.277
O–H2	0.955	0.972
C1–H3	1.078	1.087
C1–F4	1.343	1.374
C2–F5	1.341	1.366

Table 7.1 (continued)

Parameter[b]	HF/6-31G(d)	MP2/6-31G(d,p)
C2−F6	1.337	1.365
C2−H7	1.077	1.088
C1−H1−O	167.7	157.7
H1−O−H2	100.2	97.1
H3−C1−H1	106.5	108.3
F4−C1−H1	106.8	107.8
H3−C1−F4	111.8	111.3
H1−C1−C2	106.0	106.3
H3−C1−C2	114.5	112.7
F4−C1−C2	110.7	110.2
F5−C2−F6	108.1	108.5
F5−C2−H7	108.7	108.8
F6−C2−H7	109.6	109.5
F5−C2−C1	109.4	109.4
F6−C2−C1	108.2	107.6
H7−C2−C1	112.8	112.9
C1−H1−O−H2	35.7	36.5
H2...F4	2.869	2.625
CHF₂−CH₂F + OH g,g		
C1−C2	1.502	1.501
C1−H1	1.322	1.212
H1−O	1.179	1.267
O−H2	0.955	0.972
C1−H3	1.078	1.087
C1−F4	1.341	1.369
C2−H5	1.079	1.089
C2−F6	1.337	1.362

Table 7.1 (continued)

Parameter[b]	HF/6-31G(d)	MP2/6-31G(d,p)
C2−F7	1.342	1.372
C1−H1−O	171.6	162.4
H1−O−H2	100.3	98.0
H3−C1−H1	105.1	107.0
F4−C1−H1	108.3	109.3
H3−C1−F4	111.8	111.5
H1−C1−C2	106.3	106.2
H3−C1−C2	114.6	113.0
F4−C1−C2	110.3	109.7
H5−C2−F6	109.3	109.5
H5−C2−F7	108.2	107.9
F6−C2−F7	108.2	108.3
H5−C2−C1	112.7	113.4
F6−C2−C1	108.7	108.4
F7−C2−C1	109.6	109.1
C1−H1−O−H2	6.0	1.5
H2...F7	2.638	2.279
CH₂F−CHF₂ + OH		
C1−C2	1.503	1.504
C1−H1	1.319	1.212
H1−O	1.179	1.273
O−H2	0.956	0.973
C1−F3	1.323	1.354
C1−F4	1.322	1.352
C2−H5	1.082	1.088
C2−H6	1.079	1.086
C2−F7	1.363	1.391

Table 7.1 (continued)

Parameter[b]	HF/6-31G(d)	MP2/6-31G(d,p)
C1−H1−O	169.4	158.1
H1−O−H2	100.3	97.7
F3−C1−H1	108.4	109.1
F4−C1−H1	107.8	108.3
F3−C1−F4	109.5	109.5
H1−C1−C2	107.5	108.7
F3−C1−C2	111.0	110.0
F4−C1−C2	112.4	111.3
H5−C2−H6	110.4	110.7
H5−C2−F7	109.2	109.3
H6−C2−F7	109.4	109.5
H5−C2−C1	110.0	109.8
H6−C2−C1	109.9	109.8
F7−C2−C1	108.0	107.7
C1−H1−O−H2	32.1	24.9
H2...F7	2.679	2.262

CF_3-CH ˙ $+ OH$

˙2	1.504	
˛ ˙ ᴨl	1.337	
H1−O	1.173	
O−H2	0.956	
C1−H3	1.077	
C1−F4	1.337	
C2−F5	1.320	
C2−F6	1.317	
C2−F7	1.317	
C1−H1−O	171.9	

Table 7.1 (continued)

Parameter[b]	HF/6-31G(d)	MP2/6-31G(d,p)
H1−O−H2	100.8	
H3−C1−H1	105.2	
F4−C1−H1	108.0	
H3−C1−F4	112.2	
H1−C1−C2	106.6	
H3−C1−C2	113.9	
F4−C1−C2	110.5	
F5−C2−F6	108.2	
F5−C2−F7	107.9	
F6−C2−C7	108.7	
F5−C2−C1	111.1	
F6−C2−C1	109.6	
F7−C2−C1	111.3	
C1−H1−O−H2	13.9	
H2...F4	3.015	
CHF$_2$−CHF$_2$ + OH		
C1−C2	1.510	
C1−H1	1.321	
H1−O	1.176	
O−H2	0.956	
C1−F3	1.318	
C1−F4	1.318	
C2−F5	1.334	
C2−H6	1.077	
C2−F7	1.335	
C1−H1−O	174.6	
H1−O−H2	100.8	

Table 7.1 (continued)

Parameter[b]	HF/6-31G(d)	MP2/6-31G(d,p)
F3−C1−H1	107.7	
F4−C1−H1	108.6	
F3−C1−F4	110.2	
H1−C1−C2	107.0	
F3−C1−C2	111.2	
F4−C1−C2	112.0	
F5−C2−H6	109.5	
F5−C2−F7	108.5	
H6−C2−F7	109.8	
F5−C2−C1	109.2	
H6−C2−C1	111.6	
F7−C2−C1	108.2	
C1−H1−O−H2	61.2	
H2...F4	3.155	
CF₃−CHF₂ + OH		
C1−C2	1.517	
C1−H1	1.332	
H1−O	1.162	
O−H2	0.956	
C1−F3	1.318	
C1−F4	1.313	
C2−F5	1.315	
C2−F6	1.313	
C2−F7	1.311	
C1−H1−O	172.2	
H1−O−H2	101.3	
F3−C1−H1	107.9	

Table 7.1 (continued)

Parameter[b]	HF/6-31G(d)	MP2/6-31G(d,p)
F4−C1−H1	108.5	
F3−C1−F4	104.4	
H1−C1−C2	108.1	
F3−C1−C2	110.7	
F4−C1−C2	111.1	
F5−C2−F6	108.7	
F5−C2−F7	108.8	
F6−C2−F7	109.2	
F5−C2−C1	110.5	
F6−C2−C1	109.7	
F7−C2−C1	109.9	
C1−H1−O−H2	11.8	
H2...F3	2.955	

[a] Bond lengths in angstroms, angles in degrees. Atom numbering system as in Figures 1 and 2. [b] t and g refer to the abstracted H being trans and gauche to a β-F, respectively. [c] This value is equal to the one immediately above by symmetry.

For the C−H bond being broken (C1−H1) bond lengths are shorter when there are more fluorines on the α- vs. β-carbon, and for conformers where there is a β-fluorine trans rather than gauche to the abstracted hydrogen. The HF−MP2 difference is fairly constant (0.106−0.113 Å, with most values in the range 0.107−0.109 Å). For species with two or fewer fluorines, this value tends to be larger for trans and shorter for gauche conformers.

For the O−H bond being formed, H1−O lengths are longer when there are more fluorines on the α- vs. β-carbon, and for conformers where there is a β-fluorine trans rather than gauche to the abstracted hydrogen. These trends are complementary to those for C1−H1, and indicate an earlier TS in these instances. There is a general tendency to shorter lengths with increasing fluorine substitution. There is a large variation in the MP2−HF difference (0.068 −0.108 Å), with larger differences seen for trans vs. gauche conformers, and a general trend to smaller differences when the number of β-fluorines is two or more greater than the number of α-fluorines.

The bond length in the hydroxyl moiety (O−H2) is remarkably constant throughout the series, having variations of only about 0.001 Å at both levels of theory.

The C_α−H_α (C1−H3 or C1−H4) bond lengths have little variability, ranging from 1.077 −1.081 Å at HF and 1.083−1.089 Å at MP2 theory. Lengths become shorter with increasing substitution, particularly on the β-carbon, consistent with an inductive effect, as seen in Chapter 3 for the C−H bond dissociation energies. The MP2−HF differences have a range of 0.004−0.009 Å, with larger values in cases where there is an α-fluorine.

The $C_\alpha-F_\alpha$ bond lengths decrease with increasing substitution, especially when there is another α-fluorine. As with the reactants and products, inclusion of electron correlation with MP2 theory gives significantly longer bond lengths (by $0.028-0.036$ Å).

The trends in $C_\beta-H_\beta$ bond lengths are somewhat dependent on the theory used. In the HF structures, the variability in lengths ($1.077-1.086$ Å) is slightly more than was the case at the α-center. The lengths tend to be shorter when there are β-fluorines, and longer when the hydrogen is in position 5. The latter trend is also seen at the MP2 level, but not the former. The MP2$-$HF difference ranges from $0.002-0.009$ Å, with the smallest values seen when there are no β-fluorines.

The $C_\beta-F_\beta$ bond lengths are highly variable, ranging from $1.311-1.375$ Å, and $1.346-1.404$ Å, at the HF and MP2 levels, respectively. At both levels the lengths decrease with increasing fluorine substitution, especially on the β-carbon, but the correlation is not as strong at MP2. The MP2$-$HF difference is usually smaller when the fluorine is in position 5, where it will be eclipsing the SOMO of the resultant radical, or when it is trans to the abstracted hydrogen.

The $C-H-O$ angle varies more than any other through the series. Greater deviations from linearity are seen with MP2 theory, with the difference being larger when the number of α-fluorines is greater than the number at the β-carbon.

The $H-O-H$ angle tends to be smaller when there are α-fluorines; the same situation gives rise to a larger difference in values at the two levels of theory.

The magnitudes of the $H-C-H$ angles decrease in the order $H_\alpha-C1-H_\alpha$ > $H_\beta-C2-H_\beta$ > $H_\alpha-C1-H1$, where H_α can be H3 or H5, and H_β can be H5, H6, or

H7. The H_α−C1−H1 angles are about 2° larger at the MP2 level. For cases of R−CH$_3$ + OH, where there are two such angles, the largest magnitude is for the case where H_α is closest to H1, with a particularly large difference seen when H_α and H1 are eclipsed or nearly so. The H_α−C1−H_α angles are about 1° larger at the HF level. At both levels of theory the magnitude increases with increasing fluorine substitution. This trend is also seen for H_β−C2−H_β angles, which are all within ±1° of the tetrahedral value, and only very small differences are seen between the two levels of theory.

The magnitudes of the F−C−H angles also decrease in the order F_α−C1−H_α > F_β−C2−H_β > F_α−C1−H1. For cases of R−CHF$_2$ + OH, the smaller value is seen for F_α closest to H1, with the exception of CHF$_2$−CHF$_2$ + OH. The F_α−C1−H$_1$ angles tend to increase with increasing fluorine substitution, and the MP2 value is higher, by ≤ 1°, except for CH$_3$−CH$_2$F + OH, where it is −0.1° smaller. Similar trends are observed for F_α−C1−H_α angles, but the angles are larger at the HF level, with no exceptions. The magnitudes of the F_β−C2−H_β angles show little variation between the two levels of theory, being within ±0.5° in all cases, and usually within ±0.2°.

Also given in Table 7.1 are H2...Fx distances, where Fx is the closest fluorine to H2, the hydroxyl hydrogen. This gives an indication of the degree of intramolecular hydrogen bonding in the TS. Strong theoretical[236] and experimental[237] evidence for H...F intramolecular hydrogen bonding has been reported previously. Hydrogen bonding can occur when the interatomic distance from the hydrogen to the electronegative donor atom is significantly less than the sum of their effective van der Waals radii. These values are 1.2 Å for hydrogen and 1.35 Å for fluorine,[238] so in the present case an

intramolecular hydrogen bond can be deemed to be present if the H2...Fx distance is less than 2.5 Å. In all cases, except CH_3-CHF_2 + OH, where the two levels of theory give different point groups, this distance is shorter at the MP2 level, consistent with giving a more accurate geometry description when polar bonds are present.[239] Regardless of the level of theory, shorter distances are seen when at least one β-fluorine is gauche to the abstracted hydrogen, in which case the incoming hydroxyl is oriented to take advantage of an intramolecular hydrogen bond, usually such that H2 is closer to β- rather than α-fluorines. Exceptions occur for some of the more highly substituted species, where multiple β-fluorines appear to have a cancelling effect. In these cases, particularly when the β-group is CF_3, the H2...Fα distances of about 3 Å do not indicate hydrogen bonding. For the OH group to form a hydrogen bond to a trans β-fluorine, a rotation of the ethane would first have to occur, and this is not energetically favorable. Even where hydrogen bonding is occuring, the interatomic distance is only about 0.3 Å less than the sum of the van der Waals radii, so the energetic advantage should be small.

7.3 Vibrational Frequencies

Vibrational frequencies are presented in Table 7.2. The modes are ordered by increasing wavenumber at the HF level and approximate type of mode, with the order of the MP2 frequencies adjusted to match the same type at the HF level. In some cases the types of mode do not match, due to differences both from the level of theory at which the frequencies are calculated and in the optimized geometries. The assignment of modes is complicated by the lack of symmetry; many modes are strongly coupled, and

most include compensating motions in the H−O−(H) fragment. Many modes which consist primarily of motion of one carbon group also contain smaller motions of the other group. The reduced masses are often less than expected due to the couplings and compensating motions. The hydrogen being abstracted is in some cases still considered as being in the ethane, and in other cases as being in the product water molecule. This ambiguity, and the differing amounts of bond-breaking at the TS at the two levels of theory, often leads to different modes occurring at the two levels. Another effect is that it is difficult to ascertain *a priori* which modes to expect. Assignments are made based on those atoms with the largest mass-weighted motions; the descriptions can only be considered as approximate. In this context "symmetric" and "degenerate" should be interpreted loosely. For cases where equivalent groups are at both carbons, α- and β-designations are used to distinguish the motions. If no designations appear in these cases, the motion occurs in both groups.

There are six additional degrees of freedom in the TS as compared to the parent ethane. One C−H stretching mode in the reactant becomes the reaction coordinate, and one bending mode usually becomes either a C−H−O bend or a C−C−O skeletal bend, although it is retained in some cases where the hydrogen remains tightly bound to the carbon. The six additional modes consist of what is essentially a rotation of the OH group, an R−OH torsion, two H−O−H bends, an O−H stretch, and a TS symmetrical stretch.

Table 7.2: Vibrational Frequencies for Each TS at Two Levels of Theory

Frequency (cm^{-1})		Reduced mass (amu)		Approximate type of mode
HF	MP2	HF	MP2	
CH$_3$−CH$_2$F + OH				
3155i	1921i	1.065	1.109	reaction coordinate
102	100	4.158	3.543	HO−C$_2$H$_5$F torsion
151	128	1.706	2.730	CH$_3$−CH$_2$F torsion
170	229	1.205	1.072	OH rotation*
246	260	1.268	1.171	CH$_3$ rock
435	417	2.914	2.868	C−C−F bend
562	702	3.656	2.473	CH$_3$ rock + CH$_2$ scissors
865	829	1.113	1.065	CH$_2$ wag + CH$_3$ deformation
881		1.124		CH$_3$ deformation + CH$_2$ wag
	934		1.959	CH$_3$ deformation
986		2.206		CH$_3$ + CH$_2$ rock
	946		1.444	CH$_2$ wag
1186	1145	1.898	2.391	C−C stretch
1254	1222	1.654	1.605	CH$_2$ twist
1267	1178	2.621	2.363	C−F stretch
1373	1358	1.208	1.085	H−O−H bend
1497	1411	1.258	1.257	CH$_3$ + CH$_2$ rock
1569	1472	1.330	1.384	CH$_3$ symmetric deformation
1620	1542	1.046	1.043	CH$_3$ degenerate deformation
1630	1550	1.045	1.045	CH$_3$ degenerate deformation
1674	1633	1.075	1.084	H−O−H bend
3210	3143	1.039	1.036	β-C−H symmetric stretch
3280	3242	1.098	1.103	β-C−H degenerate stretch
3298	3259	1.100	1.103	β-C−H degenerate stretch

Table 7.2 (continued)

| Frequency (cm^{-1}) | | Reduced mass (amu) | | Approximate type of mode |
HF	MP2	HF	MP2	
3318	3191	1.091	1.086	α-C$-$H stretch
4036	3839	1.067	1.066	O$-$H stretch

CH$_2$F$-$CH$_3$ + OH t

3160i	1950i	1.061	1.095	reaction coordinate
73	135	1.171	1.350	OH rotation[a]
89	73	3.216	2.470	HO$-$C$_2$H$_5$F torsion
111	93	4.058	3.694	C$-$C$-$O skeletal bend
370	345	3.999	2.586	C$-$C$-$F bend
443	431	1.186	1.392	CH$_3$ rock
592		2.328		α-CH$_2$ rock + H$-$O$-$H bend
	763		1.752	β-CH$_2$ twist + H$-$O$-$H bend
848		1.263		H$-$O$-$H bend + β-CH$_2$ rock
	843		1.568	H$-$O$-$H bend + β-CH$_2$ twist
886	877	1.176	1.189	CH$_3$ deformation
1088	1007	1.756	1.706	CH$_3$ deformation + C$-$F stretch
1157		2.710		C$-$C stretch
	1117		3.373	C$-$C + C$-$F stretch
1196		2.233		C$-$F stretch + CH$_3$ deformation
	1164		1.749	CH$_3$ rock + C$-$F stretch
1300		1.385		CH$_2$ twist + CH$_3$ deformation
	1329		1.244	CH$_2$ wag + CH$_3$ ^{1}eformation
1318	1236	1.305	1.436	CH$_2$ twist
1420	1341	1.085	1.146	CH$_2$ wag
1550	1463	1.212	1.258	β-CH$_2$ rock + α-CH$_2$ scissors
1598	1485	1.056	1.048	H$-$O$-$H bend
1623	1540	1.206	1.164	α-CH$_2$ scissors + β-CH$_2$ rock

Table 7.2 (continued)

Frequency (cm^{-1})		Reduced mass (amu)		Approximate type of mode
HF	MP2	HF	MP2	
1677	1586	1.095	1.095	β-CH$_2$ scissors
3267	3156	1.058	1.058	β-C$-$H symmetric stretch
3276	3196	1.055	1.056	α-C$-$H symmetric stretch
3314	3221	1.112	1.111	β-C$-$H asymmetric stretch
3358	3286	1.112	1.110	α-C$-$H asymmetric stretch
4038	3836	1.067	1.067	O$-$H stretch

CH$_2$F$-$CH$_3$ + OH g

Frequency (cm^{-1})		Reduced mass (amu)		Approximate type of mode
HF	MP2	HF	MP2	
3185i	2109i	1.061	1.079	reaction coordinate
99	158	5.649	5.162	HO$-$C$_2$H$_5$F torsion
150	141	2.382	2.611	CH$_2$F$-$CH$_3$ torsion
284	362	1.062	1.038	OH rotation[a]
421	401	1.590	1.800	C$-$C$-$F bend + CH$_3$ rock
442	425	1.767	1.580	C$-$C$-$F bend + CH$_3$ rock
597	679	3.094	2.253	C$-$H$-$O bend
861	967	1.077	1.279	H$-$O$-$H bend
948		1.542		α-CH$_2$ wag
	893		1.502	α- + β-CH$_2$ twist
991		1.613		α-CH$_2$ twist
	951		1.695	α- + β-CH$_2$ twist
1172	1111	2.573	3.401	C$-$F stretch
1213		1.610		β-CH$_2$ twist
	1194		1.390	CH$_3$ rock
1263	1204	1.802	1.817	C$-$C stretch
1323	1342	1.234	1.138	TS symmetric stretch
1402	1298	1.087	1.088	β-CH$_2$ wag
1560	1463	1.244	1.269	β-CH$_2$ rock

Table 7.2 (continued)

Frequency (cm^{-1})		Reduced mass (amu)		Approximate type of mode
HF	MP2	HF	MP2	
1597	1513	1.197	1.156	α-CH$_2$ scissors
1644	1586	1.064	1.088	H$-$O$-$H bend
1670	1576	1.095	1.101	β-CH$_2$ scissors
3244	3149	1.061	1.058	β-CH$_2$ symmetric stretch
3279	3193	1.056	1.057	α-CH$_2$ symmetric stretch
3302	3219	1.106	1.109	β-CH$_2$ asymmetric stretch
3360	3297	1.112	1.109	α-CH$_2$ asymmetric stretch
4037	3825	1.067	1.066	O$-$H stretch

CH$_2$F$-$CH$_2$F + OH t

3198i	2024i	1.065	1.099	reaction coordinate
81	67	5.750	5.595	HO$-$C$_2$H$_4$F$_2$ torsion
95	90	3.271	3.799	C$-$C$-$O skeletal bend
155	150	4.144	5.794	CH$_2$F$-$CH$_2$F torsion
177	226	1.211	1.102	OH rotation[a]
334	305	4.702	4.049	C$-$C$-$F bend
469	475	3.153	2.818	C$-$C$-$F bend
631	757	2.146	1.692	α-CH$_2$ twist
851	884	1.161	2.106	H$-$O$-$H bend
969	950	2.173	1.475	TS symmetric stretch
994	928	1.950	2.280	β-CH$_2$ twist
1196	1133	4.499	3.676	β-C$-$F stretch
1228	1173	2.133	2.340	C$-$C stretch
1270	1191	2.838	2.233	α-C$-$F stretch
1340	1349	1.182	1.185	α-CH$_2$ scissors
1392	1297	1.119	1.095	β-CH$_2$ wag
1503	1403	1.252	1.237	α-C$-$H bend

Table 7.2 (continued)

Frequency (cm^{-1})		Reduced mass (amu)		Approximate type of mode
HF	MP2	HF	MP2	
1590	1489	1.454	1.535	β-CH$_2$ rock
1652	1560	1.079	1.093	β-CH$_2$ scissors
1665	1593	1.109	1.094	H$-$O$-$H bend
3272	3155	1.058	1.058	β-C$-$H symmetric stretch
3324	3205	1.100	1.088	α-C$-$H + β-C$-$H asymmetric stretch
3339	3232	1.098	1.108	α-C$-$H + β-C$-$H asymmetric stretch
4033	3833	1.067	1.067	O$-$H stretch

CH$_2$F$-$CH$_2$F + OH g

Frequency (cm^{-1})		Reduced mass (amu)		Approximate type of mode
HF	MP2	HF	MP2	
3248i	2153i	1.064	1.087	reaction coordinate
96	138	6.066	6.510	C$-$C$-$O skeletal bend
109	102	3.840	4.240	HO$-$C$_2$H$_4$F$_2$ torsion
173	182	4.475	5.472	CH$_2$F$-$CH$_2$F torsion
261	362	1.175	1.139	OH rotation[a]
323	311	3.632	2.952	C$-$C$-$F bend
530	495	3.093	2.585	C$-$C$-$F bend
597		2.184		α-CH$_2$ rock
	707		3.178	C$-$H$-$O bend
885	896	1.738	1.468	H$-$O$-$H bend
962	918	2.382	2.366	C$-$C stretch
1052		1.466		CH$_2$ wag
	994		1.635	β-CH$_2$ rock
1168		1.212		TS symmetric stretch
1211	1127	3.307	2.952	β-C$-$F stretch
1261	1205	1.850	1.924	CH$_2$ twist
1284	1177	2.366	2.538	α-C$-$F stretch
	1263		1.134	CH$_2$ wag

Table 7.2 (continued)

Frequency (cm^{-1})		Reduced mass (amu)		Approximate type of mode
HF	MP2	HF	MP2	
1403	1316	1.116	1.095	β-CH$_2$ wag
1520		1.422		α-C−H bend
	1433		1.348	CH$_2$ scissors
1572		1.458		β-CH$_2$ twist
	1467		1.470	β-CH$_2$ twist + α-CH$_2$ scissors
1651	1555	1.091	1.104	β-CH$_2$ scissors
1660	1583	1.072	1.112	H−O−H bend
3258	3155	1.059	1.057	β-C−H symmetric stretch
3315	3230	1.104	1.110	β-C−H antisymmetric stretch
3324	3188	1.093	1.086	α-C−H stretch
4034	3825	1.067	1.066	O−H stretch

CHF$_2$−CH$_3$ + OH g,t

3214i	2163i	1.060	1.076	reaction coordinate
73	84	6.068	6.312	C−C−O skeletal bend
100	130	5.864	6.774	HO−C$_2$H$_4$F$_2$ torsion
231	303	1.084	1.102	OH rotation[a]
351	337	6.024	4.028	CF$_2$ wag
422	409	1.118	1.139	CH$_3$ rock
506	475	3.282	3.692	CHF$_2$−CH$_3$ torsion
595	563	4.610	3.944	CF$_2$ scissor
640	718	3.067	3.232	CF$_2$ twist
892	948	1.255	1.362	H−O−H bend
966	912	2.044	2.108	CF$_2$ rock + C−C stretch
1088	1308	1.362	1.162	TS symmetric stretch
1236		2.559		C−C stretch + CF$_2$ rock
	1057		1.738	CH$_2$ + CF$_2$ rock

Table 7.2 (continued)

Frequency (cm^{-1})		Reduced mass (amu)		Approximate type of mode
HF	MP2	HF	MP2	
1253	1176	2.696	2.518	C−F stretch
1289	1183	2.396	2.543	C−F stretch
1311		1.391		CH$_3$ deformation
	1220		1.933	C−C stretch + CH$_2$ wag
1539	1441	1.186	1.205	C−H bend + CH$_2$ rock
1561	1463	1.252	1.286	C−H bend + CH$_2$ wag
1615	1522	1.356	1.277	CH$_2$ scissors + C−H bend
1629	1561	1.056	1.102	H−O−H bend
3292	3207	1.055	1.058	α-C−H symmetric stretch
3341	3203	1.091	1.087	β-C−H stretch
3380	3304	1.112	1.110	α-C−H asymmetric stretch
4036	3832	1.067	1.066	O−H stretch

CHF$_2$−CH$_3$ + OH g,g

Frequency (cm^{-1})		Reduced mass (amu)		Approximate type of mode
HF	MP2	HF	MP2	
3248i	2217i	1.060	1.074	reaction coordinate
70	80	6.200	8.053	HO−C$_2$H$_4$F$_2$ torsion
107	142	6.000	6.568	CHF$_2$−CH$_3$ torsion
191	272	1.108	1.065	OH rotation^a
389	373	1.735	1.468	CH$_2$ rock + CF$_2$ twist
438	398	1.793	2.051	CH$_3$ rock + CF$_2$ twist
496	462	3.095	3.821	CF$_2$ rock + C−H−O bend
568	559	5.743	4.513	CF$_2$ wag + C−H−O bend
652	762	2.436	3.676	CF$_2$ scissors
877	898	1.665	1.459	H−O−H bend
979	942	1.783	1.647	CH$_2$ + CF$_2$ rock
1054	990	1.737	1.913	CH$_2$ + CF$_2$ wag
1191	1298	1.307	1.261	TS symmetric stretch

Table 7.2 (continued)

| Frequency (cm⁻¹) | | Reduced mass (amu) | | Approximate type of mode |
HF	MP2	HF	MP2	
1255		2.612		C−C + C−F stretch
	1165		2.085	C−F stretch
1309		1.859		C−C + C−F stretch
	1178		2.312	C−F stretch
1312		2.193		C−F stretch
	1231		1.970	C−C stretch
1543	1438	1.332	1.333	CH₂ scissors + C−H bend
1558	1453	1.268	1.299	C−H bend + CH₂ wag
1598	1514	1.241	1.200	CH₂ scissors
1637	1561	1.084	1.100	H−O−H bend
3294	3174	1.061	1.086	C−H symmetric stretch
3309	3210	1.082	1.058	C−H symmetric stretch
3382	3304	1.113	1.110	C−H asymmetric stretch
4037	3833	1.067	1.066	O−H stretch

CH₃−CF₂H + OH

| Frequency (cm⁻¹) | | Reduced mass (amu) | | Approximate type of mode |
HF	MP2	HF	MP2	
3245i	2057i	1.067	1.108	reaction coordinate
23	176	1.438	1.183	OH rotation[a]
108	80	3.730	3.964	HO−C₂H₄F₂ torsion
139	102	2.538	3.792	CH₃−CHF₂ torsion
239	255	1.108	1.093	CH₃ rock
365	375	4.885	3.069	CF₂ rock
401	428	3.104	3.100	CF₂ twist
524	497	6.008	9.087	CF₂ scissors
674	663	4.356	3.401	CF₂ wag
844	870	1.240	1.302	H−O−H bend
991	919	2.327	2.240	C−F stretch

Table 7.2 (continued)

Frequency (cm^{-1})		Reduced mass (amu)		Approximate type of mode
HF	MP2	HF	MP2	
1088	1008	1.679	1.813	CH$_3$ rock
1203	1349	1.121	1.749	TS symmetric stretch
1258	1267	2.264	3.780	C−C stretch
1375	1216	4.311	2.209	C−F stretch
1394	1188	3.902	1.859	C−C−H bend
1570	1472	1.351	1.472	CH$_3$ symmetric deformation
1620	1536	1.054	1.048	CH$_3$ degenerate deformation
1620	1542	1.055	1.049	CH$_3$ degenerate deformation
1656	1584	1.104	1.092	H−O−H bend
3226	3154	1.039	1.035	C−H symmetric stretch
3305	3262	1.099	1.103	C−H degenerate stretch
3329	3278	1.106	1.105	C−H degenerate stretch
4034	3836	1.067	1.067	O−H stretch
CF$_3$−CH$_3$ + OH				
3281i	2280i	1.059	1.071	reaction coordinate
63	71	6.734	8.386	C−C−O skeletal bend
94	111	6.580	6.839	HO−C$_2$H$_3$F$_3$ torsion
159	230	1.092	1.065	OH rotation[a]
337	322	6.390	5.984	CF$_3$ rock
376	360	2.122	2.201	CF$_3$−CH$_3$ torsion
441	401	1.453	1.434	CH$_3$ + CF$_3$ rock
558	530	8.112	9.783	CF$_3$ degenerate deformation
583	537	7.161	7.094	CF$_3$ degenerate deformation
623	749	3.160	3.211	CH$_3$ + CF$_3$ rock
655	606	4.791	5.960	CF$_3$ symmetric deformation
850		1.552		H−O−H bend

Table 7.2 (continued)

Frequency (cm^{-1})		Reduced mass (amu)		Approximate type of mode
HF	MP2	HF	MP2	
	832		2.745	H$-$O$-$H bend + C$-$F symmetric stretch
931		4.297		C$-$F symmetric stretch
	901		1.757	H$-$O$-$H bend + C$-$F symmetric stretch
1060	1002	1.641	1.796	CH$_2$ twist
1134	1074	1.342	1.542	CH$_2$ wag
1256	1247	1.258	1.498	TS symmetric stretch
1373	1277	5.827	3.673	C$-$F degenerate stretch
1427	1329	4.249	2.622	C$-$F degenerate stretch
1450	1369	4.480	3.548	C$-$C stretch
1604	1519	1.305	1.264	CH$_2$ scissors
1629	1549	1.078	1.105	H$-$O$-$H bend
3310	3220	1.055	1.056	C$-$H symmetric stretch
3399	3319	1.114	1.111	C$-$H asymmetric stretch
4035	3835	1.067	1.066	O$-$H stretch

CHF$_2$$-CH_2$F + OH g,t

3262i	2177i	1.063	1.087	reaction coordinate
67	61	9.553	8.792	CHF$_2$$-CH_2$F torsion
84	78	8.759	8.492	HO$-$C$_2$H$_3$F$_3$ torsion
159	152	3.455	4.845	C$-$C$-$F bend
183	213	1.206	1.239	OH rotation[a]
270	247	7.338	4.323	CF$_2$ wag + C$-$C$-$F bend
418	406	5.114	5.047	C$-$H$-$O bend + CF$_2$ rock
478	457	11.287	7.495	C$-$C$-$F bend + CF$_2$ twist
622	576	9.074	10.289	CF$_2$ scissors

Table 7.2 (continued)

| Frequency (cm^{-1}) | | Reduced mass (amu) | | Approximate type of mode |
HF	MP2	HF	MP2	
642		2.125		C$-$H$-$O bend + CF$_2$ twist
	744		1.741	C$-$H$-$O bend
859	893	1.190	1.798	H$-$O$-$H bend
994	949	1.920	1.682	TS symmetric stretch
1217	1151	3.578	4.608	C$-$C + C$-$F stretch
1253	1171	4.991	5.210	C$-$F stretch
1264	1184	2.555	2.949	C$-$C + C$-$F stretch
1284	1203	3.788	2.366	C$-$F stretch
1340	1330	1.252	1.149	α-C$-$H bend
1438	1346	1.270	1.264	C$-$H bend
1541	1438	1.224	1.220	β-C$-$H bend
1603	1497	1.608	1.727	C$-$H bend
1678	1606	1.132	1.102	H$-$O$-$H bend
3341	3220	1.089	1.087	C$-$H stretch
3354	3207	1.089	1.089	C$-$H stretch
4032	3832	1.067	1.066	O$-$H stretch

CHF$_2$$-CH_2$F + OH g,g

3303i	2255i	1.062	1.082	reaction coordinate
73	70	10.162	10.045	HO$-$C$_2$H$_3$F$_3$ torsion
84	112	5.120	8.163	C$-$C$-$O skeletal bend
158	166	3.074	4.725	CHF$_2$$-CH_2$F torsion
194	270	1.383	1.106	OH rotation[a]
254	238	9.198	8.987	C$-$C$-$F bend + CF$_2$ wag
460	425	8.119	6.813	C$-$C$-$F bend + CF$_2$ scissors
516	482	4.179	3.705	C$-$C$-$F bend + CF$_2$ twist
583	758	3.072	3.730	C$-$H$-$O bend + CF$_2$ scissors

Table 7.2 (continued)

Frequency (cm^{-1})		Reduced mass (amu)		Approximate type of mode
HF	MP2	HF	MP2	
637	574	4.429	9.602	CF_2 twist + C−C−F bend
893		1.763		H−O−H bend + β-C−F bend
	898		1.392	H−O−H bend
1029		1.778		H−C−C bend
	974		1.840	H−C−C bend + β-C−F bend
1117	1120	1.123	1.481	TS symmetric stretch
1250	1482	3.656	1.843	C−C stretch
1259	1164	3.543	3.866	C−F stretch
1294	1182	3.117	4.852	C−F stretch
1298		2.440		C−F stretch
	1209		2.108	C−F stretch + C−H bend
1461		1.224		C−H bend
	1224		1.745	C−H bend + C−F stretch
1555	1370	1.280	1.213	C−H bend
1588	1448	1.914	1.258	C−H bend
1650	1572	1.058	1.100	H−O−H bend
3322	3192	1.087	1.087	C−H stretch
3346	3213	1.088	1.088	C−H stretch
4034	3832	1.067	1.066	O−H stretch

CH$_2$F−CHF$_2$ + OH

3327i	2232i	1.065	1.085	reaction coordinate
75	127	5.063	5.876	C−C−O skeletal bend
102	91	5.363	6.767	HO−C$_2$H$_3$F$_3$ torsion
138	147	4.356	5.623	CH$_2$F−CHF$_2$ torsion
211	316	1.226	1.093	OH rotation[a]
272	262	5.681	4.819	C−C−F bend + CF$_2$ rock

Table 7.2 (continued)

| Frequency (cm^{-1}) | | Reduced mass (amu) | | Approximate type of mode |
HF	MP2	HF	MP2	
373	422	6.302	5.938	CF$_2$ scissors
467	436	10.455	8.642	C−C−F bend + CF$_2$ rock
533	494	2.926	2.922	CF$_2$ twist + CH$_2$ rock
673	640	7.898	7.318	CF$_2$ wag
872	905	1.270	1.551	H−O−H bend
1005	957	2.035	1.675	CH$_2$ rock + CF$_2$ twist
1185		1.254		TS symmetric stretch
	1158		2.400	α-C−F asymmetric stretch + TS symmetric stretch
	1204		1.786	TS symmetric stretch + α-C−F asymmetric stretch
1205	1118	5.344	6.036	β-C−F stretch
1238	1245	2.790	3.724	α-C−F symmetric stretch
1348		2.780		α-C−F asymmetric stretch + CH$_2$ wag
1369	1348	1.812	2.014	C−C stretch
1435		2.473		CH$_2$ wag + α-C−F asymmetric stretch
	1284		1.276	CH$_2$ wag
1580	1461	1.592	1.533	CH$_2$ twist
1654	1558	1.108	1.097	CH$_2$ scissors
1663	1617	1.079	1.147	H−O−H bend
3272	3169	1.060	1.058	C−H symmetric stretch
3344	3252	1.109	1.111	C−H asymmetric stretch
4028	3822	1.067	1.066	O−H stretch

CF$_3$−CH$_2$F + OH

3324i		1.063		reaction coordinate
52		3.468		CF$_3$−CH$_2$F torsion

Table 7.2 (continued)

Frequency (cm^{-1})		Reduced mass (amu)		Approximate type of mode
HF	MP2	HF	MP2	
66		5.144		C−C−O skeletal bend
126		1.690		OH rotation[a]
156		4.253		HO−C$_2$H$_2$F$_4$ torsion
236		14.108		CF$_3$ rock + F−C−C bend
338		7.274		CF$_3$ rock
447		12.779		F−C−C bend + CF$_3$ rock
548		5.201		C−H−O bend + CF$_3$ symmetric deformation
591		4.010		CF$_3$ symmetric deformation + C−H−O bend
603		6.907		CF$_3$ degenerate deformation
738		8.128		CF$_3$ degenerate deformation
872		1.410		H−O−H bend
940		5.367		C−F symmetric stretch
1049		1.403		CH$_2$ wag
1254		1.333		TS symmetric stretch
1274		4.138		α-C−F stretch
1370		2.757		H−C−C bend
1395		9.418		C−F degenerate stretch
1450		3.988		C−F degenerate stretch
1566		2.646		C−C stretch
1665		1.089		H−O−H bend
3357		1.088		C−H stretch
4031		1.067		O−H stretch

CHF$_2$−CHF$_2$ + OH

3339*i*		1.066		reaction coordinate

Table 7.2 (continued)

Frequency (cm⁻¹)		Reduced mass (amu)		Approximate type of mode
HF	MP2	HF	MP2	
29		2.329		$HO-C_2H_2F_4$ torsion
64		9.542		CF_2-CHF_2 torsion
115		4.983		CF_2 wag
143		1.918		OH rotation[a]
248		12.778		CF_2 wag
263		15.038		CF_2 rock
381		8.166		CF_2 rock
451		11.629		α-CF_2 scissors + β-CF_2 twist
572		10.150		CF_2 scissors
669		13.211		α-CF_2 twist + β-CF_2 scissors
847		1.357		$H-O-H$ bend
901		3.581		α-$C-F$ symmetric stretch
990		2.297		$C-C-H_\alpha$ bend + β-CF_2 twist
1195		1.795		TS symmetric stretch + α-CF_2 twist
1264		4.686		β-$C-F$ symmetric stretch
1297		3.713		β-$C-F$ asymmetric stretch
1369		5.638		α-$C-F$ asymmetric stretch
1444		3.736		$C-C$ stretch
1547		1.276		$C-H_\beta$ bend
1599		2.043		$C-C-H_\beta$ bend
1650		1.065		$H-O-H$ bend
3361		1.090		$C-H$ stretch
4028		1.067		$O-H$ stretch

$CF_3-CHF_2 + OH$

Frequency (cm⁻¹)		Reduced mass (amu)		Approximate type of mode
3383i		1.065		reaction coordinate
56		8.041		$C-C-O$ skeletal bend

Table 7.2 (continued)

Frequency (cm^{-1})		Reduced mass (amu)		Approximate type of mode
HF	MP2	HF	MP2	
73		3.617		CHF_2-CF_3 torsion
101		1.551		OH rotation[a]
127		6.063		α-CF_2 wag
372		7.656		$HO-C_2HF_5$ torsion
392		18.023		α- + β-CF_2 scissors
456		15.239		CF_2 twist + CF_3 rock
582		17.011		CF_3 symmetric deformation
636		9.816		CF_3 degenerate deformation + CF_2 wag
639		11.397		CF_3 degenerate deformation + CF_2 twist
817		14.776		$C-F$ symmetric stretch
866		1.250		$H-O-H$ bend
1001		3.954		CF_3 degenerate deformation
1152		1.378		TS symmetric stretch
1292		9.684		$C-F$ symmetric stretch
1403		11.054		α-$C-F$ asymmetric + β-$C-F$ degenerate stretch
1412		9.542		β-$C-F$ degenerate + α-$C-F$ asymmetric stretch
1428		12.835		β-$C-F$ degenerate stretch
1550		6.758		$C-C$ stretch
1674		1.140		$H-O-H$ bend
4029		1.067		$O-H$ stretch

[a] This mode not included in ZPE.

Of the 24 internal degrees in each TS, eight are in the H_2O fragment, including the $C-H-O$ or $C-C-O$ bend. For a CX_3 group (X = H or F), there are three stretches, three deformations and two rocking motions; a CX_2 group has two stretches and four bends, normally one each of a rock, wag, scissors, and twist; a CX group has one stretch and one bend.[100] In the case of a (HF)C...H group at the α-carbon, these numbers of degrees of freedom are not additive, so it is not clear which motions to expect.

In general the frequencies are lower at the MP2 level (as expected since the systematic overestimation of *ab initio* frequencies is lower using MP2 vs. HF theory[23]), except for some of the low frequency modes which have different ordering at the two levels of theory, or where the degree of coupling between modes is more severe at one level.

In all cases the reaction coordinate is almost exclusively a motion of the hydrogen atom being abstracted away from the carbon atom and towards the oxygen. The magnitude of the vibration is always much lower at MP2 theory, consistent with the TS lying further out into the entrance channel.

For each TS there is one mode which corresponds to essentially a free rotation of the incoming OH group. As explained in Chapter 6, it is not reasonable to include this mode in the zero-point energy (ZPE), and the ZPEs presented below are adjusted accordingly. This frequency is consistently higher, thus giving a greater adjustment, at the MP2 level.

Vibrational consequences of hydrogen bonding include spectacular shifts of the

stretching frequencies, particularly the A−H mode (where A is the atom directly bonded to the hydrogen), and coupling of this mode to various other vibrations.[240] There is little evidence of coupling of the O−H stretching frequency for cases where the H2...Fx distance indicates hydrogen bonding, and only a slight decrease in the O-H stretching frequency at the MP2 level. Thus the evidence from the vibrational frequencies is that any intramolecular hydrogen bonding is of a small magnitude.

7.3 Total and Zero-Point Energies

Total energies at three levels of theory, ZPEs at two levels, and experimental heats of formation[101−104,108−114] are given in Table 7.3. Some of the energies have been reported previously (see Chapters 3 and 5 and the series of papers by Chen et al.[88−91]), but are included here for completeness. Additional total energies required for the G2 method are given in Table 7.4. As expected the energies decrease with increasing level of theory, both in terms of level of electron correlation and basis-set size. The lowest energies are obtained with the MP4/6-311G(2df,p) level, the lowest energies using the MP2 method (and second lowest overall) are obtained with the 6-311+G(3df,2p) basis set, the largest one used, and the lowest energies obtained using the 6-311G(d,p) basis set are with the QCISD(T) method, which gives the greatest degree of electron correlation. The MP2/6-311G(d,p) energies for the TS are lower when the HF geometries are used, while the MP2 geometries give lower energies for the reactants and products. This is an indication of the MP2 geometries being more accurate, since the TS is a maximum in one direction on the potential energy surface, so any deviation from

the true maximum will give a lower energy. The lower TS energies of the HF geometries are probably due to the TS being located too late on the reaction coordinate, as indicated by the geometry results above. At every level of theory, total energies for species with the same number of fluorines are lower when as many as possible are on the same carbon, consistent with the geminal effect, and preferably on the α-carbon for the radicals and TS, since the electronegative fluorine atoms will prefer to be attached to the relatively more electropositive α-carbon. For the TS there is a secondary preference for lower energy where there is a β-fluorine gauche rather than trans to the hydrogen being abstracted. This can be attributed to a stabilization from an intramolecular H-bond, as evidenced by the short H...F distances in these instances. The effect decreases both with increasing level of theory and increasing substitution by fluorine, and in all cases is less than 10 kJ mol^{-1}, in line with the geometric and vibrational evidence that only a weak hydrogen bond occurs.

The unscaled ZPEs are lower at the MP2 level, as expected since HF theory systematically overestimate vibrational frequencies by ~10%, while MP2 frequencies are only ~5% too high.[61] As with the total energies, ZPEs decrease with increasing fluorine substitution, as expected due to the larger reduced masses of the vibrations. Again, values tend to be lower for maximum substitution on one carbon, but there are no consistent trends for the α vs. β and gauche vs. trans substitution patterns.

Table 7.3: Total Energies and Zero-Point Energies, at Various Levels of Theory, and Experimental Heats of Formation[a]

Species[b]	MP2/6-311G(d,p) //HF/6-31G(d)	MP2/6-311G(d,p) //MP2/6-31G(d,p)	MP4/6-311G(d,p) //MP2/6-31G(d,p)	ZPE//HF/ 6-31G(d)	ZPE//MP2/ 6-31G(d,p)	$\Delta H_{f,298}$
TS						
CH_3-CH_3 + OH	−155.134932	−155.130898[c]	−155.190337[c]	85.415[d]	83.263[c,d]	
CH_3-CH_2F + OH	−254.207068	−254.201626	−254.264011	78.463[d]	76.316[d]	
CH_2F-CH_3+ OH t	−254.200600	−254.197664	−254.259737	78.643[d]	76.058[d]	
CH_2F-CH_3+ OH g	−254.204199	−254.201156	−254.263085	78.765[d]	76.491[d]	
CH_2F-CH_2F + OH t	−353.268973	−353.264341	−353.329561	71.496[d]	68.842[d]	
CH_2F-CH_2F + OH g	−353.270023	−353.265752	−353.331002	71.508[d]	68.953[d]	
CHF_2-CH_3 + OH g,t	−353.287614	−353.285409	−353.349222	70.884[d]	68.467[d]	
CHF_2-CH_3 + OH g,g	−353.287103	−353.284965	−353.348728	70.747[d]	68.270[d]	
CH_3-CHF_2 + OH	−353.292542	−353.286939	−353.351564	70.543[d]	68.076[d]	
CF_3-CH_3 + OH	−452.378924	−452.377420		61.940[d]	59.597[d]	
CHF_2-CH_2F + OH g,t	−452.349477	−452.345585		63.652[d]	60.935[d]	
CHF_2-CH_2F + OH g,g	−452.349958	−452.346300		63.476[d]	60.832[d]	
CH_2F-CHF_2 + OH	−452.351272	−452.346596		63.404[d]	60.867[d]	
CF_3-CH_2F + OH	−551.438967			54.674[d]		
CHF_2-CHF_2 + OH	−551.427478			55.359[d]		

Table 7.3 (continued)

Species[b]	MP2/6-311G(d,p) //HF/6-31G(d)	MP2/6-311G(d,p) //MP2/6-31G(d,p)	MP4/6-311G(d,p) //MP2/6-31G(d,p)	ZPE//HF/ 6-31G(d)	ZPE//MP2/ 6-31G(d,p)	$\Delta H_{f,298}$
CF_3-CHF_2 + OH	−650.515898			46.564[d]		
Reactants						
OH	−75.572837	−75.572879[c]	−75.588329[c]	9.106	8.758[c]	38.95[k]
CH_3-CH_3	−79.570654[c]	−79.570739[c]	−79.614234[c]	79.760[c]	77.565[c]	−83.8[l]
CH_2F-CH_3	−178.638856[c]	−178.639255[c]	−178.685358[c]	73.141[c]	70.524[c]	−263.2[m]
CH_2F-CH_2F C_2	−277.702617[c]	−277.703348[c]	−277.752149[c]	66.294[c]	63.232[c]	−443.5[i,u]
CHF_2-CH_3	−277.725742[c]	−277.726464[c]	−277.774393[c]	65.524[c]	62.798[c]	−500.8[m]
CF_3-CH_3	−376.820167[c]	−376.821147[c]		56.882[c]	54.260[c]	−745.6[m]
CHF_2-CH_2F C_1	−376.785952[c]	−376.786986[c]		58.550[c]	55.456[c]	−664.8[n]
CF_3-CH_2F	−475.877015[c]	−475.878430[c]		49.872[c]	46.968[c]	−904.2[i,u]
CHF_2-CHF_2 C_{2h}	−475.866528[c]	−475.867848[c]		50.592[c]	47.438[c]	−884.5[j,u]
CF_3-CHF_2	−575.954378[c]	−574.956045[c]		41.862[c]	38.924[c]	−1104.6[m]
Products						
H_2O	−76.263585	−76.263894[c]	−76.276272[c]	22.977	21.898[c]	−241.82[k]
CH_3-CH_2	−78.902740[f]	−78.902838[f]	−78.944350[c]	63.352[f]	61.431[c,d]	117.2[o]
CH_3-CHF	−177.975572[g]	−177.975770[f]	−178.019678[f]	61.722[f]	55.938[f]	−71.5[p]

181

Table 7.3 (continued)

Species[b]	MP2/6-311G(d,p)//HF/6-31G(d)	MP2/6-311G(d,p)//MP2/6-31G(d,p)	MP4/6-311G(d,p)//MP2/6-31G(d,p)	ZPE//HF/6-31G(d)	ZPE//MP2/6-31G(d,p)	$\Delta H_{f,298}$
CH_2F-CH_2 C_1	-177.967906[h]	-177.968344[f]	-178.012454[f]	56.814[f]	54.869[f]	
CH_2F-CHF	-277.038424[i]	-277.039136[f]	-277.085944[f]	51.229[f]	48.935[f]	
CHF_2-CH_2 C_1	-277.052193[h]	-277.052965[f]	-277.099007[f]	49.490[f]	47.515[f]	
CH_3-CF_2	-277.061025[g]	-277.061373[f]	-277.106853[f]	50.932[f]	48.937[f]	-302.5[q]
CF_3-CH_2	-376.145248[h]	-376.146393[f]		40.759[f]	39.016[f]	-517.1[r]
CHF_2-CHF	-376.118799[j]	-376.119666[f]		43.400[f]	48.935[f]	
CH_2F-CF_2 C_s	-376.119083[j]	-376.119797[f]		44.205[f]	41.884[f]	
CF_3-CHF	-475.208852[i]	-475.210073[f]		34.737[f]	32.597[f]	-680.7[s]
CHF_2-CF_2 C_s	-475.197254[j]	-475.198160[f]		36.297[f]	33.789[f]	
CF_3-CF_2	-574.285606[j]	-574.286901[f]		27.443[f]	25.298[f]	-891.2[t]

[a] Total energies in hartrees, ZPEs in millihartrees, heats of formation in kJ mol^{-1}. Some values have been reported previously, as indicated, but are included here for convenience. ZPEs are unscaled. [b] t and g refer to the abstracted H being trans and gauche to a β-F, respectively. Symmetry point groups are given where necessary to identify conformers. [c] Chapter 5. [d] Internal rotation mode removed; see Chapter 5 for details. [e] Chapter 4. [f] Chapter 3. [g] Reference 88. [h] Reference 89. [i] Reference 90. [j] Reference 91. [k] Reference 104. [l] Reference 101. [m] Reference 102. [n] Reference 103. [o] Reference 108. [p] Reference 109. [q] Reference 106. [r] Reference 111. [s] Reference 112. [t] Reference 113. [u] Calculated by the triatomic additivity method of ref 114.

Table 7.4: Total Energies at the Additional Levels of The. -y Required for G2 Method[a]

Species[b]/ G2 energy[c]	MP2/6-311+G(d,p)	MP2/6-311G(2df,p)	MP2/6-311+G(3df,2p)	MP4/6-311+G(d,p)	MP4/6-311G(2df,p)	QCISD(T)/6-311G(d,p)
TS						
CH_3-CH_2F + OH −254.422705	−254.216714	−254.321429	−254.357680	−254.280235	−254.390517	−254.267226
CH_2F-CH_3+ OH t −254.418770	−254.213508	−254.317238	−254.354520	−254.276677	−254.385980	−254.232325
CH_2F-CH_3+ OH g −254.420453	−254.215674	−254.321187	−254.356846	−254.278684	−254.389761	−254.265631
Reactants						
CH_2F-CH_3 −178.782113	−178.648072	−178.724712	−178.749351	−178.694743	−178.775024	−178.685266
CH_2F-CH_2F C_2 −277.932684	−277.719834	−277.838134	−277.873724	−277.769697	−277.893478	−277.750697
CHF_2-CH_3 −277.953302	−277.740330	−277.861834	−277.894829	−277.789372	−277.916516	−277.772646
Products						
CH_3-CHF −178.124225	−177.984552	−178.060864	−178.083417	−178.029031	−178.109094	−178.020453

Table 7.4 (continued)

Species[b]/ G2 energy[c]	MP2/6-311+G(d,p)	MP2/6-311G(2df,p)	MP2/6-311+G(3df,2p)	MP4/6-311+G(d,p)	MP4/6-311G(2df,p)	QCISD(T)/6-311G(d,p)
CH₂F−CH₂ C₁ −178.118806	−177.978043	−178.053161	−178.076799	−178.022744	−178.101577	−178.013192
CH₂F−CHF −277.274298	−277.055820	−277.173478	−277.207177	−277.103728	−277.226944	−277.085512
CHF₂−CH₂ C₁ −277.286952	−277.067720	−277.187499	−277.219477	−277.114942	−277.240391	−277.098054
CH₃−CF₂ −277.292801	−277.074986	−277.196458	−277.227268	−277.121591	−277.248812	−277.105922

ᵃ All values given are single-point energies, in hartrees, at the MP2/6-31G(d,p) geometries given above for TS, and Chapter 5 for reactants and Chapter 3 for products. The MP4/6-311G(d,p) and MP2/6-311G(d,p) single-point energies and ZPEs are given in Table 1. Values for CH₃−CH₃ + OH, OH, and H₂O are given in Chapter 6. ᵇ t and g refer to the abstracted H being trans and gauche to a β-F, respectively. Symmetry point groups are given where necessary to identify conformers. ᶜ Scaled ZPEs included. To obtain energy without ZPE correction subtract the MP2/6-31G(d,p) ZPE listed in Table 7.3 multiplied by the scaling factor of 0.9646.

7.4 Barrier Heights

Classical barrier heights, with ($\Delta E_0^{\ddagger}$) and without (V_B) ZPE corrections, at various levels of theory are given in Table 7.5. Calculations using HF geometries give the lowest barriers of the unextrapolated methods, as a result of the TS energies being lower, while reactant energies are higher, at this level of theory (see above). Barriers calculated from the MP2 geometries decrease slightly when the MP4 *cf.* MP2 method is employed (a trend noted previously in other reaction series, for *e.g.*, S_N2 reactions of halogens with methyl halides[241]), with larger decreases seen when the G2 method is used. Barriers tend to decrease with increasing fluorine substitution on the α-carbon (although not in a consistent fashion; barriers for species with two α-fluorines are slightly higher than for those with one α-fluorine), but increase with increasing β-substitution. In cases of inequivalent hydrogens being abstracted, the lower barrier occurs when the hydrogen is gauche to a β-fluorine. These trends result from the TS energy trends noted above. The trends with α- vs. β-fluorine substitution are for the most part consistent with the $C-H$ bond strength trends noted in Chapter 5, and in particular support the increase in strength from an inductive effect from β-fluorines.

Comparing calculated barriers to those obtained from experiment is not straightforward. The term "activation energy" can apply to a series of related concepts.[242] The calculated barriers presented here represent the differences between TS and reactants in potential energy (V_B) and potential energy plus ZPE ($\Delta E_0^{\ddagger}$). Corrections for $\int C_V dT$ will yield $\Delta E_T^{\ddagger}$. For bimolecular gas reactions, $\Delta E_T^{\ddagger}$ is likely to be less than $\Delta E_0^{\ddagger}$, because of a loss of translational degrees of freedom and a decrease

Table 7.5: Classical Barriers $(V_B/\Delta E_0^{\ddagger})^a$ At Various Levels of Theory, and Experimental Activation Energies, in kJ/mol

Reaction[b]	MP2/6-311G(d,p) //HF/6-31G(d)	MP2/6-311G(d,p) //MP2/6-31G(d,p)	MP4/6-311G(d,p) //MP2/6-31G(d,p)	G2	Experimental E_A[c]
CH_3-CH_3 + OH	22.6	33.4	32.6	20.1	
	14.3	26.0	24.7	12.4[d]	9.1[e]
CH_3-CH_2F + OH	12.1	27.6	26.2	15.5	
	3.1	20.1	18.7	8.0	6.2[f]
CH_2F-CH_3 + OH t	29.1	40.0	36.6	26.5	
	20.5	31.8	28.5	18.3	"
CH_2F-CH_3 + OH g	19.7	28.8	27.8	21.0	
	11.3	21.8	20.8	13.9	"
CHF_2-CH_3 + OH g,t	28.8	36.6	35.4		
	19.8	28.8	27.6		11.4[g]
CHF_2-CH_3 + OH g,g	30.1	37.7	36.7		
	20.8	29.4	28.4		"
CH_3-CHF_2 + OH	15.8	32.6	29.3		
	6.0	23.8	20.5		"
CH_2F-CH_2F + OH t	17.0	31.2	28.7		
	7.7	23.2	20.7		
CH_2F-CH_2F + OH g	14.3	27.5	24.9		
	5.0	19.8	17.2		

Table 7.5 (continued)

Reaction[b]	MP2/6-311G(d,p) //HF/6-31G(d)	MP2/6-311G(d,p) //MP2/6-31G(d,p)	MP4/6-311G(d,p) //MP2/6-31G(d,p)	G2	Experimental E_A[c]
$CF_3-CH_3 + OH$	37.0	43.6			
	27.3	34.9			18.3[h]
$CHF_2-CH_2F + OH$ g,t	24.4	37.5			
	14.8	29.2			
$CHF_2-CH_2F + OH$ g,g	23.2	34.8			
	13.2	27.0			
$CH_2F-CHF_2 + OH$	19.7	35.6			
	9.5	26.4			
$CF_3-CH_2F + OH$	28.6				
	18.3				14.5[i]
$CHF_2-CHF_2 + OH$	31.2				
	20.8				14.0[i]
$CF_3-CHF_2 + OH$	29.7				
	19.1				14.1[h]

[a] ZPEs scaled by 0.9135 at HF/6-31G(d) and 0.9646 at MP2/6-31G(d,p). [b] t and g refer to the abstracted H being trans and gauche to a β-F, respectively. [c] " refers to the E_A value being equivalent to the one immediately above since experiment does not distinguish inequivalent hydrogens in a common substrate. [d] Chapter 6. [e] Reference 245. [f] Reference 224. [g] Reference 226. [h] Reference 229. [i] Reference 231.

in C_V on activation.[242] It is often assumed that the Arrhenius activation energy, E_A, can be obtained from Tolman's theorem by adding RT to $\Delta E_T^{\ddagger}$. However, this is true only for reactions which exactly obey activated complex theory with a temperature independent transmission coefficient, κ, which will not be the case here where tunneling will be important since a proton is being transferred.[243]

Therefore, the experimental barrier heights (E_A) quoted in Table 7.5 cannot be directly compared to the calculated barriers. Furthermore, the $\overline{E}_A$ values often have large uncertainties, and values for the same reaction obtained by different groups often have large discrepancies, possibly due to reactive impurities, secondary losses of OH, and unanticipated heterogeneous processes.[229,244] Also, experiment cannot distinguish inequivalent hydrogens in a common substrate, as has been done in the calculations. Thus, the best that can be hoped for is to compare the calculated and experimental barriers in a semi-quantitative fashion. As a base for comparison, for the reaction of OH with unsubstituted ethane, E_A is 9.1 kJ mol^{-1},[245] whereas $\Delta E_0^{\ddagger}$ is 9.3 kJ mol^{-1} from a fit to experimental data.[209] The G2 results show reasonable agreement with experiment, while overall the qualitative trends in the experimental barriers are reproduced at each level of theory.

7.5 Reaction Enthalpies

Reaction enthalpies, including ZPE and thermal corrections to 298.15 K, are given in Table 7.6. Here, more dramatic effects are seen with different levels of theorv. Inclusion of electron correlation in the geometry optimization has varying effects on

Table 7.6: Reaction Enthalpies (ΔH_{298}) At Various Levels of Theory, in kJ/mol

Reaction	MP2/6-311G(d,p) //HF/6-31G(d)	MP2/6-311G(d,p) //MP2/6-31G(d,p)	MP4/6-311G(d,p) //MP2/6-31G(d,p)	G2	expt[a]
CH_3-CH_3 + OH	−64.8	−71.0	−58.4	−72.6[b]	−79.8
CH_3-CH_2F + OH	−65.8	−74.7	−60.9	−77.6	−89.1
CH_2F-CH_3 + OH	−57.2	−77.4	−44.8	−64.6	
CHF_2-CH_3 + OH	−49.1	−50.2	−37.2	−55.4	
CH_3-CHF_2 + OH	−68.8	−68.7	−54.2	−70.8	−82.5
CH_2F-CH_2F + GH	−74.6	−72.1	−58.8	−76.3	
CF_3-CH_3 + OH	−45.7	−46.8			−52.3
CHF_2-CH_2F + OH	−63.9	−44.2			
CH_2F-CHF_2 + OH	−62.6	−62.4			
CF_3-CH_2F + OH	−61.2	−63.1			−57.3
CHF_2-CHF_2 + OH	−68.9	−56.0			
CF_3-CHF_2 + OH	−57.9	−57.4			−67.4

[a] Calculated from the heats of formation given in Table 7.3. [b] In Chapter 6, this value is reported as ΔH_0.

enthalpy, while higher-order correlation corrections (MP4 vs. MP2) to the energies lower the magnitude of the enthalpy change. The reactions are about 20 kJ mol^{-1} more exothermic at G2 $cf.$ MP4 theory. Trends through the reaction series are not as consistent as for barrier heights. Reactions are more exothermic when fluorines are on the α- rather than β-carbon, since this situation lowers the energy of the product ethyl radical. Exceptions occur for the reaction of fluoroethane, at the MP2/6-311G(d,p)//MP2/6-31G(d,p) level, and trifluoroethane, at the MP2/6-311G(d,p)//HF/6-31G(d) level, where the conformers with an extra fluorine on the β-carbon result in slightly greater exothermicities. Reactions are less exothermic when as many fluorines as possible are on one carbon, as a result of the geminal effect being greater in the reactants than in the products. An exception occurs for the reaction of tetrafluoroethane, where $CF_3-CH_2F + OH$ is more exothermic at the MP2/6-311G(d,p)//MP2/6-31G(d,p) level. These exceptions are probably due to the inability of MP2 theory to adequately describe electron correlation.

The G2 values give the best agreement with experiment, although perhaps not as good as expected given this method has an average absolute deviation from experiment of atomization energies of 39 first-row compounds of 3.85 kJ mol^{-1},[41] (and also performs remarkably well in calculating ionization energies, electron affinities and proton affinities[246]) and calculation of reaction enthalpies is usually considered to give more accurate results than for atomization energies. A possible source of error is that while the same quantity is being measured by both experiment and theory, the theoretical value is from the most stable conformers of reactants to the most stable conformers of

products, while the experimental value is for a statistical average of all possible conformers in reactants and products.

7.6 Conclusions

Many of the trends seen in the optimized TS geometries are similar to those noted previously in the ethane and ethyl radical series. Variations in geometrical parameters are greater near the reaction center. Inclusion of electron correlation in the geometry optimizations gives slightly shorter $C-C$ and $C-H$ bonds, significantly longer $C-F$ bonds, greater deviations from linearity in the $C-H-O$ angles, and greater $X_\alpha-C1-H1$ angles. The HF optimized geometries have greater $H-O-H$ and $X_\alpha-C1-H_\alpha$ angles, with the remaining types of angles having about the same magnitude at the two levels of theory. Increasing fluorine substitution tends to decrease bond lengths and increase bond angles. The incoming hydroxyl group will take advantage of an intramolecular hydrogen bond to a β-fluorine, but not at the expense of having to go through a rotational barrier. The relative lengths of the $C-H$ bond being broken and the $O-H$ bond being formed, and the relative magnitudes of the imaginary frequency of the TS, both point to an earlier TS at the MP2 level of theory.

Total energy results confirm weak intramolecular hydrogen bonds in the transition states where the abstracted hydrogen is gauche to a β-fluorine. Comparison of calculated barrier heights with experiment is difficult, but the trends are at least qualitatively correct. Calculated reaction enthalpies give fairly good agreement with experiment; the

comparison of theory and experiment is difficult. Total and zero-point energies, and as a result, barrier heights and reaction enthalpies, are affected by substitution patterns. Thus, barrier heights increase with increasing β-fluorine substitution, but decrease with increasing α-fluorine substitution, and when the hydrogen being abstracted is gauche to a β-fluorine, in which case the TS is stabilized by an intramolecular hydrogen bond. The trends with fluorine substitution correlate well with those observed for the $C-H$ bond dissociation energies. The reaction exothermicity tends to increase when fluorines are on the α- rather than β-carbon, and decreases when as many fluorines as possible are on one carbon.

Chapter 8. Topological Properties of the Electronic Structures of the Reactants, Transition States, and Products of the Reactions of Hydroxyl Radical with the Series $C_2H_nF_{6-n}$, n = 1−6

8.1 Introduction

The concept of charge development at the transition state has been investigated theoretically for S_N2 reactions involving charged nucleophiles.[247] Experimental studies must look at indirect evidence such as the effect of substituents on the reaction rate. One of the most extensively studied reaction classes is hydrogen abstractions, such as is being considered here. These show interesting effects, for *e.g.*, the attack of substituted toluenes by bromine radicals correlates[248] with σ^+, and polar effects are even observed in abstractions by alkyl radicals.[249] These results show that charged species need not be involved for charge to have a significant effect on the reaction. The reactions of hydroxyl radicals (OH) with hydrofluorinated ethanes (HFEs) are formally charge neutral, but there should be significant charge development at the transition state (TS) due to the influence of the electronegative oxygen atom.

As discussed in Chapter 2, the Laplacian of the charge density, $\nabla^2\rho\,(r)$, provides information about where in space the charge is locally depleted or concentrated. If $\nabla^2\rho\,(r) < 0$, then the charge is concentrated in the region of space, while if it is $>$ 0, then the charge is depleted from the region of space. Studies of molecular systems using the properties of $\nabla^2\rho\,(r)$ show that a bond can be characterized in terms of the bond path and of the charge density at the bond critical point, $\rho(r_c)$.[250] Also, the

magnitude of the charge density at the bond critical point provides a measure of the bond strength.[251,252]

The two methods used in this study for calculating atomic charges are due to Mulliken and Bader, respectively. The Mulliken method[253] is computationally very inexpensive, but suffers at least conceptually because the overlap populations are divided equally between two bonded atoms, irrespective of their relative electronegativities. Thus, it tends to underestimate electron populations on electronegative atoms. Bader and coworkers[254] have devised a charge partitioning method in which an atom in a molecule is defined as a real space surrounded by a zero-flux surface (see Chapter 2). While this method is conceptually more rigorous, it requires much more human and computer effort, and has been criticized for overestimation the electron population on electronegative atoms.[255] For Mulliken population analysis (MPA) four levels of theory were employed: HF/6-31G(d), HF/6-311G(d,p)//HF/6-31G(d), MP2/6-311G(d,p)//HF/6-31G(d), and HF/6-311G(d,p)//MP2/6-31G(d,p). This allowed the investigation of the effects of increased basis-set size, electron correlation, and use of electron correlation in geometry optimizations, respectively (starting from a base theory of HF/6-31G(d)). For Bader population analysis (BPA), only the highest common level of theory used on all the species (MP2/6-311G(d,p)//HF/6-31G(d)) was employed.

8.2 Properties of Bond Critical Points

Properties of bond critical points for reactants, transition states, and products, are given in Tables 8.1, 8.2, and 8.3, respectively. In general, the charge densities at the

bond critical points, $\rho(x_\sigma)$ increase with increasing substitution of the species by fluorine atoms, as expected since these atoms are electron-rich and thus increase the overall charge density. Given the same number of fluorines, values of $\rho(x_\sigma)$ are affected by substitution patterns.

For C−C bond critical points, $\rho(x)$ tends to be larger when the fluorine substituents are divided as evenly as possible between the two carbons; this trend applies to reactants, TSs, and products, although the trend is weak in the latter. For the product radicals, and the TSs, there is also a trend to higher values for higher substitution on the β-carbon.

In contrast to the C−C case, values of $\rho(x)$ at C−F bond critical points are larger for species where as many fluorines as possible are on one carbon. A second trend is for higher values at α-carbons for TSs and products, although the first trend will take precedence, e.g., in CF_3−CHF values are higher on the highly substituted β-carbon.

Trends in $\rho(x)$ at C−H bond critical points are varied. For reactants and products, there is the general trend to increasing values with increasing fluorine substitution, and within a molecule, to larger values on the more substituted carbon. For TSs, values are again higher on the more substituted carbon, but the correlation of higher values with increasing number of fluorines is weaker. Values at β-carbons are lower when there is a β-fluorine gauche to the reaction centre. For the special case of the critical bond at the bond being broken in the TS (C1−H1 in Table 8.2), values are much lower than for other C−H bonds. The predominant trend here is for values to increase with the number of α-fluorines, with a secondary trend for lower values as the number

of β-fluorines increases. Values are also slightly lowered when there are β-fluorines gauche to H1.

For the bond critical point of the bond being formed (H1$-$O in Table 8.2), the magnitudes of $\rho(r)$ are again low. Higher values are seen when there are β-fluorines gauche to H1, and for increasing substitution on the β-carbon, except for CH_2F-CHF_2 + OH being higher than CHF_2-CH_2F + OH.

In contrast, $\rho(r_c)$ values in the hydroxyl group are much larger, and have much different trends. There is a weak trend to decreasing values with increasing substitution, and lower values are seen when there are β-fluorines gauche to H1. It should be noted that the range of values is small, $0.3769-0.3796$.

Most of the above trends are consistent with $\rho(r_c)$ providing a measure of bond strength.[251] Thus, the forming and breaking bonds have particularly low values. Higher values are seen in C$-$X bonds for more highly substituted carbons. For transition states, the intramolecular hydrogen bond formed when there is a β-fluorine gauche to the reaction centre (see Chapter 7) leads to higher $\rho(r_c)$ values for $C_\beta-H_\beta$ and H1$-$O bonds, the latter at the expense of the hydroxyl bond.

An exception is provided by C$-$C bonds. If bond dissociation energy (BDE) is used as a measure of bond strength, then C$-$C bonds are stronger when there is a greater electronegativity difference between the two groups (see Chapter 5), but the same trend is not seen in the $\rho(r_c)$ values. As well, the $\rho(r_c)$ values do not correlate with the C$-$C bond lengths.

Table 8.1: Properties of Bond Critical Points for Reactants

Bond[a]	$\rho(\boldsymbol{r_c})$ [b]	$\nabla^2\rho\,(\boldsymbol{r_c})$ [b]	r_A [c]	r_B [c]
OH ($C_{\infty v}$)				
O−H	0.3790	−2.7717	0.776	0.183
C_2H_6 (D_{3d})				
C−C	0.2512	−0.6697	0.764	0.764
C−H	0.2833	−1.0236	0.676	0.410
CH_2F-CH_3 (C_s)				
$C_\alpha-C_\beta$	0.2680	−0.7680	0.780	0.732
C−F	0.2295	0.5015	0.437	0.935
$C_\alpha-H_\alpha$	0.2991	−1.1402	0.688	0.395
$C_\beta-H_{\beta 0}$	0.2824	−1.0187	0.677	0.408
$C_\beta-H_{\beta 1}$	0.2848	−1.0323	0.680	0.404
CH_2F-CH_2F (C_2)[c]				
C−C	0.2826	−0.8580	0.752	0.752
C−F	0.2348	0.5029	0.436	0.931
$C-H_g$	0.2997	−1.1440	0.693	0.389
$C-H_t$	0.2997	−1.1325	0.689	0.394
CHF_2-CH_3 (C_s)				
$C_\alpha-C_\beta$	0.2804	−0.8489	0.805	0.697
$C_\alpha-F_\alpha$	0.2530	0.3911	0.431	0.915
$C_\alpha-H_\alpha$	0.3137	−1.2505	0.700	0.379
$C_\beta-H_{\beta 0}$	0.2856	−1.0370	0.685	0.398
$C_\beta-H_{\beta 1}$	0.2852	−1.0361	0.681	0.402
CF_3-CH_3 (C_{3v})				
$C_\alpha-C_\beta$	0.2845	−0.8926	0.841	0.658
$C_\alpha-F_\alpha$	0.2763	0.2283	0.428	0.897
$C_\beta-H_\beta$	0.2875	−1.0506	0.685	0.396

Table 8.1 (continued)

Bond[a]	$\rho(\mathbf{r}_c)$ [b]	$\nabla^2\rho(\mathbf{r}_c)$ [b]	r_A [c]	r_B [c]
CHF_2-CH_2F (C_1)[d]				
$C_\alpha-C_\beta$	0.2903	−0.9152	0.781	0.725
$C_\alpha-F_{\alpha g}$	0.2547	0.4119	0.430	0.913
$C_\alpha-F_{\alpha t}$	0.2590	0.4034	0.429	0.909
$C_\alpha-H_\alpha$	0.3143	−1.2566	0.704	0.374
$C_\beta-F_\beta$	0.2374	0.5171	0.434	0.928
$C_\beta-H_{\beta gt}$	0.3008	−1.1529	0.693	0.388
$C_\beta-H_{\beta gg}$	0.3008	−1.1516	0.696	0.385
CF_3-CH_2F (C_s)				
$C_\alpha-C_\beta$	0.2932	−0.9489	0.815	0.692
$C_\alpha-F_{\alpha 0}$	0.2769	0.2455	0.427	0.897
$C_\alpha-F_{\alpha 1}$	0.2823	0.2375	0.426	0.892
$C_\beta-F_\beta$	0.2437	0.4990	0.433	0.922
$C_\beta-H_\beta$	0.3022	−1.1632	0.697	0.383
CHF_2-CHF_2 (C_{2h})				
$C-C$	0.2977	−0.9663	0.755	0.755
$C-F$	0.2612	0.4084	0.429	0.907
$C-H$	0.3145	−1.2599	0.708	0.370
CF_3-CHF_2 (C_s)				
$C_\alpha-C_\beta$	0.2991	−0.9836	0.790	0.727
$C_\alpha-F_{\alpha 0}$	0.2879	0.2437	0.424	0.887
$C_\alpha-F_{\alpha 1}$	0.2831	0.2433	0.425	0.891
$C_\beta-F_\beta$	0.2668	0.3861	0.428	0.903
$C_\beta-H_\beta$	0.3156	−1.2690	0.709	0.368

[a] Only bonds which are unique by symmetry are given. The α-C is the most highly substituted one. An atom labelled with 0 is in the symmetry plane, 1 is not. See Figure

6 for individual geometries. [b] In atomic units. [c] For bond A−B, r_A and r_B are the distances, in Å, from the bond critical point to atoms A and B, respectively. [c] The designations g and t indicate the atom is gauche or trans, respectively, to a fluorine.

Table 8.2: Properties of Bond Critical Points for Transition States

Bond[a]	$\rho\,(r_c)$ [b]	$\nabla^2\rho\,(r_c)$ [b]	r_A [c]	r_B [c]
C_2H_6 + OH[d]				
H1−O	0.1723	−0.1257	0.348	0.870
O−H2	0.3796	−2.7384	0.771	0.184
C1−H1	0.1578	−0.2879	0.866	0.434
C1−C2	0.2572	−0.6981	0.777	0.736
C1−H3/4	0.2877	−1.0493	0.682	0.400
C2−H5	0.2809	−1.0063	0.679	0.409
C2−H6/7	0.2854	−1.0371	0.680	0.404
$CH_3−CH_2F$ + OH				
H1−O	0.1763	−0.1314	0.346	0.864
O−H2	0.3785	−2.7481	0.773	0.182
C1−H1	0.1671	−0.3299	0.878	0.421
C1−C2	0.2716	−0.7870	0.793	0.707
C1−H3	0.3008	−1.1486	0.695	0.385
C1−F4	0.2398	0.5737	0.432	0.922
C2−H5	0.2825	−1.0166	0.683	0.404
C2−H6	0.2848	−1.0346	0.682	0.402
C2−H7	0.2861	−1.0413	0.684	0.399
$CH_2F−CH_3$ + OH t				
H1−O	0.1794	−0.1701	0.338	0.863
O−H2	0.3788	−2.7462	0.772	0.182
C1−H1	0.1524	−0.2629	0.874	0.438
C1−C2	0.2713	−0.7824	0.750	0.755
C1−H3	0.2891	−1.0584	0.687	0.393
C1−H4	0.2884	−1.0544	0.684	0.396
C2−F5	0.2295	0.4791	0.438	0.936

Table 8.2 (continued)

Bond[a]	$\rho\,(\boldsymbol{r_c})$ [b]	$\nabla^2\rho\,(\boldsymbol{r_c})$ [b]	r_A [c]	r_B [c]
C2−H6	0.3013	−1.1562	0.691	0.389
C2−H7	0.3011	−1.1547	0.691	0.390
CH₂F−CH₃ + OH g				
H1−O[e]				
O−H2	0.3778	−2.7615	0.775	0.180
C1−H1	0.1525	−0.2599	0.879	0.438
C1−C2	0.2733	−0.7923	0.739	0.763
C1−H3	0.2887	−1.0551	0.686	0.394
C1−H4	0.2872	−1.0464	0.685	0.395
C2−H5	0.2979	−1.1317	0.692	0.392
C2−F6	0.2277	0.4958	0.438	0.937
C2−H7	0.3011	−1.1542	0.692	0.389
CH₂F−CH₂F + OH t				
H1−O	0.1809	−0.1609	0.340	0.859
O−H2	0.3776	−2.7511	0.774	0.181
C1−H1	0.1628	−0.3089	0.884	0.424
C1−C2	0.2840	−0.8640	0.768	0.729
C1−H3	0.3011	−1.1519	0.699	0.380
C1−F4	0.2453	0.5872	0.430	0.917
C2−F5	0.2342	0.4790	0.437	0.931
C2−H6	0.3004	−1.1513	0.694	0.388
C2−H7	0.3012	−1.1552	0.695	0.385
CH₂F−CH₂F + OH g				
H1−O	0.1843	−0.1839	0.335	0.856
O−H2	0.3772	−2.7638	0.776	0.179
C1−H1	0.1610	−0.2978	0.890	0.424
C1−C2	0.2844	−0.8643	0.760	0.737

Table 8.2 (continued)

Bond[a]	$\rho\,(\mathbf{r}_c)$ [b]	$\nabla^2\rho\,(\mathbf{r}_c)$ [b]	r_A [c]	r_B [c]
C1—H3	0.2997	−1.1421	0.697	0.383
C1—F4	0.2475	0.5841	0.429	0.915
C2—H5	0.2987	−1.1369	0.695	0.387
C2—H6	0.3005	−1.1517	0.693	0.388
C2—F7	0.2330	0.4929	0.437	0.932
CHF₂—CH₃ + OH g,t				
H1—O	0.1869	−0.2182	0.330	0.855
O—H2	0.3778	−2.7608	0.775	0.180
C1—H1	0.1500	−0.2483	0.883	0.439
C1—C2	0.2842	−0.8635	0.710	0.787
C1—H3	0.2892	−1.0595	0.689	0.390
C1—H4	0.2892	−1.0591	0.690	0.389
C2—F5	0.2549	0.3724	0.431	0.913
C2—H6	0.3157	−1.2668	0.704	0.374
C2—F7	0.2518	0.3828	0.432	0.916
CHF₂—CH₃ + OH g,g				
H1—O	0.1881	−0.2300	0.328	0.854
O—H2	0.3777	−2.7633	0.776	0.180
C1—H1	0.1484	−0.2401	0.888	0.439
C1—C2	0.2837	−0.8602	0.706	0.790
C1—H3	0.2896	−1.0623	0.688	0.391
C1—H4	0.2893	−1.0595	0.689	0.389
C2—H5	0.3126	−1.2428	0.704	0.376
C2—F6	0.2577	0.3805	0.430	0.911
C2—F7	0.2513	0.3774	0.432	0.917
CH₃—CF₂H + OH[d]				
H1—O	0.1821	−0.1580	0.340	0.857

Table 8.2 (continued)

Bond[a]	$\rho\,(\boldsymbol{r}_c)$ [b]	$\nabla^2\rho\,(\boldsymbol{r}_c)$ [b]	r_A [c]	r_B [c]
O−H2	0.3778	−2.7497	0.774	0.181
C1−H1	0.1717	−0.3483	0.893	0.410
C1−C2	0.2781	−0.8396	0.821	0.675
C1−F3/4	0.2634	0.4577	0.426	0.903
C2−H5	0.2837	−1.0238	0.687	0.398
C2−H6/7	0.2874	−1.0511	0.686	0.396
CF$_3$−CH$_3$ + OH				
H1−O	0.1919	−0.2577	0.323	0.850
O−H2	0.3777	−2.7621	0.776	0.180
C1−H1	0.1470	−0.2333	0.892	0.440
C1−C2	0.2878	−0.9007	0.671	0.824
C1−H3	0.2913	−1.0744	0.692	0.386
C1−H4	0.2908	−1.0710	0.693	0.385
C2−F5	0.2781	0.2034	0.428	0.896
C2−F6	0.2748	0.2102	0.429	0.899
C2−F7	0.2811	0.2136	0.427	0.893
CHF$_2$−CH$_2$F + OH g,t				
H1−O	0.1874	−0.2034	0.332	0.853
O−H2	0.3778	−2.7578	0.775	0.181
C1−H1	0.1599	−0.2921	0.893	0.425
C1−C2	0.2912	−0.9135	0.741	0.761
C1−H3	0.3015	−1.1556	0.702	0.376
C1−F4	0.2477	0.5998	0.429	0.915
C2−F5	0.2583	0.3777	0.430	0.910
C2−F6	0.2603	0.3961	0.429	0.908
C2−H7	0.3156	−1.2684	0.707	0.370
CHF$_2$−CH$_2$F + OH g,g				

Table 8.2 (continued)

Bond[a]	$\rho\,(\mathbf{r}_c)$ [b]	$\nabla^2\rho\,(\mathbf{r}_c)$ [b]	r_A [c]	r_B [c]
H1−O	0.1893	−0.2201	0.329	0.851
O−H2	0.3773	−2.7641	0.776	0.179
C1−H1	0.1580	−0.2809	0.897	0.425
C1−C2	0.2910	−0.9112	0.734	0.768
C1−H3	0.3016	−1.1563	0.700	0.378
C1−F4	0.2499	0.5986	0.428	0.913
C2−H5	0.3132	−1.2483	0.707	0.372
C2−F6	0.2607	0.4000	0.429	0.908
C2−F7	0.2569	0.3867	0.430	0.911
CH$_2$F−CHF$_2$ + OH				
H1−O	0.1898	−0.2121	0.330	0.850
O−H2	0.3770	−2.7605	0.776	0.179
C1−H1	0.1656	−0.3156	0.905	0.414
C1−C2	0.2879	−0.9003	0.789	0.714
C1−F3	0.2673	0.4889	0.425	0.899
C1−F4	0.2687	0.4773	0.424	0.898
C2−H5	0.2997	−1.1439	0.698	0.383
C2−H6	0.3029	−1.1690	0.697	0.382
C2−F7	0.2373	0.5096	0.435	0.928
CF$_3$−CH$_2$F + OH				
H1−O	0.1924	−0.2411	0.325	0.847
O−H2	0.3772	−2.7622	0.776	0.180
C1−H1	0.1569	−0.2744	0.901	0.426
C1−C2	0.2944	−0.9421	0.706	0.798
C1−H3	0.3028	−1.1166	0.704	0.374
C1−F4	0.2540	0.5882	0.427	0.909
C2−F5	0.2817	0.2140	0.427	0.893

Table 8.2 (continued)

Bond[a] ·	$\rho\ (\boldsymbol{r}_c)$ [b]	$\nabla^2\rho\ (\boldsymbol{r}_c)$ [b]	r_A [c]	r_B [c]
C2−F6	0.2829	0.2321	0.426	0.892
C2−F7	0.2836	0.2243	0.426	0.891
CHF₂−CHF₂ + OH				
H1−O	0.1917	−0.2237	0.328	0.847
O−H2	0.3769	−2.7589	0.776	0.180
C1−H1	0.1646	−0.3096	0.907	0.414
C1−C2	0.2941	−0.9410	0.768	0.742
C1−F3	0.2723	0.4895	0.423	0.895
C1−F4	0.2729	0.4865	0.423	0.894
C2−F5	0.2640	0.3745	0.429	0.905
C2−H6	0.3162	−1.2742	0.709	0.368
C2−F7	0.2629	0.3894	0.429	0.906
CF₃−CHF₂ + OH				
H1−O	0.2063	−0.3948	0.311	0.852
O−H2	0.3699	−2.5308	0.763	0.192
C1−H1	0.1467	−0.2034	0.918	0.414
C1−C2	0.2809	−0.7922	0.754	0.763
C1−F3	0.2776	0.1802	0.436	0.882
C1−F4	0.2813	0.2006	0.434	0.879
C2−F5	0.2846	−0.0396	0.439	0.876
C2−F6	0.2913	−0.0392	0.438	0.874
C2−F7	0.2923	−0.0358	0.438	0.874

[a] All species are asymmetrical, except where noted. For numbering scheme, see Figure 8 for C_2H_6 + OH, and Figure 11 for other species. The designations g and t refer to the hydrogen being abstracted as gauche and trans, respectively, to a β-F. [b] In atomic units. [c] For bond A−B, r_A and r_B are the distances, in Å, from the bond critical point to atoms A and B, respectively. [d] C_s symmetry. [e] Bond critical point not found.

Table 8.3: Properties of Bond Critical Points for Products

Bond[a]	$\rho\,(\mathbf{r}_c)$ [b]	$\nabla^2\rho\,(\mathbf{r}_c)$ [b]	r_A [c]	r_B [c]
H_2O (C_{2v})				
$O-H$	0.3842	-2.7953	0.767	0.181
C_2H_5 (C_s)				
$C_\alpha-C_\beta$	0.2628	-0.7198	0.761	0.737
$C_\alpha-H_\alpha$	0.2880	-1.0395	0.677	0.398
$C_\beta-H_{\beta 0}$	0.2783	-0.9882	0.681	0.410
$C_\beta-H_{\beta 1/2}$	0.2834	-1.0235	0.678	0.407
CH_2F-CH_2 (C_1)				
$C_\alpha-C_\beta$	0.2774	-0.8072	0.733	0.756
$C_\alpha-H_{\alpha 1}$	0.2891	-1.0475	0.684	0.390
$C_\alpha-H_{\alpha 2}$	0.2884	-1.0440	0.680	0.394
$C_\beta-F_{\beta 1}$	0.2320	0.4757	0.437	0.934
$C_\beta-H_{\beta 0}$	0.2950	-1.1105	0.692	0.395
$C_\beta-H_{\beta 2}$	0.2980	-1.1327	0.691	0.393
CH_3-CHF (C_1)				
$C_\alpha-C_\beta$	0.2742	-0.7936	0.779	0.711
$C_\alpha-F_{\alpha 1}$	0.2436	0.7171	0.427	0.913
$C_\alpha-H_{\alpha 2}$	0.2983	-1.1216	0.689	0.387
$C_\beta-H_{\beta 0}$	0.2840	-1.0296	0.680	0.404
$C_\beta-H_{\beta 1}$	0.2799	-0.9980	0.684	0.405
$C_\beta-H_{\beta 2}$	0.2842	-1.0285	0.683	0.402
CH_2F-CHF (a) (C_1)				
$C_\alpha-C_\beta$	0.2879	-0.8771	0.757	0.725
$C_\alpha-F_{\alpha 2}$	0.2501	0.7331	0.425	0.916
$C_\alpha-H_{\alpha 1}$	0.2996	-1.1322	0.693	0.381
$C_\beta-F_{\beta 0}$	0.2308	0.4240	0.440	0.935

Table 8.3 (continued)

Bond[a]	$\rho\ (\boldsymbol{r}_c)$ [b]	$\nabla^2\rho\ (\boldsymbol{r}_c)$ [b]	r_A [c]	r_B [c]
$C_\beta - H_{\beta 1}$	0.2998	-1.1467	0.691	0.390
$C_\beta - H_{\beta 2}$	0.3005	-1.1507	0.694	0.386
$CHF_2 - CH_2$ (C_1)				
$C_\alpha - C_\beta$	0.2883	-0.8780	0.706	0.778
$C_\alpha - H_{\alpha 1}$	0.2906	-1.0604	0.684	0.389
$C_\alpha - H_{\alpha 2}$	0.2905	-1.0589	0.687	0.386
$C_\beta - F_{\beta 0}$	0.2517	0.3267	0.434	0.917
$C_\beta - F_{\beta 2}$	0.2555	0.3732	0.431	0.913
$C_\beta - H_{\beta 1}$	0.3141	-1.2543	0.702	0.377
$CH_3 - CF_2$ (C_s)				
$C_\alpha - C_\beta$	0.2780	-0.8358	0.809	0.682
$C_\alpha - F_\alpha$	0.2632	0.5771	0.424	0.899
$C_\beta - H_{\beta 0}$	0.2819	-1.0106	0.687	0.400
$C_\beta - H_{\beta 1/2}$	0.2867	-1.0468	0.684	0.398
$CF_3 - CH_2$ (C_s)				
$C_\alpha - C_\beta$	0.2927	-0.9176	0.670	0.813
$C_\alpha - H_\alpha$	0.2924	-1.0732	0.689	0.382
$C_\beta - F_{\beta 0}$	0.2759	0.1703	0.430	0.898
$C_\beta - F_{\beta 1/2}$	0.2785	0.2011	0.428	0.896
$CHF_2 - CHF$ (a) (C_1)				
$C_\alpha - C_\beta$	0.2952	-0.9289	0.730	0.760
$C_\alpha - F_{\alpha 2}$	0.2535	0.7462	0.424	0.904
$C_\alpha - H_{\alpha 1}$	0.2999	-1.1373	0.698	0.376
$C_\beta - F_{\beta 0}$	0.2585	0.3834	0.430	0.910
$C_\beta - F_{\beta 2}$	0.2558	0.3390	0.433	0.913
$C_\beta - H_{\beta 1}$	0.3149	-1.2625	0.706	0.372
$CH_2F - CF_2$ (C_s)				

Table 8.3 (continued)

Bond[a]	$\rho\,(r_c)$ [b]	$\nabla^2\rho\,(r_c)$ [b]	r_A [c]	r_B [c]
$C_\alpha-C_\beta$	0.2892	−0.9068	0.786	0.705
$C_\alpha-F_\alpha$	0.2692	0.5966	0.422	0.893
$C_\beta-F_\beta$	0.2373	0.4374	0.437	0.929
$C_\beta-H_\beta$	0.3019	−1.1618	0.696	0.384
CF_3-CHF (C_1)				
$C_\alpha-C_\beta$	0.2983	−0.9559	0.699	0.793
$C_\alpha-F_{\alpha1}$	0.2602	0.7367	0.423	0.898
$C_\alpha-H_{\alpha2}$	0.3015	−1.1499	0.699	0.373
$C_\beta-F_{\beta0}$	0.2807	0.2213	0.427	0.894
$C_\beta-F_{\beta1}$	0.2799	0.1842	0.428	0.895
$C_\beta-F_{\beta2}$	0.2844	0.2056	0.426	0.891
CHF_2-CF_2 (C_s)				
$C_\alpha-C_\beta$	0.2933	−0.9337	0.763	0.741
$C_\alpha-F_\alpha$	0.2725	0.6029	0.421	0.891
$C_\beta-F_\beta$	0.2650	0.3750	0.428	0.904
$C_\beta-H_\beta$	0.3125	−1.2428	0.710	0.371
CF_3-CF_2 (C_s)				
$C_\alpha-C_\beta$	0.2976	−0.9613	0.733	0.774
$C_\alpha-F_\alpha$	0.2778	0.5978	0.420	0.886
$C_\beta-F_{\beta0}$	0.2846	0.1920	0.427	0.891
$C_\beta-F_{\beta1/2}$	0.2875	0.2134	0.425	0.888

[a] Only bonds which are unique by symmetry are given. The α-C is the radical centre. Atom numbering scheme is as in Figure 2. See Figure 1 for individual geometries. [b] In atomic units. [c] For bond A−B, r_A and r_B are the distances, in Å, from the bond critical point to atoms A and B, respectively.

Many of the trends in the charge densities are seen again in the Laplacian of the charge density, $\nabla^2\rho\,(r)$. For most bonds in this study $\nabla^2\rho\,(r)$ is negative at the bond critical point, indicating a local concentration of charge. All $C-F$ bonds have positive values, except for slightly negative values in the CF_3 group of the $CF_3-CHF_2 + OH$ TS. The anomalous values of $\nabla^2\rho\,(r_c)$ for the $C-F$ bonds derives from the unique behaviour of the Laplacian distributions for fluorine atoms, where the charge density is tightly bound and very localized in all of its compounds.[256]

For the $C-C$ critical points, the trends are particularly similar to those for the charge density, with the following exceptions: in the products, the trend to larger magnitudes for more symmetrically substituted radicals, which was weak for the charge densities, is now more effective (see for example the cases for $C_2H_2F_3$); for transition states, there is a strong dependence on the number of fluorines, but no consistent trends with substitution patterns.

The trends in $\nabla^2\rho\,(r)$ values for $C-F$ bond critical points are at variance with their $\rho\,(r)$ trends, and also vary with category, $i.e.$, reactants, products, or TS. For reactants, within a molecule the higher values are on the less substituted carbon. Higher values are also seen in symmetrically substituted molecules, and there is a general trend to higher values with increasing number of fluorines. For transition states, values are usually higher on the α-carbon, with an exception for $CH_2F-CHF_2 + OH$. On both α- and β-carbons, $\nabla^2\rho\,(r_c)$ decreases with increasing number of fluorines on that carbon. For products, within a radical much larger values are seen at the α-carbon. For isomers

with the same number of fluorines, $\nabla^2\rho\,(x_c)$ is higher in the case where fluorines are distributed as evenly as possible between the carbons; this trend is particularly pronounced for values at the β-centre.

Values of $\nabla^2\rho\,(x)$ at C$-$H bond critical points are almost always more negative on the more highly substituted carbon, and as fluorine substitution as a whole increases. For TSs, magnitudes on the β-carbon are lower for hydrogens gauche to the reaction centre. Magnitudes of $\nabla^2\rho\,(x_c)$ for C1$-$H1 are much lower than for other C$-$H bonds. They are higher when there are α-fluorines, but decrease when there are β-fluorines. There is no dependence on the total number of fluorines.

For H1$-$O, $\nabla^2\rho\,(x_c)$ is more negative when there are β-fluorines, especially if they are gauche to H1. There is a general increase in magnitude with increasing substitution. Magnitudes of $\nabla^2\rho\,(x_c)$ for O$-$H2 are by far the highest of any bond types in this study. Starting from the parent C_2H_6 + OH reaction, values increase for mono-substituted systems, then are fairly steady (between -2.7497 and -2.7641) when there are two or more fluorines, with more negative values when there are β-fluorines, particularly if they are gauche to H1.

A relatively large negative value of $\nabla^2\rho\,(x_c)$ together with a relatively large $\rho\,(x_c)$ value indicate a strong covalent bond.[257] Thus, it is again seen that the forming and breaking bonds are weak, and bonds are stronger when there is a high degree of substitution by electronegative fluorine atoms, and for cases of intramolecular hydrogen bonding. Particularly strong bonds are seen in the hydroxyl units.

On the other hand, the positive values of $\nabla^2\rho\ (r)$ seen at the $C-F$ bond critical points do not indicate that these are weak bonds. Rather, as a result of charge transfer in these polar bonds, the bond critical point moves closer to the carbon nucleus (see below) and the associated bonded charge concentration now lies within the boundary of the fluorine atom.[258]

The sum of the distances (r_A and r_B) from the bond critical point to the associated nuclei is usually longer than the bond length, due to curvature in the bond path (the bond critical point will only lie on the internuclear axis if this axis coincides with an axis of symmetry[259]). These distances can be used as a one-dimensional indication of the size of the atom within the molecule, and assuming fairly constant bond (or bond path) lengths, trends in the absolute difference between r_A and r_B for a given bond type can be used as an indication of substituent effects on that bond type.

For $C-C$ bonds, the larger atom is the more highly substituted one, and for TSs and products α-carbons are larger in case of equal substitution. For reactants, the r_A-r_B difference is seen to increase with an increasing difference in the fluorine substitution at the two carbons, and with the total number of fluorines.

For $C-F$ bonds, the r_A-r_B difference decreases slightly with increasing number of fluorines. For TSs and products, the difference is larger at β-carbons.

For $C-H$ bonds, the r_A-r_B difference is larger at the more substituted carbon, at least for reactants and TSs, and for the latter larger differences are seen at the α-carbon when there is equal substitution at the two carbons. For products, the difference in a given radical is largest at the α-carbon, except when there are two β-fluorines. For

reactants and products there is a general increase in $r_A - r_B$ differences with increasing substitution.

For the bond in the hydroxyl unit, whose length is remarkably constant through the series (see Chapter 7), the $r_A - r_B$ difference is also nearly constant, except for $CF_3 - CHF_2$ + OH, where the bond critical point is closer to the oxygen atom than it is in other TSs.

There is a larger variance in lengths for the bonds being broken (C1 — H1) and formed (H1 — O) at the TS. Here a better measure of substituent effects on a bond type is the relative length from the critical point to the nearest atom. For H1 — O this is fairly constant (28±0.6%). More variance is seen for C1 — H1 (31.1 — 33.4%), with a slight trend to lower values with increasing substitution. For a given number of fluorines, lower values are seen for the TS where they are distributed as evenly as possible between the two carbons.

The above results in the position of the bond critical point are consistent with those seen previously for binary hydrides.[260] There it was noted that the position of r_c correlated, although not in a linear fashion, to the electronegativity of the non-hydrogen atom, i.e., as the electronegativity increased, r_c moved closer to the hydrogen (this correlation led to a method for calculating group electronegativities[261]). Here, r_c is closer to the least electronegative atom, or to the atom which has less electronegative substituents. Thus, the carbon atom with the largest atomic basin is that which is more substituted with fluorines, or is closer to the incoming oxygen. The same factors lead to smaller hydrogen atoms.

8.3 Atomic Charges

Atomic charges calculated by MPA at four levels of theory, and by BPA at the MP2/6-311G(d,p)//HF/6-31G(d) level, for all heavy atoms plus the hydrogen being abstracted, are given in Table 8.4. Starting from the base theory of HF/6-31G(d), the following trends can be seen as the level of theory is increased. Employing a larger basis set (6-311G(d,p)) has dramatic effects, usually reducing the magnitude of the charge. Including electron correlation at the MP2 level has varying effects depending on the atom, similar to previous results.[262,263] Carbon atoms become more negative or less positive. Hydrogens usually become more positive, with some exceptions for more highly substituted species, where the positive charge lessens slightly. Oxygens become less negative in OH and H_2O, and more negative in TSs, with the degree of difference increasing with the number of α-fluorines. Fluorines are less negative, by about 0.8. When electron correlation is employed in the geometry optimizations, varying effects are seen. In general, the change in charge is greater for greater geometry changes, and on the oxygen atoms.

The BPA charges are often much larger than MPA, and in cases of moderate magnitudes the signs are often different. While experiment cannot give us numbers with which to compare to, given their opposing trends noted above with regards to electronegative atoms, the two methods should give results on either side of the expected "actual charges". Simple chemical intuition is not always reliable in judging the relative accuracy of the results. For example, in all the commonly used electronegativity scales carbon is slightly more electronegative than hydrogen, so it is reasonable to expect that

in ethane the carbons should have a slight negative charge and the hydrogens should be slightly positive. This is the case for the MPA results, but the opposite situation is seen in the BPA results. However, the dipole moment derivatives for methane correspond to to a bond dipole in the sense C^+-H^-,[264] and this conclusion is supported by an analysis[265] of natural population analysis charges (which do not have the basis set dependence of MPA charges). A more general conclusion is that MPA leads to the wrong charge distribution in most $C-H$ bonds.[266] The high ionic character for $C-F$ bonds as indicated by the BPA charges also seems surprising at first. However, carbon and hydrogen have roughly the same electronegativity, and it is generally recognized that HF has a large ionic character.

For individual atom types, the following trends are noted at the various levels of theory. Charges at α-carbons are more negative than at β-carbons, except when the number of α-fluorines is greater then the number of β-fluorines. With MPA β-fluorines are usually more negative than α-fluorines, except when there are more fluorines on the β-carbon. With BPA there is less variance, and the trends are sometimes opposite. For example, in CH_2F-CHF, MPA gives more negative results for the β-fluorine, but at BPA the more negative value is for the α-fluorine. Charges on hydrogens roughly correlate with the electronegativity of nearby atoms, i.e., as the number of nearby electronegative atoms increases, so does the positive charge on the hydrogen. Charges on oxygen atoms are smallest in the reactant (OH), largest in the product (H_2O), and vary little in the TS. Smaller magnitudes are seen when MP2 geometries are used.

Table 8.4: MPA Atomic Charges at Four Levels of Theory, and BPA Atomic Charges at the MP2/6-311G(d,p)//HF/6-31G(d) Level

Atom[a]	HF/6-31G(d)	HF/6-311G(d,p) //HF/6-31G(d)	MP2/6-311G(d,p) //HF/6-31G(d)	HF/6-311G(d,p) //MP2/6-31G(d,p)	BPA
OH					
O	−0.443	−0.252	−0.239	−0.251	−0.595
C$_2$H$_6$					
C	−0.477	−0.257	−0.310	−0.256	0.162
H	0.159	0.086	0.103	0.085	−0.054
C$_2$H$_6$ + OH					
C$_\alpha$	−0.460	−0.278	−0.315	−0.307	−0.006
C$_\beta$	−0.487	−0.252	−0.210	−0.245	0.166
H	0.403	0.221	0.256	0.191	0.295
O	−0.757	−0.443	−0.464	−0.340	−0.907
H$_2$O					
O	−0.864	−0.500	−0.476	−0.497	−1.196
H	0.432	0.250	0.238	0.248	0.598
CH$_3$−CH$_2$					
C$_\alpha$	−0.327	−0.250	−0.263	−0.249	−0.016
C$_\beta$	−0.496	−0.249	−0.308	−0.248	0.164

Table 8.4 (continued)

Atom[a]	HF/6-31G(d)	HF/6-311G(d,p) //HF/6-31G(d)	MP2/6-311G(d,p) //HF/6-31G(d)	HF/6-311G(d,p) //MP2/6-31G(d,p)	BPA
CH₂F−CH₃					
C_α	−0.520	−0.285	−0.341	−0.282	0.157
C_β	0.111	0.211	0.123	0.213	0.705
F_β	−0.428	−0.360	−0.283	−0.376	−0.719
H_β	0.162	0.073	0.083	0.088	−0.040
$H_{\alpha 0}$	0.181	0.101	0.103	0.102	−0.028
$H_{\alpha 1/2}$	0.157	0.087	0.116	0.076	−0.024
CH₂F−CH₃ + OH t					
C_α	−0.491	−0.310	−0.349	−0.334	−0.004
C_β	0.127	0.233	0.137	0.232	0.724
F_β	−0.409	−0.357	−0.275	−0.377	−0.714
H	0.292	0.209	0.242	0.183	0.305
O	−0.693	−0.431	−0.448	−0.337	−0.907
CH₂F−CH₃ + OH g					
C_α	−0.505	−0.304	−0.340	−0.324	−0.004
C_β	0.107	0.201	0.106	0.193	0.699

Table 8.4 (continued)

Atom[a]	HF/6-31G(d)	HF/6-311G(d,p) //HF/6-31G(d)	MP2/6-311G(d,p) //HF/6-31G(d)	HF/6-311G(d,p) //MP2/6-31G(d,p)	BPA
F_β	−0.413	−0.363	−0.280	−0.390	−0.719
H	0.333	0.221	0.250	0.197	NA[b]
O	−0.709	−0.430	−0.444	−0.351	NA[b]
CH₂F−CH₂ C₁					
C_α	−0.358	−0.275	−0.289	−0.271	−0.010
C_β	0.101	0.222	0.128	0.225	0.718
F_β	−0.397	−0.356	−0.280	−0.372	−0.716
CH₃−CH₂F + OH					
C_α	0.119	0.157	0.070	0.146	0.570
C_β	−0.526	−0.272	−0.331	−0.268	0.167
F_α	−0.375	−0.330	−0.237	−0.373	−0.716
H	0.305	0.203	0.242	0.168	0.304
O	−0.707	−0.434	−0.470	−0.332	−0.905
CH₃−CHF					
C_α	0.214	0.168	0.095	0.174	0.599
C_β	−0.544	−0.269	−0.329	−0.266	0.162

Table 8.4 (continued)

Atom[a]	HF/6-31G(d)	HF/6-311G(d,p) //HF/6-31G(d)	MP2/6-311G(d,p) //HF/6-31G(d)	HF/6-311G(d,p) //MP2/6-31G(d,p)	BPA
F_α	−0.368	−0.307	−0.224	−0.322	−0.720
CH₂F−CH₂F					
C	0.076	0.182	0.092	0.186	0.717
F	−0.406	−0.346	−0.271	−0.361	−0.711
H_g	0.155	0.075	0.082	0.080	−0.013
H_t	0.176	0.090	0.097	0.095	0.006
CH₂F−CH₂F + OH t					
C_α	0.080	0.128	0.040	0.118	0.590
C_β	0.090	0.204	0.108	0.205	0.733
F_α	−0.368	−0.314	−0.221	−0.354	−0.708
F_β	−0.399	−0.345	−0.264	−0.363	−0.706
H	0.289	0.192	0.229	0.163	0.309
O	−0.695	−0.425	−0.461	−0.327	−0.903
CH₂F−CH₂F + OH g					
C_α	0.080	0.136	0.054	0.131	0.604
C_β	0.075	0.182	0.086	0.171	0.718

Table 8.4 (continued)

Atom[a]	HF/6-31G(d)	HF/6-311G(d,p) //HF/6-31G(d)	MP2/6-311G(d,p) //HF/6-31G(d)	HF/6-311G(d,p) //MP2/6-31G(d,p)	BPA
F_α	−0.364	−0.309	−0.217	−0.343	−0.706
F_β	−0.402	−0.350	−0.268	−0.377	−0.710
H	0.322	0.205	0.237	0.185	0.321
O	−0.706	−0.422	−0.454	−0.339	−0.904
CH_2F-CHF					
C_α	0.191	0.140	0.067	0.149	0.623
C_β	0.053	0.208	0.108	0.213	0.728
F_α	−0.365	−0.287	−0.203	−0.299	−0.712
F_β	−0.389	−0.351	−0.276	−0.369	−0.706
CHF_2-CH_3					
C_α	−0.559	−0.298	−0.355	−0.292	0.166
C_β	0.634	0.549	0.412	0.559	1.287
F_β	−0.399	−0.322	−0.246	−0.338	−0.721
$H_{\alpha 0}$	0.199	0.115	0.127	0.118	0.000
$H_{\alpha 1/2}$	0.184	0.105	0.119	0.107	−0.015
H_β	0.155	0.067	0.069	0.077	0.017

Table 8.4 (continued)

Atom[a]	HF/6-31G(d)	HF/6-311G(d,p) //HF/6-31G(d)	MP2/6-311G(d,p) //HF/6-31G(d)	HF/6-311G(d,p) //MP2/6-31G(d,p)	BPA
CHF$_2$−CH$_3$ + OH gt					
C$_\alpha$	−0.541	−0.321	−0.358	−0.339	0.014
C$_\beta$	0.638	0.556	0.412	0.559	1.296
F$_g$	−0.391	−0.325	−0.245	−0.354	−0.720
F$_t$	−0.380	−0.314	−0.234	−0.332	−0.716
H	0.328	0.218	0.246	0.199	0.321
O	−0.701	−0.420	−0.433	−0.341	−0.908
CHF$_2$−CH$_3$ + OH gg					
C$_\alpha$	−0.535	−0.310	−0.346	−0.334	0.017
C$_\beta$	0.625	0.537	0.394	0.543	1.291
F$_{\beta1}$	−0.376	−0.309	−0.230	−0.327	−0.717
F$_{\beta2}$	−0.390	−0.325	−0.245	−0.355	−0.720
H	0.341	0.221	0.246	0.207	0.329
O	−0.703	−0.416	−0.431	−0.339	−0.904
CHF$_2$−CH$_2$ C$_1$					
C$_\alpha$	−0.372	−0.274	−0.285	−0.264	0.027

Table 8.4 (continued)

Atom[a]	HF/6-31G(d)	HF/6-311G(d,p) //HF/6-31G(d)	MP2/6-311G(d,p) //HF/6-31G(d)	HF/6-311G(d,p) //MP2/6-31G(d,p)	BPA
C_β	0.611	0.571	0.423	0.582	1.305
$F_{\beta1}$	−0.374	−0.321	−0.245	−0.341	−0.716
$F_{\beta2}$	−0.386	−0.317	−0.244	−0.334	−0.718
$CH_3-CHF_2 + OH$					
C_α	0.639	0.483	0.341	0.492	1.200
C_β	−0.555	−0.285	−0.344	−0.282	0.180
F_α	−0.369	−0.292	−0.200	−0.324	−0.715
H	0.341	0.195	0.233	0.169	0.319
O	−0.754	−0.422	−0.472	−0.323	−0.897
CH_3-CF_2					
C_α	0.700	0.489	0.356	0.512	1.250
C_β	−0.582	−0.275	−0.337	−0.271	0.174
F_α	−0.353	−0.284	−0.205	−0.301	−0.717
CF_3-CH_3					
C_α	−0.589	−0.310	−0.372	−0.300	0.198
C_β	1.104	0.806	0.614	0.838	1.932

Table 8.4 (continued)

Atom[a]	HF/6-31G(d)	HF/6-311G(d,p) //HF/6-31G(d)	MP2/6-311G(d,p) //HF/6-31G(d)	HF/6-311G(d,p) //MP2/6-31G(d,p)	BPA
F	−0.377	−0.287	−0.214	−0.305	−0.721
H	0.205	0.122	0.133	0.126	0.010
$CF_3-CH_3 + OH$					
C_α	−0.570	−0.330	−0.369	−0.351	0.061
C_β	1.092	0.814	0.616	0.838	1.952
$F_{\beta1}$	−0.355	−0.280	−0.203	−0.299	−0.716
$F_{\beta2}$	−0.366	−0.291	−0.214	−0.320	−0.721
$F_{\beta3}$	−0.351	−0.274	−0.198	−0.293	−0.717
H	0.339	0.223	0.247	0.212	0.331
O	−0.397	−0.408	−0.425	−0.330	−0.899
CF_3-CH_2					
C_α	−0.446	−0.281	−0.297	−0.267	0.078
C_β	1.092	0.838	0.634	0.868	1.960
$F_{\beta0}$	−0.362	−0.286	−0.212	−0.304	−0.717
$F_{\beta1/2}$	−0.361	−0.284	−0.212	−0.300	−0.719
CHF_2-CH_2F					

Table 8.4 (continued)

Atom[a]	HF/6-31G(d)	HF/6-311G(d,p) //HF/6-31G(d)	MP2/6-311G(d,p) //HF/6-31G(d)	HF/6-311G(d,p) //MP2/6-31G(d,p)	BPA
C_α	0.042	0.165	0.072	0.171	0.729
C_β	0.589	0.521	0.380	0.533	1.313
F_α	−0.393	−0.339	−0.265	−0.352	−0.706
$F_{\beta 1}$	−0.391	−0.318	−0.242	−0.333	−0.715
$F_{\beta 2}$	−0.380	−0.307	−0.232	−0.322	−0.712
$H_{\alpha 1}$	0.175	0.094	0.099	0.100	0.013
$H_{\alpha 2}$	0.187	0.101	0.105	0.107	0.027
H_β	0.170	0.083	0.082	0.095	0.042
$CHF_2-CH_2F + OH$ gg					
C_α	0.043	0.115	0.033	0.110	0.634
C_β	0.599	0.522	0.377	0.523	1.324
F_α	−0.358	−0.302	−0.211	−0.334	−0.702
$F_{\beta 1}$	−0.378	−0.312	−0.231	−0.340	−0.713
$F_{\beta 2}$	−0.371	−0.303	−0.223	−0.320	−0.711
H	0.328	0.207	0.236	0.195	0.332
O	−0.697	−0.402	−0.442	−0.324	−0.894

Table 8.4 (continued)

Atom[a]	HF/6-31G(d)	HF/6-311G(d,p) //HF/6-31G(d)	MP2/6-311G(d,p) //HF/6-31G(d)	HF/6-311G(d,p) //MP2/6-31G(d,p)	BPA
CHF_2-CH_2F + OH gt					
C_α	0.031	0.101	0.013	0.096	0.618
C_β	0.616	0.548	0.404	0.555	1.347
F_α	−0.363	−0.308	−0.216	−0.346	−0.704
$F_{\beta 1}$	−0.375	−0.306	−0.227	−0.325	−0.708
$F_{\beta 2}$	−0.372	−0.302	−0.223	−0.324	−0.710
H	0.317	0.205	0.237	0.182	0.323
O	−0.692	−0.406	−0.443	−0.318	−0.898
CHF_2-CHF					
C_α	0.152	0.134	0.057	0.147	0.668
C_β	0.584	0.553	0.404	0.566	1.337
F_α	−0.348	−0.280	−0.198	−0.292	−0.706
$F_{\beta 1}$	−0.379	−0.311	−0.236	−0.329	−0.709
$F_{\beta 2}$	−0.379	−0.310	−0.236	−0.325	−0.713
CH_2F-CHF_2 + OH					
C_α	0.598	0.474	0.332	0.481	1.248

Table 8.4 (continued)

Atom[a]	HF/6-31G(d)	HF/6-311G(d,p) //HF/6-31G(d)	MP2/6-311G(d,p) //HF/6-31G(d)	HF/6-311G(d,p) //MP2/6-31G(d,p)	BPA
C_β	0.046	0.170	0.076	0.159	0.739
$F_{\alpha1}$	−0.343	−0.277	−0.186	−0.310	−0.706
$F_{\alpha2}$	−0.351	−0.286	−0.194	−0.320	−0.707
F_β	−0.395	−0.340	−0.259	−0.366	−0.706
H	−0.311	0.195	0.227	0.182	0.336
O	−0.703	−0.408	−0.456	−0.322	−0.895
CH_2F-CF_2					
C_α	0.694	0.462	0.325	0.487	1.291
C_β	0.034	0.204	0.103	0.210	0.761
F_α	−0.356	−0.268	−0.189	−0.283	−0.707
F_β	−0.379	−0.336	−0.264	−0.351	−0.696
CF_3-CH_2F					
C_α	0.019	0.151	0.054	0.162	0.787
C_β	1.091	0.790	0.593	0.821	1.977
F_α	−0.381	−0.323	−0.252	−0.336	−0.697
$F_{\beta0}$	−0.378	−0.287	−0.214	−0.302	−0.716

Table 8.4 (continued)

Atom[a]	HF/6-31G(d)	HF/6-311G(d,p) //HF/6-31G(d)	MP2/6-311G(d,p) //HF/6-31G(d)	HF/6-311G(d,p) //MP2/6-31G(d,p)	BPA
$F_{\beta1/2}$	-0.372	-0.273	-0.202	-0.288	-0.712
H	0.196	0.108	0.111	0.116	0.035
$CF_3 - CH_2F + OH$					
C_α	0.005	0.088	-0.000		0.680
C_β	1.082	0.815	0.614		2.013
F_α	-0.349	-0.292	-0.202		-0.695
$F_{\beta1}$	-0.349	-0.273	-0.196		-0.708
$F_{\beta2}$	-0.348	-0.271	-0.194		-0.712
$F_{\beta3}$	-0.349	-0.272	-0.197		-0.710
H	0.326	0.208	0.236		0.335
O	-0.690	-0.397	-0.436		-0.890
$CF_3 - CHF$					
C_α	0.129	0.126	0.043	0.143	0.736
C_β	1.057	0.828	0.623	0.861	2.008
F_α	-0.334	-0.264	-0.183	-0.274	-0.696
$F_{\beta1}$	-0.353	-0.276	-0.199	-0.294	-0.710

226

Table 8.4 (continued)

Atom[a]	HF/6-31G(d)	HF/6-311G(d,p) //HF/6-31G(d)	MP2/6-311G(d,p) //HF/6-31G(d)	HF/6-311G(d,p) //MP2/6-31G(d,p)	BPA
$F_{\beta2}$	−0.357	−0.279	−0.208	−0.294	−0.714
$F_{\beta3}$	−0.348	−0.269	−0.183	−0.284	−0.710
CHF$_2$−CHF$_2$ t					
C	0.563	0.507	0.364	0.523	1.349
F	−0.373	−0.302	−0.229	−0.316	−0.708
H	0.190	0.097	0.093	0.110	0.063
CHF$_2$−CHF$_2$ + OH					
C_α	0.585	0.463	0.319		1.290
C_β	0.589	0.526	0.381		1.384
$F_{\alpha1}$	−0.337	−0.269	−0.179		−0.697
$F_{\alpha2}$	−0.341	−0.273	−0.182		−0.699
$F_{\beta1}$	−0.365	−0.293	−0.216		−0.699
$F_{\beta2}$	−0.370	−0.301	−0.221		−0.706
H	0.296	0.189	0.221		0.336
O	−0.695	−0.403	−0.456		−0.890

227

Table 8.4 (continued)

Atom[a]	HF/6-31G(d)	HF/6-311G(d,p) //HF/6-31G(d)	MP2/6-311G(d,p) //HF/6-31G(d)	HF/6-311G(d,p) //MP2/6-31G(d,p)	BPA
CHF_2-CF_2					
C_α	0.666	0.469	0.327	0.500	1.362
C_β	0.561	0.546	0.397	0.559	1.396
F_α	−0.332	−0.262	−0.185	−0.277	−0.702
F_β	−0.366	−0.295	−0.224	−0.309	−0.706
CF_3-CHF_2					
C_α	0.542	0.494	0.346	0.515	1.416
C_β	1.040	0.788	0.587	0.822	2.036
F_α	−0.363	−0.289	−0.219	−0.303	−0.700
$F_{\beta0}$	−0.342	−0.262	−0.192	−0.275	−0.703
$F_{\beta1,2}$	−0.351	−0.273	−0.202	−0.287	−0.708
H	0.188	0.106	0.100	0.120	0.071
$CF_3-CHF_2 + OH$					
C_α	0.531	0.423	0.275		1.211
C_β	0.068	0.813	0.611		1.921
$F_{\alpha1}$	−0.327	−0.258	−0.168		−0.619

228

Table 8.4 (continued)

Atom[a]	HF/6-31G(d)	HF/6-311G(d,p) //HF/6-31G(d)	MP2/6-311G(d,p) //HF/6-31G(d)	HF/6-311G(d,p) //MP2/6-31G(d,p)	BPA
$F_{\alpha 2}$	−0.335	−0.268	−0.180		−0.614
$F_{\beta 1}$	−0.344	−0.264	−0.189		−0.632
$F_{\beta 2}$	−0.338	−0.259	−0.183		−0.638
$F_{\beta 3}$	−0.341	−0.263	−0.187		−0.638
H	0.322	0.202	0.230		0.394
O	−0.689	−0.384	−0.437		−0.942
CF₃−CF₂					
C_α	0.660	0.461	0.311	0.498	1.433
C_β	1.083	0.832	0.624	0.864	2.075
F_α	−0.335	−0.249	−0.174	−0.262	−0.694
$F_{\beta 0}$	−0.361	−0.267	−0.198	−0.282	−0.701
$F_{\beta 1/2}$	−0.356	−0.264	−0.195	−0.278	−0.707

[a] The α-C is always that written on the right. Atom labelling scheme is generally the same as in Table 8.3. [b] A bond critical point was not found for the forming H−O bond, rendering the charge integrations for these atoms meaningless.

8.4 Charge Development in the Reactions

The changes in atomic charges from the reactant to transition state, and from TS to product, are given for each reaction by both MPA and BPA methods, at the MP2/6-311G(d,p)//HF/6-31G(d) level of theory, in Table 8.5. In going from reactant to TS, C_α always becomes more negative with the BPA method. MPA results are smaller by a factor of up to 10, and the change is often positive when there are no α-fluorines. Less drastic changes are seen at C_β, which in most cases has a slight positive change, and there is better agreement between the two methods.

Fluorines attached to the α-carbon become slightly more positive, by about 0.05 with MPA, and < 0.01 with BPA. For β-fluorines little change is seen, with relatively larger ΔQ_{r-ts} values with MPA. The abstracted hydrogen becomes more positive, and the oxygen more negative, with greater changes seen using BPA.

The above results are consistent with the influence of the incoming, electronegative oxygen atom, which will draw charge density away from the hydrogen. The impending loss of a relatively electropositive substituent, and/or an inductive effect from the oxygen atom, leaves more electrons at the α-carbon, and a concomitant slight decrease in charge at the remaining substituents.

As the reaction proceeds to products, the oxygen atom moves away from the ethyl radical, so its influence is no longer felt, and many of the changes in atomic charges are reversed. In going from TS to product, C_α always becomes more positive with MPA (except in $CH_2F - CHF_2 + OH$), in some cases more than compensating for the buildup of charge at the TS. The BPA changes are smaller, with varying signs. If the change

in charge from reactant to product is considered, BPA always predicts that C_α is more negative in the product (except in the case of CF_3-CHF_2 + OH), consistent with the increase in electronegativity in going from an sp^3- to sp^2-hybridized carbon.

The MPA results for C_β usually continue the trend to positive changes observed in going from reactant to TS. Signs for the BPA changes vary, and the magnitude is often smaller than for MPA, with CF_3-CHF_2 + OH again being a notable exception.

For α-fluorines, the trend of MPA results to more positive values, which was seen for the change from reactant to TS, continues but with slightly smaller values, and a few exceptions where the value is slightly negative. With BPA the values of ΔQ_{ts-p} are slightly negative. Both methods give very small magnitudes for β-fluorine values.

For the reacting hydrogen atom the BPA method continues the trend to more positive charge, although the effect is smaller than before. Much smaller magnitudes are seen in the MPA results, where the sign of the change varies. The oxygen atom undergoes similar trends as for reactants to TSs, with the effect again being much smaller with MPA.

A general trend seen in these results is that there is a buildup of charge in the TS, concentrated near the reaction centre. The charge buildup on α-carbon atoms dissipates somewhat as the reaction proceeds to products. For other atoms the buildup or depletion of charge continues, but the effect is smaller.

Table 8.5: Change in Atomic Charges from Reactants to Transition State, and from Transition State to Products, at MP2/6-311G(d,p)//HF/6-31G(d) Level of Theory

Reaction[a]	Atom	ΔQ_{r-ts}		ΔQ_{ts-p}	
		MPA	BPA	MPA	BPA
C_2H_6 + OH	C_α	−0.005	−0.168	0.052	−0.010
	C_β	0.000	0.004	0.002	−0.002
	H	0.153	0.349	−0.018	0.303
	O	−0.225	−0.312	−0.012	−0.289
CH_2F-CH_3 + OH t	C_α	−0.008	−0.161	0.060	−0.006
	C_β	0.014	0.019	−0.009	−0.006
	F_β	0.008	0.005	−0.005	−0.002
	H	0.139	0.345	0.004	0.293
	O	−0.209	−0.312	−0.028	−0.289
CH_2F-CH_3 + OH g	C_α	0.001	−0.161	0.051	−0.006
	C_β	−0.017	−0.006	0.022	0.019
	F_β	0.003	0.000	0.000	0.003
	H[b]	0.134		0.012	
	O[b]	−0.205		−0.046	
CH_3-CH_2F + OH	C_α	−0.053	−0.135	0.025	0.029
	C_β	0.010	0.010	0.002	−0.005
	F_α	0.046	0.003	0.013	−0.004
	H	0.159	0.328	−0.004	0.294
	O	−0.231	−0.310	−0.006	−0.291
CH_2F-CH_2F + OH t	C_α	−0.052	−0.127	0.027	0.033
	C_β	0.016	0.016	0.000	−0.005
	F_α	0.050	0.003	0.018	−0.004
	F_β	0.007	0.005	−0.012	0.000
	H	0.132	0.322	0.009	0.289

Table 8.5 (continued)

Reaction[a]	Atom	ΔQ_{r-ts} MPA	ΔQ_{r-ts} BPA	ΔQ_{ts-p} MPA	ΔQ_{ts-p} BPA
	O	−0.222	−0.308	−0.015	−0.293
$CH_2F-CH_2F + OH$ g	C_α	−0.038	−0.113	0.013	0.019
	C_β	−0.006	0.001	0.014	0.010
	F_α	0.054	0.005	0.014	−0.006
	F_β	0.003	0.001	−0.008	0.004
	H	0.155	0.315	0.001	0.277
	O	−0.215	−0.309	−0.022	−0.292
$CHF_2-CH_3 + OH$ gt	C_α	−0.003	−0.152	0.073	0.013
	C_β	0.000	0.009	0.011	0.009
	F_g	0.001	0.001	0.001	0.002
	F_t	0.012	0.005	−0.011	0.000
	H	0.127	0.336	−0.008	0.277
	O	−0.194	−0.313	−0.043	−0.288
$CHF_2-CH_3 + OH$ gg	C_α	0.009	−0.149	0.061	0.010
	C_β	−0.018	0.004	0.029	0.014
	$F_{\beta1}$	0.016	0.004	−0.015	0.001
	$F_{\beta2}$	0.001	0.001	0.001	0.002
	H	0.119	0.329	−0.008	0.269
	O	−0.192	−0.309	−0.045	−0.292
$CH_3-CHF_2 + OH$	C_α	−0.071	−0.087	0.015	0.050
	C_β	0.011	0.014	0.007	−0.006
	F	0.046	0.006	−0.005	−0.002
	H	0.164	0.302	0.005	0.279
	O	−0.233	−0.302	−0.004	−0.299
$CF_3-CH_3 + OH$	C_α	0.003	−0.137	0.072	0.017
	C_β	0.002	0.020	0.018	0.008

Table 8.5 (continued)

Reaction[a]	Atom	$\Delta Q_{r\rightarrow ts}$		$\Delta Q_{ts\rightarrow p}$	
		MPA	BPA	MPA	BPA
	$F_{\beta 1}$	0.011	0.005	−0.009	−0.001
	$F_{\beta 2}$	0.000	0.000	0.002	0.002
	$F_{\beta 3}$	0.016	0.004	−0.014	−0.002
	H	0.114	0.321	−0.009	0.267
	O	−0.186	−0.304	−0.051	−0.297
$CHF_2-CH_2F + OH$ gg	C_α	−0.039	−0.095	0.024	0.034
	C_β	−0.003	0.011	0.027	0.013
	F_α	0.054	0.004	0.013	−0.004
	$F_{\beta 1}$	0.011	−0.001	−0.005	0.004
	$F_{\beta 2}$	0.009	0.004	−0.013	−0.002
	H	0.131	0.305	0.002	0.266
	O	−0.203	−0.299	−0.034	−0.302
$CHF_2-CH_2F + OH$ gt	C_α	−0.059	−0.111	0.044	0.050
	C_β	0.024	0.034	0.000	−0.010
	F_α	0.049	0.002	0.018	−0.002
	$F_{\beta 1}$	0.015	0.004	−0.009	−0.001
	$F_{\beta 2}$	0.009	0.005	−0.013	−0.003
	H	0.138	0.310	0.001	0.275
	O	−0.204	−0.303	−0.033	−0.298
$CH_2F-CHF_2 + OH$	C_α	−0.048	−0.065	−0.007	0.043
	C_β	0.004	0.010	0.027	0.022
	$F_{\alpha 1}$	0.046	0.006	−0.003	−0.001
	$F_{\alpha 2}$	0.048	0.008	0.005	0.000
	F_β	0.006	0.000	−0.005	0.010
	H	0.145	0.294	0.011	0.262
	O	−0.217	−0.300	−0.020	−0.301

Table 8.5 (continued)

Reaction[a]	Atom	$\Delta Q_{r\text{-}ts}$		$\Delta Q_{ts\text{-}p}$	
		MPA	BPA	MPA	BPA
$CF_3-CH_2F + OH$	C_α	−0.054	−0.107	0.043	0.056
	C_β	0.021	0.036	0.009	−0.005
	F_α	0.050	0.002	0.019	−0.001
	$F_{\beta1}$	0.006	0.004	−0.003	−0.002
	$F_{\beta2}$	0.020	0.004	−0.014	−0.002
	$F_{\beta3}$	0.005	0.002	0.014	0.000
	H	0.125	0.300	0.002	0.263
	O	−0.197	−0.295	−0.040	−0.306
$CHF_2-CHF_2 + OH$	C_α	−0.045	−0.059	0.008	0.072
	C_β	0.017	0.035	0.016	0.012
	$F_{\alpha1}$	0.050	0.011	−0.006	−0.005
	$F_{\alpha2}$	0.047	0.009	−0.003	−0.003
	$F_{\beta1}$	0.013	0.009	−0.008	−0.007
	$F_{\beta2}$	0.008	0.002	−0.003	0.000
	H	0.128	0.273	0.017	0.262
	O	−0.217	−0.295	−0.020	−0.306
$CF_3-CHF_2 + OH$	C_α	−0.071	−0.205	0.036	0.222
	C_β	0.024	−0.115	0.013	0.154
	$F_{\alpha1}$	0.051	0.081	−0.006	−0.075
	$F_{\alpha2}$	0.039	0.086	0.006	−0.080
	$F_{\beta1}$	0.003	0.071	−0.009	−0.069
	$F_{\beta2}$	0.019	0.070	−0.012	−0.069
	$F_{\beta3}$	0.015	0.070	−0.008	−0.069
	H	0.130	0.323	0.008	0.204
	O	−0.198	−0.347	−0.039	−0.254

[a] As written the second carbon is attached to the reaction centre (α). The g and t designations refer to the abstracted H being gauche or trans, respectively, to a β-F. [b] BPA numbers not available since the bond critical point for the forming H$-$O bond was not found.

8.5 Conclusions

The magnitudes of the charge density and its Laplacian at the bond critical points are in most cases correlated with the bond strength. The position of the bond critical point is influenced by the electronegativity of the surrounding atoms.

There is a buildup of charge in the TS, concentrated near the reaction centre. As the reaction proceeds to products the charge buildup on the α-carbon dissipates somewhat, while for other atoms the buildup or depletion of charge continues, but at a lesser rate.

Of the two methods used to calculate atomic charges, BPA is more sophisticated, but MPA appears to give more realistic results, at least when relative atomic electronegativities are considered. However, the BPA results are consistent with bond polarities determined in previous studies, and they give a reasonable picture of the charge development in the reactions.

Chapter 9. Global Conclusions and Suggestions for Further Study

Results from the total energy calculations show that for fluorinated ethanes and fluorinated ethyl radicals the most stable isomer is always that in which as many fluorines as possible are on one carbon. The gauche effect operates in radicals as well as in saturated molecules.

The computed $C-C$ BDEs show some intriguing trends, which can be largely explained using electronegativity arguments. The net result of these trends is that CF_3-CH_3 has the greatest $C-C$ bond dissociation energy. Trends in the computed $C-H$ BDEs suggest that an inductive effect from an electronegative β-group can stabilize $C-H$ bonds. Where hydrogen atom abstraction is possible from inequivalent positions in the parent molecules, the favourability of the process is controlled by the nature of the products, rather than the reactants.

The inclusion of electron correlation in the geometry optimizations leads to improvements in structural parameters, most notably the $C-F$ bond lengths, and in total energies, but has a negligible effect on the calculated BDEs.

These results compare favourably with those from experimental studies. However, the incompleteness of the experimental data for these molecules, and some conflicting results where more than one value has been reported, render an absolute determination of the accuracy of these results impossible. From the comparisons that are possible, it appears that the MP2/6-311G(d,p) level of theory gives accurate predictions for the bond dissociation energies and the associated trends, and that accurate geometries

can be obtained with the MP2/6-31G(d,p) level.

Similarly, hyperfine structural parameters for the series of ethyl radicals, calculated with a gradient-corrected density functional method, give satisfactory agreement with experiment, where comparison is possible, and the remaining results should be useful as a guide in completing the experiments in the series.

Good agreement with experiment is also observed in the results of Chapter 6, which presents the most detailed description to date of the potential energy surface for the reaction of hydroxyl with ethane. The calculated barrier height and width, reaction enthalpy, and vibrational frequencies are all close to values measured by or inferred from experiment.

For the reactions of the series of fluorinated ethanes with hydroxyl radicals, variations in geometrical parameters are greater near the reaction centre, and many of the trends, both through the series and between the two levels of theory, are similar to those found for the parent molecules. When there is a β-fluorine gauche to the reaction centre, an intramolecular hydrogen bond forms. The calculated geometries and frequencies both indicate an earlier TS at the MP2 level of theory, consistent with these being exothermic reactions.

Total and zero-point energies, and thence barrier heights and reaction enthalpies, are affected by substitution patterns. Opposing trends are given by increasing fluorine substitution on the α- and β-carbons, and barrier heights are decreased when there is an intramolecular hydrogen bond. Relative trends in experimental energy values are reproduced.

Topological studies of the reactants, transition states, and products of these reactions show that the properties of the charge density at bond critical points correlate with the bond strength, and that these properties are influenced by the electronegativity of nearby atoms. There is a buildup of charge in the transition states of the reactions, concentrated near the reaction centre. The charge buildup is again consistent with electronegativity arguments.

Results from the various chapters are for the most part consistent with each other. While bond strength does not always correlate with bond length, it does correlate with the reactivity of the hydrogen atoms when they are abstracted by hydroxyl radicals. The central factor tying together the trends discussed in this thesis is the influence of electronegativity. This reaffirms that the seminal work done by Linus Pauling on the nature of the chemical bond[93] in the 1930's still has a profound effect on chemical research.

While this thesis represent an extensive and systematic study, further work could be done. Trivially, as more computer power becomes available work could be repeated at higher levels of theory. The analysis of trends in geometrical parameters could be extended by searching for relations between the bond lengths and bond angles. An interesting feature of some of the ethyl radicals is the inversion which takes place at the radical centre, and this could be studied in detail. Work on the reactions could be extended by looking at their dynamics. The topological analyses could be extended to include calculation of group electronegativities, and mapping the electron density over

the entire molecule for some of the more symmetrical species. Tracing the bond paths would allow determination of the degree of bond bending, which could be used to further explain some of the geometry trends.

Finally, it is my hope that in some small way this work will be of use to researchers attempting to solve pressing global environmental problems occurring in the Earth's atmosphere.

References

1. Molina, M.J.; Rowland, F.S. *Nature* **1974**, *249*, 810.

2. Farman, J.C.; Gardiner, B.G.; Shankin, J.D. *Nature* **1985**, *315*, 207.

3. Montreal Protocol on Substances that Deplete the Ozone Layer, UNEP **1987**.

4. WMO/UNEP *Global Ozone Research and Monitoring Project, Report No. 25*, World Meteorological Organization; Geneva: 1992.

5. Anderson, J.G.; Toon, O.B. *Geophys. Res. Lett.* **1993**, *20*, 2499, and other articles in this issue.

6. Austin, J.; Butchart, N.; Shine, K.P. *Nature* **1992**, *360*, 221.

7. Proffitt, M.H.; Fahey, D.W.; Kelly, K.K.; Tuck, A.F. *Nature* **1989**, *342*, 233.

8. Rowland, F.S. *Environ. Conserv.* **1986**, *13*, 193.

9. Anderson, J.G.; Toohey, D.W.; Brune, W.H. *Science* **1991**, *251*, 39.

10. Ravishankara, A.R.; Solomon, S,; Turnipseed, A.A.; Warren, R.F. *Science*, **1993**, *259*, 194.

11. Makide, Y.; Rowland, F.S. *Proc. Natl. Acad. Sci. U.S.A.* **1981**, *78*, 5933.

12. Fisher, D.A.; Hales, C.H.; Filkin, D.L.; Ko, M.K.W.; Sze, N.D.; Connell, P.S.; Wuebbles, D.J.; Isaksen, I.S.A.; Stordal, F. *Nature* **1990**, *344*, 508.

13. Solomon, S.; Albritton, D.L. *Nature* **1992**, *357*, 33.

14. Stolarski, R.S.; Rundel, R.D. *Geophys. Res. Lett.* **1975**, *2*, 443.

15. Francisco, J.S.; Williams, I.H. In *Proceedings of the 16th Annual Meeting of the National Organization of Black Chemists and Chemical Engineers*, NOBCChE: Pleasanton, CA, 1989; Vol. 16, p 59.

16. Nielsen, O.J.; Sehested, J. *Chem. Phys. Lett.* **1993**, *213*, 433.

17. Ravishankara, A.R.; Turnipseed, A.A.; Jensen, N.R.; Barone, S.; Mills, M.; Howard, C.J.; Solomon, S. *Science* **1994**, *263*, 71.

18. Atkinson, R. *J. Phys. Chem. Ref. Data, Monograph 1* **1989.**

19. Sehested, J.; Nielsen, O.J. *Chem. Phys. Lett.* **1993**, *206*, 349.

20. Ko, M.K.W.; Sze, N.-D.; Rodriguez, J.M.; Weisenstein, D.K.; Heisey, C.W.; Wayne, R.P.; Biggs, P.; Canosa-Mas, C.E.; Sidebottom, H.W.; Treacy, J. *Geophys. Res. Lett.* **1994**, *21*, 101.

21. Wallington, T.J.; Schneider, W.F.; Worsnop, D.R.; Nielsen, O.J.; Sehested, J.; Debruyn, W.J.; Shorter, J.A. *Environ. Sci. Technol.* **1994**, *28*, 321.

22. *Chem. Eng. News*, **1992**, June 22, p 7.

23. Hehre, W.J.; Radom, L.; Schleyer, P.v.R.; Pople, J.A. *Ab Initio Molecular Orbital Theory*; Wiley: New York, 1986.

24. McQuarrie, D.A. *Quantum Chemistry*; University Science Books: Mill Valley, CA, 1983.

25. Schrödinger, E. *Ann. Physik* **1926**, *79*, 361.

26. Born, M.; Oppenheimer, J.R. *Ann. Physik* **1927**, *84*, 457.

27. Slater, J.C. *Phys. Rev.* **1930**, *36*, 57.

28. Boys, S.F. *Proc. Roy. Soc. (London)* **1950**, *A200*, 542.

29. Levine, I.N. *Quantum Chemistry*, 3rd ed.; Allyn and Bacon, Inc.: Boston, 1983.

30. Eriksson, L.A. Ph. D. thesis, Uppsala University, 1992.

31. Hartree, D.R. *Cambridge Phil. Soc.* **1928**, *24*, 89.

32. Fock, V. *Z. Physik* **1930**, *61*, 126.

33. Roothaan, C.C.J. *Rev. Mod. Phys.* **1951**, *23*, 69.

34. Hall, G.G. *Proc. Roy. Soc. (London)* **1951**, *A205*, 541.

35. Pople, J.A.; Nesbet, R.K. *J. Chem. Phys.* **1954**, *22*, 571.

36. Møller, C.; Plesset, M.S. *Phys. Rev.* **1934**, *46*, 618.

37. Schrödinger, E. *Ann. Phys.* **1926**, *80*, 437.

38. Pople, J.A.; Head-Gordon, M.; Raghavachari, K. *J. Chem. Phys.* **1987**, *87*, 5968.

39. Schlegel, H.B. In *New Theoretical Concepts for Understanding Organic Reactions*; Bertrán, J., Csizmadia, I.G., Eds.; Kluwer Academic Publishers: Dordrecht, 1989.

40. Schlegel, H.B. *Adv. Chem. Phys.* **1987**, *67*, 249.

41. Curtiss, L.A.; Raghavachari, K.; Trucks, G.W.; Pople, J.A. *J. Chem. Phys.* **1991**, *94*, 7221.

42. Pople, J.A.; Head-Gordon, M.; Fox, D.J.; Raghavachari, K.; Curtiss, L.A. *J. Chem. Phys.* **1989**, *90*, 5622.

43. Parr, R.G.; Yang, W. *Density-Functional Theory of Atoms and Molecules*; Oxford University Press: Oxford, 1989.

44. Thomas, L.H. *Proc. Cambridge Phil. Soc.* **1927**, *23*, 542.

45. Fermi, E. *Z. Physik* **1928**, *48*, 73.

46. Slater, J.C. *Phys. Rev.* **1951**, *81*, 385; **1951**, *82*, 538.

47. Gáspár, R. *Acta Phys. Hung.* **1954**, *3*, 263.

48. Hohenberg, P.; Kohn, W. *Phys. Rev. B* **1964**, *136*, 864.

49. Kohn, W.; Sham, L.J. *Phys. Rev. A* **1965**, *140*, 1133.

50. Bader, R.F.W. *Atoms in Molecules: A Quantum Theory*; Clarendon Press: Oxford, 1990.

51. Shi, Z. Ph.D. thesis, Dalhousie University, 1989.

52. (a) Bader, R.F.W.; Tal, Y.; Anderson, S.G.; Nguyen-Dang, T.T. *Isr. J. Chem.* **1980**, *19*, 8. (b) Bader, R.F.W.; Nguyen-dang, T.T. *Adv. Quant. Chem.* **1981**, *14*, 63. (c) Bader, R.F.W.; Nguyen-Dang, T.T.; Tal, Y. *Rept. Prog. Phys.* **1981**, *44*, 893. (d) Bader, R.F.W.; Essén, H. *J. Chem. Phys.* **1984**, *80*, 1943.

53. Bader, R.F.W.; Anderson, S.G.; Duke, A.J. *J. Am. Chem. Soc.* **1979**, *101*, 1389.

54. *Gaussian 90*, Frisch, M.J.; Head-Gordon, M.; Trucks, G.W.; Foresman, J.B.; Schlegel, H.B.; Raghavachari, K.; Robb, M.A.; Binkley, J.S.; Gonzalez, C.; DeFrees, D.J.; Fox, D.J.; Whiteside, R.A.; Seeger, R.; Melius, C.F.; Baker, J.; Martin, R.L.; Kahn, L.R.; Stewart, J.J.P.; Topiol, S.; Pople, J.A. Gaussian Inc. Pittsburgh PA, 1990.

55. *Gaussian 92/DFT*, Frisch, M.J.; Trucks, G.W.; Schlegel, H.B.; Gill, P.M.W.; Johnson, B.G.; Wong, M.W.; Foresman, J.B.; Robb, M.A.; Head-Gordon, M.; Repogle, E.S.; Gomperts, R.; Andres, J.L.; Raghavachari, K.; Binkley, J.S.; Gonzalez, C.; Martin, R.L.; Fox, D.J.; DeFrees, D.J.; Baker, J.; Stewart, J.J.P.; and Pople, J.A., Gaussian Inc. Pittsburgh PA, 1993.

56. Hariharan, P.C.; Pople, J.A. *Theor. Chim. Acta* **1973**, *28*, 213.

57. Schlegel, H.B. *J. Comp. Chem.* **1982**, *3*, 214.

58. Krishnan, R.; Binkley, J.S.; Seeger, R.; Pople, J.A. *J. Chem. Phys.* **1980**, *72*, 650.

59. Gonzalez, C.; Schlegel, H.B. *J. Phys. Chem.* **1989**, *93*, 2154. *ibid*, **1990**, *94*, 5523.

60. Pople, J.A.; Schlegel, H.B.; Krishnan, R.; DeFrees, D.J.; Binkley, J.S.; Frisch, M.J.; Whiteside, R.A.; Hout, R.F.; Hehre, W.J. *Int. J. Quantum Chem. Symp.*, **1981**, *15*, 269.

61. Pople, J.A.; Scott, A.P.; Wong, M.W.; Radom, L. *Isr. J. Chem.* **1993**, *33*, 345.

62. Reference 23, p 280.

63. Reference 23, p 259.

64. (a) St-Amant, A.; Salahub, D.R. *Chewm. Phys. Lett.* **1990**, *169*, 387. (b) Salahub, D.R.; Fournier, R.; Mlynarski, P.; Papai, I.; St-Amant, A.; Ushio, J. In *Density Functional Methods in Chemistry*; Labanowski, J.; Andzelm, J., Eds.; Springer-Verlag; New York, 1991. (c) St-Amant, A. Ph.D. Thesis, Université de Montréal, 1991.

65. Eriksson, L.A.; Pettersson, L.G.M.; Siegbahn, P.E.M.; Wahlgren, U. *J. Chem. Phys.* **1995**, *102*, 872.

66. (a) Kutzelnigg, W.; Fleischer, U.; Schindler, M. *NMR - Basic Principles and Progress*; Springer-Verlag: Heidelberg, 1990; p 165, Vol. 23. (b) Huzinaga, S. *J. Chem. Phys.* **1965**, *42*, 1293. (c) Huzinaga, S.; Sakai, Y. *J. Chem. Phys.* **1969**, *50*, 1371.

67. (a) Eriksson, L.A.; Malkin, V.G.; Malkina, O.L.; Salahub, D.R. *J. Chem. Phys.* **1993**, *99*, 9756. (b) Eriksson, L.A.; Malkina, O.L.; Malkin, V.G.; Salahub, D.R. *J. Chem. Phys.* **1994**, *100*, 5066. (c) Malkin, V.G.; Malkina, O.L.; Eriksson, L.A.; Salahub, D.R. In *Theoretical and Computational Chemistry, Vol. 2*; Politzer, P., Seminario, J.M., Eds.; Elsevier Scientific: Amsterdam, 1995.

68. Vosko, S.H.; Wilk, L; Nusair, M. *Can. J. Phys.* **1980**, *58*, 1200.

69. Perdew, J.P.; Wang, Y. *Phys. Rev. B* **1986**, *33*, 8800.

70. Perdew, J.P. *Phys. Rev. B* **1986**, *33*, 8822; **1986**, *34*, 3098.

71. Biegler-König, F.W.; Bader, R.F.W.; Tang, J. *J. Comput. Chem.* **1982**, *3*, 317.

72. Bernardi, F.; Cherry, W.; Shaik, S.; Epiotis, N.D. *J. Am. Chem. Soc.* **1978**, *100*, 1352.

73. Leroy, G.; Peeters, D. *J. Mol. Struct. (THEOCHEM)*, **1981**, *85*, 133.

74. Baird, N.C. *Can. J. Chem.* **1983**, *61*, 1567.

75. Luke, B.T.; Loew, G.H.; McLean, A.D. *J. Am. Chem. Soc.* **1987**, *109*, 1307.

76. Pasto, D.J.; Krasnansky, R.; Zercher, C. *J. Org. Chem.* **1987**, *52*, 3062.

77. Leroy, G.; Peeters, D.; Wilante, C. *J. Mol. Struct. (THEOCHEM)* **1982**, *103*, 217.

78. Dearden, D.V.; Hudgens, J.W.; Johnson, R.D.; Tsai, B.P.; Kafafi, S.A. *J. Phys. Chem.* **1992**, *96*, 585.

79. Pacansky, J.; Yoshimine, M. *J. Phys. Chem.* **1985**, *89*, 1880. Pacansky, J.; Liu, B.; Defrees, D. *J. Org. Chem.* **1986**, *51*, 3270. Honjou, N.; Yoshimine, M.; Pacansky, J. *J. Phys. Chem.* **1987**, *91*, 4455. Schubert, W.; Yoshimine, M.; Pacansky, J. *J. Phys. Chem.* **1981**, 85, 1340.

80. Pacansky, J.; Koch, W.; Miller, M.D. *J. Am. Chem. Soc.* **1991**, *113*, 317.

81. Schlegel, H.B. *J. Phys. Chem.* **1982**, *86*, 4878.

82. Paddon-Row, M.N.; Houk, K.N. *J. Phys. Chem.* **1985**, *89*, 3771.

83. Paddon-Row, M.N.; Thomson, C.; Ball, J.R. *J. Mol. Struct. (THEOCHEM)* **1987**, *150*, 93.

84. Paddon-Row, M.N.; Wong, S.S. *J. Mol. Struct. (THEOCHEM)* **1981**, *150*, 109.

85. Pross, A.; Radom, L. *Tetrahedron* **1980**, *36*, 1999.

86. Brum, J.L.; Johnson, R.D.; Hudgens, J.W. *J. Phys. Chem.* **1994**, *98*, 3645.

87. Chen, Y. Ph.D. Thesis, University of Calgary, 1992.

88. Chen, Y.; Rauk, A.; Tschuikow-Roux, E. *J. Chem. Phys.* **1990**, *93*, 1187.

89. Chen, Y.; Rauk, A.; Tschuikow-Roux, E. *J. Chem. Phys.* **1990**, *93*, 6620.

90. Chen, Y.; Rauk, A.; Tschuikow-Roux, E. *J. Chem. Phys.* **1991**, *94*, 7299.

91. Chen, Y.; Rauk, A.; Tschuikow-Roux, E. *J. Chem. Phys.* **1991**, *95*, 2774.

92. Bent, H.A. *Chem. Rev.* **1961**, *61*, 275.

93. Pauling, L. *The Nature of the Chemical Bond*, 3rd ed.; Cornell University Press: Ithaca, NY, 1960; p 116.

94. Pauling, L. *J. Chem. Phys.* **1969**, *51*, 2767.

95. Ignacio, E.W.; Schlegel, H.B. *J. Phys. Chem.* **1992**, *96*, 5830.

96. Jacox, M.E. *J. Mol. Spectrosc.* **1980**, *81*, 349.

97. Jacox, M.E. *Chem. Phys.* **1981**, *58*, 289.

98. Jacox, M.E. *J. Phys. Chem.* **1984**, *88*, 445.

99. Snelson, A.; Cyvin, B.N.; Cyvin, S.J. *Z. Anorg. Allg. Chem.* **1981**, *482*, 133.

100. Shimanouchi, T. *Tables of Molecular Vibrational Frequencies, Vol. 1, NSRDS-NBS 39*; U.S. Department of Commerce: Washington, 1972.

101. Pedley, J.B.; Naylor, R.D.; Kirby, S.P. *Thermochemical Data of Organic Compounds*, 2nd ed.; Chapman and Hall: London, 1986.

102. Chen, S.S.; Rodgers, A.S.; Chao, J.; Wilhoit, R.C.; Zwolinski, B.J. *J. Phys. Chem. Ref. Data* **1975**, *4*, 441.

103. Lacher, J.R.; Skinner, H.A. *J. Chem. Soc. (A)* **1968**, 1034.

104. Chase, M.W., Jr.; Davies, C.A.; Downey, J.R., Jr.; Frurip, D.J.; McDonald, R.A.; Syverud, A.N. JANAF Thermochemical Tables; *J. Phys. Chem. Ref. Data* **1985**, *14* (Suppl. 1).

105. Cadman, P.; Kirk, A.W.; Trotman-Dickenson, A.F. *J. Chem. Soc., Faraday Trans. 1* **1976**, *72*, 996.

106. Pickard, J.M.; Rodgers, A.S. *Int. J. Chem. Kinet.* **1983**, *15*, 569.

107. Tschuikow-Roux, E.; Paddison, S. *Int. J. Chem. Kinet.* **1987**, *19*, 15.

108. Castelhano, A.L.; Griller, D. *J. Am. Chem. Soc.* **1982**, *104*, 3655.

109. Tschuikow-Roux, E.; Salomon, D.R. *J. Phys. Chem.* **1987**, *91*, 699.

110. Pickard, J.M.; Rodgers, A.S. *J. Am. Chem. Soc.* **1977**, *99*, 691.

111. Wu, E.-C.; Rodgers, A.S. *J. Phys. Chem.* **1974**, *78*, 2315.

112. Martin, J.P.; Paraskevopoulos, G. *Can. J. Chem.* **1983**, *61*, 861.

113. Wu, E.-C.; Rodgers, A.S. *J. Am. Chem. Soc.* **1976**, *98*, 6112.

114. Somayajulu, G.R.; Zwolinski, B.J. *J. Chem. Soc., Faraday Trans 2*, **1974**, *70*, 973.

115. Leroy, G.; Sana, M.; Wilante, C. *J. Mol. Struct. (THEOCHEM)* **1991**, *228*, 37.

116. Reference 23, p 356 ff.

117. Wolfe, S. *Acc. Chem. Res.* **1972**, *5*, 102.

118. Fessenden, R.W. *J. Phys. Chem.* **1967**, *71*, 74.

119. Fessenden, R.W.; Schuler, R.H. *J. Chem. Phys.* **1963**, *39*, 2147.

120. Bowles, A.J.; Hudson, A.; Jackson, R.A. *Chem. Phys. Lett.* **1970**, *5*, 552.

121. Chen, K.S.; Krusic, P.J.; Meakin, P.; Kochi, J.K. *J. Phys. Chem.* **1974**, *78*, 2014.

122. Chen, K.S.; Kochi, J.K. *Can. J. Chem.* **1974**, *52*, 3529.

123. Jinguji, M.; Lin, K.C.; McDowell, C.A.; Raghunathan, P. *J. Chem. Phys.* **1976**, *65*, 3910.

124. Krusic, P.J.; Bingham, R.C. *J. Am. Chem. Soc.* **1976**, *98*, 230.

125. McDowell, C.A.; Raghunathan, P.; Shimokoshi, K. *J. Chem. Phys.* **1973**, *58*, 114.

126. Adrian, F.J.; Cochran, E.L.; Bowers, V.A. *J. Chem. Phys.* **1973**, *59*, 3946.

127. Toriyama, K.; Iwasaki, M.; Nunome, K.; Muto, H. *J. Chem. Phys.* **1981**, *75*, 1633.

128. Hasegawa, A.; Wakabayashi, T.; Hayashi, M.; Symons, M.C.R. *J. Chem. Soc., Faraday Trans. 1*, **1983**, *79*, 941.

129. Chipman, D.M. *J. Chem. Phys.* **1991**, *94*, 6632.

130. Carmichael, I. *J. Phys. Chem.* **1991**, *95*, 6198.

131. Nakano, T.; Morihashi, K.; Kikuchi, O. *Bull. Chem. Soc. Jpn.* **1992**, *65*, 603.

132. Guerra, M. (a) *Chem. Phys. Lett.* **1987**, *139*, 463. (b) *J. Am. Chem. Soc.* **1992**, *114*, 2077.

133. (a) Lunell, S.; Eriksson, L.A.; Huang, M.-B. *J. Mol. Struct. (THEOCHEM)* **1991**, *230*, 263. (b) Eriksson, L.A.; Sjöqvist, L.; Lunell, S.; Shiotani, M.; Usui, M.; Lund, A. *J. Am. Chem. Soc.* **1993**, *115*, 3244. (c) Knight, L.B., Jr.; Kerr, K.; Villanueva, M.; McKinley, A.J.; Feller, D. *J. Chem. Phys.* **1992**, *97*, 5363.

134. (a) Austen, M.A.; Eriksson, L.A.; Boyd, R.J. *Can. J. Chem.* **1994**, *72*, 695. (b) Eriksson, L.A.; Malkin, V.G.; Malkina, O.L.; Salahub, D.R. *Int. J. Quantum Chem.* **1994**, *52*, 879. (c) Tschinke, V.; Ziegler, T. *Can. J. Chem.* **1988**, *67*, 460. (d) Fan, L.; Ziegler, T. *J. Chem. Phys.* **1991**, *94*, 6057.

135. Wertz, J.E.; Bolton, J.R. *Electron Spin Resonance*; Chapman and Hall: New York, 1986.

136. Hudson, A.; Root, K.D.J. *Adv. Magn. Resonance* **1971**, *5*, 1.

137. Fessenden, R.W.; Schuler, R.H. *J. Chem. Phys.* **1965**, *43*, 2704.

138. (a) Bingham, R.C.; Dewar, M.J.S. *J. Am. Chem. Soc.* **1973**, *95*, 7182. (b) Krusic, P.J.; Bingham, R.C. *J. Am. Chem. Soc.* **1976**, *98*, 230.

139. (a) Dobbs, A.J.; Gilbert, B.C.; Norman, R.O.C. *J. Chem. Soc. A* **1971**, 124. (b) Beckwith, A.L.J.; Tindal, P.K. *Aust. J. Chem.* **1971**, *24*, 2099. (c) Cooper, J.; Hudson, A.; Jackson, R.A. *Mol. Phys.* **1972**, *23*, 209.

140. Martell, J.M.; Boyd, R.J.; Eriksson, L.A. *J. Phys. Chem.* **1995**, *99*, 623.

141. (a) Barone, V.; Adamo, C.; Russo, N. *Chem. Phys. Lett.* **1993**, *212*, 5. (b) Dickson, R.M.; Becke, A.D. *J. Chem. Phys.* **1993**, *99*, 3898.

142. Chen, Y.; Rauk, A.; Tschuikow-Roux, E. *J. Chem. Phys.* **1990**, *93*, 1187.

143. Kong, J.; Eriksson, L.A.; Boyd, R.J. *Chem. Phys. Lett.* **1994**, *24*, 217.

144. Ruelle, P.; Sandorfy, C. *Int. J. Quantum Chem.* **1982**, *21*, 691.

145. Sana, M.; Leroy, G. ᵔeters, D.; Wilante, C. *J. Mol. Struct. (THEOCHEM)* **1988**, *164*, 249.

146. Challocombe, M.; C ᵎsiowski, J. *J. Chem. Phys.* **1991**, *95*, 1064.

147. Greenberg, A.; Liebman, J.F.; Dolbier, W.R., Jr.; Medinger, K.S. *Tetrahedron*, **1983**, *39*, 1533.

148. Speis, M.; Buss, V. *J. Comput. Chem.* **1992**, *13*, 142.

149. Cooper, D.L.; Allan, N.R.; Powell, R.L. *J. Fluorine Chem.* **1990**, *46*, 317.

150. Cooper, D.L.; Wright, S.C.; Allan, N.L.; Winterton, N. *J. Fluorine Chem.* **1990**, *47*, 489.

151. Mastryukov, V.S.; Boggs, J.E.; Samdal, S. *J. Mol. Struct. (THEOCHEM)* **1993**, *283*, 199.

152. Magnusson, E. *Aust. J. Chem.* **1986**, *39*, 747.

153. Magnusson, E. *J. Am. Chem. Soc.* **1986**, *108*, 11.

154. Wiberg, K.B.; Breneman, C.M. *J. Am. Chem. Soc.* **1990**, *112*, 8765.

155. Gutiérrez, A.; Jackson, J.E.; Mislow, K. *J. Am. Chem. Soc.* **1985**, *107*, 2880.

156. Hehre, W.J.; Pau, C.-F.; Headley, A.D.; Taft, R.W. *J. Am. Chem. Soc.* **1986**, *108*, 1711.

157. Esseffar, M.; El Mouhtadi, M.; López, V.; Yáñez, M. *J. Mol. Struct. (THEOCHEM)* **1992**, *255*, 393.

158. Chen, Y.; Paddison, S.J.; Tschuikow-Roux, E. *J. Phys. Chem.* **1994**, *98*, 1100.

159. Papasavva, S.; Tai. S.; Esslinger, A.; Illenger, K.H.; Kenny, J.E. *J. Phys. Chem.* **1995**, *99*, 3438.

160. Smart, B.E. In *Molecular Structure and Energetics*; Liebman, J.F., Greenberg, A., Eds.; VCH Publishers: Deerfield Beach, FL, 1986; Vol. 3, pp 156-159.

161. Musso, G.F.; Magnaso, V. *Mol. Phys.* **1984**, *53*, 615.

162. Smits, G.F.; Krol, M.C.; Van Kampen, P.N.; Altona, C. *J. Mol. Struct. (THEOCHEM)* **1986**, *139*, 247.

163. Radom, L.; Baker, J.; Gill, P.M.W.; Nobes, R.H.; Riggs, N.V. *J. Mol. Struct. (THEOCHEM)* **1985**, *126*, 271.

164. Wiberg, K.B.; Murcko, M.A. *J. Phys. Chem.* **1987**, *91*, 3616.

165. Miyajima, T.; Kurita, Y.; Hirano, T. *J. Phys. Chem.* **1987**, *91*, 3954.

166. Dixon, D.A.; Smart, B.E. *J. Phys. Chem.* **1988**, *92*, 2729.

167. Dixon, D.A.; Matsuzawa, N.; Walker, S.C. *J. Phys. Chem.* **1992**, *96*, 10740.

168. Ha, T.-K.; Günthard, H.H. *Chem. Phys.* **1989**, *143*, 203.

169. Allinger, N.L.; Schäfer, L.; Siam, K.; Klimkowski, V.J.; Van Alsenoy, C. *J. Comput. Chem.*, **1985**, *6*, 331.

170. Durig, J.R.; Liu, J.; Little, T.S.; Kalasinsky, V.F. *J. Phys. Chem.* **1992**, *96*, 8224.

171. Martell, J.M.; Boyd, R.J. *J. Phys. Chem.* **1992**, *96*, 6287.

172. Martell, J.M.; Boyd, R.J.; Shi, Z. *J. Phys. Chem.* **1993**, *97*, 7208.

173. References 165 and 167 and references therein.

174. Coulson, C.A. *Valence*; Oxford University Press: London, 1952; p 200.

175. Reference 23, p 146 ff.

176. Bühl, M.; Schleyer, P.v.R. *J. Am. Chem. Soc.* **1992**, *114*, 477.

177. Schleyer, P.v.R.; Gauss, J.; Bühl, M.; Greatrex, R,; Fox, M.A. *J. Chem. Soc., Chem. Commun.* **1993**, 1766.

178. Harmony, M.D.; Laurie, V.W.; Kuczkowski, R.L.; Schwendeman, R.H.; Ramsay, D.A.; Lovas, F.J.; Lafferty, W.J. *J. Phys. Chem. Ref. Data* **1979**, *8*, 619.

179. Takeo, H.; Matsumura, C.; Morino, Y. *J. Chem. Phys.* **1986**, *84*, 4205.

180. Wiberg, K.B.; Murcko, M.A.; Laidig, K.E.; MacDougall, P.J. *J. Phys. Chem.* **1990**, *94*, 6956.

181. Runtz, G.; Bader, R.F.W.; Messer, R.R. *Can. J. Chem.* **1977**, *55*, 3040.

182. Boyd, R.J.; Glover, J.N.M.; Pincock, J.A. *J. Am. Chem. Soc.* **1989**, *111*, 5152.

183. Glassman, I. *Combustion*; Academic Press: New York, 1977.

184. Makide, Y.; Rowland, F.S. *Proc. Natl. Acad. Sci. U.S.A.* **1981**, *78*, 5933.

185. Overend, R. P.; Paraskevopoulos, G.; Cvetanovic, R. J. *Can. J. Chem.* **1975**, *53*, 3374.

186. Howard, C. J.; Evenson, K. M. *J. Chem. Phys.* **1976**, *64*, 4303.

187. Lee, J. H.; Tang, I. N. *J. Chem Phys.* **1982**, *77*, 4459.

188. Margitan, J. J.; Watson, T. *J. Phys. Chem.* **1982**, *86*, 3819.

189. Tully, F. P.; Ravishankara, A. R.; Carr, K. *Int. J. Chem. Kinet.* **1983**, *15*, 1111.

190. Jeong, K. -M.; Hsu, K. -J.; Jeffries, J. B.; Kaufman, F. *J. Phys. Chem.*, **1984**, *88*, 1222.

191. Smith, C. A.; Molina, L. T.; Lamb, J. J.; Molina, M. J. *Int. J. Chem. Kinet.* **1984**, *16*, 41.

192. Devolder, P.; Carlier, M.; Pauwels, J.F.; Sochet, L.R. *Chem. Phys. Lett.* **1984**, *111*, 94.

193. Baulch, D.L.; Craven, R.J.B; Dim, M.; Drysdale, D.D; Grant, S.; Richardson, D.J.; Walker, A.; Watling, G. *J. Chem. Soc. Faraday Trans. 1*, **1985**, *81*, 259.

194. Tully, F.P.; Droege, A.T.; Koszykowski, M.L.; Melius, C.F. *J. Phys. Chem.* **1986**, *90*, 691.

195. Stachnik, R.A.; Molina, R.T.; Lamb, J.J.; Molina, M.J. *J. Phys. Chem.* **1986**, *90*, 277.

196. Nielsen, O.J.; Munk, J.; Pagsberg, P.; Sillesen, A. *Chem. Phys. Lett.*, **1986**, *128*, 168.

197. Wallington, T.J.; Neuman, D.M.; Kurylo, M.J. *Int. J. Chem. Kinet.* **1987**, *19*, 725.

198. Bourmada, N.; Lafage, C.; Devolder, P. *Chem. Phys. Lett.* **1987**, *136*, 209.

199. Leu; M.-T. *J. Phys. Chem.* **1979**, *70*, 1662.

200. Schmidt, V.; Zhu, G.Y.; Becker, K.H.; Fink, E.H. *Ber. Bunsenges. Phys. Chem.* **1985**, *89*, 321.

201. Zabarnik, S.; Fleming, J.W.; Lin, M.C. *Int. J. Chem. Kinet.* **1988**, *20*, 117.

202. Abbatt, J.P.D.; Demerjian, K.L.; Anderson, J.G. *J. Phys. Chem.* **1990**, *94*, 4566.

203. Bott, J.F.; Cohen, N. *Int. J. Chem. Kinet.* **1991**, *23*, 1019.

204. Schiffman, A.; Nelson, D.D.; Robinson, M.S.; Nesbitt, D.J. *J. Phys. Chem.* **1991**, *95*, 2629.

205. Sharkey, P.; Smith, I.W.M. *J. Chem. Soc. Faraday Trans.* **1993**, *89*, 631.

206. Talukdar, R.K.; Mellouki, A.; Gierczak, T.; Barone, S.; Chiang, S.-Y.; Ravishankara, A.R. *Int. J. Chem. Kinet.* **1994**, *26*, 973.

207. Atkinson, R.; Baulch, D.L.; Cox, R.A.; Hampson, R.F.; Kerr, J.A.; Troe, J. *J. Phys. Chem. Ref. Data* **1989**, *18*, 881.

208. Melissas, V.S.; Truhlar, D.G. *J. Phys. Chem.* **1994**, *98*, 875.

209. Martell, J.M.; Mehta, A.K.; Pacey, P.D.; Boyd, R.J. *J. Phys. Chem.* **1995**, *99*, 8661.

210. Gonzalez, C.; McDouall, J.J.W; Schlegel, H.B. *J. Phys. Chem.* **1990**, *94*, 7467.

211. Pardo, L.; Banfelder, J.R.; Osman, R. *J. Am. Chem. Soc.* **1992**, *114*, 2382.

212. Dunning, T.H. *J. Chem. Phys.* **1989**, *90*, 1007.

213. Allinger, N.L.; Rahman, M.; Lii, J.-H. *J. Am. Chem. Soc.* **1990**, *112*, 8293.

214. Allinger, N.L.; Yuh, Y.H.; Lii, J.-H. *J. Am. Chem. Soc.* **1989**, *111*, 8551.

215. Baer, M. In *Theory of Chemical Reaction Dynamics*; Baer, M., Ed.; CRC Press: Boca Raton, FL, 1985; Vol. 1 p. 93.

216. Delves, L.M. *Nucl. Phys.* **1959**, *9*, 391.

217. Jones, S.A.L.; Pacey, P.D. *J. Phys. Chem.* **1992**, *96*, 1764.

218. Gordon, M.S.; Truhlar, D.G. *J. Am. Chem. Soc.* **1986**, *108*, 5412.

219. Pacey, P.D.; Wimalasena, J.H. *J. Phys. Chem.* **1984**, *88*, 5657.

220. Pittam, D.A.; Pilcher, G. *J. Chem. Soc. Faraday Trans. 1* **1972**, *68*, 2224.

221. Berkowitz, J.; Ellison, G.B.; Gutman, D. *J. Phys. Chem.* **1994**, *98*, 2744.

222. (a) Reference 23, p 227. (b) Gaussian, Inc., personal communication.

223. Makide, Y.; Rowland, F.S. *Proc. Natl. Acad. Sci. U.S.A.* **1981**, *78*, 5933.

224. Schmoltner, A.M.; Talukdar, R.K.; Warren, R.F.; Mellouki, A.; Goldfarb, L.; Gierczak, T.; McKeen, S.A.; Ravishankara, A.R. *J. Phys. Chem.* **1993**, *97*, 8976.

225. Hsu, K.-J.; DeMore, W.B. *J. Phys. Chem.* **1995**, *99*, 1235.

226. Brown, A.C.; Canosa-Mas, C.E.; Parr, A.D.; Wayne, R.P. *Atmos. Environ.* **1990**, *24A*, 2499.

227. Nielsen, O.J. *Chem. Phys. Lett.* **1991**, *187*, 286.

228. Gierczak, T.; Talukdar, R.; Vaghjiani, G.L.; Lovejoy, E.R.; Ravishankara, A.R. *J. Geophys. Res. D* **1991**, *96*, 5001.

229. Talukdar, R.; Mellouki, A.; Gierczak, T.; Burkholder, J.B.; McKeen, S.A.; Ravishankara, A.R. *J. Phys. Chem.* **1991**, *95*, 5815.

230. Zhang, Z.; Huie, R.E.; Kurylo, M.J. *J. Phys. Chem.* **1992**, *96*, 1533.

231. Demore, W.B. *Geophys. Res. Lett.* **1993**, *20*, 1359.

232. Cohen, N.; Benson, S.W. *J. Phys. Chem.* **1987**, *91*, 162.

233. Cohen, N.; Benson, S.W. *J. Phys. Chem.* **1987**, *91*, 171.

234. Gonzalez, C.; McDouall, J.J.W; Schlegel, H.B. *J. Phys. Chem.* **1990**, *94*, 7467.

235. Pardo, L.; Banfelder, J.R.; Osman, R. *J. Am. Chem. Soc.* **1992**, *114*, 2382.

236. Choi, S.C.; Boyd, R.J. *Can. J. Chem.* **1986**, *64*, 2042.

237. Drummond, D.F.; McMahon, T.B. *J. Phys. Chem.* **1981**, *85*, 3746.

238. Reference 93, p 260.

239. DeFrees, D.J.; Levi, B.A.; Pollack, S.K.; Hehre, W.J.; Binkley, J.S.; Pople, J.A. *J. Am. Chem. Soc.* **1979**, *101*, 4085.

240. Ceulemans, A. In *Intermolecular Forces*; Huyskens, P.L., Luck, W.A.P., Zeegers-Huyskens, T., Eds.; Springer-Verlag: Berlin, 1991.

241. Deng, L.; Branchadell, V.; Ziegler, T. *J. Am. Chem. Soc.* **1994**, *116*, 10645.

242. Pacey, P.D. *J. Chem. Educ.* **1981**, *58*, 613.

243. Garrett, B.C.; Truhlar, D.G. *J. Phys. Chem.* **1979**, *83*, 1052.

244. Wayne, R.P.; Canosa-Mas, C.E.; Heard, A.C.; Parr, A.D. *Atmos. Environ.* **1992**, *26A*, 2371.

245. Talukdar, R.K.; Mellouki, A.; Gierczak, T.; Barone, S.; Chiang, S.-Y.; Ravishankara, A.R. *Int. J. Chem. Kinet.* **1994**, *26*, 973.

246. Curtiss, L.A.; Raghavachari, K. In *Quantum Mechanical Electronic Structure Calculations with Chemical Accuracy*; Langhoff, S.R., Ed.; Kluwer: Dordrecht, in press.

247. Shi,Z.; Boyd, R.J. *J. Am. Chem. Soc.* **1991**, *113*, 1072.

248. Kim, S.S.; Choi, S.Y.; Kong, C.H. *J. Am. Chem. Soc.* **1985**, *85*, 4234.

249. Héberger, K. *J. Phys. Org. Chem.* **1994**, *7*, 244.

250. Wiberg, K.B.; Bader, R.F.W.; Lau, C.D.H. *J. Am. Chem. Soc.* **1987**, *109*, 985.

251. Bader, R.F.W.; Tang, T.H.; Tal, Y.; Biegler-König, F.W. *J. Am. Chem. Soc.* **1982**, *104*, 946.

252. (a) Boyd, R.J. In Kobayashi, M., Ed. *Studies in Organic Chemistry*; Elsevier Scientific: Amsterdam, 1987; Vol. 31, p 485. (b) Knop, O.; Boyd, R.J.; Choi, S.C. *J. Am. Chem. Soc.* **1988**, *110*, 7299.

253. Mulliken, R.S. *J. Chem. Phys.* **1955**, *23*, 1833.

254. Bader, R.F.W.; Nguyen-Dang, T.T. *Adv. Quantum Chem.* **1981**, *14*, 63.

255. Perrin, C.L. *J. Am. Chem. Soc.* **1991**, *113*, 2865.

256. Reference 50, p 274.

257. Reference 50, p 290.

258. Reference 50, p 278.

259. Runtz, G.; Bader, R.F.W.; Messer, R.R. *Can. J. Chem.* **1977**, *55*, 3040.

260. (a) Edgecombe, K.E. Ph.D. thesis, Dalhousie University, 1987. (b) Boyd, R.J.; Edgecombe, K.E. *J. Comput. Chem.* **1987**, *8*, 489. (c) Edgecombe, K.E.; Boyd, R.J. *Int. J. Quantum Chem.* **1986**, *29*, 959.

261. Boyd, R.J.; Edgecombe, K.E. *J. Am. Chem. Soc.* **1988**, *110*, 4182.

262. Wang, L.-C.; Boyd, R.J. *J. Chem. Phys.* **1989**, *90*, 1083.

263. Boyd, R.J.; Wang, L.-C. *J. Comput. Chem.* **1989**, *10*, 367.

264. Wiberg, K.B.; Wendoloski, J. *J. Phys. Chem.* **1984**, *88*, 586.

265. Reed, A.E.; Weinhold, F. *J. Chem. Phys.* **1986**, *84*, 2428.

266. Cioslowski, J. *J. Am. Chem. Soc.* **1989**, *111*, 8333.